Novel Sensors for the Detection of Biologically Important Species

Li, Meng

Award date:
2015

Awarding institution:
University of Bath

Novel Sensors for the Detection of Biologically Important Species

Meng Li

A thesis submitted for the degree of Doctor of Philosophy

University of Bath

Department of Chemistry

June 2015

COPYRIGHT

I want to bring out the secrets of nature and apply them for the happiness of man. I don't know of any better service to offer for the short time we are in the world.

--Thomas Edison

Abstract

The ability to monitor the presence of analytes is of great importance both in industrial applications and physiological systems. Since the crucial recognition events of chemistry, biology, and materials science occur in a much smaller world, it is very difficult to gather this kind of information. Therefore much effort has been devoted to the detection of chosen molecules selectively and signalling this presence. This thesis highlighted the uniqueness and utility of both fluorescent sensor and electrochemical sensor to investigate biologically important species.

The determination of copper(II) ion is very crucial to both environment and human health. To utilise the fluorescent sensors for recognition has plenty of advantages, such as high sensitivity, "on-off" switch ability and submillisecond temporal resolution. Naphthalimide based probes has always been the key point of the chemosensors due to its excellent photophysical properties. Therefore, the aim of the project is to investigate boronic acid receptor linked to the naphthalimide fluorophore for copper(II) detection. And the utility of boronic acid as binding site is one of the rare examples of fluorescent chemosensors for Cu^{2+} detection.

Neutral molecules such as glutathione (GSH) play a crucial role in maintaining appropriate redox homeostasis in biological systems. We creatively use the chromophore of dicyanomethylene-4H-pyran(DCM) for the design of probe, due to its emission located at the red or near infra-red (NIR) region, which is particularly suitable for application in biological samples. GSH, the most abundant cellular thiol, is of great importance in cellular defence against toxins and free radicals. Therefore we developed a colorimetric and NIR fluorescence turn-on thiol probe containing DCM as the fluorophore and DNBS as the fluorescence quencher and recognition moiety.

The interaction of ferrocene-boronic acid with fructose is investigated in aqueous 0.1 M phosphate buffer at pH 7, 8, and 9. Two voltammetric methods, (i) based on a dual-plate generator-collector micro-trench electrode (steady state) and (ii) based on square-wave voltammetry (transient), are applied and compared in terms of mechanistic resolution. A combination of experimental data is employed to obtain new insights into the binding rates and the cumulative binding constants for both the reduced ferrocene-

boronic acid (pH dependent and weakly binding) and for the oxidised ferrocene-boronic acid (pH independent and strongly binding).

Finally, a redox-activated fluorescence switch based on a ferrocene - fluorophore - boronic ester conjugate was investigated. The development of multifunctional systems that can integrate individual basic logic gates into combinational circuits has drawn much attention to smart materials. A novel electrochemically and fluorescence active boronic ester sensor molecule has been developed containing ferrocence and naphthalimide as the redox and fluorophore units. The solid state electrochemical characterisation of the compound was investigated in aqueous media and it indicates a direct interaction with fluoride anions. The fluorescence can also be modulated through photoinduced electron transfer (PET) by a redox process. An OFF-ON fluorescence response occurs when the ferrocene is oxidised by Fe^{3+}. While in the presence of F^-, the fluorescence enhancement was offset. Therefore, the combinations of iron (Fe^{3+}) ions, sodium L-ascorbate, and fluoride (F^-) ions can be used to produce a molecular system displaying INHIBIT logic gate, due to indirect fluorescence quenching.

Contents

Acknowledgement

I owe a great deal of thanks to many people who help me make my research work. First, I'd like to thank Prof. Tony James from University of Bath and Prof. Weihong Zhu from East China University of Science and Technology. Without the cooperation between the two labs, I would not get the chance to start my PhD degree in University of Bath. I am most grateful to them for answering all my stupid questions and for being the kindest mans in the world to let me work freely in the lab. Second, I'd like to thank Prof. Frank Marken for giving me the chance to understand the electrochemistry world. And also I would like to thank China Scholarship Council (CSC) for financial support and University of Bath for Full Fees Scholarship.

Many thanks to all the TDJ group members in University of Bath. Of particular note: Steve Flower, for being so friendly and patient to help me out a lot since I started and creating a good working atmosphere in the lab; Suying Xu, for giving me specific guidance on my lab work and getting me settled down in Bath.

And also many thanks to all my collaboration partners at Bath: Haobe Ge and Dr Rory Arrowsmith, Dr. Vincenzo Mirabello from Dr Sofia Pascu's group, for giving me tremendous help by recording the confocal imaging of my compounds; Dr. Andrew J. Gross From Prof. Frank Marken's group for helping me with dual-plate generator-collector voltammetry study.

Thanks go to all the support staff who works in the department. Particularly I would like to take this opportunity to thank Anneke Lubben for Mass Spectra analysis and John Lowe for NMR studies.

Furthermore, I would like to thank University of Bath for the award of Global Research Scholarship Scheme. I am most grateful to Prof. Juyoung Yoon to look after me during my two months placements in Ewha Womans University. I would like to extend particular thanks to various members in Yoon's group who made me feel welcome and comfortable: Ying Hu, Songyi Li, Jiyeong Kim, Hyunsu Kim, Jiyeon Ohm, Gina Kim and Nahyun Kwon.

Also I want to thank all my friends I met in Bath. It is them who make my life in Bath full of happiness and joy. In particular, to Jiangning Gao, Yuanyang Rong, Wentao

Deng, Boyang Mao and Qianlong Wang, over the past three years, I have received plenty of encouragement from you. It is you who made me feel the warmth at home and gave me good suggestions when I run into a problem.

Finally, I would like to dedicate this thesis to my parents, Mr. Zhibiao Li and Mrs. Jinmei Shang for their unconditional love and support that made my doctoral research success. Without their continuous support and understanding, I could not go through the ups and downs of the past years.

Abbreviations

AIE	aggregation induced emission
Ar	aryl
bp	by product
BODIPY	dipyrromethene difluoride
br	broad
°C	degree Celsius
$CDCl_3$	deuterated chloroform
cm^3	cubic centimetre
cm^{-1}	wave numbers
δ	chemical shift in parts per million
D	deuterium (^2H)
d	doublet
dd	doublet of doublet
D-A	donor-acceptor
DCM	dichloromethane/ dicyanomethylene-4H-pyran
dm^3	cubic decimetre
DMSO	dimethyl sulfoxide
DMF	Dimethylformamide
ds	doublet and singlet
dt	doublet of treplet
e^-	electron
ESI-MS	Electrospray Ionization Mass Spectrometry
Et	ethyl
EtOAc	ethyl acetate
EtOH	ethanol
eq./equiv.	Equivalent
FCS	foetal calf serum
FRET	Froster resonance energy transfer
g	gram
h	hours
$h\nu$	incident light
HOMO	highest occupied molecular orbital
HOTs	hydroxylated organotins

I	fluorescence intensity
I/I_0	relative fluorescence intensity
ICT	internal charge transfer
J	coupling constant
K_a	association constant
kJ	kilojoules
λ	Wavelength
λ_{em}	emission wavelength
λ_{ex}	excitation wavelength
L	Litre
LUMO	lowest unoccupied molecular orbital
μM	micromolar
μm	micrometre
μL	microlitre
μg	microgram
m	*meta*
m	unresolved multiplet / minutes
M^{-1}	cubic decimetres per mole
$[M]^+$	parent molecular ion
Me	methyl
MeCN	acetonitrile
MeOD	deuterated D4 methanol
MeOH	methanol
mg	milligram
MHz	megahertz
MLCT	metal-ligand charge transfer
mm	millimetre
mM	millimolar
mmol	millimole
mol	mole
m.p.	melting point
MS	mass spectra
NBS	*N*-bromosuccinimide
nm	nanometer

NCL	native chemical ligation
NIR	near infrared
NMR	nuclear magnetic resonance
ns	nanosecond
o	*ortho*
p	*para*
PBA	phenylboronic acid
PET	photoinduced electron transfer
pK_a	- log K_a
ppm	parts per million
q	quartet
R^2	goodness of curve fitting
R_f	retardance factor
RET	resonance energy transfer
rt	room temperature
s	singlet / second
S_0	singlet electronic ground state
S_1	first singlet electronic excited state
S_2	second singlet electronic excited state
SFM	serum free medium
t	triplet
tt	triplet of triplet
T_1	first triplet electronic excited state
TEA	triethylamine
THF	tetrahydrofuran
TICT	twisted intramolecular charge transfer
TLC	thin layer chromatography
TMS	tetramethylsilane
UV	ultraviolet
wt%	weight percent

CHAPTER ONE

Introduction

1 Introduction

1.1 Overview of Introduction

The interaction between a receptor site and a reporter site are always involved in sensor constructs. It is interesting that recognition is not just defined as a binding event but requires selectivity between the receptor and guest sites. And the electronic, geometric and polar elements are very important in the selection process. Therefore, we need to make intelligent structural design with appropriate functional group complementarities to synthesise a potential receptor for a suitable guest

Fluorescent sensor

Chemosensors consist of receptors and fluorophores constructed by linkage or integration, able to produce "grip-and-tell" operations (Scheme 1). The binding of a sensor to a guest will disturb the original relationship with respect to electron or charge transfer between the reporter and receptor in the sensors' excited or ground state, and finally change emission wavelength or intensity.[1] Here, the general sensing mechanisms involved in designing fluorescent sensors will be introduced.

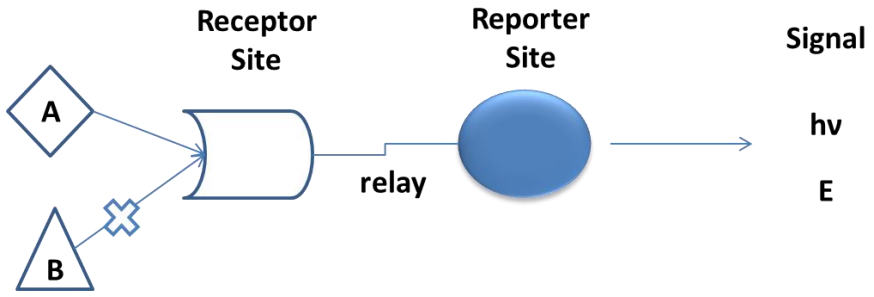

Scheme 1 The schematic depiction of chemosensor action.

Metal-coordination based fluorescent sensor

The transition or d-block metal ions such as manganese, iron, cobalt, nickel, copper, and zinc have been shown to be important for biological systems. Coordination chemistry plays an essential role in the design of fluorescent probes for these metal ions. Metal coordination to organic dyes induces distinct optical responses which signal the presence of metal species of interest. The principles governing metal ligand complex

stability and specificity depend on the properties of both the metal ion and the chelating agent. Here, the fluorescent sensors based on different fluorphores for the detection of copper(II) ion will be illustrated.

Reaction based fluorescent sensor

While the traditional sensors were developed on the basis of supramolecular interactions, which is often subject to limitations. Reaction based chemosensor system have attracted considerable attentions due to the high selectivity and sensitivity towards substrates. As a result, increasing attention within the fluorescent sensor community is turning to the use of analyte-specific molecular indicators, where substrate-triggered reactions are used to detect the presence of a given analyte. Glutathione is the most common and important biothiols in biological system. Therefore, the reaction based fluorescent sensor for the detection of biothiols will be presented.

Electrochemical sensor

Besides fluorescent sensor, electrochemical sensors also provide an attractive means to analyse the content of biological samples due to the direct conversion of a biological event to an electronic signal. The most common traditional techniques, such as cyclic voltammetry, differential pulse voltammetry, square wave, impedance spectroscopy, and dual-plate junction based methods are well explored in this field. Surface modification, electrochemical transduction mechanisms, and the choice of the recognition receptor molecules all influence the ultimate sensitivity of the sensor. Here, the electrochemical sensing with boronic acid for saccharides recognition will be introduced.

Molecular switches and logic gates

Molecular switches relate to molecules whose electronic and optical properties can change reversibly in terms of various environmental incentives.[2] Among the various switching materials, fluorescence is one of the most attractive owing to its high sensitivity and the easy monitoring of the luminescence changes.[3] The photo induced electron transfer (PET) mechanism is often used in fluorescence switches. In the off state of the switch, fluorescence is quenched by PET either to or from the fluorophore. Although fluorescent switches have been extensively explored,[4] fluorescence switches

based on a redox reaction centre such as ferrocene (Fc) are rare and much less well studied.[5, 6] Here, the electrochemical-fluorescence sensors and molecular logic gate systems will be introduced.

1.2 The Principles of Fluorescence

1.2.1 Fluorescence Spectroscopy

Fluorescence is the emission of light by a substance that has absorbed light or other electromagnetic radiation which is a form of luminescence that can be split into two categories: fluorescence and phosphorescence. The Jablonski diagram (Figure 1) clearly explains the relationship between photoluminescence and molecular energy states.[7]

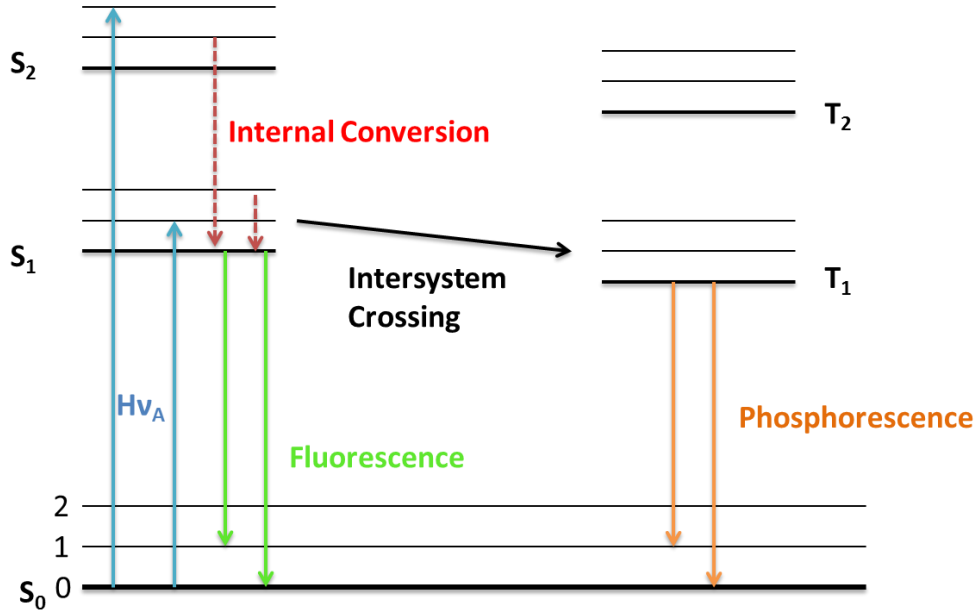

Figure 1 Example of a Jablonski diagram and illustration of the relative positions of absorption, fluorescence and phosphorescence spectra.

After the absorption of a certain wavelength of light, the molecules will enter their excited states such as S_1 and S_2. The energy absorbed from light is strongly correlated to the excitation of fluorophores from ground state to excited state, and also relates to emission of light *via* a fluorescent or phosphorescent mechanism. This amount of energy is measured in quantic terms as expressed by the equation:

$$E = h\nu = hc/\lambda$$

This equation is known as Planck's Law, where E represents the energy, h is Planck's constant, ν and λ are the frequency and wavelength of the incoming light and c is the speed of light. Planck's Law states that the energy absorbed from photon is directly

relative to the frequency and inversely proportional to the wavelength of incoming light, which means that the incoming light with shorter wavelength carries a higher quantum of energy.

After the excitation, the return to the vibrational state S_0 is quick and produces the radiative emission in the form of fluorescence. The decay of the excited electron from a singlet excited state (S_1) to the ground state (S_0) is a spin-allowed process as it has opposite spin to the electron in the ground-state orbital. Thus the typical fluorescence lifetime is about 10 ns.[7] But some undergo a nonradiative transition which arises through several different mechanisms, which means that excited molecules can also undergo a spin conversion to a triplet state T_1, in which the electron in the excited orbital has the same spin orientation as the ground-state electron. The conversion from S_1 to T_1 is called intersystem conversion. Thus this type of nonradiative transition can give rise to phosphorescence. The decay from T_1 to S_0 is typically with a longer lifetime as it is spin-prohibited. Some phosphorescence can take a few hours at 80 K.

There are several distinctive parameters of fluorescence, such as the Stokes shift, lifetime, maximum emission wavelength and fluorescent intensity, *etc*. In most cases, the emitted light has a longer wavelength, and therefore lower energy, than the absorbed radiation due to internal conversion. The difference between locations of the band maxima of the absorption and emission spectra of the same electronic transition is called Stokes shift. And usually the emission spectrum is often the mirror image of absorption since the electronic transitions are vertical, which means that the nucleus does not move and the vibrational levels of the excited state is similar to the vibrational levels of the ground state. The fluorescence lifetime indicates the average time the molecule stays in its excited state before emitting a photon.

As for fluorescence, due to its high sensitivity and selectivity down to the single molecule, it plays a crucial role in recognition events of chemistry, biology, and materials science. There are three basic mechanisms used for sensing: internal charge transfer (ICT), photoinduced electron transfer (PET) and fluorescence resonance energy transfer (FRET).

1.2.2 Types of Sensing Mechanisms

The mechanisms commonly used for sensing design include internal charge transfer (ICT)[8], photoinduced electron transfer (PET)[9, 10] and fluorescence resonance energy transfer (FRET).

1.2.2.1 Sensing Systems Based on Internal Charge Transfer (ICT)

A typical internal charge transfer (ICT) molecule contains an electron donating group (D) and an electron accepter group (A) linked by a conjugated π system, namely D-π-A system. Both in the ground state and excited state, the molecules are characterised by a polarised structure. When the photon is excited, the intramolecular electron conjugated system can be used as a charge transfer channel, to further increase the charge transfer of electron donor to electron acceptor, which produces the ICT process.[11, 12]

The charge transfer of the D-π-A conjugated molecular structure is controlled by the electrons' gain and loss, so it is possible to recognise different species by changing the ability of the electrons' gain and loss in ICT systems (Figure 2). When the electron donor is used as recognition group, because of the coordination effect of the receptor and guest, the ability of donating electrons will be reduced, causing the systems' ground state to rise, which creates a blue shift; Whereas when the electron acceptor is used as recognition groups, the changes of the molecular energy level is opposite to the former one, thus creating a red shift.[13]

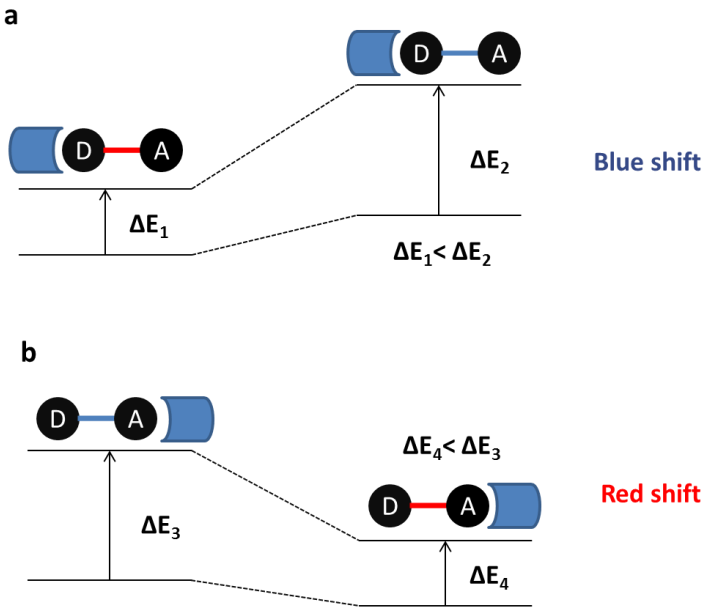

Figure 2 ICT systems: an analyte interacts with (a) donor group and (b) acceptor group.[13]

An example of ICT sensor for copper(II) ion sensing was developed by the Qian group.[14] They designed a ratiometric fluorescent sensor **1** based on naphthalimide fluorophore. In aqueous ethanol solution, the addition of Cu^{2+} induces an increasing fluorescent emission centred at 475 nm at the cost of the fluorescent emission of **1** centred at 525 nm, which forms a 1:1 metal - ligand complex. The detention of Cu^{2+} by the receptor showed a 50 nm blue shift of fluorescence emission, which resulted from the reduction of the electron-donating ability of the two amino groups conjugated to the naphthalene ring. The system provided high selectivity for Cu^{2+} over other metal ions.

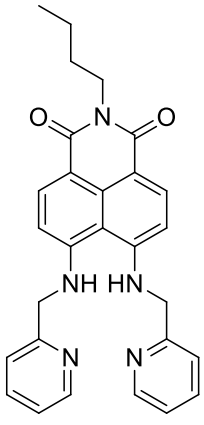

1

1.2.2.2 Sensing Systems through Photoinduced Electron Transfer (PET)

A typical photoinduced electron transfer (PET) molecule usually contains an electron donating group, an electron acceptor group and a linker. Fluorescent signalling *via* the PET strategy is distinguished by its intrinsically supramolecular nature, since distinct components perform each one (or more) of the necessary functions (Figure 3). A fluorophore module is the site of both photonic transactions of excitation and emission. A receptor module is responsible for guest complexation and decomplexation. A spacer module holds the fluorophore and receptor close together, but it is separate from each other. This also means that true molecular engineering applies, i.e., the optical guest-binding and redox properties of the components allow the quantitative prediction of the signalling parameters of the supramolecular system. Furthermore, PET signalling systems have natural "all or none" switch ability: guest-induced "off-on" and "on-off" fluorescence are both designable. The mechanism of PET fluorescent sensors can also be explained using frontier orbital theory.[15-17]

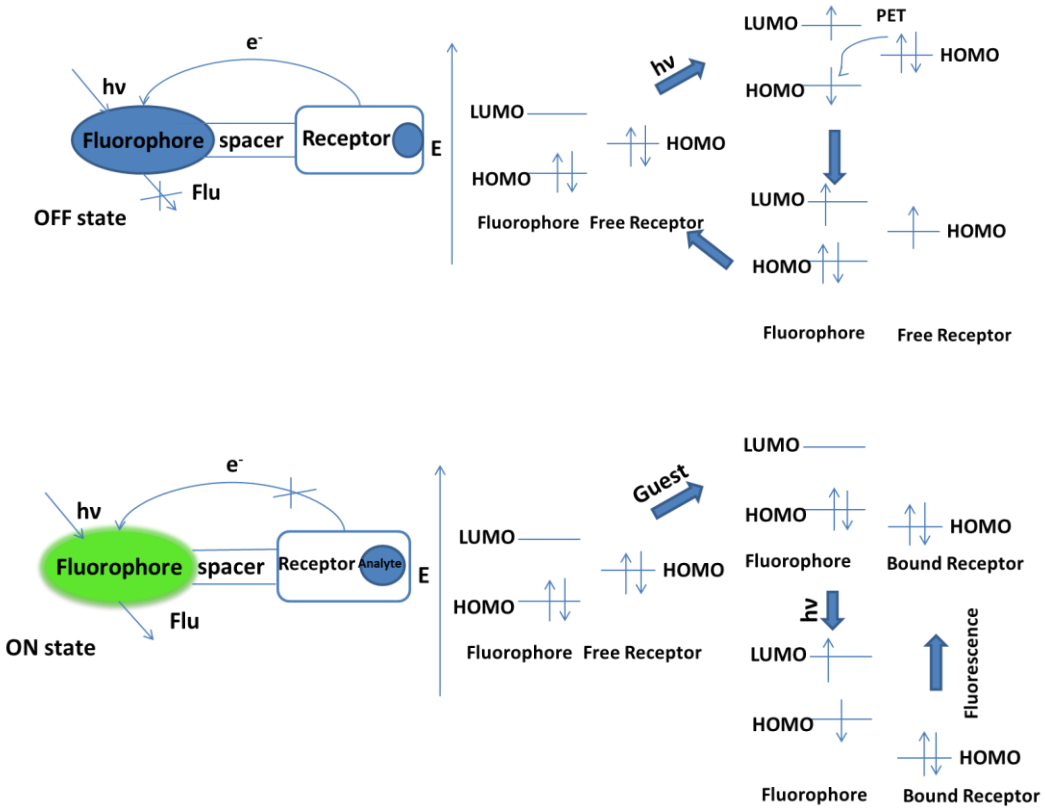

Figure 3 Abridged general view of principle of PET fluorescent switches and frontier orbital energy diagrams illustrating thermodynamics of PET.[18]

A PET sensor for detection of copper(II) ion was reported by Duan's group.[19] A fluorescent turn-on probe **2** was prepared by incorporating coumarin fluorophores within the benzil dihydrazone moiety (Figure 4). Because of the quenching behaviour of paramagnetic copper(II) ion it is still difficult to design PET sensors. However, in aqueous acetonitrile solution, the presence of Cu^{2+} did not induce an absorbance spectral change; the conservation of the emission wavelength with significant fluorescence enhancement suggested a PET mechanism. Given the excellent selectivity and sensitivity of the probe, it has also been used to detect Cu^{2+} in living cells.

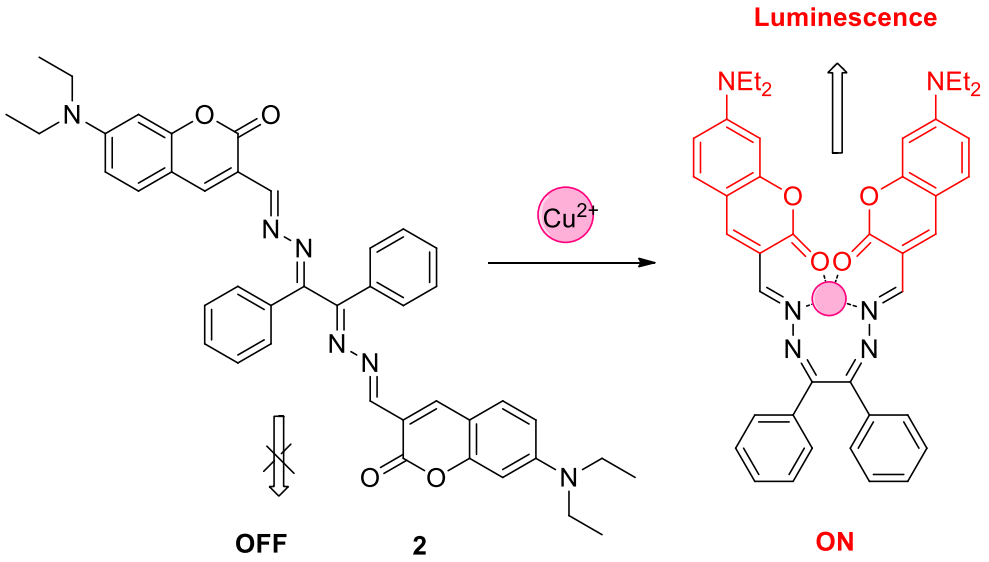

Figure 4 The chemical structure and proposed binding mode of **2** to Cu^{2+}, showing the possibility of blocking the PET process upon metal binding.

1.2.2.3 Fluorescence Resonance Energy Transfer (FRET) System

Another important process that occurs in the excited state is resonance energy transfer (RET). Whenever the emission spectrum of a fluorophore overlaps with the absorption spectrum of another molecule, RET process occurs. Such overlap is illustrated in Figure 5. The acceptor does not need to be fluorescent. It is vital to understand that RET does not involve emission of light by the donor. RET is not the result of emission from the donor being absorbed by the acceptor. Such reabsorption processes are dependent on the overall concentration of the acceptor and on non-molecular factors such as sample size, and thus are of less interest. There is no intermediate photon in RET. The donor and acceptor are coupled by a dipole-dipole interaction. For these reasons the term RET is preferred over the term fluorescence resonance energy transfer (FRET), which is also in common use.[20, 21]

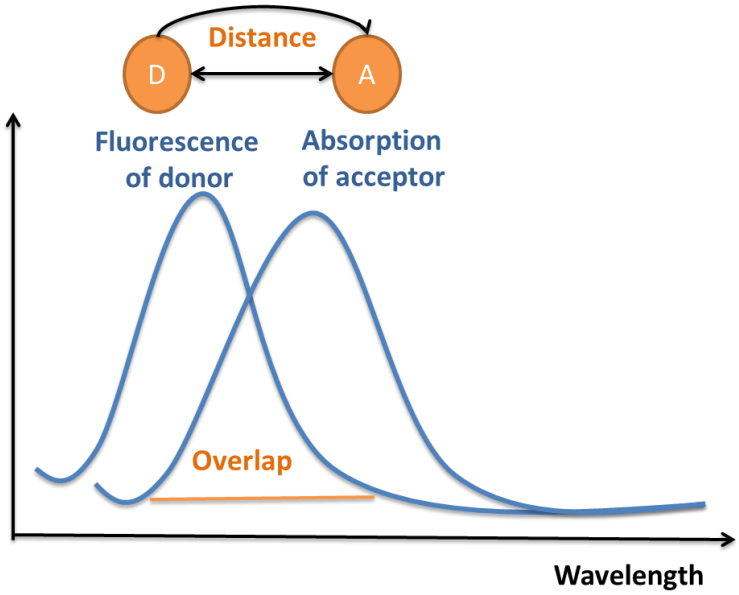

Figure 5 Spectral overlap for fluorescence resonance energy transfer (FRET).

An example of a FRET sensor for Cu^{2+} detection was designed by Hu's group.[22] They employed a facile one-step Cu(I)-catalysed "click" reaction to fabricate a novel FRET ratiometric "off-on" fluorescent probe **3**. The emission of the donor, a dansyl group, overlaps well with the absorption of the acceptor, xanthene in the open-ring fluorophore rhodamine, which shows high selectivity to Cu^{2+}. A 28-fold enhancement of the emission ratio (I_{568}/I_{540}) was achieved on addition of Cu^{2+} with an approximate linear relationship between emission ratios and the concentrations of Cu^{2+} from 10 to 50 μM. The system has also been used for the fluorescence imaging of intracellular Cu^{2+}.

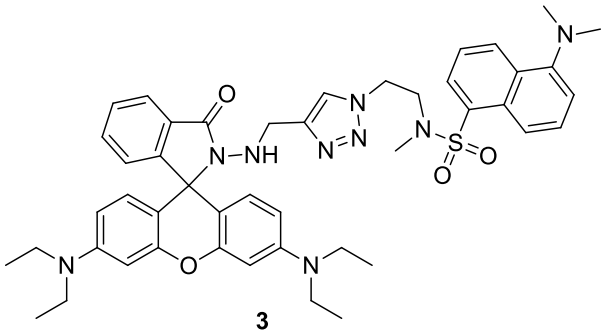

3

1.2.2.4 Alternative Sensing Mechanism

Except for above mentioned mechanisms, other emissive phenomenon are also utilised in synthetic receptors, like metal-ligand charge transfer (MLCT), twisted intramolecular charge transfer (TICT), aggregation-induced emission (AIE) and C=N isomerisation, which could be ascribed to fluorescence changes *via* conformation restriction.[23, 24]

1.3 Developments in the Field of Chemosensors for the Detection of Copper(II) Ions

1.3.1 Sensors for Copper(II) Ions

Sensors based on the ion-induced changes in fluorescence have been widely investigated in the biological and environmental systems due to the simplicity and high detection limit of fluorescence.[25] A couple of other methods, such as high-performance liquid chromatography (HPLC), mass spectrometry (MS), atomic absorption spectroscopy, inductively coupled plasma atomic emission spectrometry, electrochemical sensing, etc., have been used to analyse the targets concerned.[26, 27] However, these methods have some limitations such as extensive and time-consuming procedures that involve the use of sophisticated instrumentation. Fluorescent probes are preferable approaches for the measurement of these analytes because fluorimetry is rapidly performed and it is highly sensitive. Above all, it is suitable for high-throughput screening applications, and can afford real information on the localisation and quantity of the targets of interest.[28, 29] Various fluorophores with different photochemical properties have been employed as signal reporters for chemosensors, some recent examples are coumarin, pyrene, 1,8-naphthalimide, rhodamine, fluorescein, xanthenes, squaraine, cyanine, boron dipyrromethene difluoride (BODIPY), nitrobenzofurazan, etc.[30, 31]

Coumarin is a popular fluorescent dye with widespread applications as a fluorescent chemosensor due to its high molar absorption coefficients and high fluorescence quantum yields. Wu and coworkers recently reported a copper(II) sensor **4** (related to **2**) containing a coumarin group as the fluorophore and a phenol hydrazone moiety as a selective and sensitive receptor for copper(II).[32] Among other metal ions, only on the addition of Cu^{2+} induced significant fluorescence quenching. The Job plot's curve demonstrated that the binding ratio of the **4**-Cu^{2+} complexes was 2: 1 and the association constant (K_a) for Cu^{2+} binding with **4** was calculated to be 9.56×10^9 M^{-1}. Moreover, fluorescence confocal experiments indicated that **4** could be employed for detecting Cu^{2+} in living cells.

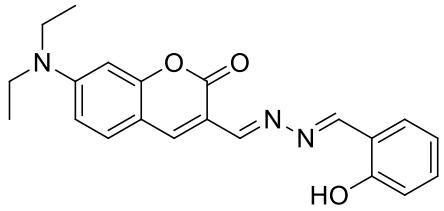

4

Besides Coumarin, rhodamine is highly favourable for the design of fluorescent sensor due to its large Stokes shift, and high photostability. Therefore, several examples of rhodamine based sensors for the detection of copper(II) ions have been developed. A rhodamine-pyrene derivative **5** (related to **3**) has been synthesised as a ratiometric and off-on sensor for the detection of Cu^{2+} by Yoon's group (Figure 6).[33] When Cu^{2+} was added to the solution, a significant decrease in the fluorescence intensity at 424 nm and a new fluorescence emission band centred at 575 nm was observed, which was attributed to the Cu^{2+}-induced ring-opening of the spirolactam moiety. Upon addition of up to 7 equiv. Cu^{2+}, the solution changed colour from primrose yellow to pink.

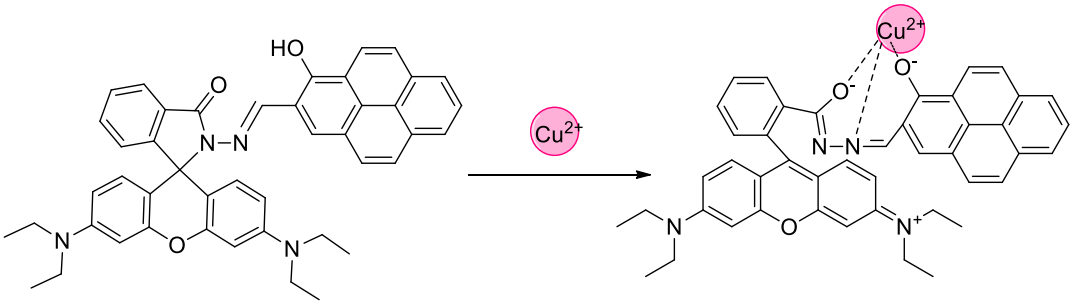

5

Figure 6 Proposed binding modes.[33]

Kim *et al.*, reported the design and synthesis of a new rhodamine-based derivative **6** (related to **5**), bearing an *N*-butyl-1, 8-naphthalimide group (Figure 7).[34] This compound displayed selective colorimetric and fluorescence "turn-on" changes at 550 nm *via* selective rhodamine ring-opening by Cu^{2+}. This compound forms a 2: 2 complex with Cu^{2+}. As expected, the naphthalimide moiety allowed for ratiometric analysis.

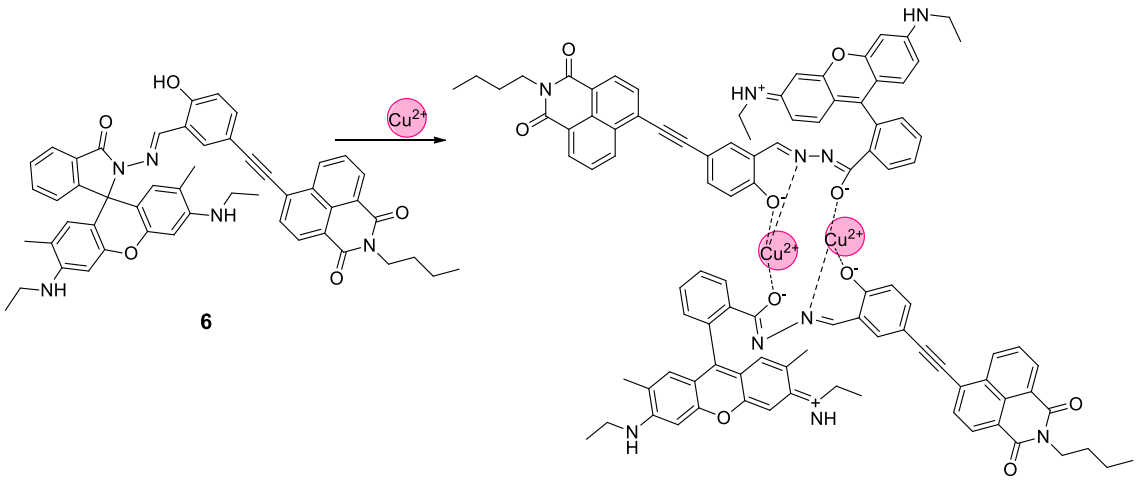

Figure 7 Proposed binding mechanisms of the compound **6**.[34]

In addition to rhodamine, boron dipyrromethene difluoride (BODIPY) is also very favourable for the design of fluorescent sensors because of its unique characteristics, such as sharp and intense absorption and fluorescence peaks in the visible spectral region and stability against light and chemicals. It is also modifiable to make the absorption and emission bands shift to the red or near infra-red (NIR) range so that it is suitable for applications in biological systems. Dehaen and coworkers firstly reported a colorimetric and NIR fluorescent turn-on chemosensor **7** for Cu^{2+} based on BODIPY.[35] This probe displays a significantly sensitive and selective fluorescent enhancement on the addition of Cu^{2+} among various metal ions with an excitation at 620 nm in acetonitrile. The 1: 1 stoichiometry for the **7**-Cu^{2+} complex was obtained by non-linear fitting of the fluorometric titration data with K_d = 8.7 ± 0.5 μM in acetonitrile, which was confirmed by mass spectra as well.

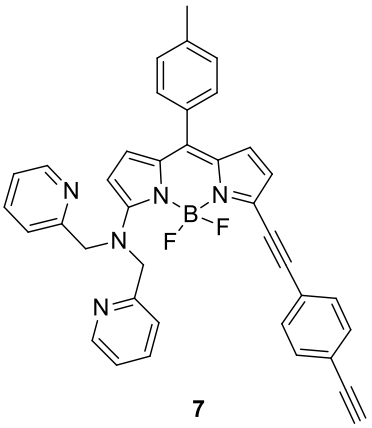

7

Juang *et al* have prepared a fluoro-chromogenic chemosensor **8** based on BODIPY-functionalised gold nanoparticles.[36] To take advantage of nanoparticles as solid supports has resulted in the development of hybrid materials with improved functionalities such as sensitivity and water solubility. In the presence of Cu^{2+} in aqueous solution (10% CH_3CN), **8** displayed a colour change along with a blue-shift of the absorption band and quenching of the fluorescence at room temperature. According to the fluorescence titration data, a detection limit of 1 μM was achieved, which is much lower than the US EPA limit (~20 μM) in drinking water. Moreover, confocal imaging experiments confirmed that **8** can be used to detect Cu^{2+} in living cells (Figure 8).

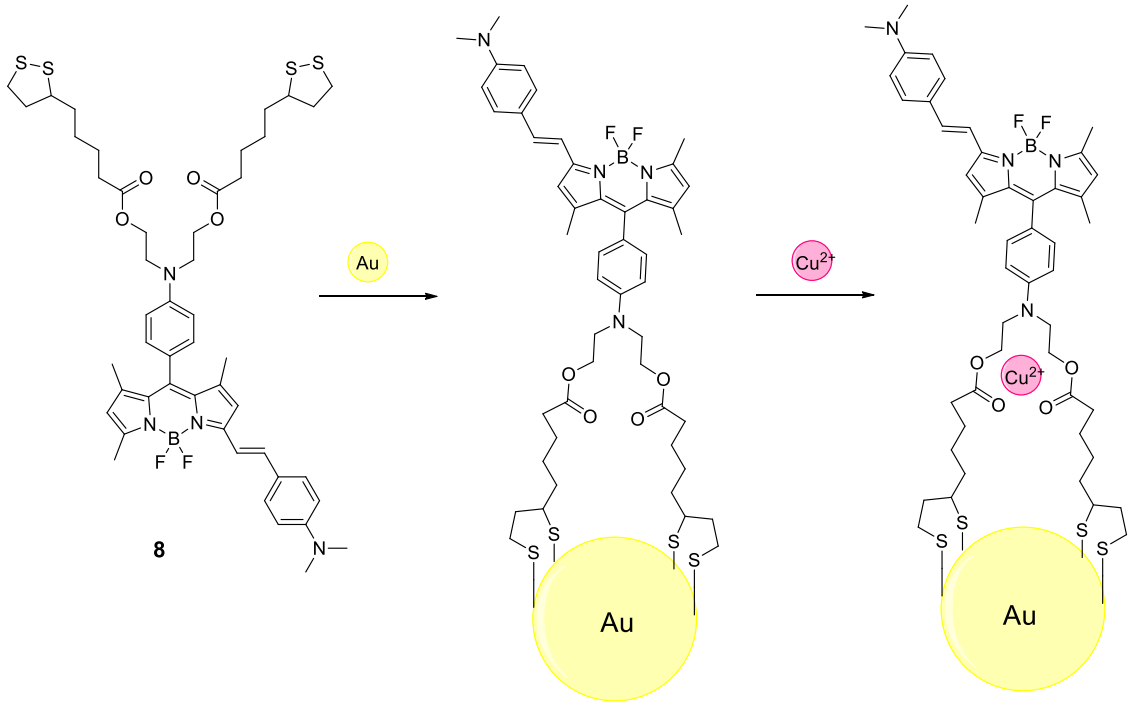

Figure 8 Synthesis of BODIPY-functionalised gold nanoparticles **8**.

1.3.2 Naphthalimide Based Sensors in Copper(II) Sensing

Among all the other fluorophores developed, 1,8-naphthalimide is highly favourable because of its excellent photophysical properties, such as high extinction coefficients, excellent quantum yields, great photostability, and relatively long emission wavelengths. Compared to rhodamine, BODIPY and cyanine based sensor, 1,8-naphthalimide derivatives are also more stable and easy to synthesise. And they are typical fluorophores with an ICT nature, which is a critical design feature as it leads to sensitivity to changes in the microenvironment. In addition, they have relatively simple structures for which facile and straightforward syntheses have been established. At the same time, they can be modified with two or more separate side chains in sequence, e.g. derivation sites for the 4,5- or 3,4-positions and the imide position.[37]

Recently, Yu and coworkers designed a fluorescent sensor **9** derived from naphthalimide bearing a pyridine group for the detection of Cu^{2+} (Figure 9).[38] The probe exhibited high selectivity and sensitivity to Cu^{2+} in aqueous ethanol media with a detection limit of 0.03 μM. The result of Job's plot experiment suggested a 1:1 complex of **9** with Cu^{2+}, which was also supported by mass spectral analysis.

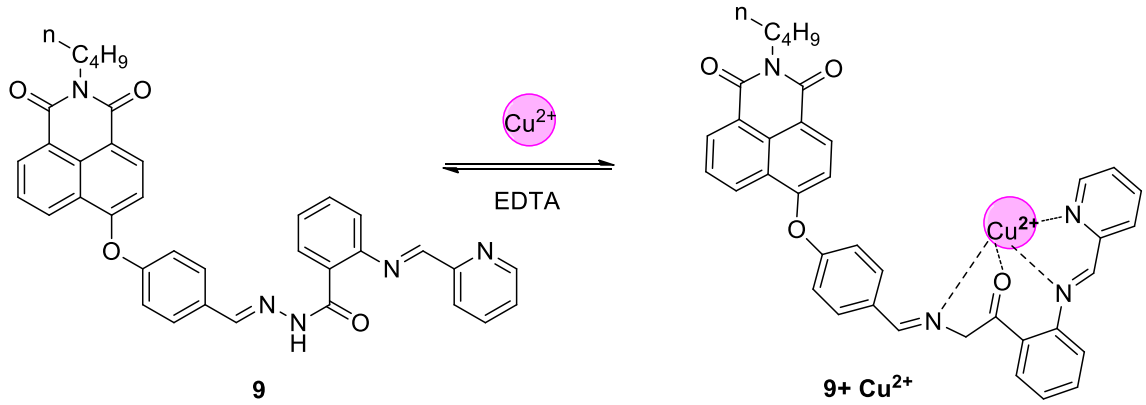

Figure 9 The mode of formation of **9**-Cu^{2+} complex.

Cui and co-workers also developed a fluorescence turn-on probe **10** for detecting Cu^{2+} both in *vitro* and *vivo*.[39] They employed the N-butylbenzene-1,2-diamine as a new recognition moiety for copper(II) ion. By coordinating with Cu^{2+} 20-fold fluorescence enhancement was achieved while no fluorescence change can be found on addition of other metal ions. The results of ^{1}HNMR titration, time-resolved fluorescence decay

measurements, and computational optimisation confirmed that the binding ratio was 1:1. Furthermore, the probe was used in confocal fluorescence imaging to detect Cu^{2+} in living cells.

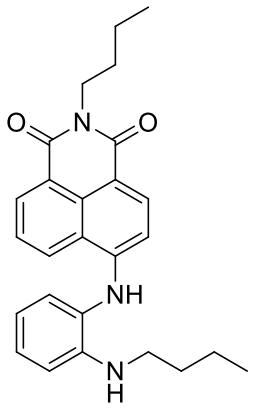

10

Wang *et al.*, have reported a fluorescence turn-on chemosensor **11** based on naphthalimide derivatives for detection of copper(II) ion (Figure 10).[40] The fluorescence spectrum displays a 4.5-fold enhancement in the intensity of the signal at 519 nm on binding with Cu^{2+}. The detection limit is calculated to be 0.15 μM, which indicated that the compound is quite sensitive to Cu^{2+}. The binding mechanism could be the copper(II) ions' restructure of C=N bond.

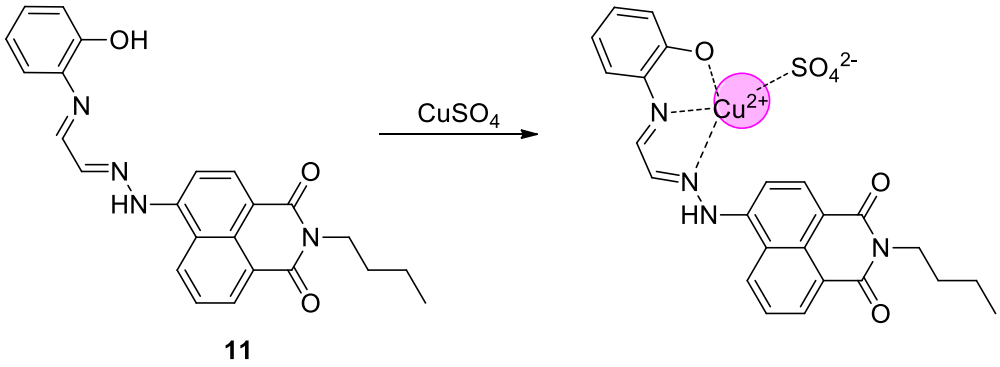

11

Figure 10 Binding action of a turn-on chemosensor.[40]

Liu and co-workers reported a new ratiometric fluorescent sensor **12** for Cu^{2+}, which has been developed by integrating a 1,8-naphthalimide fluorophore with 8-aminoquinoline (Figure 11).[41] This compound not only exhibits a highly selective ratiometric response to Cu^{2+} in aqueous media, but has also been used for the practical

ratiometric imaging of intracellular Cu^{2+} in human breast adenocarcinoma cells (MCF-7 cells) using a confocal microscope.

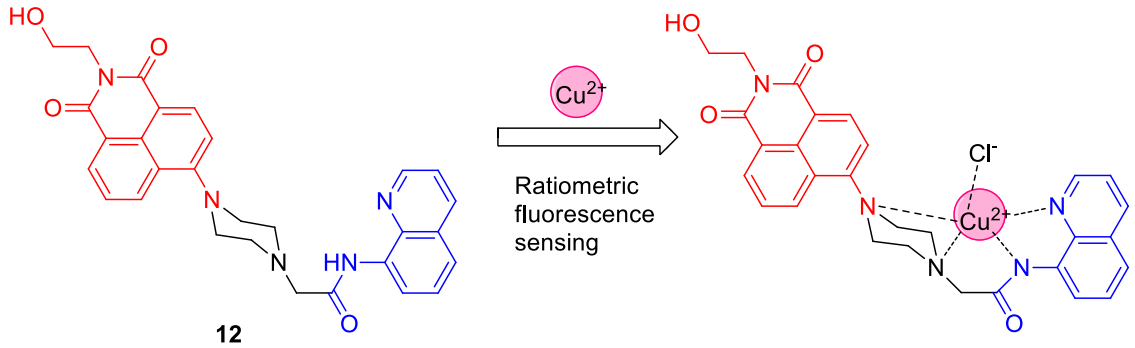

Figure 11 A ratiometric fluorescent sensor for Cu^{2+}.[41]

Qian *et al.*, have reported a fluorescent sensor **13** based on the *peri*-disubstituted naphthalimide with side chains (Figure 12).[42] Diethanolamine is a weaker metal ion ligand and a better water-soluble group than di(pyridin-2-ylmethyl)amine, which makes it more advantageous of the two receptors. In addition, the on-off fluorescence response in emission at 543 nm makes the compound serve as a naked eye, dual-channel colorimetric and fluorescence probe for Cu^{2+}.

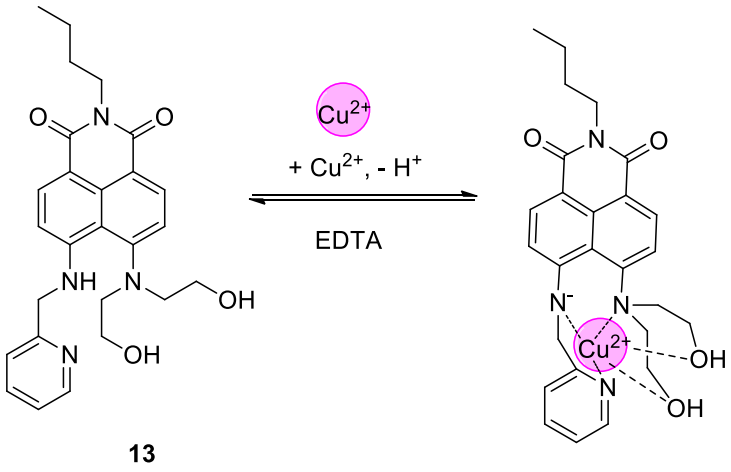

Figure 12 The proposed binding mode.[42]

1.3.3 Boronic Acid Based Sensors for Metal Ion Sensing

Boronic acids are well known to have high affinities for substances that contain vicinal diol groups[43] and, consequently, they have been used in fluorescent chemosensors for carbohydrates.[44] Limited precedents exist for the use of boronic acid-linked fluorescent sensors to detect metal ions directly. Therefore, it is very interesting to explore the use of boronic acids as the binding site of metal ions.

The first example of a boronic acid-linked fluorescent and colorimetric chemosensor **14**, **15** for copper(II) ions was prepared by Yoon,[45] which involves the unique ring-opening process of rhodamine and the fluorescein derivatives (Figure 13). In addition, the practical use of the probe is demonstrated by its application to the detection of copper(II) ions in mammalian cells and vertebrate organisms.

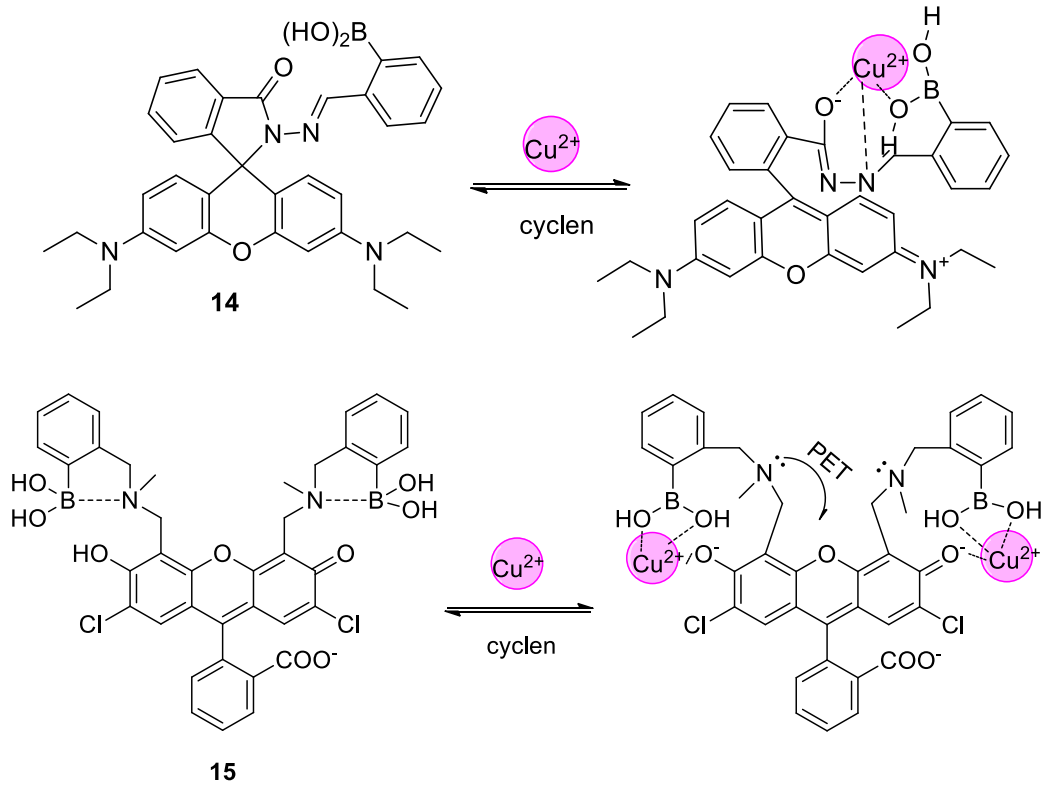

Figure 13 Binding modes of the two compounds.[45]

In 2010, Yoon and co-workers reported another two rhodamine B (RB) derivatives **16**, **17** bearing mono and bis-boronic acid groups as Hg^{2+} selective fluorescent and colorimetric sensors (Figure 14).[46] These derivatives are the first examples of reversible fluorescent chemosensors for Hg^{2+} which utilised boronic acid groups as binding sites. The two new RB-boronic acid derivatives displayed selective 'Off-On'-type fluorescent enhancements and distinct colour changes with Hg^{2+}. The selective fluorescent enhancement of two rhodamine derivatives was attributed to ring opening of the spirolactam (nonfluorescent) to ring-opened amide (fluorescent).

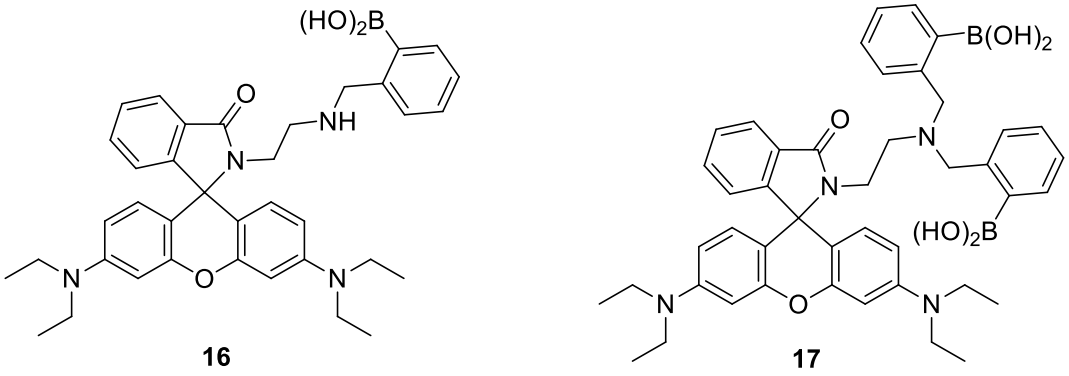

Figure 14 Structures of the two compounds.

Xu and coworkers developed a highly selective fluorescent receptor **18** for hydroxylated organotins(HOTs) in aqueous solution (Figure 15).[47] The new receptor nicely combines the binding character of an o-hydroxyl Schiff base for the transition metal and boronic acid for the vicinal diol. And this is the first example of a fluorescent receptor for hydroxylated metal species. They demonstrated that boronic acid acted as an efficient receptor group for metal-centred diols. This may lead to important applications of boronic acid in molecular recognition in further studies.

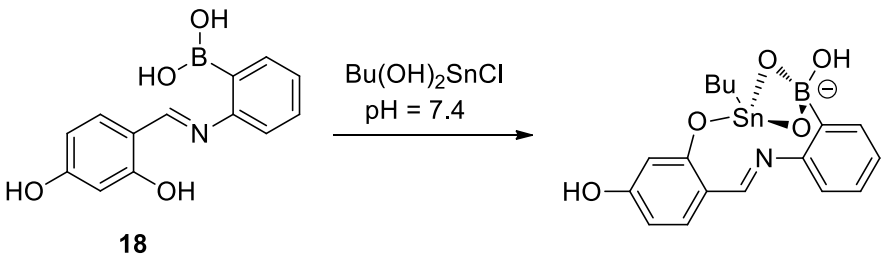

Figure 15 Binding modes of the compound **18**.

1.4 Developments of Chemodosimeters for the Detection of Biothiols

1.4.1 Reaction Based Sensors for Biothiols

Biological small molecules such as glutathione (GSH), cysteine (Cys), and homo-cysteine (Hcy) play crucial roles in living organisms, which are also involved in a number of biological processes. It has also been proposed that abnormal levels of biothiols have been correlated with various diseases.[48, 49] GSH, the most abundant cellular non-protein thiol,[50] assists many cellular functions, such as intracellular signal transduction, maintenance of intracellular redox activities, xenobiotic metabolism, and gene regulation.[51]

Given that biothiols are very important in biological, clinical, and environmental analysis, they have drawn great attention to design new analytical methodologies for their detection. A number of sophisticated analytical techniques for the detection of thiols have been reported, e.g., MS,[52] HPLC,[53] capillary electrophoresis[54] and electrochemical detection.[55] However, these methods have some limitations, e.g., only measuring total thiol content, high equipment costs, complex sample preparation, and running times, which make them unpractical for some applications such as high-throughput routine clinical or research purposes. Therefore, a cheap and simple method for quantifying thiols is vital for real-time monitoring of biological samples.

Among the various methods optical probes for thiols have proven to be some of the most efficient means and have therefore become a dynamic research area in recent years. Particularly, great effort has been devoted to the development of fluorescent sensors due to the low detection limits, ease of handling and monitoring intracellular analytes. Most of the fluorescent sensors for thiols are reaction based sensor. The discussion below covers a variety of sensing mechanisms such as Michael addition, cyclisation with aldehydes, conjugate addition-cyclisation, cleavage of sulfonamide and sulfonate esters, thiol-halogen nucleophilic substitution, disulfide exchange, native chemical ligation (NCL), metal complex-displace coordination and nanomaterial-related chemosensors.

Related to Michael addition of thiols

It is well known that the derivatives of α, β -unsaturated carbonyl moieties undergo favourable nucleophilic addition with sulfhydryl groups. In 1970, Kanaoka and coworkers designed a fluorescent chemodosimeters for detection of thiol that utilised the addition of a thiol to a maleimide group, which is one of the most renowned electrophiles.[56]

Kim and coworkers reported a selective fluorescence turn-on probe **19** for biothiols (Cys, Hcy, GSH) (Figure 16).[57] In the presence of biothiols, it exhibited a sensitive and selective fluorescence enhancement through the Michael addition of a thiol group to the α, β -unsaturated malonitrile unit, the reaction does not work with other natural amino acids. In 0.1 M DMSO-HEPES buffer (pH 7.4, 1: 2, v/v), Cys induced a dramatic increase in the fluorescence intensity (F/F_o = 19) while Hcy and GSH turn on the fluorescence intensity of **19** by 12- and 5.6-fold, respectively. Moreover, the probe was employed for detecting cellular biothiols in HeLa cells by confocal imaging experiments.

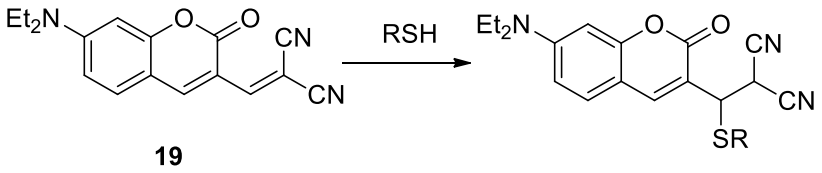

19

Figure 16 Proposed reaction mechanism of **19** with thiols.

Jung *et al.* developed a chemodosimeter **20** which showed good selectivity for Cys over other similar amino acids, Hcy and GSH.[58] On the addition of Cys a Michael-type reaction occurred with fluorescence enhancement (Figure 17). Under physiological conditions Cys could generate a stronger nucleophile and modify the host, in this case a larger nucleophile experiences more steric hindrance in getting to the electrophilic centre, which has been observed *via* the low reaction rate constant in the second-order reaction and the highest interaction energy (calc.) with GSH. Furthermore, confocal microscopic experiments were employed for fluorescence imaging of Cys in HepG2 cells.

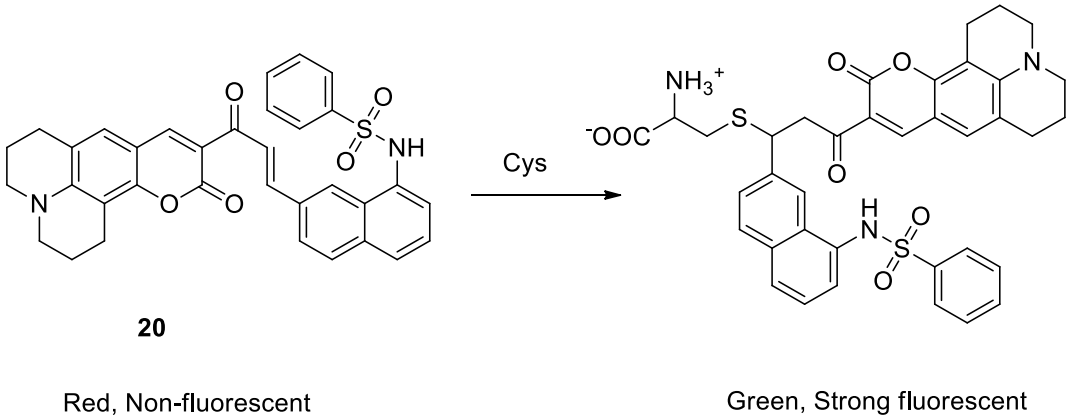

Figure 17 Chemodosimetric reaction of **20** with Cys.

Related to cleavage of sulfonamide and sulfonate esters by thiols

Nucleophilic substitution reactions of sulfonate esters and amides of phenols or amines, has been used for the fluorescent detection of thiols.

Thiol probe **21** was reported by Ji *et al.* and showed an off-on red-emitting phosphorescence (Figure 18).[59] In acetonitrile aqueous solution, **21** showed no fluorescence as the metal to ligand charge transfer (MLCT) was disrupted by electron transfer from Ru(II) to 2,4-dinitrobenzenesulfonyl group. In presence of thiols, the electron sink was cleaved and the MLCT was re-established, which induced phosphorescence at 598 nm with a 143 nm Stokes shift and a 1.1 μs luminescence lifetime.

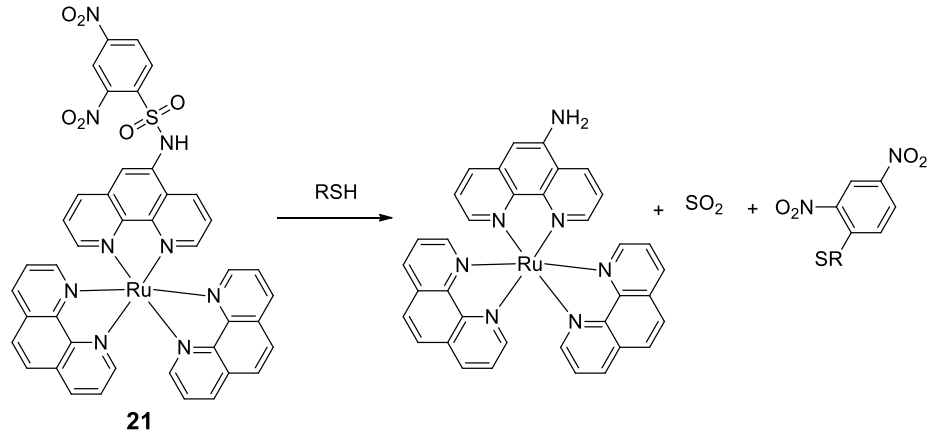

Figure 18 Thiol sensing mechanism of **21**.

A new series of NIR fluorescent dyes was prepared by Yuan *et al.*, which are superior to traditional fluorescein dyes with both absorption and emission in the NIR region (Figure 19).[60] In the presence of Cys at pH 7.4 PBS buffer (30% CH_3CN), probe **22** produced a 50-fold fluorescence enhancement with a new emission peak appearing at 716 nm. Additionally, quantum chemical calculations with the B3LYP exchange function was employed to explain the structure-optical properties of these new NIR dyes. Moreover, confocal imaging experiments were used to confirm that **22** was suitable for NIR fluorescence imaging of thiols in both macrophage cells and *in vivo*.

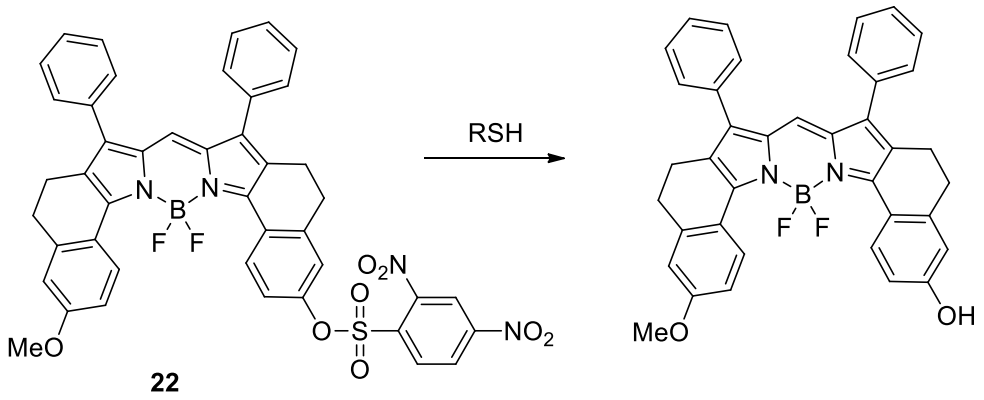

Figure 19 Schematic illustration of the reaction of **22** with thiols.

Related to thiol-halogen nucleophilic substitution by thiols

Due to the similar structure and reactivity, there has been much difficulty to discriminate GSH from Cys and Hcy with one fluorescent probe. Although a number of excellent chemosensors for detection of thiols have been published, there still scope to develop systems with improved selectivity. Herein, Niu and coworkers recently reported a BODIPY-based ratiometric fluorescence sensor **23**, which could effectively recognise GSH from Cys and Hcy (Figure 20).[61] The mechanism is that the chlorine of **23** could be rapidly displaced by the thiolate of biothiols through thiol-halogen nucleophilic substitution. Except for GSH, only the amino groups of Cys/Hcy could replace the thiolate to form an amino-substituted probe. In 20 mM HEPES buffer (pH 7.4, 5% CH_3CN), the fluorescence intensity of **23** was dramatically enhanced on the addition of GSH, with a linear range of 0-60 μM. The detection limit was 8.6×10^{-8} M (S/N = 3) with a coefficient of R = 0.993. Moreover, **23** was used for confocal microscopic detection of GSH in HepG2 cells.

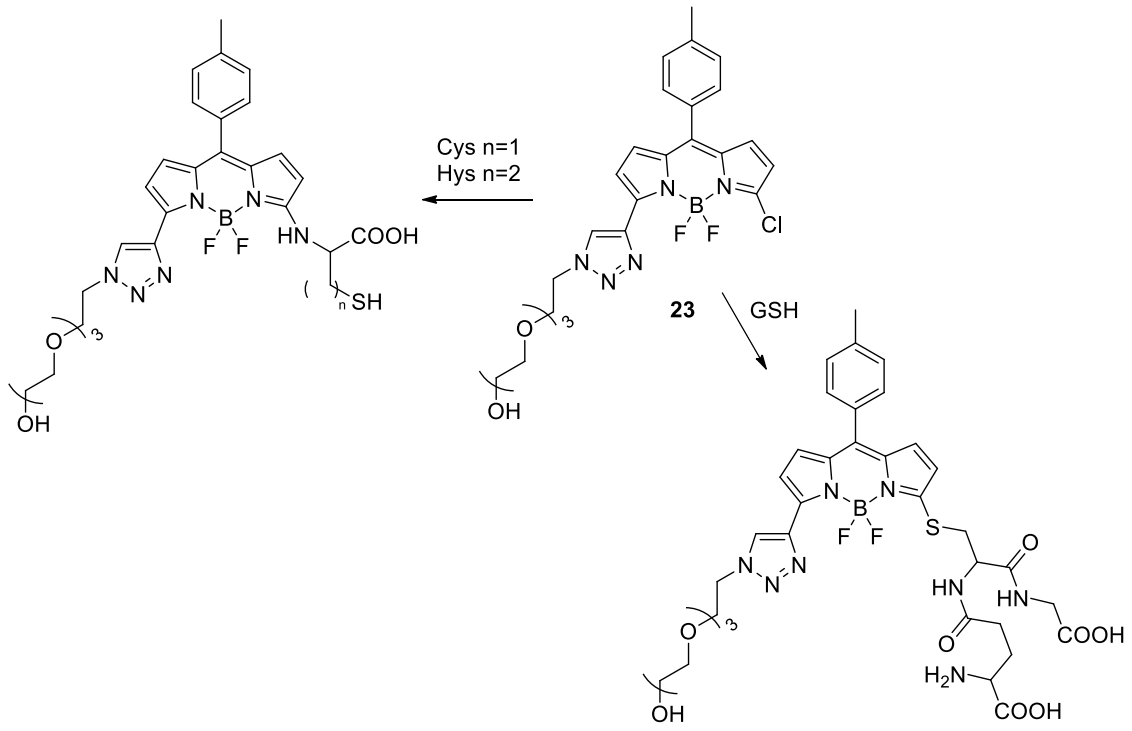

Figure 20 Reaction mechanisms of **23** for thiols.

Related to disulfide exchange reaction by thiols

A galactose-appended naphthalimide based probe **24** was reported by Lee *et al.* for detection of hepatic thiol both in *vitro* and in living cells and animals (Figure 21).[62] The galactose subunit was used to target hepatocytes, while exposed to cellular thiols the disulfide-link was cleaved to release the naphthalimide moiety with fluorescence enhanced at 540 nm. As a control compound, **25** without galactose was used to confirm the mechanism, no selectivity for any particular organ was observed.

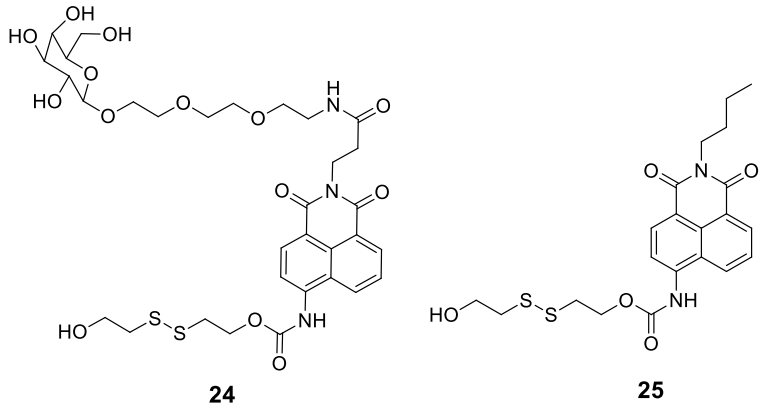

Figure 21 Structures of probes **24** and **25**.

Zhu and coworkers designed a ratiometric fluorescent probe **26** containing a naphthalimide moiety as the fluorophore and a disulfide group as the receptor (Figure 22).[63] In pH 7.4 PBS buffer (20 mM, 10% EtOH), in the presence of GSH, the maximum absorption peak displayed an 85 nm red-shift with the colour of the solution changed from colourless to fluorescent green. And the maximum emission peak experienced a 48 nm red-shifted and the ratio of fluorescence intensities (F_{533}/F_{485}) changed from 0.5 to 5.7. Moreover, in terms of ratiometric sensing, probe **26** exhibited high sensitivity towards GSH with the detection limit as low as 28 μM, and also probe **26** showed significant ratiometric fluorescence changes in confocal imaging of HeLa cells.

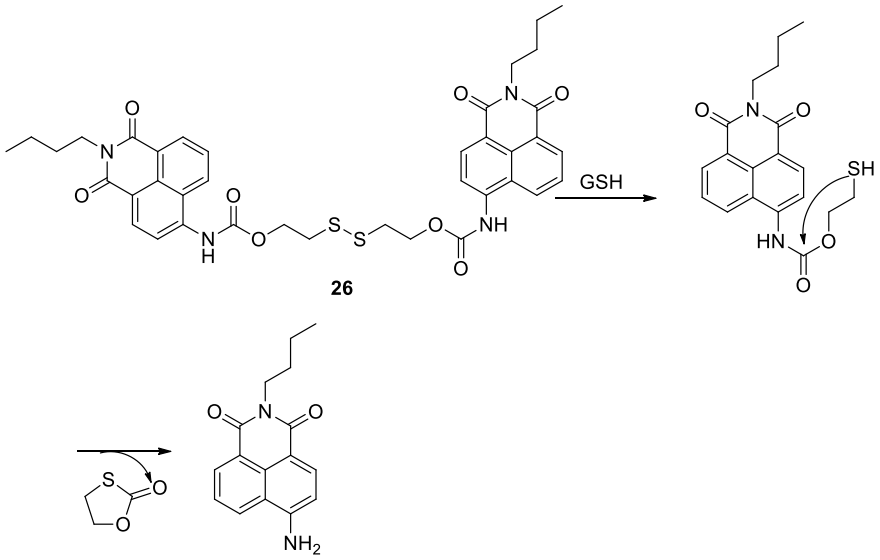

Figure 22 Disulfide bond cleavage mechanism in **26** towards thiols.

Related to cleavage of Se-N by thiols

Zhu and coworkers developed a fluorescent probe by cleavage of the Se-N bond in presence of strong nucleophilic thiols (Figure 23).[64] In a mixed solution of DMF-H_2O (8:2, v/v), the interaction of GSH with the pyridylvinylene derivative **27** produced a 19 nm red-shift in the absorption spectra and a fluorescence intensity enhancement at 440 nm. According to the titration data, probe **27** showed a linear relationship between fluorescence and the concentration of GSH in the range of 2 - 12 μM with a detection limit of 0.03 μM.

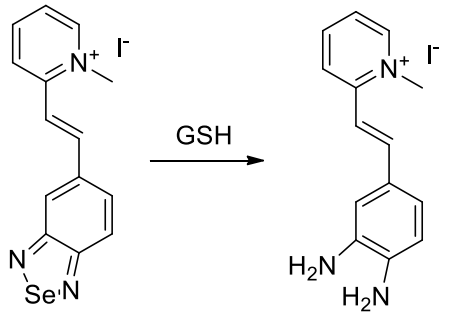

Figure 23 Reactions of **27** with GSH.

Recently, two NIR fluorescent thiol probes **28** and **29** were adopted by Wang *et al.* (Figure 24).[65] After incubation at 25 ^{o}C for 3 mins in PBS buffer (15 mM, pH 7.4), probes **28** and **29** displayed almost no fluorescence upon excitation at 635 nm due to a donor-excited photoinduced electron transfer (d-PET) process. In the presence of GSH, there was a strong emission band at 750 nm with a significant fluorescence enhancement. In addition, probes **28** and **29** showed a linear relationship between the fluorescence intensity and the amount of Cys in the 0-5 μM range. Moreover, confocal imaging experiments were carried out to confirm that the two probes could detect thiols in living RAW 264.7 cells and fresh rat liver tissue.

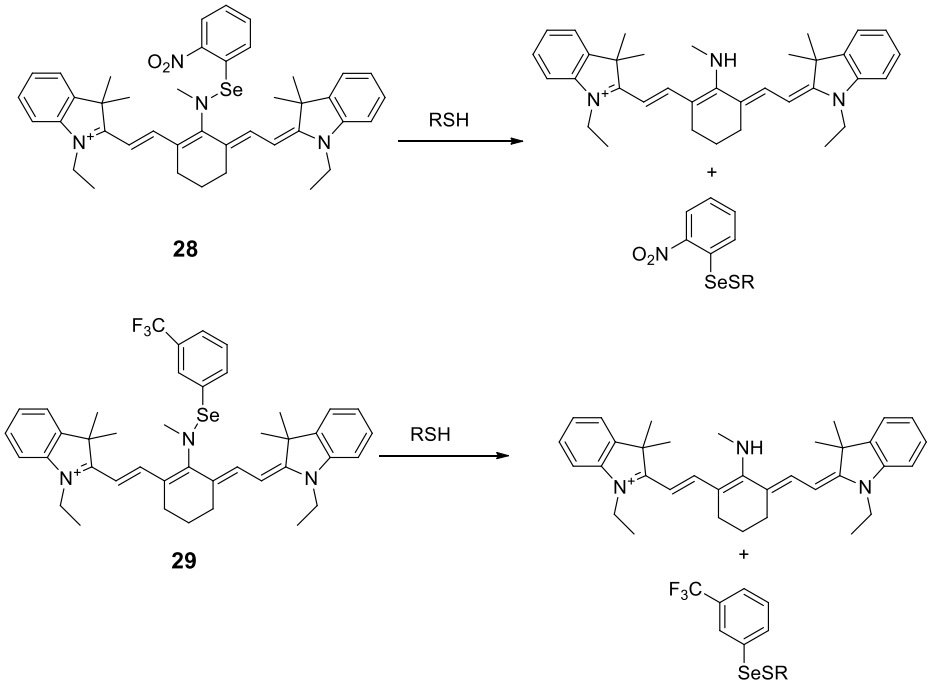

Figure 24 Reaction mechanisms of probe **28** and **29** with thiols.

Related to the native chemical ligation (NCL) mechanism for aminothiols

In the area of biology and chemistry, the native chemical ligation (NCL) reaction has been well developed to prepare proteins by total or semi-synthesis. Cascade reactions between a peptide-a-thioester and an N-terminal cysteine peptide were included in NCL of peptide segments.

A ratiometric FRET fluorescent probe for thiol detection was prepared by Long and co-workers inspired by the chemoselective and biocompatible characters of the NCL reaction (Figure 25).[66] In pH 7.4 CH_3CN-phosphate buffer (25 μM, 9:11, v/v), probe **30** alone exhibits remarkable emission of the rhodamine at 590 nm, but almost no BODIPY emission at 510 nm owing to the overlap of the emission band of the BODIPY with the absorption band of the rhodamine. However, in the presence of Cys, the emission band of the BODIPY increased at 510 nm and the rhodamine emission band at 590 nm gradually reduced due to the NCL reaction. The emission ratio (I_{510}/I_{590}) indicates a 270-fold enhancement with a detection limit of 82 nM towards Cys. Moreover, probe **30** has been proven to have the potential to detect Cys in HeLa cells.

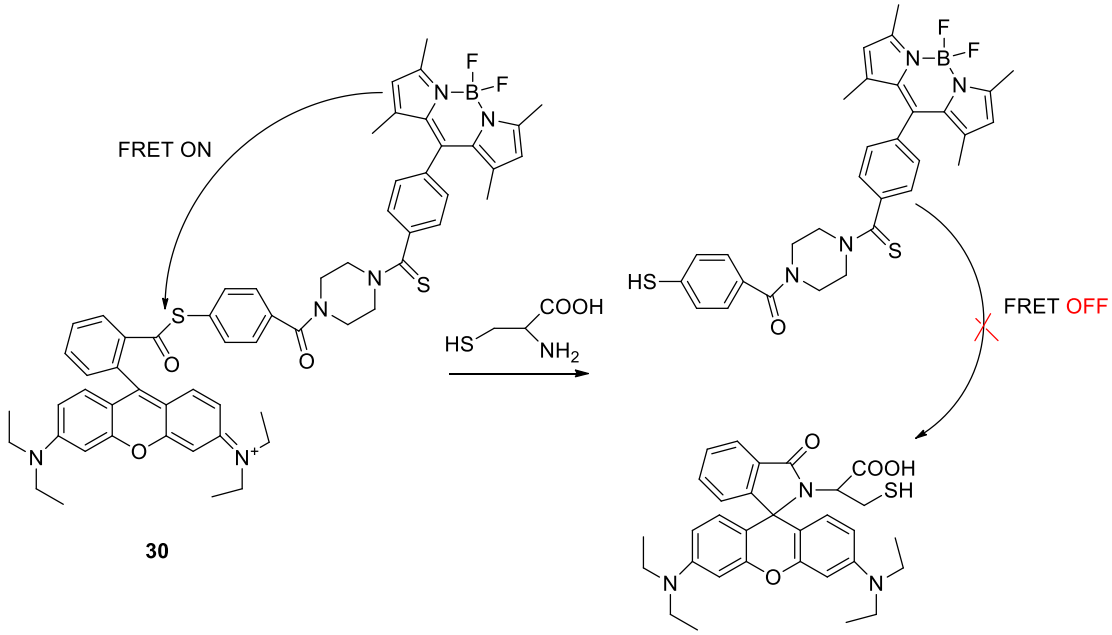

Figure 25 Structure of ratiometric fluorescent thiol probe **30** based on the NCL reaction.

Metal complex related: displacement of coordination by thiols

It is well known that thiols have high affinity towards metal ions. Therefore, great effort has been made to develop chemodosimeters for thiols using a nucleophilic displacement approach.

Jung and coworkers designed an iminocoumarin-Cu^{2+} ensemble probe for thiol detection (Figure 26).[67] On the addition of thiol-containing amino acids probe **31** displays a red to green colour change and an enhancement in fluorescence at 514 nm in 10 mM PBS solution (pH 7.4, 1.0% DMSO). The detection limit for GSH was determined to be 10^{-8} M in aqueous solution. Furthermore, the confocal imaging experiments demonstrate that complex **31**-Cu^{2+} was a promising candidate for the detection of thiols in HepG2 cells.

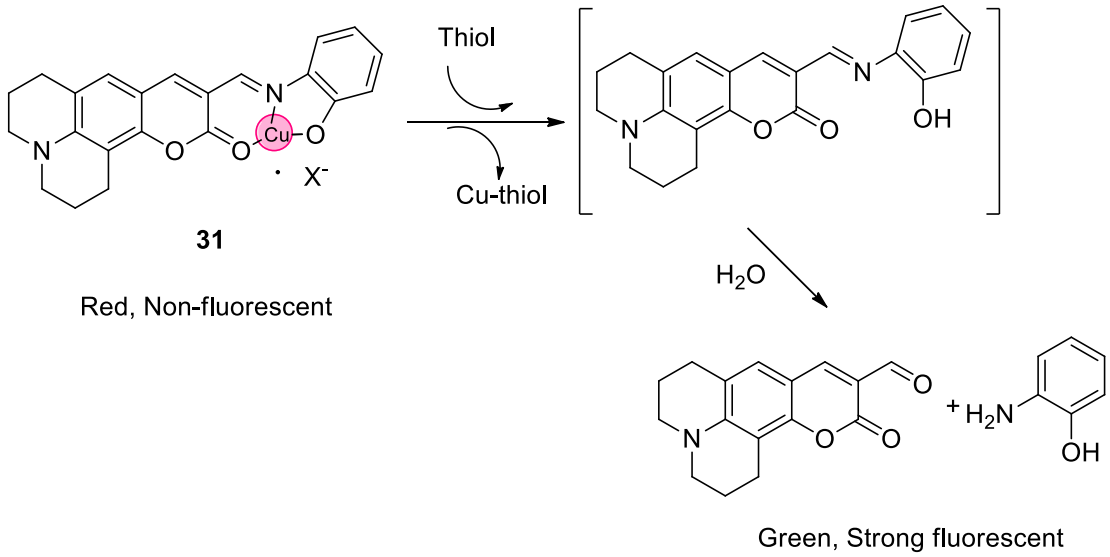

Figure 26 Schematic illustration of the thiol detecting the chemodosietric mechanism of **31**-Cu^{2+} in aqueous media.

Nano-material related

Recently, nanoparticles have drawn great attention in the field of analytical chemistry. A novel unmodified carbon nanodot (C-Dot) fluorescence probe for Hg^{2+} and biothiol detection was prepared by Zhou *et al.* (Figure 27).[68] The fluorescence of the C-Dots was quenched by Hg^{2+} owing to a charge transfer process. While in the presence of thiols, the displacement of Hg^{2+} from the surface of the C-Dots to form Hg^{2+}-S bonds displayed a significant fluorescence enhancement. A good linear curve between the fluorescence intensity and the concentration of Cys in the range of 0.01-5 μM indicates

a good sensitivity of the probe towards thiols with the detection limit of 4.9 nM. Other amino acids were employed to test the selectivity. The results indicate no fluorescence increase for any other amino acid. Fetal bovine serum (FBS) was used for estimating the applicability of the probe in biological samples. The method provided good recoveries ranging from 96.1% to 104.9%, using Cys as the standard and showed great potential for detecting thiols in practical sample analysis.

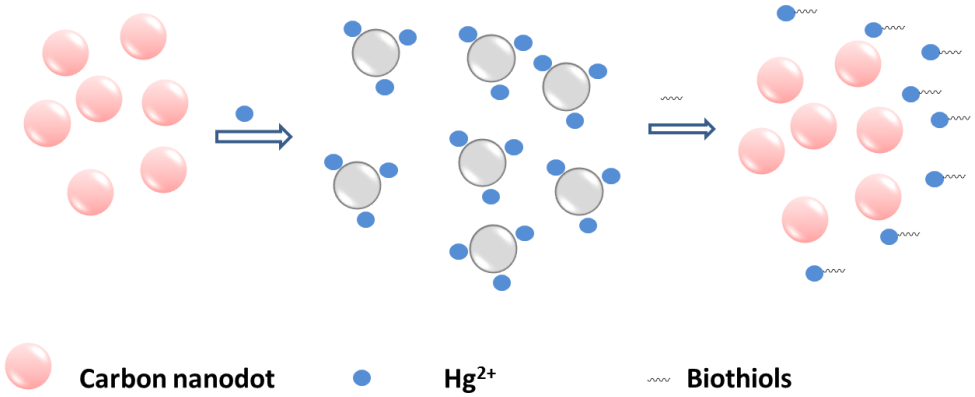

Figure 27 Schematic illustration of the detection mechanism of Hg^{2+} and biothiols using the carbon nanodots.

1.4.2 Dicyanomethylene-4H-pyran (DCM) Based Sensors

Due to their lower background fluorescence with less scattering and deep tissue penetration and limited toxicity, long wavelength (far-red to NIR) analyte-responsive fluorescent probes have drawn great interest in the sensing world. Therefore, much effort has been made to develop novel NIR analyte-responsive fluorescent probes over recent years. Dicyanomethylene-4H-pyran (DCM) chromophore is one of the promising long wavelength dyes with typical donor-π-acceptor (D-π-A) type with a broad absorption band resulting from an ultra-fast internal charge-transfer (ICT) process. Thus, various DCM-type derivatives have emerged due to their excellent optical-electronic properties and varied structural modification. Generally, DCM chromophores have a typical D-π-A structure with a broad absorption band produced from an ultra-fast internal charge-transfer (ICT) process (Figure 28),[69, 70] resulting in several advantages such as: (i) high sensitivity to electron disturbance; (ii) long emission wavelength (red light); and (iii) high fluorescent yield. In 1989, Tang and co-workers reported a DCM derivative as a highly fluorescent dopant in organic electroluminescent diodes (OLEDs).[71] Therefore, a number of DCM derivatives have been developed due to their excellent optical-electronic properties and easy structural modification.[72]

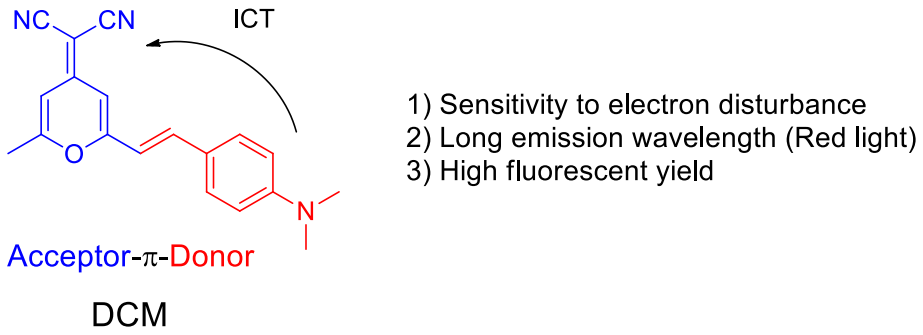

Figure 28 Schematic diagram of an ICT proess in a DCM chromophore.[72]

DCM fluorophore based fluorescent sensors have drawn much attention because of their unique advantages such as long wavelength emission, high quantum yield, and simple structural modification. A typical fluorescent chemosensor is usually composed of two parts: a receptor and a fluorophore, which are linked with a spacer for converting

the recognition event into the fluorescence signal. The ICT mechanism has been widely employed for sensing and molecular switching using the DCM fluorophore.[73, 74]

Recently, Zhu and coworkers reported a DCM based fluorescent sensor **32** (Figure 29), showing fluorescence enhancement in the long red wavelength region with high selectivity for the PPi anion.[75] It is well known that metal complexes can bind anions more efficiently than water, therefore the method of using a metal ion complex as a binding site for PPi has become more and more popular. Probe **32** showed good selectivity to PPi over other phosphates, displaying high sensitivity towards PPi with an association constant (K_a) of 4.6 × 10^5 M^{-1}. Mass spectral analysis was used to confirm that DCCP-Cu^{2+} forms a 1: 1 complex with PPi.

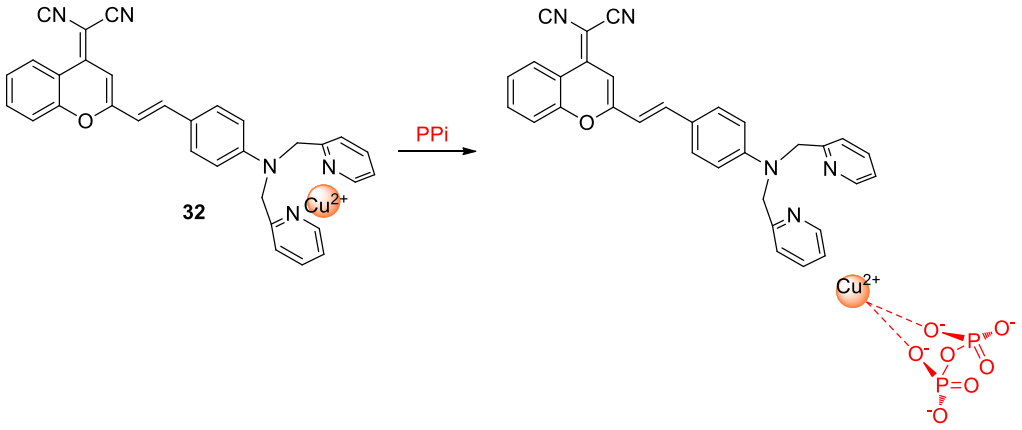

Figure 29 Sensing mechanism of **32** with PPi.

Subsequently, another DCM based fluorescent probe **33** for PPi detection in 100% aqueous solution was designed by Zhu and co-workers (Figure 30).[76] An α-amino acid was used as a good chelating ligand for Cu^{2+} and incorporation of the lithium iminodiacetate group induced a large improvement in water solubility. In the presence of PPi, **33**-Cu^{2+} displayed a dramatically enhanced fluorescence emission at 675 nm, thus making the wavelength fall in the desired NIR region, which is suitable for bioimaging. Therefore, confocal microscopic experiments were carried out for PPi detection in KB cells (human nasopharyngeal epidermal carcinoma cells).

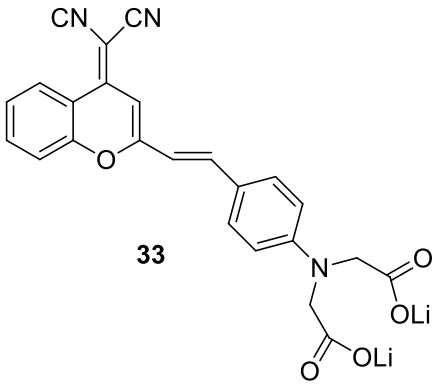

Figure 30 Chemical structures of **33**.

Interesting functional materials based on polymeric sensors have been developed due to easy preparation and modification. Therefore, Guo and co-workers prepared a hydrophilic copolymer poly(HEMA-co-DCPDP) containing the DCM group as a fluorescent film sensor for Cu^{2+} and PPi detection (Figure 31).[77] The hydrophilic copolymer poly(HEMA-co-DCPDP) was composed of two parts: poly(2-hydroxyethyl methacrylate) (PHEMA) as a hydrophilic chain segment to improve the permeability of ions into the polymer backbone, and the DCM fluorophore was attached onto the polymer backbone as metal ion-sensing units. Thus, the copolymer experienced a fluorescence ON-OFF-ON process in presence of Cu^{2+} and PPi. Moreover, the co-polymer showed high sensitivity towards PPi with an association constant (K_a) of 3.1 × 10^4 M^{-1}.

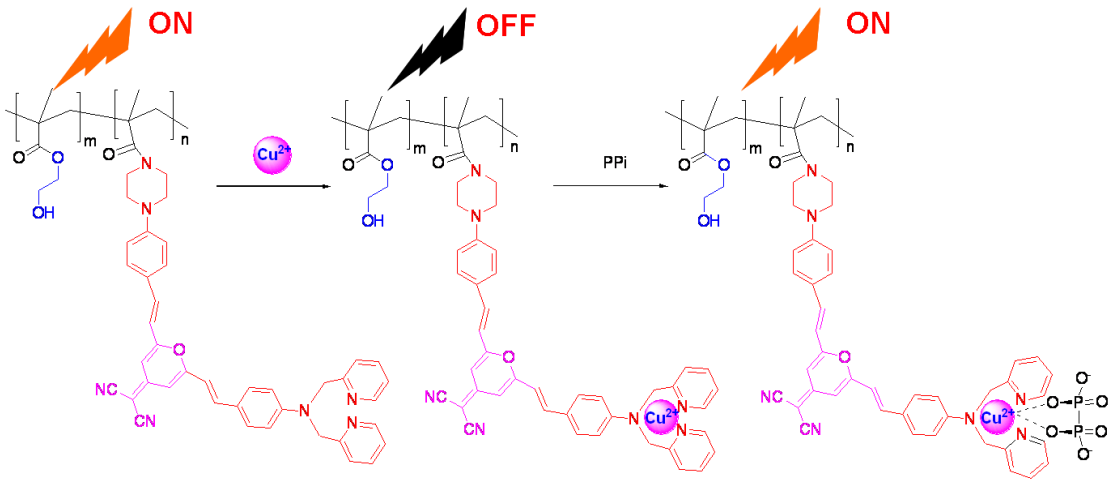

Figure 31 Schematic representation of Cu^{2+} and PPi sensors based onthe fluorescence ‘‘ON-OFF’’ and ‘‘OFF-ON’’ of poly(HEMA-co-DCPDP) and poly(HEMA-co-DCPDP)-Cu^{2+}, respectively.

In addition to PPi chemosensors, a DCM chromophore based NIR fluorescent chemodosimeter **34** for fluoride detection was designed by Zhao *et al.* (Figure 32).[78] This is the first NIR turn-on fluorescence sensor for F^- based on the ICT mechanism. In the absence of F^-, chemodosimeter **34** exhibited one major absorption band centred at 447 nm. However, on addition of F^-, the absorption at 454 nm decreased with a concomitant new band at 645 nm appearing. The F^- triggered specific Si-O cleavage of **34** to release DCPO induced dramatic colour changes and distinct NIR fluorescence enhancement at 718 nm. Furthermore, NMR and mass spectroscopic analysis was used to confirm the sensing mechanism.

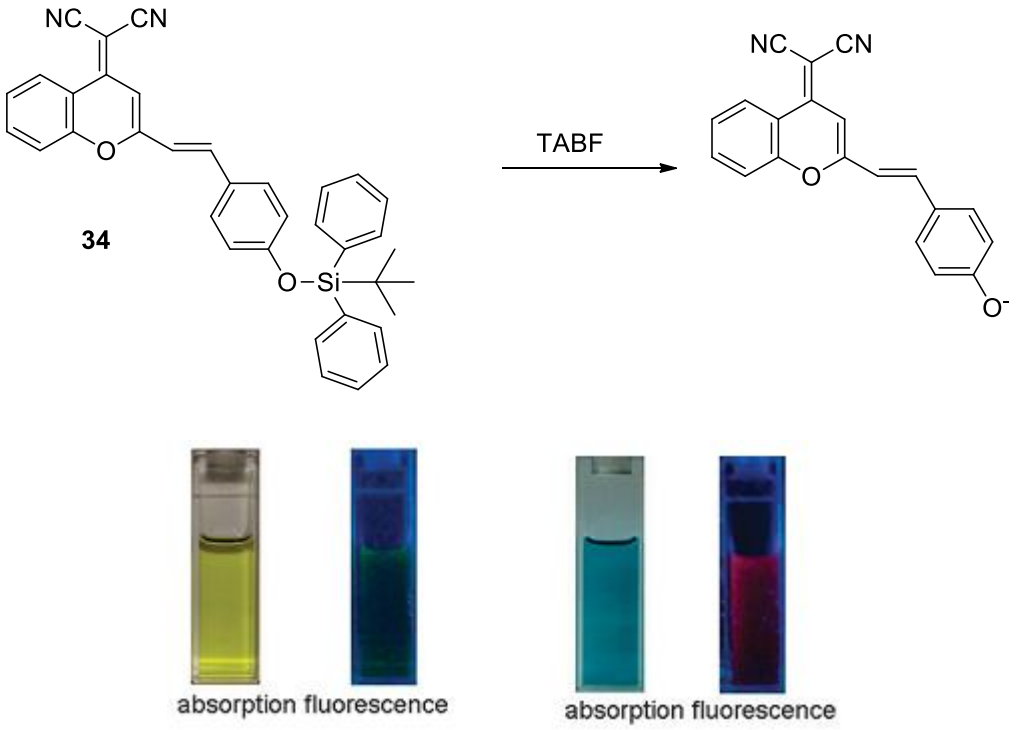

Figure 32 The F-triggered specific Si–O cleavage of **34** to release DCPO with a change in colour and fluorescence.

1.5 Electrochemical Sensing with Boronic Acid for Saccharides

1.5.1 Introduction to Electrochemistry

Electrochemistry brings up a varied field that can generally be defined as the study of the combination of electricity and chemical systems, which include the chemical reactions that take place at the interface of an electrode and the electrolyte. These reactions involve electron transfer between the electrodes and the electrolyte. Essentially, the study of charge transfer that occurs between electrodes and redox species both at an interface and the space in between is of the most interest. Generally, charge transfer can occur in two directions. Take Mn^{3+} as an example, a redox species can either gain an electron from the electrode to form the reduced species, or it can donate an electron to the electrode surface to form the oxidised species.[79]

$$Mn^{3+}_{(aq)} + e^- \longrightarrow Mn^{2+}_{(aq)} \qquad \text{Equation 1}$$

$$Mn^{2+}_{(aq)} \longrightarrow Mn^{3+}_{(aq)} + e^- \qquad \text{Equation 2}$$

With the employment of a potential to an electrochemical system, the interaction between electrical energy and chemical change can be obtained. In addition, other parameters could also control the rate of charge transfer including different types of working electrode surface and the reactivity of the reactant. The redox processes are exhibited as the observed current, otherwise known as a Faradaic current, the magnitude of which is given by Equation 3 where i = current, n = the number of electrons, A = electrode area, F = Faraday constant, and j = flux.[79]

$$i = nAFj \qquad \text{Equation 3}$$

An electrochemical cell is often used for setting up the work station with a number of possible electrode setups, and the most common is a three-electrode arrangement using a potentiostatic sweeping-voltage analysis technique. In this three-electrode arrangement, the electrochemical cell contains a reference electrode, counter electrode, and a working electrode (Figure 33a). A potentiostat is a hardware required to control the three-electrode cell and run electroanalytical experiments.

Most importantly, the reaction at the surface of working electrode and the interfacial potential between this surface and the solution are carried on in electrochemical experiments. A reference electrode, which has a constant and known potential, is used to provide the correct changes in current to the working electrode (Figure 33b). Therefore, the measured potential difference is derived from the difference between this known reference value and the potential at the working electrode. Furthermore, a counter electrode is added to the cell to make sure there is a closed circuit while the reference electrode is present to provide a stable and fixed potential. As a result, the potential difference at the electrode | electrolyte interface is allowed to be measured and controlled by a potentiostat in this system.

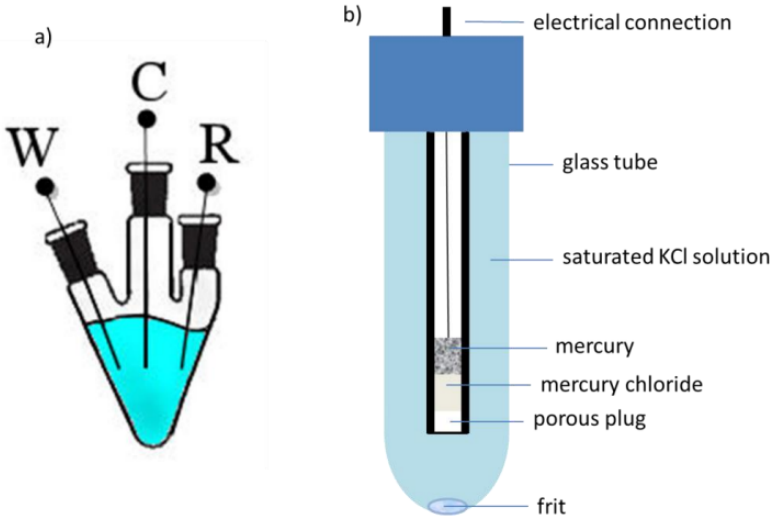

Figure 33 a) A typical three-electrode cell set-up, and b) a schematic representation of a saturated calomel electrode.[80]

1.5.2 Electrochemical Analysis

Electrochemical techniques have attracted much attention for designing sensors due to their high selectivity and sensitivity. The electrochemical sensor refers to the measurement of a physical quantity of an analyte and converts it into an electrical signal which can be read out by a potentiostat. So far, there has been much research focused on electrochemical sensing such as measuring the amount of glucose in the blood through its redox potential, gas detection (Figure 34), and proteins detection, *etc*. Among those, anion transfer detection has drawn much attention owing to its occurring quite often in nature and industry.

Figure 34 Carbon monoxide alarm with electrochemical sensor and 90 to 270 V AC operating voltage.[81]

1.5.3 Recent Developments of Electrochemical Sensing with Boronic Acid for Saccharides

The interaction of a boronic acid with a diol is covalent in nature and involves the rapid and reversible formation of a cyclic boronate ester.[82-84] Therefore, boronic acid functionalised compounds and materials have been widely used as the recognition matrix for chemo/biosensing of diol-containing biomolecules, such as saccharides, dopamine and glycoproteins, *etc*.[85-90] The Lewis acidic nature of boron has also led to the development of anion receptors and sensors (Figure 35).[91-94]

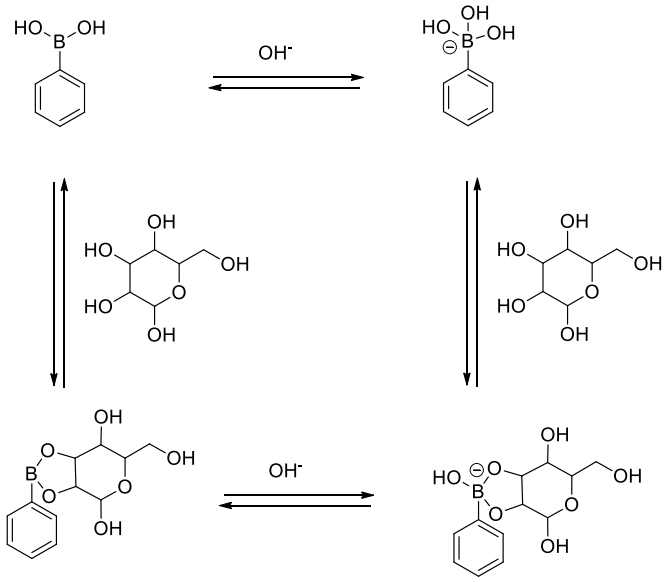

Figure 35 Scheme of binding equilibria of phenylboronic acid to sugar and OH^- ion.

Electrochemical sensors provide an attractive means to analyse biological samples due to the direct conversion of a biological event to an electronic signal.[95-98] They are usually constructed by modifying the surface of metal and carbon electrodes with materials such as polymers, self-assembled monolayers, and water-immiscible organic oils, *etc*.[99-101] The output signal of sensors is generated through the specific binding or replacement or a catalytic reaction at the electrode surface. The properties of boronic acids have led to them being exploited in sensing and separation systems for saccharides (diols).[102, 103] Therefore, electrochemical sensing using boronic acids potentially provides a method to monitor blood glucose level for treatment of diabetes.

Boronic acid functionality has been employed in electrochemical sensing systems

predominantly based on direct effects of analyte binding on current and/or potential responses in voltammetric experiments. Most widely studied are soluble ferrocenylboronic acid redox probes which were first synthesised by Nesmayanov[104] and have been shown to allow direct electrochemical diol and anion sensing in aqueous media.

The potential use of ferrocenylboronic acid (FcBA) for the electrochemical determination of a wider range of sugars was investigated by Lucina and Skládal.[105] They detected the free and bound forms of FcBA in the boronate complex by using voltammetric and amperometric measurements (Figure 36). In this way, the complexation interaction was studied with saccharides as model diols giving distinct voltammetric behaviour. In addition, in this study electrodes modified with sorbitol and 1,6-hexanediol were used to immobilise FcBA to the surface of the electrode through boronate ester bonds. Thus, FcBA-modified electrodes could be useful as reagent-free sensors for recognition of sugars and related compounds in replacement assays.

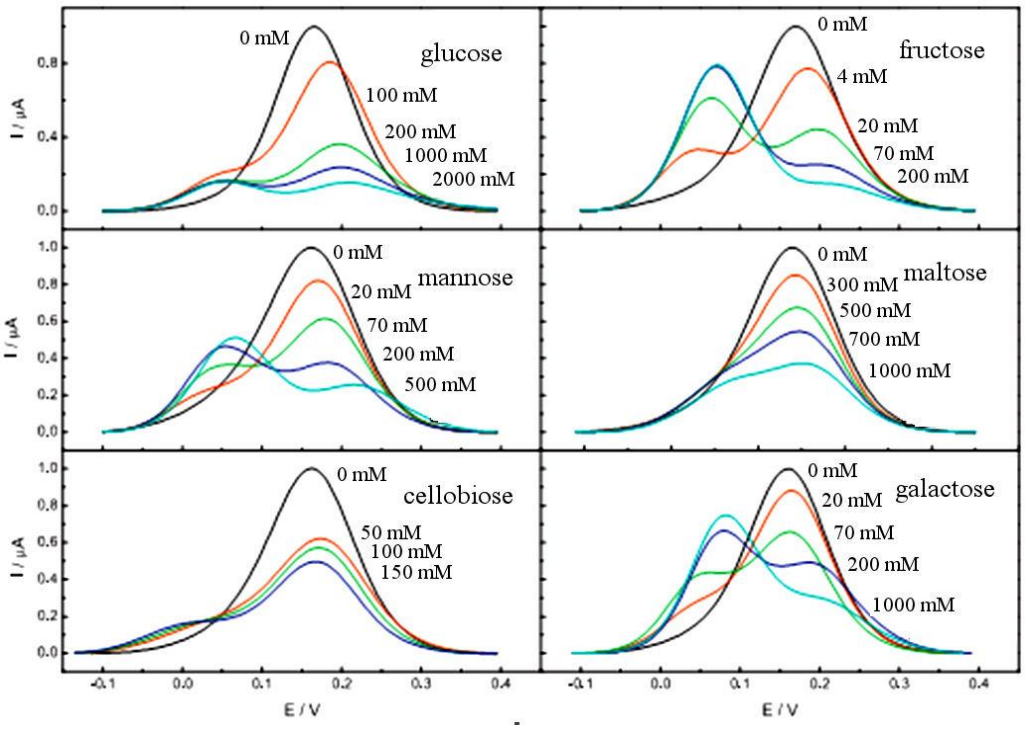

Figure 36 Differential pulse voltammograms for 1 mM FcBA in the presence of polyols demonstrating characteristic features for each saccharide.[102]

Compared to solution processes, surface immobilized processes are more convenient in applications. They also offer more sensitivity and selectivity due to additional interactions with the analyte at the electrode/solution interface. Strategies for the preparation of boronic acid functionalised electrode surfaces can be divided into (i) polymer-bound deposits (ii) covalently bound or grafted structures, (iii) self-assembled films.

Modified electrodes are commonly developed based on the polymer components with environmental stability, electrical (hopping) conductivity, and pH-dependent redox behaviour. Senel and coworkers prepared a polymer based on aniline boronic acid, which was formed by the electro-co-polymerization of aniline and aniline boronic acid with application in the detection of glucose (Figure 37).[106] This poly-aniline-boronic acid (PABA) monolayer provides a conducting polymer coated surface and was used in the immobilization of FAD (flavine adenine dinucleotide binding directly to the boronic acid) and reconstitution of apo-glucose oxidase (apo-GOx) onto the resulting FAD monolayer. After a series of optimisation experiments, pH 7.5 was selected as buffer medium for the determination of glucose and 0.5 V was chosen as the applied potential for amperometric detection of glucose concentration. Under optimum conditions, glucose could be determined in a linear range from 1.0 to 17 mM with a correlation coefficient of 0.9979 and a detection limit of 0.24 mM at 3 S/N. Applicability to blood analysis was evaluated.

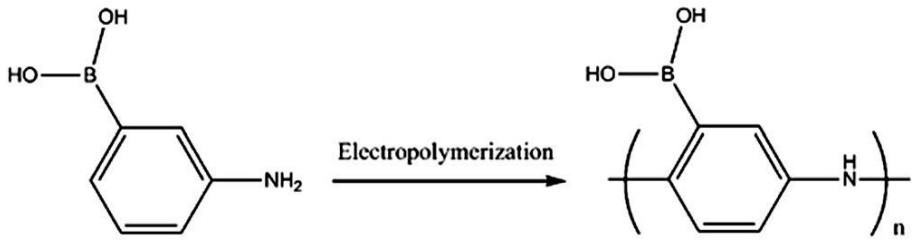

Figure 37 Electro-polymerization of aniline boronic acid on the glassy carbon electrode.

Diazonium chemistry provides a versatile tool to produce stable organic layers successfully on carbon electrodes, metals, and on semiconductors. In general, this method uses a chemical generation of radicals, followed by formation of covalent bonding between the radicals and the electrode surface. The process is easily and rapidly carried out in one step. The covalent bond between the modifier and the electrode surface is particularly attractive for construction of chemo-sensors or bio-

sensors due to stability in different measurement conditions, e.g. at different pH values and temperatures.

Teramae *et al.* investigated covalently grafted multilayers of phenylboronic acid (PBA) on glassy carbon for the detection of glucose.[107] 3-Aminophenylboronic acid (3-APBA) was used to form the multilayers controlled by the concentration of precursor 3-APBA and the number of potential cycles applied during the grafting procedure (Figure 38). Cyclic voltammetry and electrochemical impedance spectroscopy were used to characterise the grafting of the PBA group. The barrier properties of the grafted electrodes were studied in the presence of $Fe(CN)_6^{3-/4-}$. The resultant PBA multilayer was applied for glucose detection utilising $Fe(CN)_6^{3-/4-}$ as a redox probe by impedance. Non-Faradic impedance measurements for reagentless detection of glucose were reported. A linear response to the glucose concentration was found, which reflects formation of the glucose-PBA complex on the electrode surface.

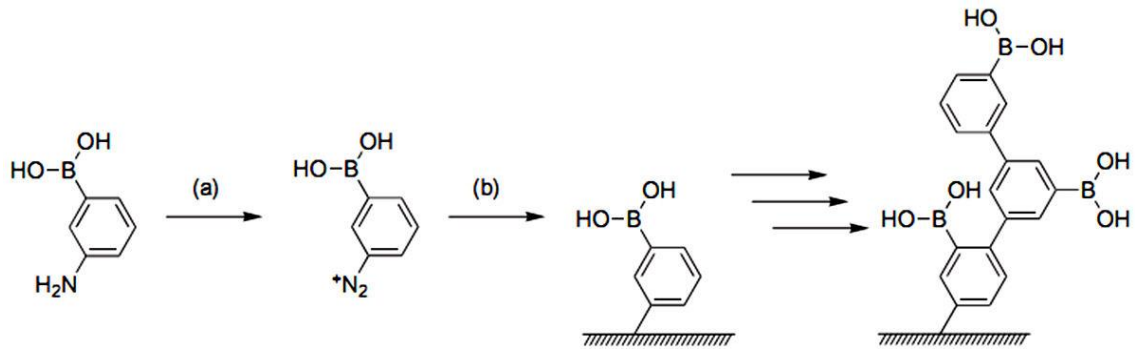

Figure 38 Schematic illustration of the electrode surface grafting by the electrochemical reduction of in situ generated 3-APBA diazonium cation. (a) Five eqiv. $NaNO_2$, 1 M HCl, 4 ℃; (b) Potential cycling between +0.6 and -0.4 V vs. Ag/AgCl, 4 ℃, formation of sub-monolayer to multilayer structures.

Over recent years, carbon nanotubes and graphene oxide have been the most common carbon materials for electrode modification due to the high surface area accessible for boronic acid functionalisation. Graphene oxide (GO) can provide a matrix for sensing. Recenly, Boukherroub and Szunerits reported a novel interface strategy for sugar sensing based on specific boronic acid-diol binding.[108] 4-Aminophenylboronic acid (APBA) was stirred with a suspension of graphene oxide (GO) for 12 h at 100 ^oC to form a reduced graphene oxide (rGO) with APBA incorporated into the rGO matrix (Figure 39). In order to determinate sugars, differential pulse voltammetry (DPV) was used on glassy carbon electrode modified with rGO/APBA. Importantly, this investigation shows excellent sensitivity for saccharides with a wide linear range with

detection limits of 100 nM for fructose, and around 800 nM for mannose and glucose. The sensor proved to be useful for exploring the sugar content of more complex matrixes such as apple juice thus resulting in an interesting alternative to other sensors.

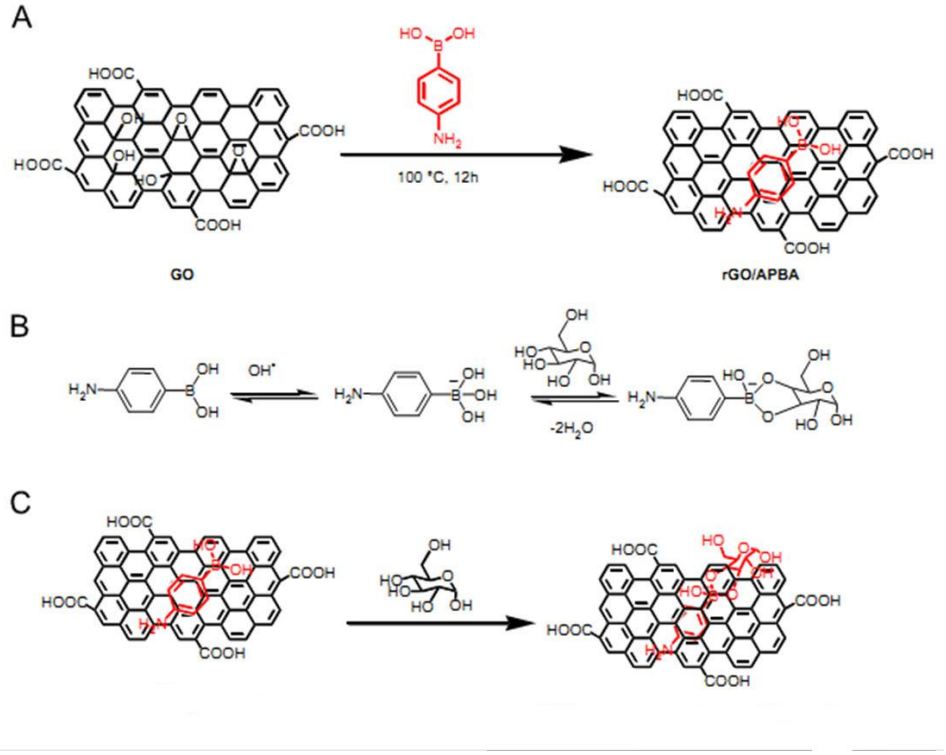

Figure 39 (A) Schematic illustration of the formation of rGO/APBA nanosheests; (B) mechanism by which α-glucose can be linked to rGO/APBA nanocomposite interfaces and (C) detection principle employed.

Given the affinity between gold and sulphur, gold electrodes cab be modified by self-assembled sulphur containing molecules. Long and coworkers developed a bis-boronic acid modified electrode for the sensitive and selective determination of glucose.[109] The compound was designed to contain a glucose selective chemosensor unit (bis-boronic acid) and surface anchoring unit (sulphur) (Figure 40). Cyclic voltammetry and electrochemical impedance spectroscopy were used for investigation of the sensor's response to glucose, fructose, galactose and mannose. The sensor surface shows high sensitivity to glucose with a good linear response with impedance spectroscopy. The stability constants obtained are: D-glucose ($1.7 \pm 0.3 \times 10^5\ M^{-1}$), D-galactose ($9.1 \pm 1.2 \times 10^4\ M^{-1}$), D-fructose ($4.6 \pm 0.5 \times 10^4\ M^{-1}$) and D-mannose ($1.2 \pm 0.1 \times 10^2\ M^{-1}$).

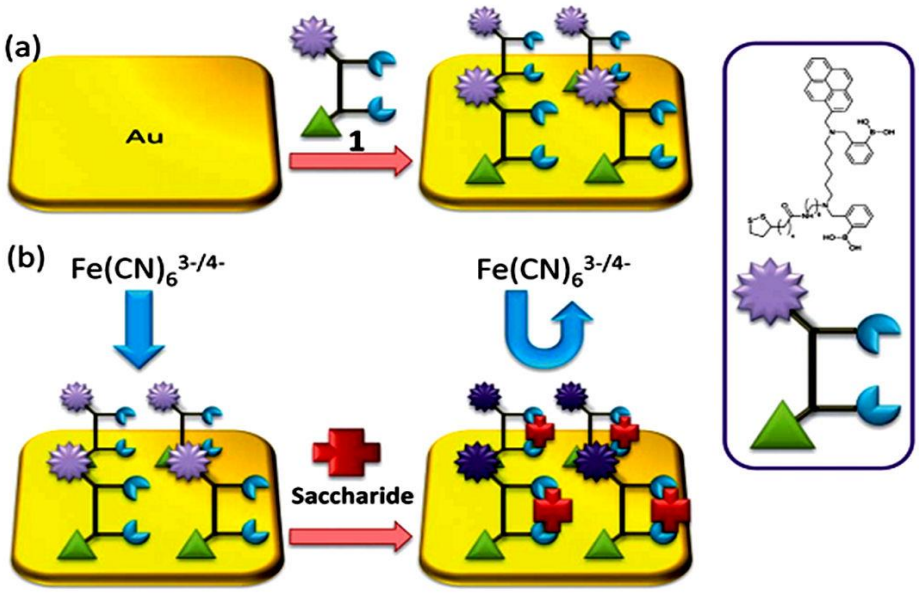

Figure 40 (a) Representation of gold surface functionalisation by the receptor unit and (b) saccharide binding.

The electrochemical sensors mentioned above have demonstrated that electrochemical sensing with boronic acids is one of the most effective methods for biologically and medically important species detection in addition to fluorescent sensing. Both methods will be employed in this thesis to develop new types of sensor mechanisms.

1.6 The Development of Molecular Switches and Logic Gates

1.6.1 Molecular Switches

A molecular switch is a molecule that can be reversibly change between two or more stable states.[110] The molecules may change between the states in response to external effects, such as changes in pH, light, heat, exposure to chemicals, an electrical current, microenvironment, or magnetic field. In some circumstances, it is required a combination of stimuli. pH indicators are the best examples for synthetic molecular switches, which reversibly change colour in response to changing the pH of a medium. So far, synthetic molecular switches have been of great interest in the field of nanoelectronic devices. Besides, molecular switches are important to biological researches due to their biological functions, such as allosteric regulation and vision. Moreover, they are also one of the simplest examples of molecular machines.

Photochromic molecular switches

Photochromic compounds have been widely studied since they can switch between electronic configurations when exited at a certain wavelength of light. UV-*Vis* spectroscopy is employed to measure the absorption maximum for each state. There are a diversity of photochromic compounds including azobenzenes, diarylethenes, dithienylethenes, fulgides, stilbenes, spiropyrans and phenoxynaphthacene quinones, which have been used to design photochromic molecular switches.

Zhu and co-workers have developed a novel photoswitching system based on bis(dithiazole)ethene moiety (Figure 41).[111] The two states are both thermally stable and quantitative photoswitching of the full cycle, which can be realised by light illumination with excellent fatigue resistance and reversibility. Due to its admirable properties such as quantitative photoswitching and fatigue resistance, it supports the proof-of-concept for photo-optical modulation using $\mathbf{35_O}$ and $\mathbf{35_C}$ as bistable complements. As a result, it can transmit information in the lasers to other passing light waves and launch it into the optical fibre. Therefore a new method of modulating light

with encoded information has been developed using the fundamental properties of molecular photoswitches.

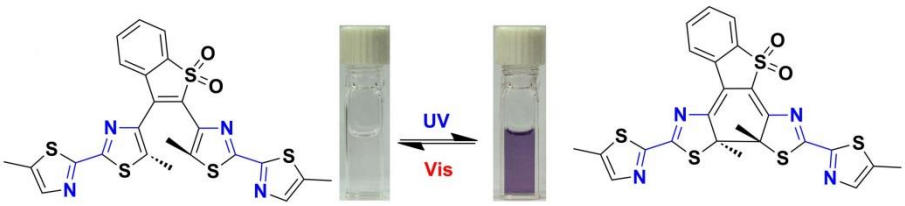

35o **35c**

Figure 41 Reversible and quantitative UV and visible-light shuttle bis(dithiazole)ethene between its bistable states $\mathbf{35_O}$ and $\mathbf{35_C}$.

Host-guest molecular switches

In host-guest chemistry the difference between two stable states in the affinity for guests has been used to design host-guest molecular switch.

In 1980 Shinkai was the first to use the unit as a reporter in favour of an azobenzene moiety and find an on-off signalling of the molecule (Figure 42).[112] In this molecule, light induced a trans-cis isomerisation of the azo group causes a cavity contration. In the *trans* form the crown binds favourably to ammonium, lithium and sodium ions, however, in the *cis* form potassium and rubidium are more favourably bound. The reverse isomerisation takes place in the dark. In order to mimic the biochemical action of monensin and nigericin,[113, 114] this devices was employed for the actual ion transport in a biphasic system of ions triggered by light.

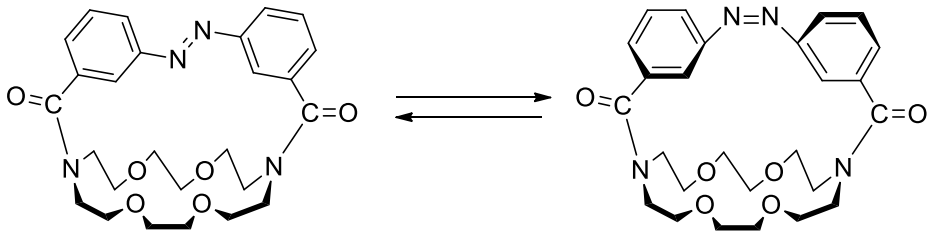

36

Figure 42 Structure of compound **36**.

1.6.2 Electro-optical Switches

Molecular switches whose electronic and optical properties can change reversibly in response to various chemicals and electrical input are called electro-optical switches. Among the various switching materials, fluorescence and electrochemical components have drawn much attention due to the high sensitivity and the easy observing of the signals.[3]

Recently, fluorescent switches have been widely explored, however, fluorescent switches allocating a redox reaction centre ferrocene (Fc) for multifunctional signals still need further studies.[5] Therefore, it is interesting to modulate the changes in emission of fluorophore by redox reaction of the Fc group (Scheme 2).

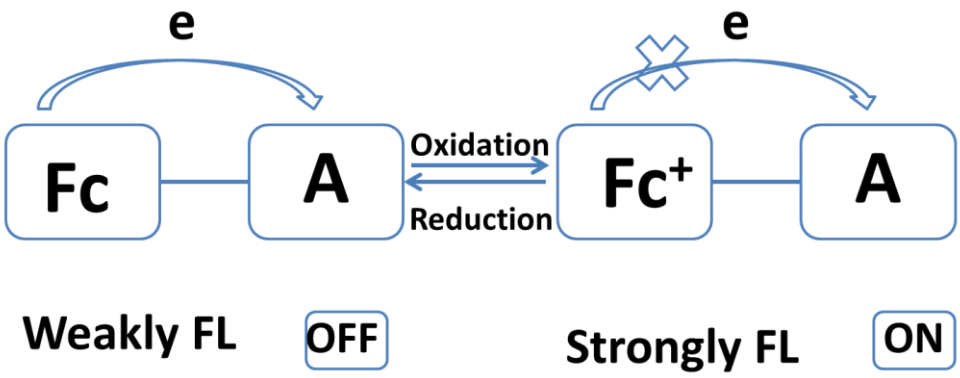

Scheme 2 Illustration of a redox fluorescence switch based on an Fc-type electron donor.

Veciana and coworkers have reported a reversible redox-fluorescence molecular switch based on a 1,4-disubstituted azine with ferrocene and pyrene units (Figure 43).[115] The emission fluorescence intensity of **37** in solution can be reversibly modulated by the redox of ferrocene. As an electron donor active unit, ferrocene was linked to the pyrene acceptor unit which fluoresces efficiently. Spectroelectrochemical studies were carried out to confirm that the fluorescence intensity was recovered after each step.

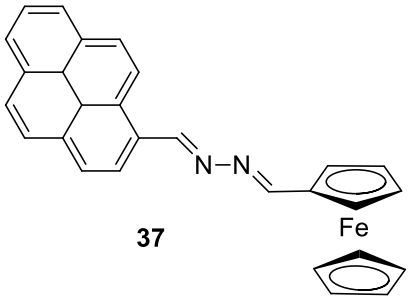

37

Figure 43 Structure of compound **37.**

Yao *et al.* have developed a redox-fluorescence switch **38** based on a triad containing ferrocene and perylene diimide moieties (Figure 44).[116] In the presence of Fe^{3+}, compound **38** displays a dramatic fluorescence enhancement due to the interruption of PET process, which demonstrates that **38** can be used as a redox-fluorescence switch. Therefore, in use of electrochemical oxidation and reduction method, the fluorescence intensity of the solution can be reversibly modulated. And no fatigue was observed even after several cycles of electrochemical redox.

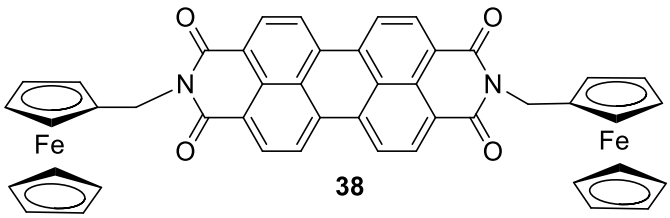

38

Figure 44 Structure of compound **38**.

Zhu and co-workers have also reported a new photochromic bisthienylethene system in which the ferrocene unit is directly linked to a naphthalimide chromophore (Figure 45).[117] The ferrocene component in the photochromic system plays an important role in the optical adjustments, such as fluorescence changes through photoinduced electron transfer (PET), a two-step oxidation process and a decrease in the photochromic cyclisation quantum yield. Especially, the fluorescence can be modulated not only with $Fe(ClO_4)_3$ as an oxidant and LAS as a reducing agent but also by electrochemical redox process. Therefore, the system is suitable for potential applications in sensing and signalling, as well as in data manipulation on a molecular level.

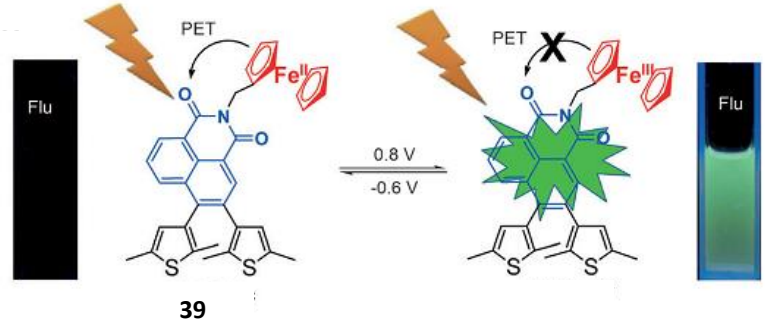

39

Figure 45 Structural changes and fluorescence images of **39** before- and after electrochemical redox processes.

1.6.3 Logic Gates

The development of highly sensitive and selective chemosensors has become an active area in supramolecular chemistry, especially in biology and the environment. The remarkable progress in the development of molecular logic gates has brought chemists closer to the realisation of molecular-scale calculators since the first report of molecular AND logic gate based on chemosensors by A. P. de Silva *et al.*.[118] Compared with the modern semiconductor IT industry, molecular logic gates can be viewed as computational devices that process physical or chemical "inputs" to generate "outputs" based on a set of logical operators. The molecular logic systems can also make themselves to convenient reconfiguring, especially for application in the life sciences. The "bottom-up" method exhibits a distinct advantage over conventional semiconductor counterparts. As a consequence, molecular logic function can be designed in chemical and intracellular sensing, small object recognition and intelligent diagnostics.

AND logic gate

A. P. de Silva and co-workers have designed a new compound with three receptors (Figure 46).[119] In the new compound, there are three PET processes, which result in the fluorescence of fluorophore anthracene being quenched. Only when the three ligands Zn^{2+}, Na^{+}, H^{+} coordinate with compound **40** together, the intramolecular PET process can be effectively inhibited, thus making the fluorescence increase. With three ligands as three input AND logic gates, corresponding to the combination of logic output, the output signal can be "1" in the truth table only when the three inputs are "1".

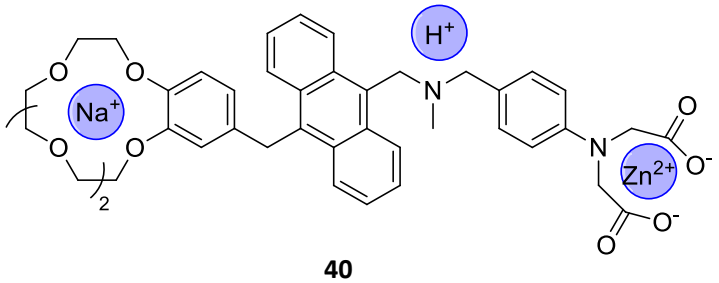

40

Figure 46 Diagram of compound **40** sensing for ions and AND logic gate.

Akkaya and co-workers proposed a photodynamic therapy agent **41** that was an AND logic gate (Figure 47). **41** would release singlet oxygen (output) at a much larger rate, when two cancer related cellular parameters (inputs) are above a threshold value within the same spatiotemporal coordinates.[120] It is believed that Na^+ and H^+ concentrations (pH) could be potential targets as cancer related cellular parameters. In tumour tissue, the pH can be quite low while the intracellular sodium ion concentration is high. Therefore, the molecular system is to search for higher concentration of both hydrogen and sodium ions, and release the cytotoxic agent (singlet oxygen) only when both concentrations are high, which also means that **41** can be employed in the fields of treatment, logic calculation and molecular sensing.

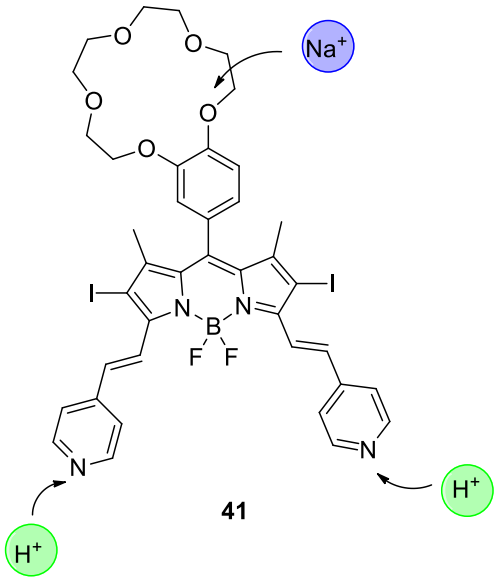

Figure 47 Diagram of compound **41** sensing for ions and AND logic gate.

INHIBIT GATE

An INHIBIT logic gate is based on two-input AND gates with one input carrying a NOT gate. Through reasonable design of the molecular structure, the INHIBIT logic gate can be prepared within a single molecule, compared with the traditional logic circuit to avoid the logic gate circuit connection.

An example of a "lockable" logic gate and a double INHIBIT logic gate **42** was first reported by Tian *et al.* based on a multiple-configurational rotaxane moiety (Figure 48).[121] They employed both submolecular position control and chemical modification to design a polymer film with INHIBIT logic gate function. In terms of different input combinations of 380 nm, 313 nm, and protons, different configuration states and fluorescence changes, a lockable INHIBIT logic gate as well as a complicated double INHIBIT logic gate can be developed using this rotaxane. Above all, several different supramolecular configurations can be represented by the output 0 and 1 states of the current logic circuits.

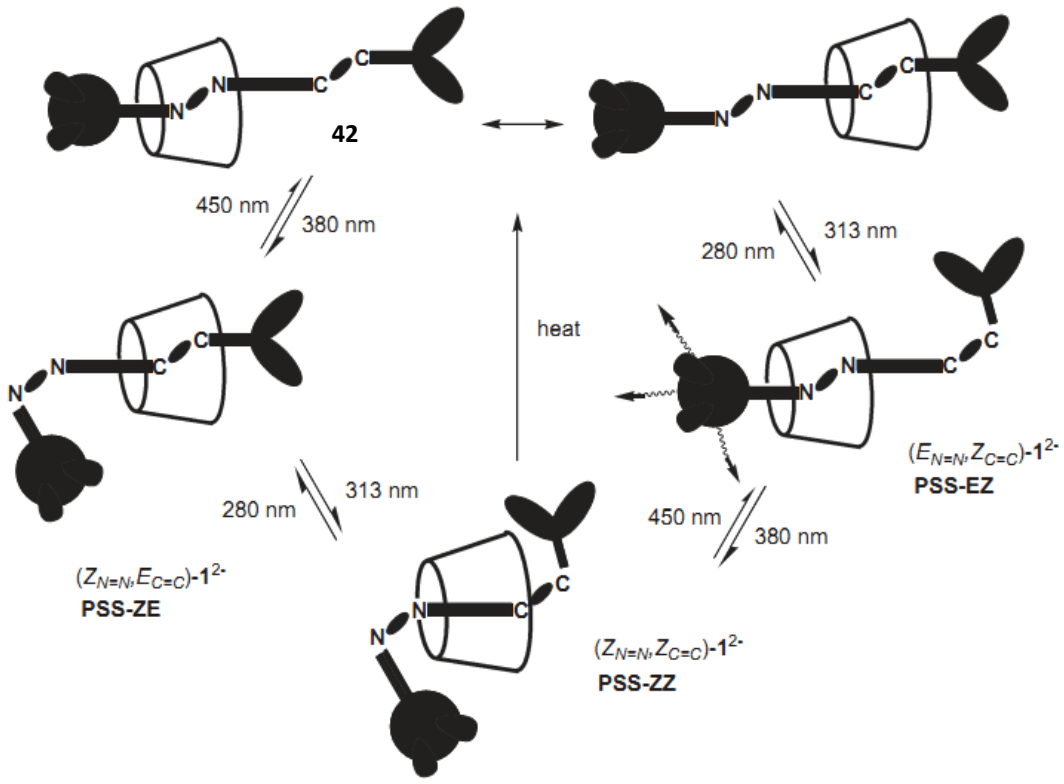

Figure 48 Double INHIBIT logic gate employing configuration and fluorescence changes.

XOR gate

The XOR gate is a digital logic gate that carries out an exclusive or, which means that a true output results if one, and only one, of the inputs to the gate is true. If both inputs are false or both are true, a false output is produced. XOR represents the inequality function, that is to say the output is true if the inputs are not alike otherwise the output is false.

A. P. de Silva and co-workers designed a fluorescent sensor **43** containing two separate receptors for Ca^{2+} and H^{+} within a push pull chromophore (Figure 49).[122] If the output is viewed as transmittance, XOR logic is produced. When electron donor recognition is combined with Ca^{2+}, the electron donating ability of the nitrogen is reduced due to the coordination effect, thus reducing the effect of the push-pull electronic interaction and resulting in the blue shift of the absorption spectrum; When the receptor part of quinoline was acidified, the molecular level of the system is changed resulting in red shift of absorption spectrum. When two inputs Ca^{2+} and H^{+} are added together, the ICT process of push-pull electronic effects of **43** are balanced, and the absorption spectrum returns to the initial state. The change of transmittance spectra at 390 nm corresponds to the truth table of XOR gate logic operation.

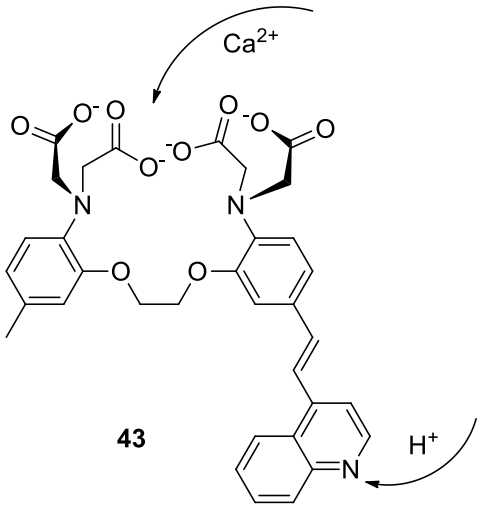

Figure 49 Diagram of compound **43** sensing for ions and absorption spectra.

1.7 Summary of Chapter 1

Firstly, a brief introduction was given about different types of fluorescent sensors and electrochemical sensors. Next, fluorescent techniques together with different types of fluorescence sensing mechanisms were presented.

The Literature was reviewed for progress on copper(II) ion detection using a variety of different fluorophores. Besides, the boronic acid receptors for metal ion detection was also introduced.[123] [124, 125] The employment of different fluorophores for copper(II) ion was reviewed. Specifically, the recent achievements in copper(II) ion sensing based on naphthalimide fluorophore were discussed. As coordination based sensors, the naphthalimide based probes can selectively bind with Cu^{2+}, reducing the synthetic effort and enhancing solubility. Factors which affect the binding constants and selectivity were studied in terms of the development of modular sensors.

Furthermore, progress towards biothiol sensing was reviewed in terms of reaction based probes. Intracellular thiols, as reduced species in cells, serve many cellular functions, including the maintenance of intracellular redox activities, intracellular signal transduction, and so on. Therefore, much attention has been devoted to the development of fluorescent sensors for thiol detection. The sensing mechanisms which cover a diversity of sensing syststems such as Michael addition, cyclisation with aldehydes, conjugate addition-cyclisation, cleavage of sulfonamide and sulfonate esters, and thiol-halogen nucleophilic substitution were discussed.

Moreover, the introduction to electrochemistry was introduced and also the electrochemical sensors using boronic acid for saccharides detection were presented. In particular, the recent progress of boronic acid-based electrochemical sensors both in solution processes and surface processes was reviewed.

Finally, molecular switches and logic gates were presented. Molecular switches based on photochromic switches, host-guest switches and electro-optical switches were discussed and three fundamental logic gates: AND gate, INHIBIT gate and XOR gate were illustrated.

CHAPTER TWO

Results and Discussion

Published - Li, M., Ge, H., Arrowsmith, R. L., Mirabello, V., Botchway, S. W., Zhu, W., Pascu, S. I. and James, T. D., Ditopic boronic acid and imine-based naphthalimide fluorescence sensor for copper(ii). *Chem. Comm.* 2014, **50 (80)**, 11806-11809.

2 Results and Discussion: New Fluorescent Chemosensors Based on Naphthalimide for the Detection of Copper(II) Ions

2.1 Overview of Fluorescent Chemosensors Based on Naphthalimide for the Detection of Copper(II) Ions

2.1.1 Importance of Copper(II) Ions

Recently, the importance of metal ions to the vital functions of living organisms, hence their health and well-being, has become interestingly apparent. As an essential soft transition metal ion, copper(II) plays a crucial role in biological, environmental and chemical systems. [126-128] The copper(II) ion is also used as a catalytic cofactor for a variety of metalloenzymes, including superoxide dismutase, cytochrome c oxidase and tyrosinase. In addition, under excessive levels, copper(II) exhibits toxicity that causes neurodegenerative diseases[129-131] (e.g., Alzheimer's and Wilson's diseases), probably by its involvement in the production of reactive oxygen species. While copper(II) deficiency may also lead to hematological manifestations and a number of other problems. In this regard, chemosensors for copper(II) ions are extensively employed as the signal output owing to their high sensitivity and the simplicity of the equipment requirements.[132-135] It is also important to note the medical emphasis in the need for copper(II) sensors, reaffirming fluorescence as a desirable signalling method to monitor the movement and location of Cu^{2+} in living cells.

2.1.2 Receptors for Sensing Copper(II) Ions

In chemistry, a coordination complex or metal complex consists of a central atom or ion, which is usually metallic and is called the coordination centre, and a surrounding array of bound molecules, that are in turn known as ligands or complexing agents. There are many kinds of ligands. Generally, the Schiff base moiety has been used as ligand for metal ions due to its high affinity and excellent selectivity in coordination chemistry.[136] The imine nitrogen in the Schiff base moiety acts as an electron-donating substituent whose donor character strongly depends on cation coordination (Scheme 3).

While, boronic acids have been well studied as the receptors for saccharides and fluoride. However, there are just a few examples where a boronic acid conjugated fluorescent chemosensors for metal ions has been developed. Therefore, this is a promising area to explore.

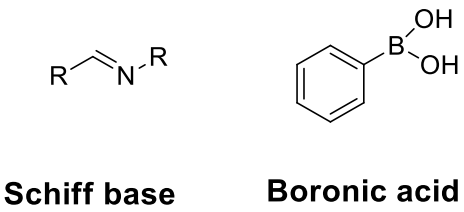

Scheme 3 The structures of two receptors.

2.2 Aim and Objective

The synthesis of naphthalimide chemosensors was performed and their potential as selective sensors for various metal ions was investigated. The derivatives were also examined for their interaction with monosaccharides, and potentially develop multifunctional molecules.

The 1,8-naphthalimide moiety has been shown to be a good reporter for chemosensing applications, however, only a few boron-modified naphthalimide compounds have been reported for copper(II) recognition. Confocal microscopic cellular imaging was used to evaluate the probes developed for Cu^{2+} detection, in collaboration with Dr. Sofia Pascu's group.

2.3 A Boronic Acid-Naphthalimide Based Fluorescent Sensor for the Recognition of Copper(II) Ions

2.3.1 Synthesis of the Fluorescent Sensor and Reference Compounds

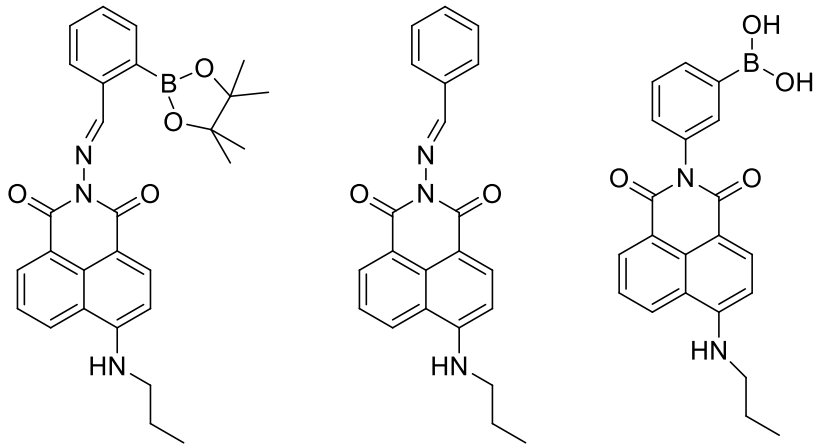

47 **48** **50**

Figure 50 The structures of target compound and its reference compounds.

Compound **47** is the target compound and compounds **48** and **50** are reference compounds (Figure 50). Previous work[137, 138] showed that a Schiff base is always used as a typical receptor for copper(II) ion and also the boronic acid can be used to coordinate with metal ions. Therefore, we designed a compound to combine those units, in order to improve the copper(II) sensing selectivity and sensitivity. In the meantime, we can't ignore the performance of the boronic acid for the recognition of saccharides. Therefore, we can use this compound to measure the binding ability with saccharides. Since naphthalimide fluorophore has excellent spectroscopic characteristics, we decided to use the same fluorophore together with the above moieties to synthesise a multi-functional molecule. The reference compounds are used to probe the function of the Schiff base and the boronic acid units.

Synthesis of compound 47 and 48

47 and **48** was obtained by a three-step procedure (Scheme 4). Firstly, intermediate **45** was synthesised through imide formation. Under nitrogen atmosphere, anhydride naphthalene **44** was dissolved in absolute ethanol. Then an excess of hydrazine hydrate was added, after having refluxed for 4 h, the mixture was cooled and the precipitated solids were filtered and recrystallised from ethanol to give a yellow solid.

46 was obtained by mixing 1.0 equiv. of **45** and 10.0 equiv. propylamine and refluxing in 2-methoxyethanol under nitrogen. This reaction is a typical nucleophilic aromatic substitution reaction. ^{1}H NMR spectrum showing the peaks at 0.9 - 1.1, 1.6 - 1.8, 3.2 - 3.5 ppm implied the completion of this reaction.

Besides the nucleophilic substitution of bromine and propylamine, the last reaction is an example of hydrazone formation of an amine to a carbonyl group followed by dehydration to the Schiff base. The Schiff base is an electrophile which easily reacts *via* electrophilic addition with compounds containing an acidic proton. Therefore, we protected the boronic acid prior to reaction with the aldehyde. ^{1}H NMR analysis indicates a sharp peak at 1.25 ppm and two peaks at 1.70 - 1.77 ppm, which is an indication of successfully coupling the two molecules together. Compound **48** was prepared using the same procedure.

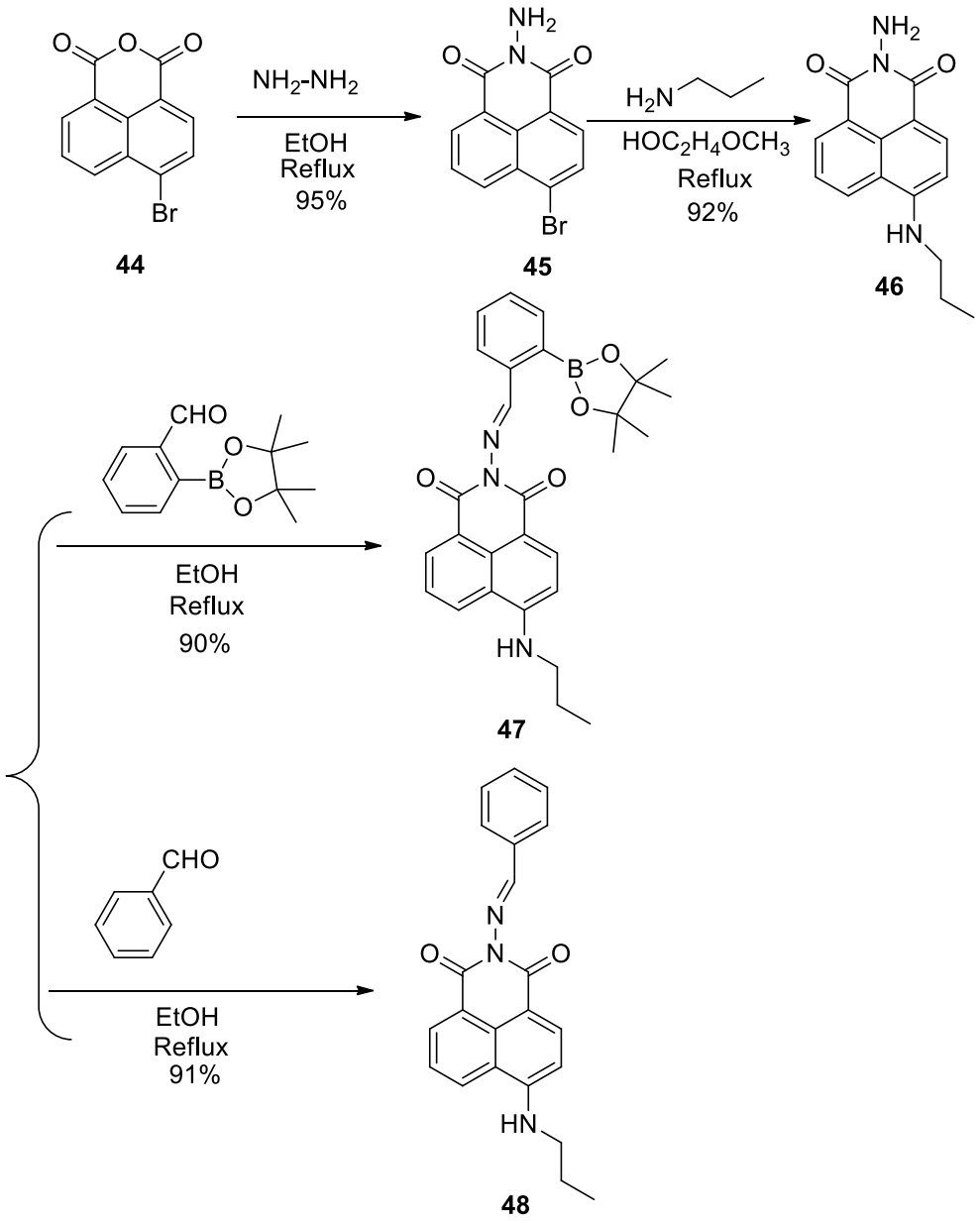

Scheme 4 Preparation of compound **47**, **48**.

*Synthesis of compound **50***

A parallel protocol was used for the preparation of compound **50** (Scheme 5). Compared with compound **47** and **48**, the boronic acid was linked to naphthalimide moiety directly without a Schiff base unit and acts as a reference compound. Compound **49** was obtained by treating compound **44** with 3-aminoboronic acid. The reactant mixture was stirred in ethanol under reflux overnight before concentrating under vacuum. The resultant product was washed with hexane to give a yellow solid with a yield of 90%. Compound **50** was obtained by the same procedure as compound **47**. In order to get the pure compound, the residue was purified by column chromatography to give a yellow solid with a yield of 92%. The ^{1}H NMR spectrum showing the peak at 1.0 - 2.0 ppm and 8.0 - 9.0 ppm implied the completion of this reaction.

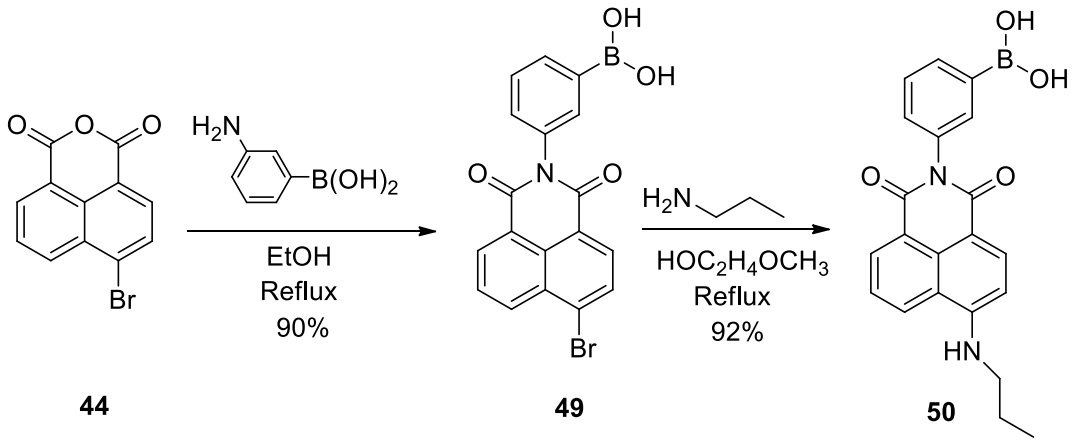

44 **49** **50**

Scheme 5 Preparation of Compound **50**.

2.3.2 Investigations of Copper(II) Ion Sensing

2.3.2.1 Measurements for Compound **47**

Effects of water

In order to employ our sensor under physiological conditions the effect of water was investigated. Due to the strong polarity of water, it is easy to exchange the energy between the excited state of fluorescent dyes and the solvent, thus leading to fluorescence quenching or decrease of the chemosensor. When choosing the test system, it is important not only to achieve good solubility of the fluorescent sensor in water, but also to ensure the fluorescent properties of the dyes. Figure 51 indicates that only 10 percent of water affects the recognition of copper(II). Therefore, we evaluate the compound in absolute methanol.

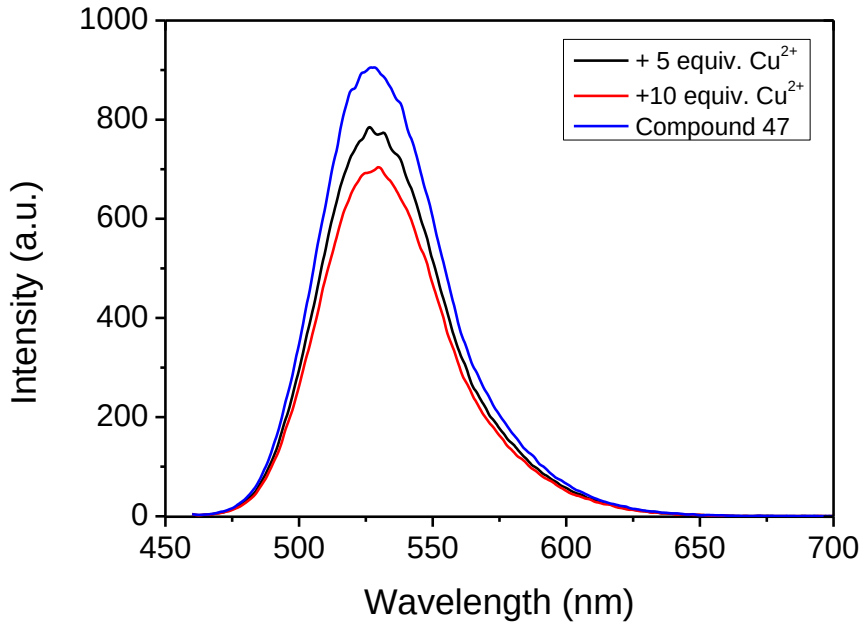

Figure 51 Emission spectra of Compound **47** (10 μM) with excitation wavelength at 450 nm in a mixture of methanol-water (90: 10, v / v) upon titration of Cu^{2+}.

*The selectivity of compound **47** to Cu^{2+}*

From Figure 52, only in presence of Cu^{2+}, causes significant quenching of the fluorescence. The other metal ions, such as Cd^{2+}, Hg^{2+}, Ag^{+}, Fe^{3+}, Fe^{2+}, Na^{+} and Pb^{2+} show minimal effect on the fluorescence of the compound, while Zn^{2+} shows some interference. Therefore, compound **47** can be employed as a chemosensor for detecting Cu^{2+}.

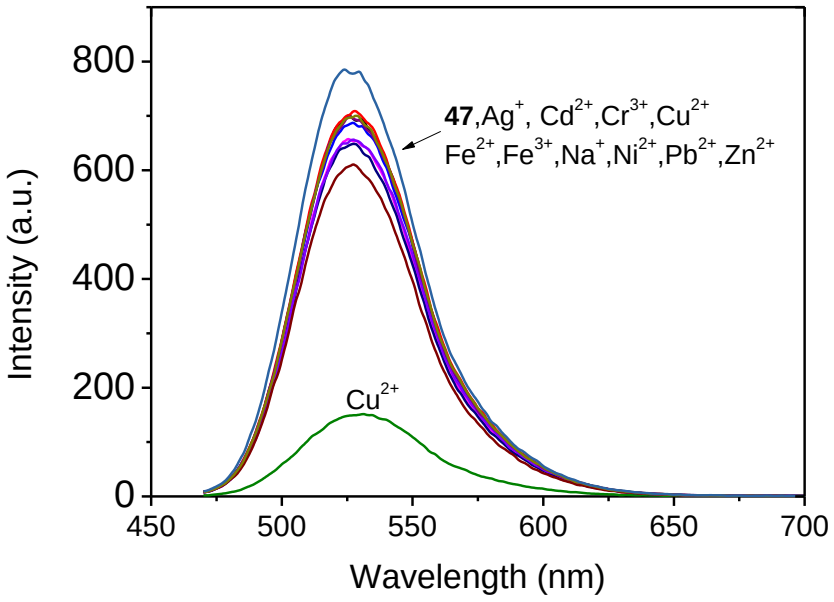

Figure 52 Fluorescent changes of compound **47** (10 μM) with various metal ions (100 μM) in methanol (λ_{ex} = 450 nm, λ_{em} = 525 nm).

*Absorption and fluorescence titration of compound **47** with Cu^{2+}*

To obtain insight into compound **47**, its absorption (Figure 53) and emission spectra (Figure 54) upon titration with Cu^{2+} were recorded. Compound **47** in methanol shows a strong band in the UV-*vis* spectrum with a maximum absorbance at 450 nm. Upon increasing the concentration of Cu^{2+} (0 - 300 μM), an absorption enhancement could be observed with a red-shift to 465 nm in the absorption maximum which indicates the formation of an complex between **47** and Cu^{2+}. The fluorescence at 525 nm is simultaneously quenched, which was attributable to the coordination of the paramagnetic Cu^{2+} centre as reported in previous studies.[139, 140] Based upon these results of the fluorescence titration experiments, the association constant of **47** for Cu^{2+} was determined to be 3.39×10^{5} M^{-1} (Figure 55). In agreement with the stoichiometry

of the reaction the best fitting of the binding model displays a second binding constant which was found to be 50 M^{-1}. The discrepancy of the two values indicates the presence of a secondary event in solution which is slower but necessary to complete the "turn-off" process.

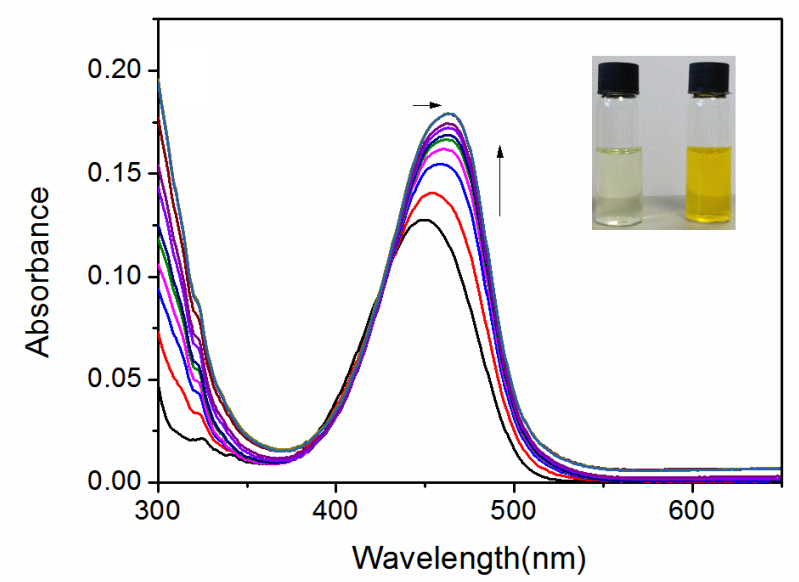

Figure 53 Absorption spectra of **47** (10 μM) in methanol in the presence of different amounts of Cu^{2+} (0 -30 equiv).

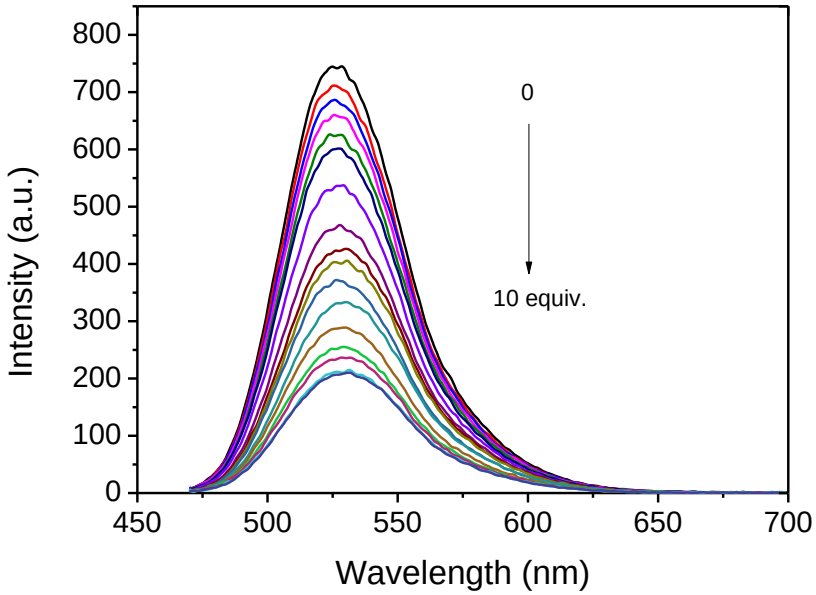

Figure 54 Fluorescent titrations of compound **47** (10 μM) with Cu^{2+} in methanol (ex = 450 nm).

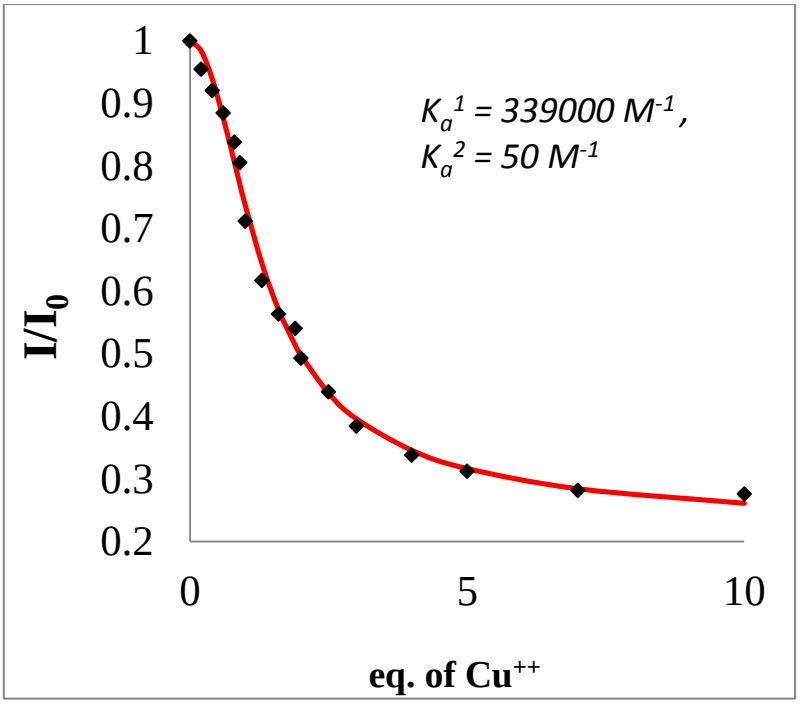

Figure 55 Fluorescence quenching response of compound **47** to the increments of Cu^{2+} equivalent in solution. Association constants, K_a^1 and K_a^2, were calculated by using MATLAB® m-files and fitted for 2:1 BNP: Cu^{2+} binding isotherm (*Thodarson, P., Chem. Soc. Rev.* 2011, *40*, 1305–1323). Experimental data points, (black markers) and fitting curve (red line) for such equilibrium are reported in figures here together with standard error and covariance of fit.

*Stability of compound **47** in phosphate buffer solution (pH = 8.21, 51% methanol)*

It is well known that boronic acid has high affinity to diols. Therefore, we want to explore the potential recognition of our sensor with saccharides. Since saccharides are in human body, the test system should be similar to the biological environment. In the previous experiment of our lab, we use pH 8.21 phosphate buffer (containing 52.1 *wt* % methanol) to do the saccharides' titration. However, there is a Schiff base moiety in compound **47**, which might be very sensitive to water. Therefore, the fluorescent stability test of **47** in pH = 8.21 phosphate buffer (containing 52.1 *wt* % methanol) was measured. Figure 56 indicates that the fluorescence intensity doesn't change after 1 h in the buffer solution, which indicates that the compound is stable in the buffer solution.

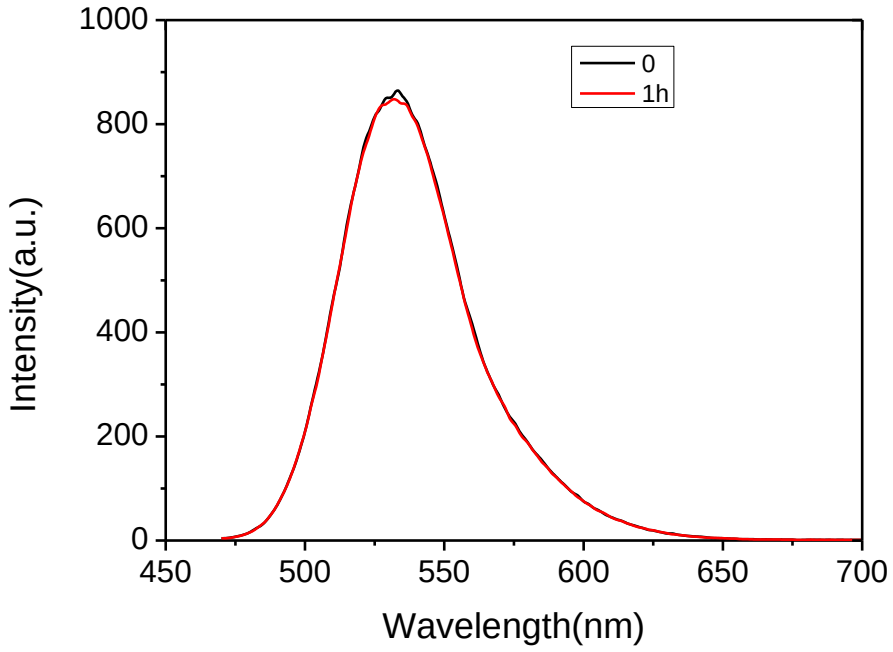

Figure 56 Emission spectra of compound **47** in buffer solution. The concentration of compound **47** was 10 μM (λ_{ex} = 450 nm, λ_{em} = 525).

*Selectivity of saccharides for compound **47** in buffer solution (pH=8.21, 51% methanol)*

Since compound **47** is quite stable in pH 8.21 phosphate buffer (containing 52.1 *wt* % methanol), thus, we used **47** to detect monosaccharides. However, the result shows that the **47** shows no selectivity to the four monosaccharides and no decrease of the fluorescence intensity, which suggests that the binding of the boronic acid and saccharides induces no effect on the naphthalimide fluorophore (Figure 57).

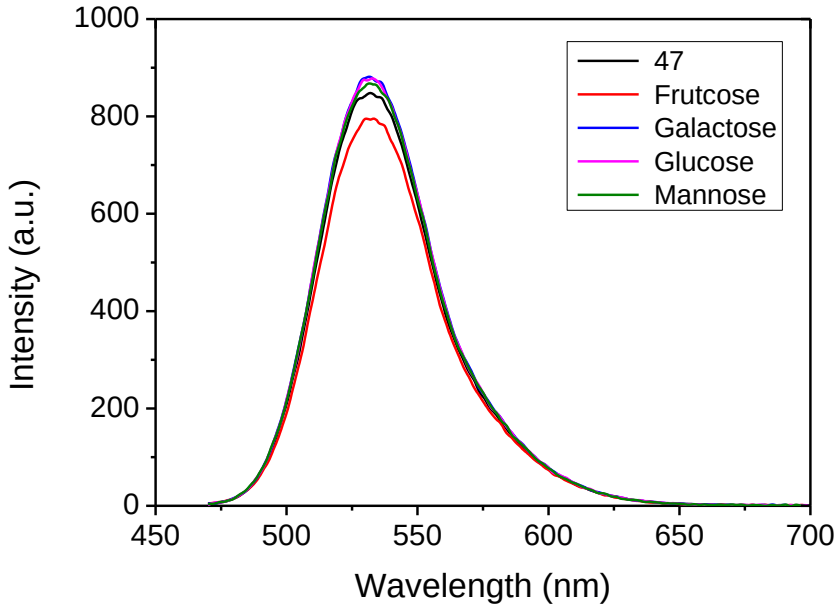

Figure 57 Emission spectra of compound **47** upon addition of 100 mM each relevant analyst with excitation wavelength at 450 nm in buffer solution. The concentration of compound **47** was 10 μM.

*Fluorescence titration of compound **47**-Cu^{2+} with fructose*

While compound **47** did not show any fluorescent changes upon addition of saccharides, the addition of fructose to a solution of **47**-Cu^{2+} coordination compound resulted in a fluorescence enhancement. Considering the solubility of the saccharide in methanol, we only tested fructose. Therefore, we added 2 equivalents of Cu^{2+} to a solution of compound and the fluorescence intensity decreased from 851 to 530. However, after adding up to 200 mM fructose, the fluorescence recovered to 832. Figure 58 illustrates that the fluorescence intensity increased after adding different amounts of fructose, which indicates that the complex can be used to recognise fructose.

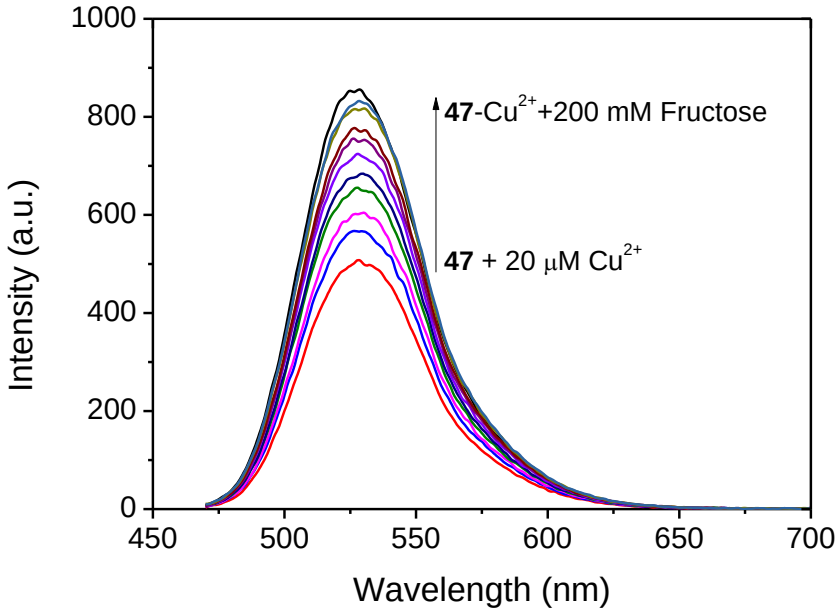

Figure 58 Emission spectra of compound **47**-Cu^{2+} upon addition of different amount of fructose with excitation wavelength at 450 nm in methanol. The concentration of compound **47** was 10 μM.

Logic gates

In terms of the results above, while **47** did not show any fluorescent changes upon addition of fructose, the addition fructose to a solution of **47**-Cu^{2+} resulted in a fluorescence enhancement. When 2 equivalents of Cu^{2+} are added to a solution of **47** followed by fructose addition the system behaves like a fluorescence INHIBIT logic gate (Figure 59), which means that fructose inhibits the fluorescence quenching and Cu^{2+} alone can quench the fluorescence.

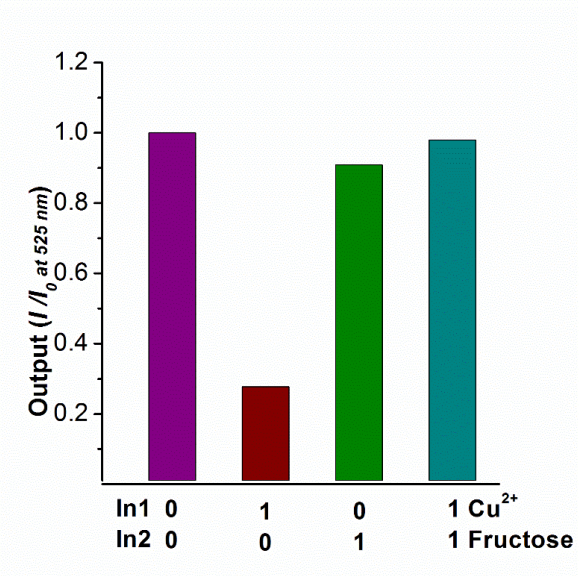

Figure 59 Outputs with Cu^{2+} (50 μM) and D-fructose (200 mM) as inputs.

Two-photon emission spectra

In collaboration with Dr. Sofia Pascu's group, the capacity of the boronic acid-linked **47** to detect copper(II) ions was investigated in HeLa cells using confocal imaging and fluorescence lifetime imaging (FLIM).

Fluorescence lifetime is often considered as a means of distinguishing between different fluorophores, different energy states of the same fluorophore and environmental effects such as quenching caused by binding of intracellular ions such as Cl^- or Ca^{2+} or oxygen. FLIM was likewise used to monitor the stability and demetallation of copper(II) complexes in cells.[141, 142] Therefore by utilising an approach of fluorescence lifetime imaging the presence of Cu(II) ions could be investigated by mapping the submicron cellular localisation on ions. Furthermore, a recent study showed that a variant of human apocarbonic anhydrase II could monitor Cu(II) ions in cells *via* FLIM, whereby an increase in Cu(II) ions produced a decline in the average lifetime observed.[143, 144] We have combined FLIM and Multiphoton excitation in this study to offer reduced effect of the excitation light since the use of near infrared leads to reduced cellular phototoxicity. Further advantages of two-photon excitation is that imaging occurs only from the focal plane, and causes less damage to cells than single-photon microscopy and decreases photo-bleaching, whilst improving imaging depth. [145, 31]

Two photon excitation of the boronic acid-linked **47**, its quenching by Cu^{2+} and recovery upon addition of fructose was investigated in DMSO solution at 10 mM. DMSO was used due to its low volatility in comparison to methanol and was also employed for the stock solution in the cellular experiments (0.5% DMSO). When **47** was excited at 910 nm, an intense emission was observed, which was quenched after addition of 5 equivalents of Cu^{2+}. However, an additional 5 equivalents of fructose led to an enhancement of the fluorescence (Figure 60). Moreover, the Time-Correlated Single Photon Counting (TCSPC) was measured (Figure 61). For **47** the first lifetime component (τ_1) was 2.0 ns (25.0%), with a second component (τ_2) of 9.4 ns (75.0%) and a mean lifetime (τ_m) of 7.6 ns. By adding 5 equiv. Cu^{2+}, the lifetime of **47** decreased to 4.5 ns. Furthermore, upon addition of fructose, the lifetime component decreased further to 4.1 ns.

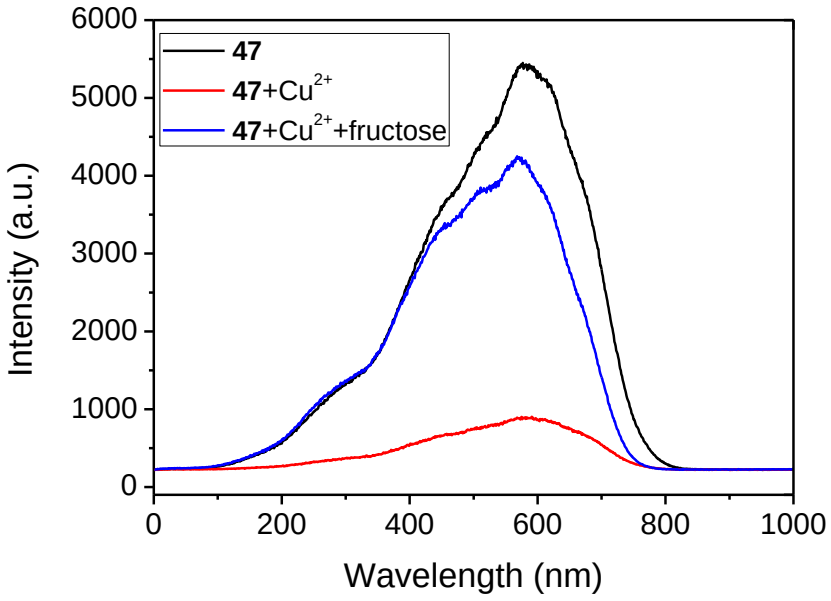

Figure 60 Emission spectra of **47** (10 mM), **47** plus 5 equiv. Cu^{2+} and **47**-Cu^{2+} plus 5 equiv. fructose with two-photon excitation at 910 nm.

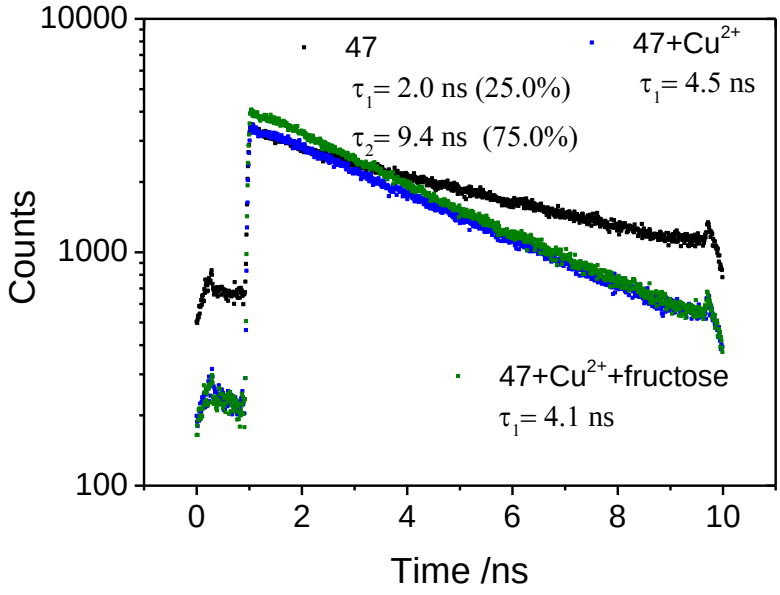

Figure 61 Nanosecond decay curves for **47**, **47** plus 5 equiv. Cu^{2+}, **47**-Cu^{2+} plus 5 equiv. fructose.

Confocal image

The fluorescence imaging was recorded at the Research Complex at Harwell by Haobo Ge, under the supervision of Dr Sofia Pascu and Dr Stan Botchway, and the results will be discussed below.

Confocal microscopy shows that **47** enters cells and displays strong fluorescence in the absence of external copper(II) ions (Figure 62, a-c). Furthermore lifetime distribution curve from the FLIM data of **47** showed a τ_1 of 1.5 ns ± 0.6 ns, when incubated in HeLa cells, which was comparable to the 2.0 ns τ_1 observed in solution confirming the presence of the **47** ligand in cells and indicated that the lifetime was not significantly different between DMSO solution and in cells (Figure 63).

Contrastingly, when 5 equivalents of copper(II) ions (250 μM) were added a very weak fluorescence response was observed, indicating quenching (Figure 62, d-f). Moreover, the fluorescence lifetime was observed to have a τ_1 of 4.4 ns ± 0.5 ns, which was consistent with data observed in DMSO solution. Further work may shed light upon the interaction of **47** and copper(II) in cells and to fully understand its potential as a copper(II) sensor (Figure 63).

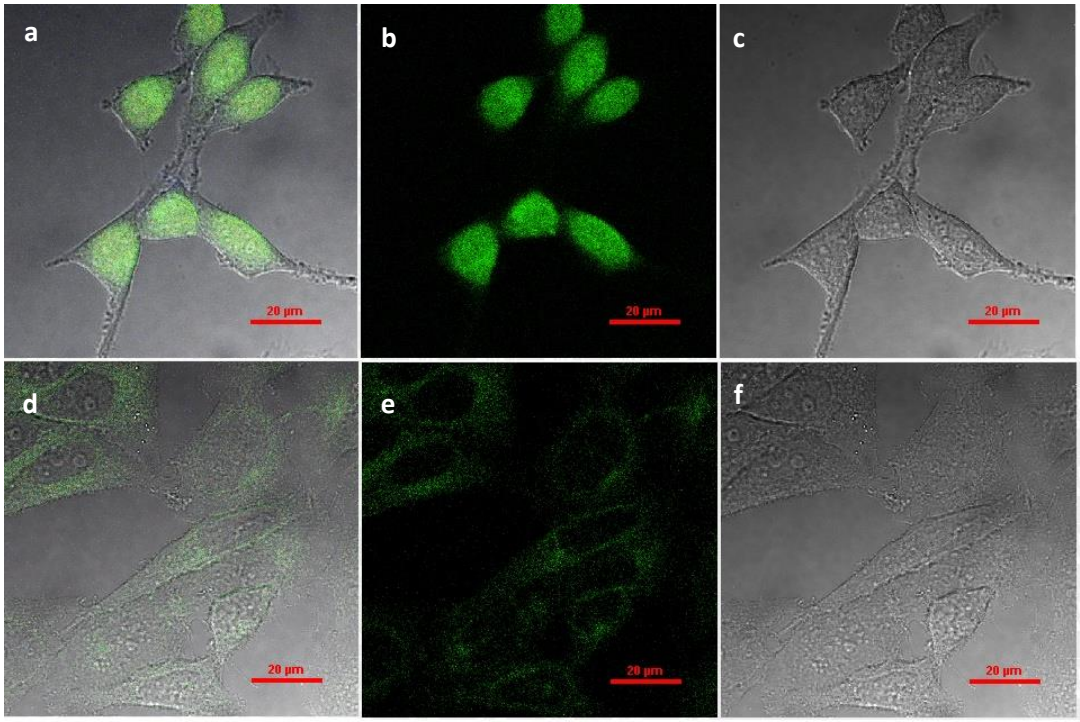

Figure 62 Laser scanning confocal imaging of **47** in absence of Cu^{2+} (a-c), and **47** in presence of Cu^{2+} in HeLa cells (d-f). (a) overlay image of (b) and (c), (d) overlay image of (e) and (f). (b, e) fluorescence micrographs with excitation at 405 nm and the emission long path filtered at 515 nm, (c, f) differential interference contrast micrograph.

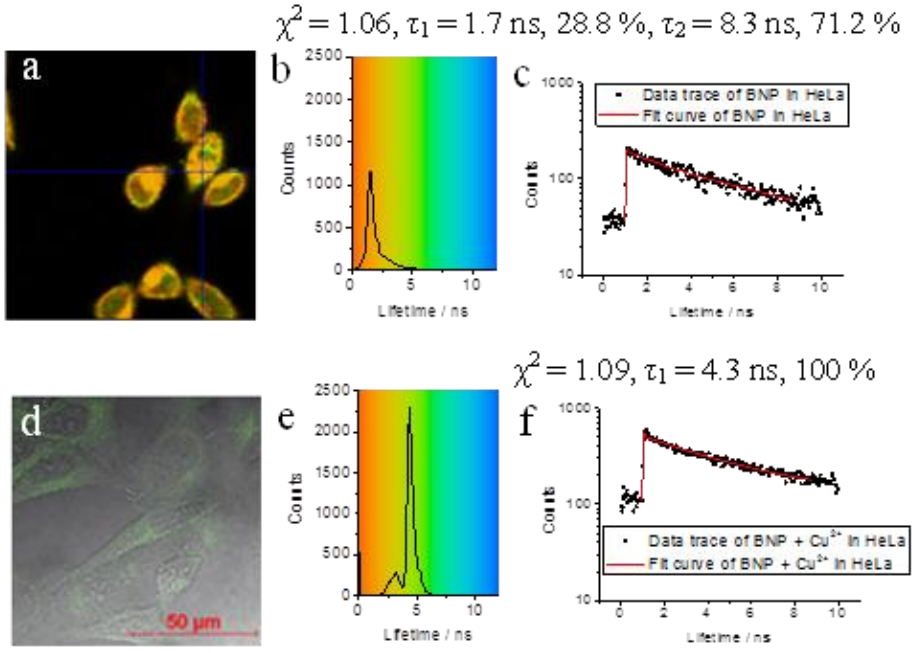

Figure 63 Two-photon lifetime imaging at 910 nm, 15 min incubation of 50 µM **47** in HeLa cells (0.5% DMSO, 2.5 mW,) (a - c) and 50 µM **47** + 250 µM Cu^{2+}, 5.6 mW (d - f). Images show: (a) fluorescence lifetime mapping for τ_1 and (d) confocal overlay image of Figure 62 e and 62 f, (b and e) corresponding fluorescence lifetime distribution curves, (c and f) sample point decay trace inside the cell.

2.3.2.2 Selectivity of Control Compounds **48** and **50** and Proposed Binding Mode

In order to probe the role played by the boronic acid group in copper(II) ion binding and fluorescence quenching, compound **48** was treated with Cu^{2+} in methanol. No changes in the fluorescence properties of **48** were observed, suggesting the importance of the boronic acid moiety in **48** for the binding of copper(II) ions (Figure 64). As another control, the simple boronic acid derivative **50** without the imine metal recognition site was investigated with Cu^{2+} under the same conditions. In this system fluorescence quenching was not observed, which indicates that the imine group plays a role in the coordination of Cu^{2+} (Figure 65).[146] This suggests that the boronic acid and Schiff base work together to bind copper (II) ions in polar environments. A Job plot indicates that the binding of **47** with Cu^{2+} has 2: 1 stoichiometry (Figure 66). Further analysis of mass spectra and single crystal data is needed for the proposed binding mode.

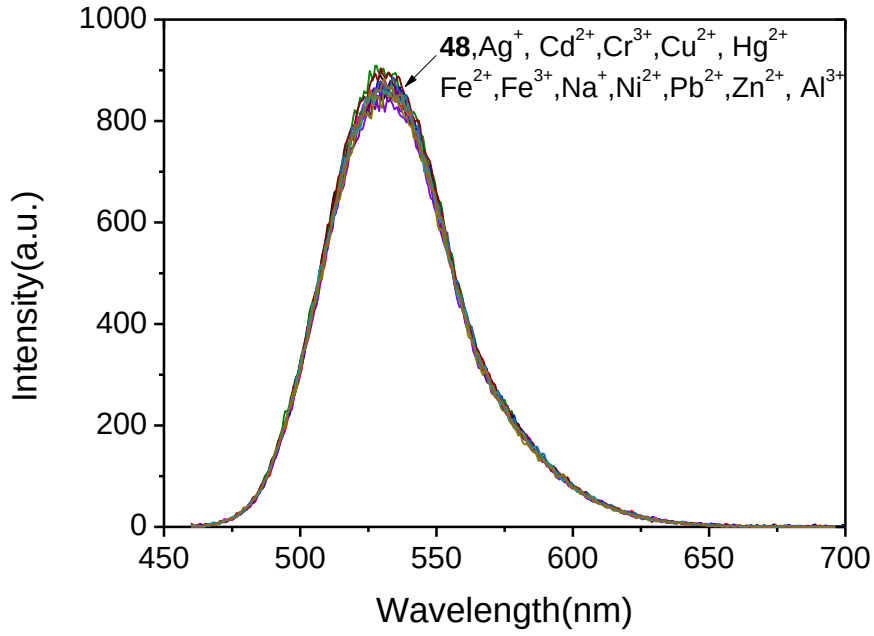

Figure 64 Emission spectra of control **48** upon addition 10 equiv. various metal ion with excitation wavelength at 450 nm in methanol. The concentration of **48** was 10 μM.

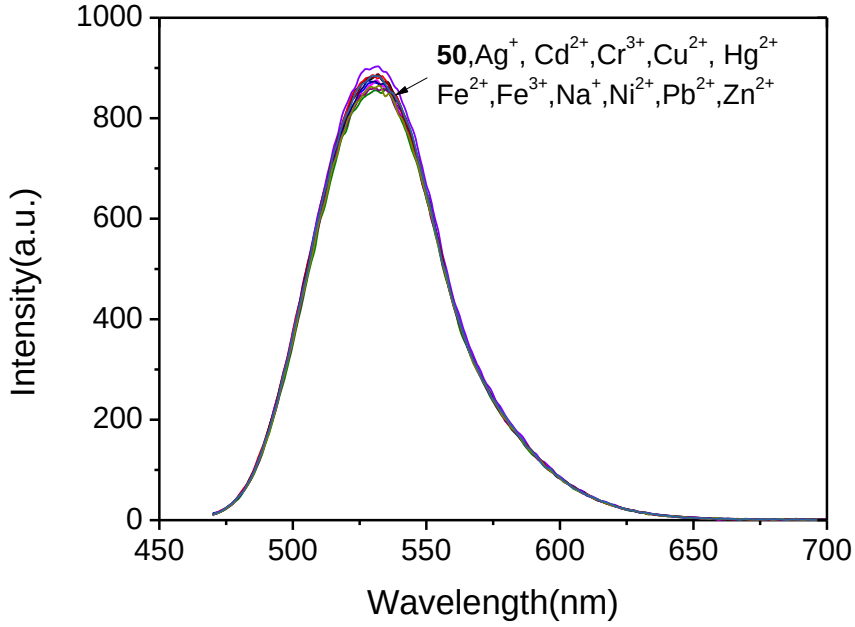

Figure 65 Emission spectra of control compound **50** upon addition 10 equiv. various metal ion with excitation wavelength at 450 nm in methanol. The concentration of **50** was 10 μM.

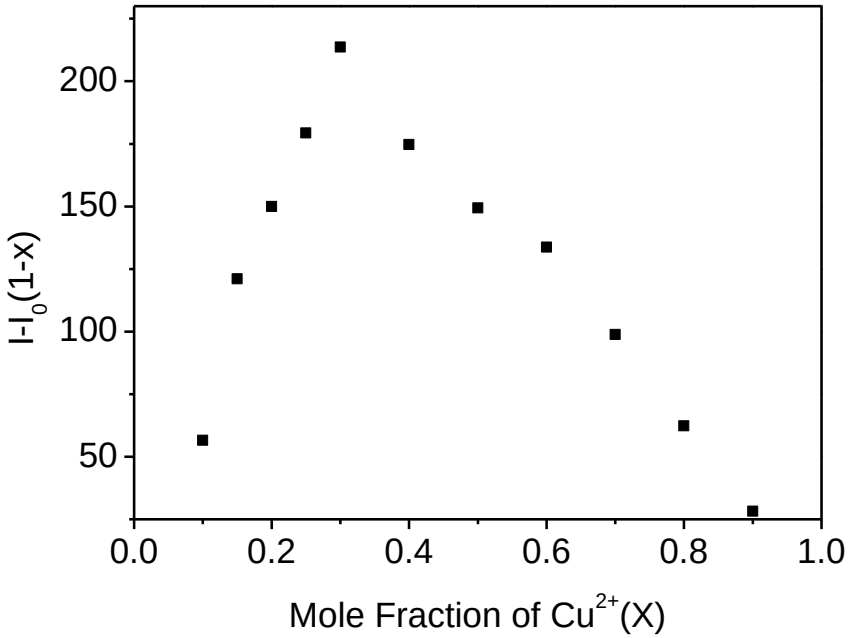

Figure 66 The Job's plot of sensor **47** in methanol. The total concentration of sensor **47** and Cu^{2+} is 20.0 μM.

2.4 Summary of Chapter 2

A robust naphthalimide based fluorescence sensor bearing a monoboronic acid group and its reference compounds were developed. The potential abilities of these compounds for recognising metal ions were investigated. The sensor displays high selectivity for copper(II) ions in living cells, which is one of the few examples of boronic acid based fluorescent chemosensors as a copper(II) binding site. With this research we demonstrated that boronic acids can be used to bind metal ions as well as diols. The chelate, **47**-Cu^{2+}, displayed fluorescence enhancement with fructose, and the system could be described as a fluorescence INHIBIT logic gate. We believe that these results will be of particular interest for the further development of the next generation of molecular ion sensory systems.

CHAPTER THREE

Results and Discussion

Published - Li, M., Wu, X., Wang, Y., Li, Y., Zhu, W. and James, T. D., A near-infrared colorimetric fluorescent chemodosimeter for the detection of glutathione in living cells. *Chem. Comm.* 2014, **50 (14)**, 1751-1753.

3 Results and Discussion: Fluorescent Chemodosimeters Based on Dicyanomethylene-4*H*-pyran Chromophore for Glutathione Recognition

3.1 Background

3.1.1 The Importance of Biothiols

Biothiols such as glutathione (GSH), cysteine (Cys), and homocysteine (HCys) play a crucial role in maintaining appropriate redox homeostasis in biological systems.[147, 148] GSH, the most abundant cellular thiol, is of great importance in cellular defence against toxins and free radicals.[149] Changes in the level of GSH concentration has been correlated with various diseases, such as AIDS, leukocyte loss, liver damage, cancer and neurodegenerative diseases.[150] Therefore, much effort has been devoted to the development of efficient methods for the detection of GSH, which is of significant interest in the fields of chemical, environmental and biological sciences.[151, 152]

3.1.2 Dicyanomethylene-4H-pyran (DCM) Chromophore

Compared to the nathalimide fluorophore, DCM chromophores have a typical donor-π-acceptor (D-π-A) structure with a broad absorption band resulting from an ultra-fast internal charge-transfer (ICT) process[8] (Scheme 6), which have several strengths such as: (i) high sensitivity to electron disturbance; (ii) long emission wavelength; and (iii) high fluorescence. In 1989, Tang and coworkers were the first to introduce a DCM derivative as a highly fluorescent dopant in organic electroluminescent diodes (OLEDs).[71] Up to now, a variety of DCM derivatives have drawn much attention due to their excellent optical-electronic properties and different structural modification.

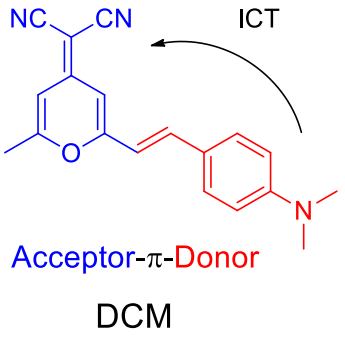

Scheme 6 Schematic diagram of an ICT process in a DCM chromophore.

3.2 Aim and Objective

Previous studies have demonstrated that Dicyanomethylene-4*H*-pyran (DCM) chromophore is a near-infrared fluorophore, which has many beneficial photophysical properties. Though the dicyanomethylene-4*H*-pyran (DCM) chromophore has been shown to be a good reporter for chemosensing applications, few DCM fluorophore based sensors were reported for redox species. Within this project, two 2,4-dinitrobenzenesulfonyl (DNBS)-containing and boronic acid-containing dicyanomethylene-4*H*-pyran (DCM) probes were synthesised. Using the specific redox reaction of GSH, in order to release the phenolate moiety of the DCM, which facilitates charge transfer and results in fluorescence turn on and longer wavelength of spectral changes. The application of the sensor for detection of glutathione can also be used in cellular imaging experiments.

3.3 Investigations on Thiols Sensing

*3.3.1 Synthesis of Compound **53***

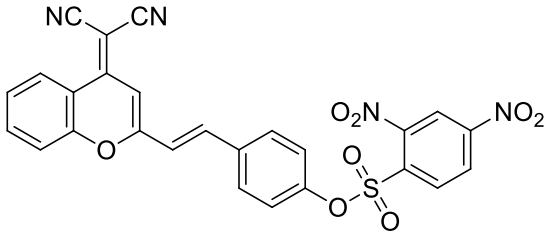

53

Figure 67 Structure of target compound **53**.

Compound **53** (Figure 67) was synthesised following literature procedure,[153] the synthetic route shown in Scheme 7. The intermediate **52** was synthesised by refluxing 2-(2-methyl-4H-chromen-4-ylidene)malononitrile **51** and 4-hydroxybenzaldehyde in toluene overnight, which is a typical Knoevenagel-type condensation reaction. A Dean-Stark head was used to remove the byproduct water, which could increase the reaction yield. Acetic acid and piperidine were employed as the catalysts, which is an acid under base catalysing. After completion of this reaction, the mixture was evaporated under vacuum and the crude products were purified by chromatography with 40% yield. From the ^{1}H NMR spectrum, the emergence of the peak at 10.16 ppm implied the completion of this reaction. Next, the target compound **53** was synthesised through sulfate formation. Intermediate **52** was dissolved in dry CH_2Cl_2 and 0.5 ml pyridine was added. The mixture was then cooled to 0℃ and a solution of 2,4-dinitrobenzensulfonyl chloride in dry CH_2Cl_2 was added dropwise. After being stirred at 0℃for 30 minutes, the mixture continues to stir at room temperature for 3h. After the completion of the reaction, the mixture was evporated under reduced pressure and the residue was purified using column chromatography. The disappearance of the peak at 10.16 ppm and the emergence of the peaks around 8.4 - 9.9 ppm in the ^{1}H NMR spectrum implied the completion of this reaction.

Detail experimental reaction conditions and full characterisations of all these compounds were listed in Chapter 7 of the thesis (Experimental).

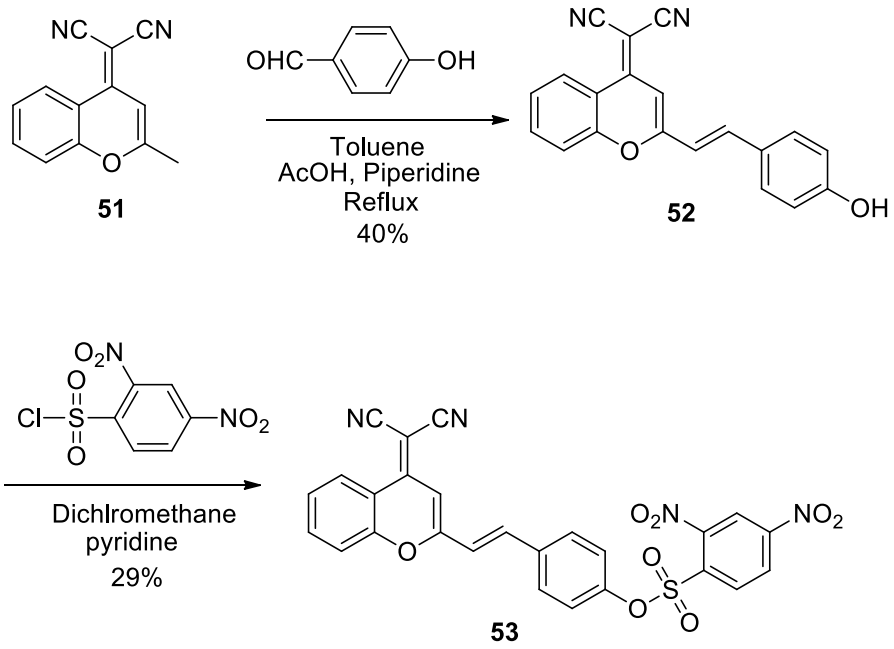

Scheme 7 Synthetic route of Compound **53.**

3.3.2 UV Absorption and Fluorescence Emission Measurements

Initially, UV-*vis* absorption of probe **53** was investigated. Probe **53** has an intense absorption at 414 nm (Figure 68a) in DMSO/ PBS buffer solution (pH = 7.4, 50/ 50, v/v) at 37 ℃. With the addition of GSH, the colour of the solution turned from slight yellow to pink, which was clearly recognisable by the naked eye. At the same time, a concomitant increase of a new absorption band at 560 nm was observed with an isosbestic point at 446 nm. As illustrated in Figure 68a, due to the specific O-S cleavage, a distinct 146 nm red shift in absorbance was observed (Scheme 8). Since the phenolate group is a much stronger electron donor than the sulfonate group, the ICT efficiency should be significantly enhanced by the interaction of probe **53** with GSH and thus shift the absorption to a longer wavelength.

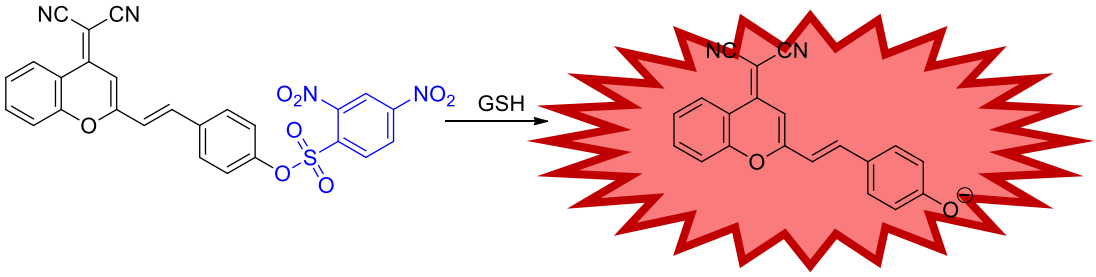

Scheme 8 Synthesis of probe **53** and GSH-promoted release of **52**$^{-}$.

Subsequently, the fluorescence spectra of probe **53** in the absence and presence of GSH was measured. The probe alone exhibits almost no emission when excited at 560 nm and no distinct variations are observed over time, suggesting that probe **53** is stable and has no tendency to convert into **52**$^{-}$ under the measurement conditions. In the presence of GSH, however fluorescence at 690 nm was dramatically enhanced (Figure 68b). The departure of the electron-withdrawing DNBS moiety *via* a GSH-induced O-S bond cleavage releases **52**$^{-}$, which possesses strong ICT and induces a turn-on NIR fluorescence response with high off/on ratio. On the other hand, the large Stokes shift of ~130 nm is important in decreasing the background fluorescence andenhancing the signal fidelity. Moreover, the response rate of **53** to GSH was tested by time-course fluorescence measurement. In the presence of GSH, the fluorescence intensity at 690 nm increases gradually and reaches a plateau after about 5 min (Figure 69), indicating the end of the reaction. Furthermore, the fluorescence intensities at 690 nm follows a

linear relationship (R = 0.98) within the GSH concentrations from 1 to 10 μM, and the detection limit was evaluated to be 1.8 × 10^{-8} M, indicating that probe **53** is particularly sensitive to the detection of GSH (Figure 70).

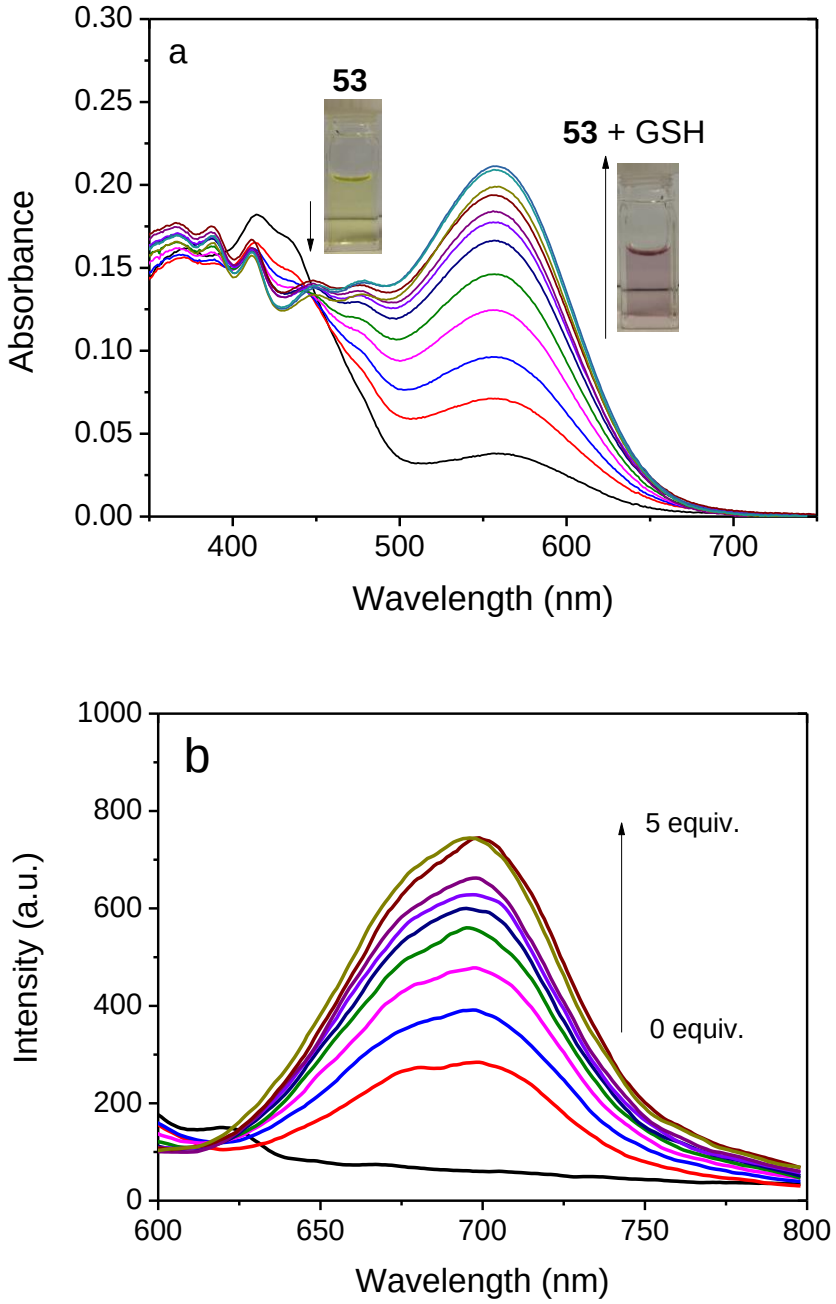

Figure 68 a) Absorption spectra of probe **53** (1 × 10^{-5} M) in the presence of different concentrations of GSH (0, 0.1, 0.2, 0.3, 0.4, 0.5, 0.6, 0.7, 0.8, 1.0, 2.0, 5.0 equiv.) in a mixture of DMSO–water (50: 50, v/v) with a PBS buffer solution (10 mM, pH = 7.4). Insets: colour changes of probe **53** upon additions of GSH (5 equiv.). (b) Fluorescence spectra of probe **53** (1 × 10^{-5} M) in the presence of different concentrations of GSH when excited at 560 nm.

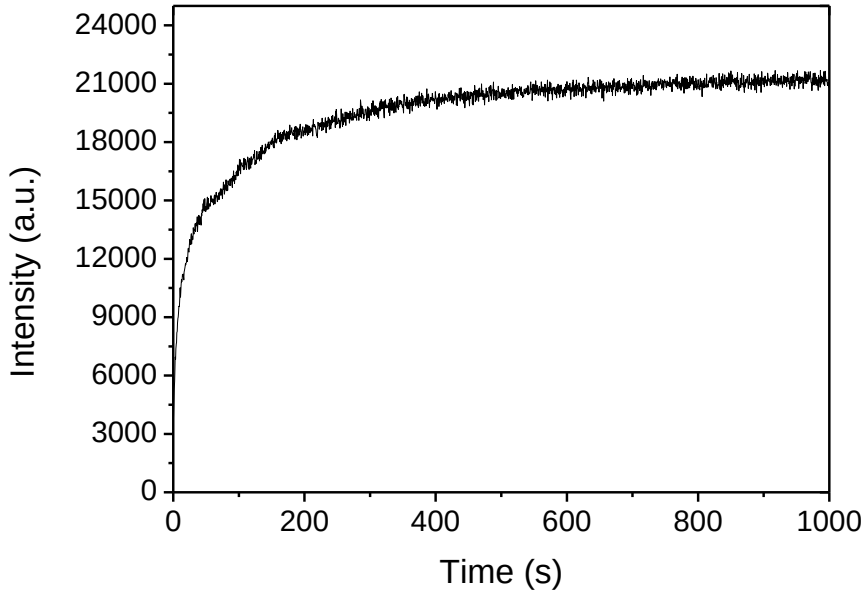

Figure 69 Kinetics of fluorescence enhancement profile of probe **53** (1×10^{-5} M) at 690 nm in the presence of GSH (5 equiv) upon excitation at 560 nm. All fluorescence changes were measured at 37 ℃ in PBS buffer (pH 7.4).

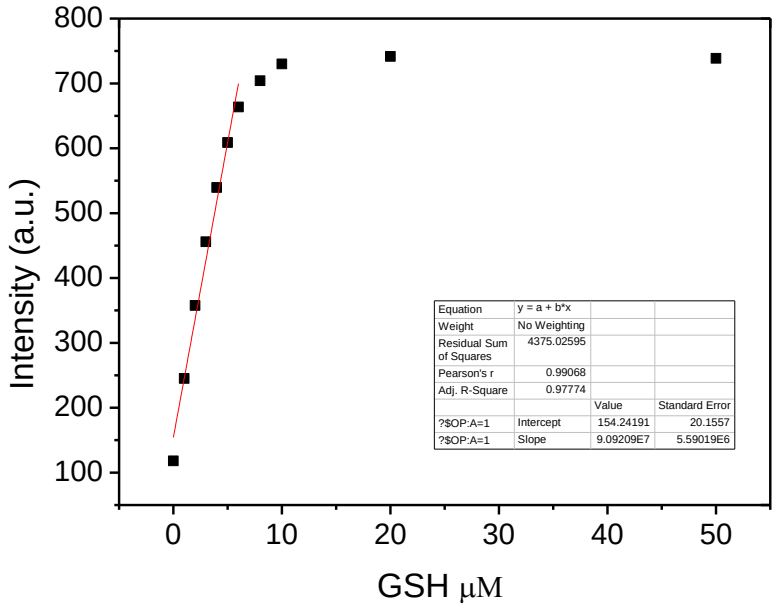

Figure 70 Response of fluorescence signals to GSH concentrations, a linear regression curve was then fitted to these fluorescent intensity data. The Standard Deviation was obtained by fluorescence responses to be σ = 0.5327, therefore, the detection limit was calculated by the formula ($3\sigma/k$) and gave a result as 1.8×10^{-8} M.

The results above were achieved at the excitation of 560 nm, which is the maximum absorption wavelength. However, when probe **53** is excited at the isobestic point (446 nm, Figure 71) a fluorescence increase at 581 nm is observed and is ascribed to release of the DNBS quenching group. Conversely, when probe **53** is excited at 560 nm the large observed increase in fluorescence at 690 nm is due to the fluorescence of the **52**$^{-}$ produced on cleavage of the DNBS from probe **53**.

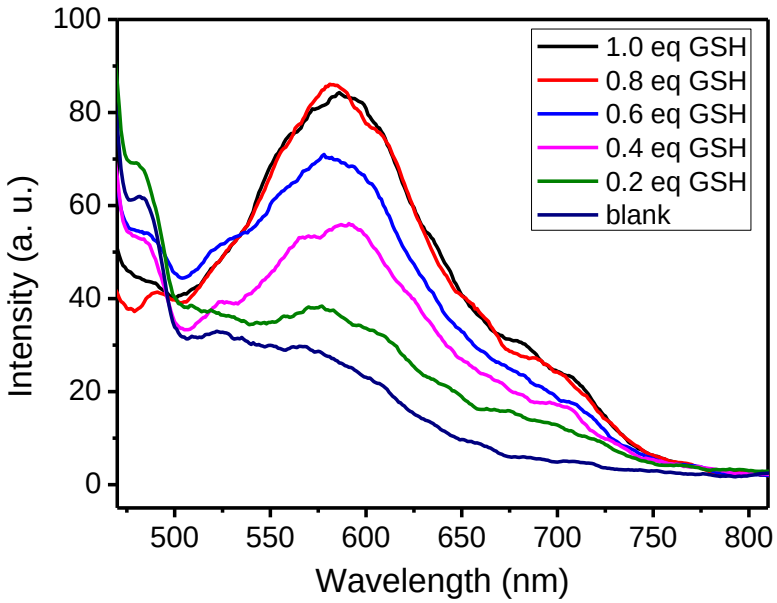

Figure 71 Fluorescence spectra of probe **53** (1×10^{-5} M) in the presence of different concentrations of GSH when excited at 446 nm.

3.3.3 Selectivity Screen

To evaluate the selectivity of the developed probe **53** for sulfydryl-containing species, a series of amino acids were examined. Not surprisingly, except for GSH, probe **53** shows similar response to other sulfhydryl-containing compounds such as cysteine, homocysteine, dithiothreitol, while no measurable fluorescence enhancement could be triggered by the treatment of other amino acids (Figure 72). In fact, the plausible disturbance of DTT, Cys and Hcy can be neglected due to their relatively low concentrations in biological system.

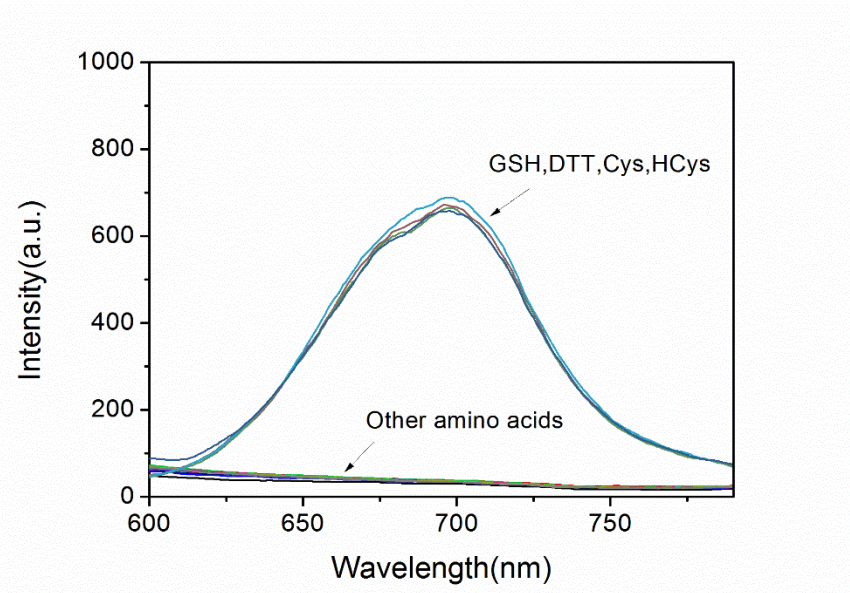

Figure 72 Fluorescence spectra of probe **53** in absence and presence of various amino acids and GSH, DTT, Cys, HCys in a mixture of DMSO-water (50: 50, v/v) with a PBS buffer solution (10 mM, pH = 7.4) The amino acids are: arginine, threonine, serine, isoleucine, asparaginic acid, sarcosine, valine, glutamine, tryptophan, glutamic acid, proline, leucine, histidine, glycine, phenylalanine, alanine, asparagine, methionine.

*3.3.4 pH Dependency of Compound **52** and **53***

The fluorescence of **52** may be sensitive to pH value because of the phenolic group; therefore, the effect of pH on the photophysical properties of **52** was investigated (Figure 73). And probe **53** was then investigated (Figure 75). As illustrated, we believed that the probe is quite stable in aqueous media up to pH 8, whereas **52** displays a corresponding fluorescence enhancement in the pH range of 5.7 - 8.0, which clearly demonstrates that the fluorescence response of probe **53** in the physiological pH range is due to the presence of thiols and verifies the generation of **52**$^{-}$ after the treatment with GSH. Therefore, we decided to employ the probe for fluorescent imaging of cellular thiols. The pK_a of **52** was calculated as 8.70 (Figure 74).

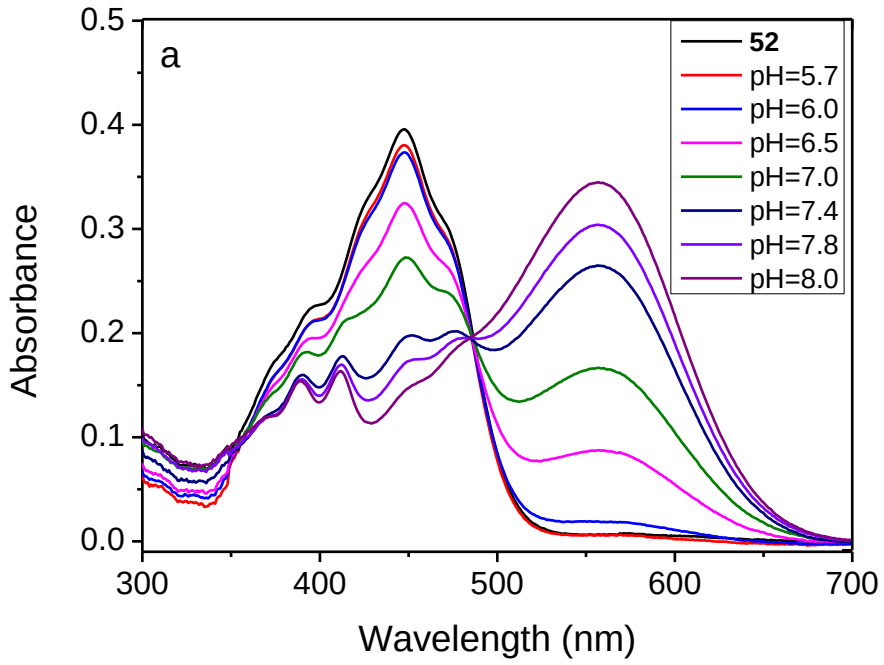

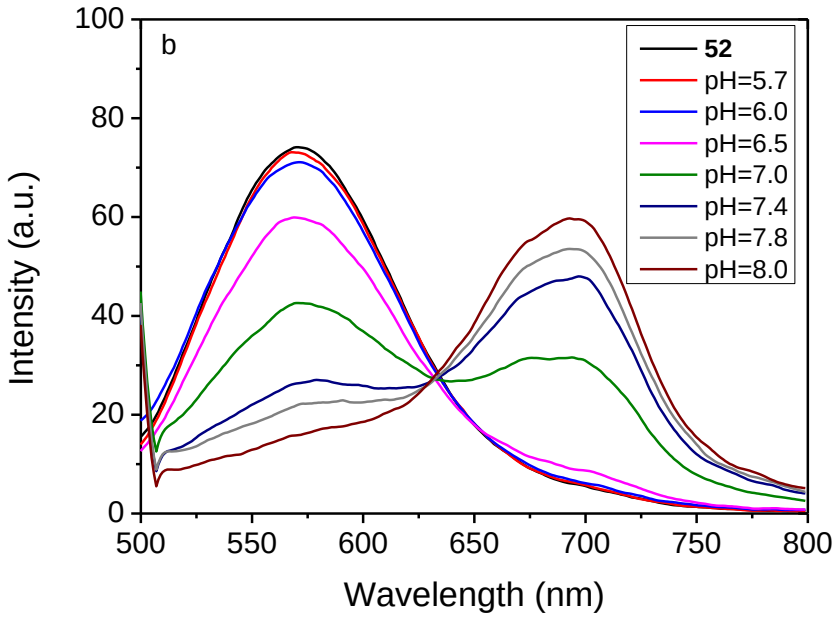

Figure 73 (a) Absorption spectra of **52** in buffer solution as a function of pH. (b) Corresponding emission spectra (λex = 486 nm). The pH was adjusted by NaH_2PO_4 and Na_2HPO_4.

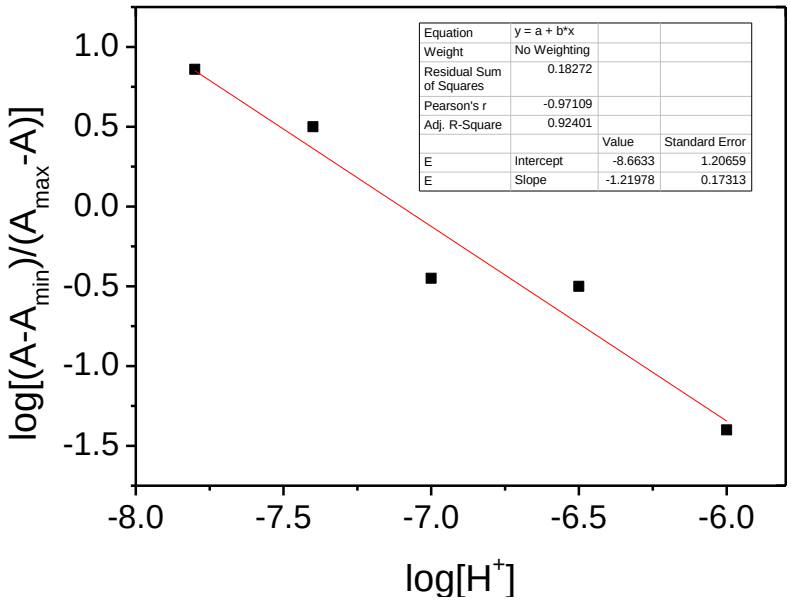

Figure 74 pH-dependent absorbance calculation at 557 nm of **52**. The pKa of **52** was calulated using: log[(A - Amin) / (Amax - A)] = log[Ka]+ nlog [H+], giving a pKa of 8.70 in terms of the intercept.

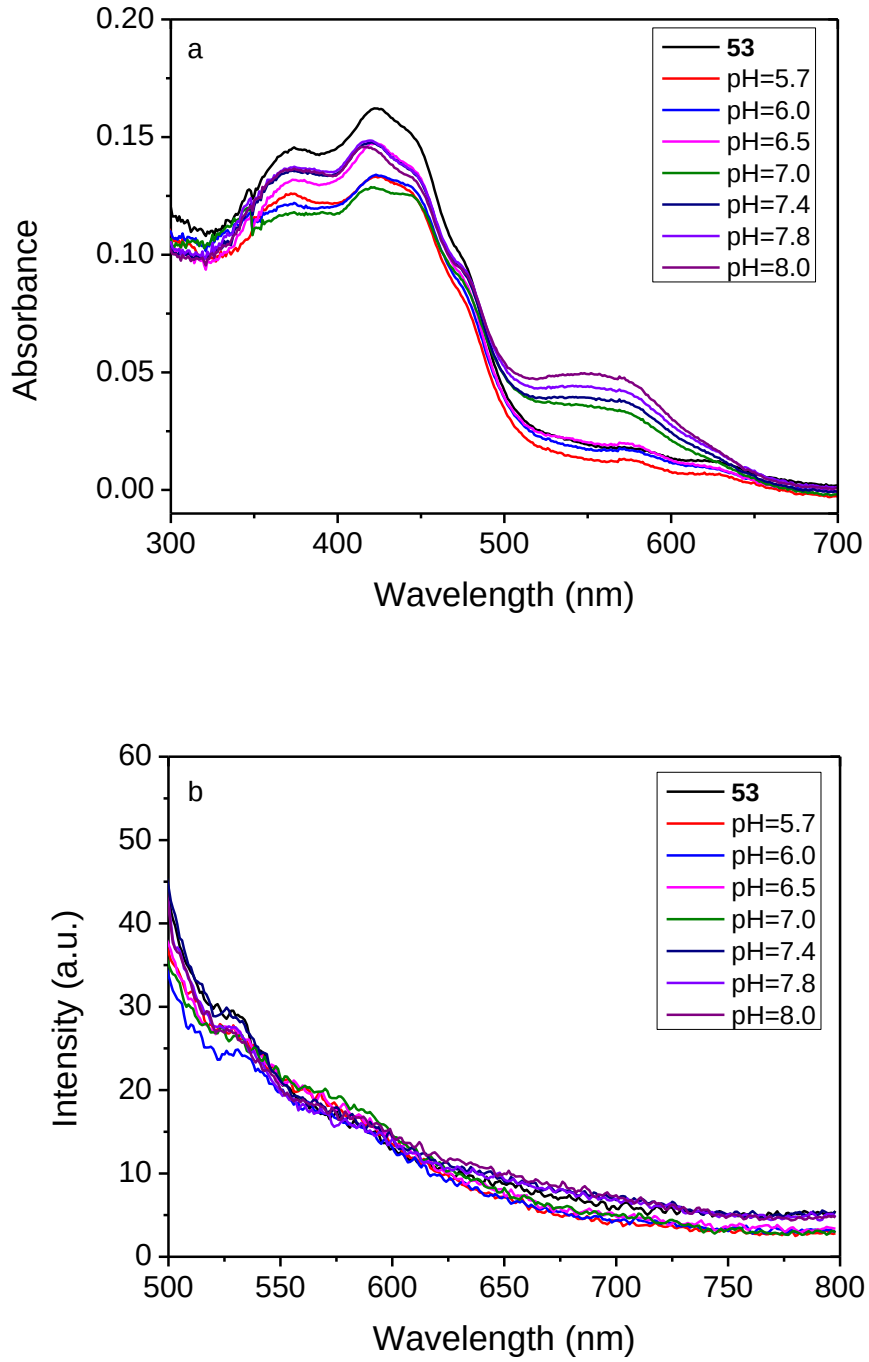

Figure 75 (a) Absorption spectra of probe **53** in buffer solution as a function of pH. (b) Corresponding emission spectra (λex = 486 nm). The pH was adjusted by NaH_2PO_4 and Na_2HPO_4.

3.3.5 Sensing Mechanism

A number of sensing mechanisms have been employed for thiol detection, including Michael addition,[154] to –CHO attached fluorophores,[155] and deprotection of 2,4-dinitrobenzenesulfonyl (DNBS), [59, 156, 157] *etc*. Among them, the DNBS group is especially preferable as an efficient recognition unit for thiols due to its unique sensitivity and high reactivity toward thiolate anions with OFF-ON signalling. To gain insight into the sensing mechanism, mass spectral analysis was performed. The reaction between probe **53** and GSH that occurred by the cleavage of O-S with the release of **52**$^{-}$ was confirmed by the peak of 311.0828 in the mass spectrum (Figure 76). The other peaks at 424.7963 and 500. 8092 could be impurities.

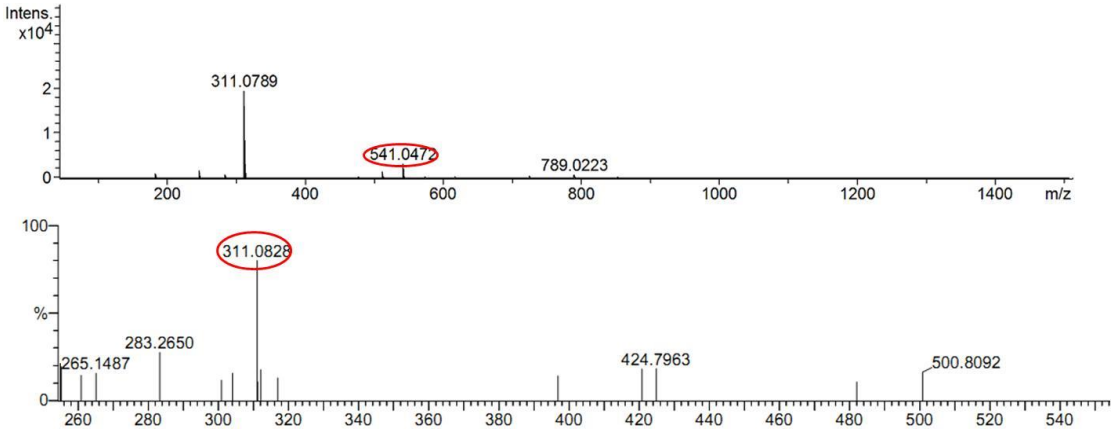

Figure 76 Mass spectra of probe **53** and probe **53**+ GSH systems.

3.3.6 Cell Imaging Application

The ability of probe **53** to detect GSH in HeLa cells was examined with the use of a confocal fluorescence microscope (Figure 77). HeLa cells were cultured in RPMI 1640 supplemented with 10% FCS and then incubated with 10% fetal bovine serum followed by 20 μM of probe **53** in PBS for 30 min. 2.5% DMSO was used in the cell culture process. Bright-field measurements confirmed that the cells after treatment with probe **53** were viable throughout the imaging experiments, indicating the superior biocompatibility of probe **53**. After the co-culture with probe **53**, the intracellular NIR fluorescence could be detected. The overlay of fluorescence and bright-field images indicates that the fluorescence localises mainly in the cytosol, indicative of the subcellular distribution of GSH and excellent membrane permeability of probe **53**. In contrast, cells that are not treated with probe **53** display nearly no fluorescence, verifying the fluorescence source of the **53**-treated cells. Moreover, the images also indicate that the probe has low toxicity since the cellular morphology is maintained. With this bioimaging experiment we have demonstrated the potential of probe **53** for the imaging of GSH in living cells.

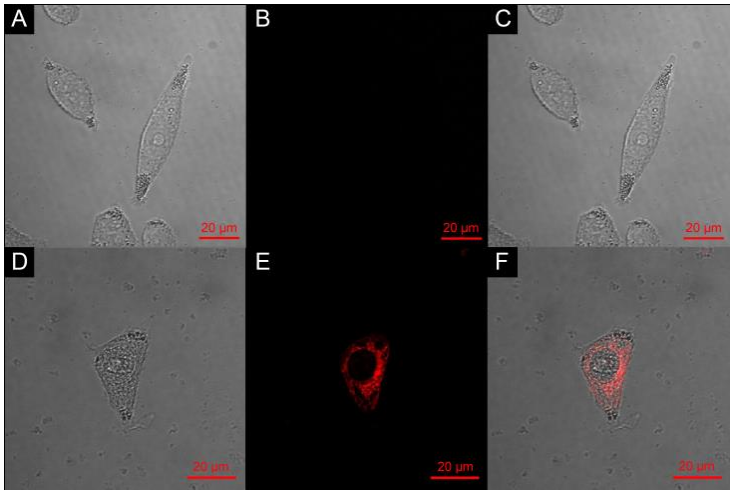

Figure 77 Confocal fluorescence images in HeLa cells: Top, (A–C) cell incubated without probe **53**. Bottom,(D–F) cell incubated with probe **53** (20 μM) for 0.5 h. Emission was collected at 660–740 nm upon excitation at 488 nm. Bright field (A and D), fluorescence (B and E) and overlap field (C and F).

3.4 Summary of Chapter 3

The photophysical properties of the DCM core and its applications in glutathione recognition were presented.

In conclusion, we have designed and synthesised a NIR fluorescent chemodosimeter for GSH based on the DCM framework, showing a subcellular distribution of GSH and good cell membrane permeability. The fluorescence enhancement mechanism is based on the cleavage of DNBS from the fluorophore by GSH, which switches the dark excited state to an emissive excited state. Probe **53** displays a colour change from yellow to pink upon addition of GSH, and thus can serve as a ‘‘naked-eye’’ probe for GSH. Furthermore, we have also demonstrated that the probe can be used for the fluorescent imaging of cellular thiols. Since our DCM based system is very easy to prepare with long emission wavelength, high photo-stability, we believe that it will become the probe of choice for biological applications.

CHAPTER FOUR

Results and Discussion

Published - Li, M., Xu, S., Gross, A. J., Hammond, J. L., Estrela, P., Weber, J., Lacina, K., James, T. D., Marken, F., *ChemElectroChem*, 2015, Ferrocene-Boronic Acid – Fructose Binding Based on Dual-Plate Generator-Collector Voltammetry and Square-Wave Voltammetry. DOI: 10.1002/celc.201500016.

Acknowledgment – Cooperation with Dr. Andrew Gross for dual-plate microtrench voltammetry and help with DigiElch simulation are gratefully acknowledged.

4 Results and Discussion: Ferrocene-Boronic Acid – Fructose Binding Based on Dual-Plate Generator-Collector Voltammetry and Square-Wave Voltammetry

4.1 Introduction to Ferrocene-Boronic Sensing for Saccharides

Boronic acids have emerged as key components in analytical processes and devices,[158] for example for the detection and monitoring of glucose levels[82] and for the separation of glycated and glycosylated proteins,[87] both of which are applications with considerable potential for impact in medicinal technologies. Chemically, boronic acids are attractive due to their capability to reversibly form bonds to diols,[43] quinols,[159] α-hydroxy-carboxylates,[160] and a range of other hard nucleophiles, in particular fluoride[93] and phosphate.[161] New types of boronic acids have been developed to report binding events *via* fluorescence response[162] or *via* electrochemical response[163] for operation in more opaque or non-transparent media. The ferrocene-boronic acid compound (Figure 78) may be regarded as the prototypical electrochemical "reporter" system.[105, 164, 165]

Most electrochemically active boronic acid systems have a structurally defined "redox" moiety and a separate "boronic receptor" moiety without strong interaction between the two. As a result, the electrochemical signal is not strongly affected upon binding (only the diffusion coefficient changes; no significant changes in midpoint potential are observed). However, in ferrocene-boronic acid a stronger "coupling" occurs with the Fe(II/III) redox state directly affecting the binding kinetics and binding energies. The classic "square scheme" mechanism in Figure 78 can be applied (although further complexity due to intermediates and ternary complexes for example with phosphate clearly exists).[166]

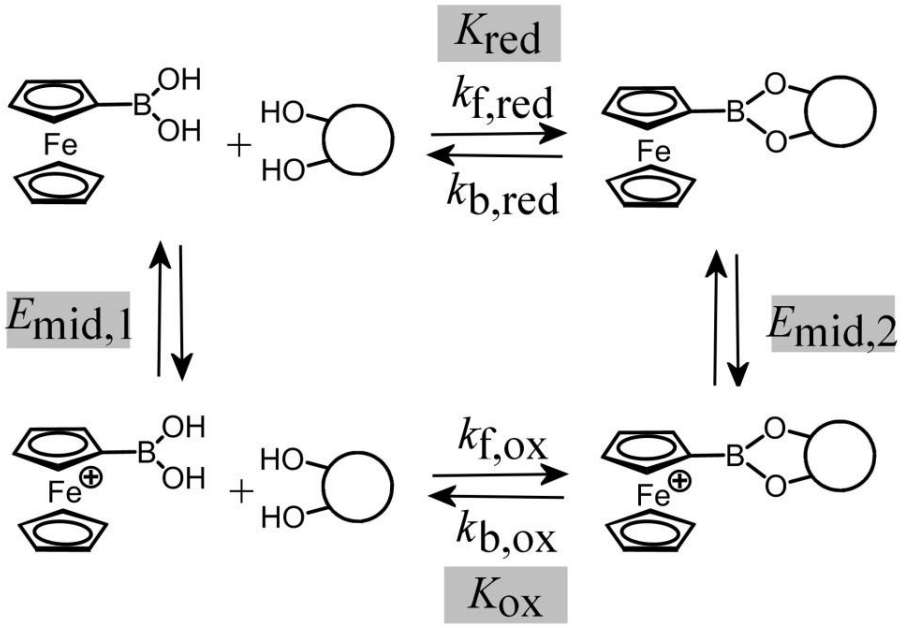

Figure 78 Schematic representation of the "square scheme" mechanism[167] for binding of fructose to ferrocene-boronic acid in two different redox states.

4.2 Aim and Objective

The fact that the ferrocene-boronic redox signal can be employed directly to report on fructose (or other saccharides) binding is of interest and the conditions required for two distinct signals to be detected are important. Therefore, in this chapter the binding process is investigated with two voltammetric methods: a "steady state" method (dual-plate generator-collector voltammetry)[168, 169] and a method that is "transient" in nature (square wave voltammetry).[170] The abilities of these two experimental tools to distinguish and quantify "bound" and "unbound" ferrocene-boronic acid are compared.

When detecting two distinct voltammetric signals associated with "unbound" and "bound" configurations, it may be tempting to interpret these signals in terms of equilibrium concentrations and binding constants (K_{red}, K_{ox}). However, within the limit of fast experimental tools, it is more likely that the rate of binding is responsible for the splitting and magnitude of the voltammetric responses ($k_{f,ox}$, $k_{f,red}$). In order to dissect and determine the true binding constants (as a function of pH), deeper analysis of data is required. In the (simplified) scheme in Figure 78 there are 5 unknown parameters (two midpoint potentials and four rate constants minus one thermodynamic relationship linking these, *vide infra*) all of which are shown to be relevant. Data have been analysed for pH 7, 8, and 9 to demonstrate distinct trends in the interaction of fructose to ferrocene- and ferricenium-boronic acid.

4.3 Investigations on Fructose Binding

4.3.1 Fabrication and Calibration of Pt-Pt Dual-Plate Electrodes and the Diffusion Coefficient Determination

Platinum-platinum (Pt-Pt) dual-plate micro-trench electrodes were fabricated following a previously reported protocol.[171] Glass slides were plasma treated (Oxford Instruments PlasmaPro 100) prior to deposition to improve adhesion. Using an electron beam evaporator (Edwards FL-400) a 50 nm Ti adhesion layer followed immediately by 150 nm Pt (99.99% purity; Testbourne) were deposited at 10^{-6} torr through a custom stainless steel shadow mask (Tecan). Film thicknesses were confirmed using a mechanical contact profilometer (Dektak 6M). The glass slide was subsequently cut into 8 mm x 25 mm Pt substrates using a diamond cutter (Buehler, Isomet 1000 precision saw) then cleaned by rinsing with demineralised water and heat-treatment at 450 ℃. The dual-plate electrode was prepared by spin-coating a single layer of SU-8-2002 photoresist (MicroChem) onto two individual Pt substrates at 500 rpm for 15s then 3000 rpm for 30s. Next, the two electrodes were pushed together, vis-à-vis, then placed onto a hot plate at 90 ℃ for 2 minutes. The temperature was then ramped to 160 ℃ and held for a further 5 minutes. After cooling to room temperature, the end of the dual-plate electrode was sliced using the diamond cutter. The electrode was then immersed in Piranha solution (1:5 v/v H_2O_2:H_2SO_4; *Warning: Piranha solution is highly corrosive and appropriate precautions are needed*) for 30 min to etch the photoresist to give a micro-trench with dimensions of width = 2.5 mm and inter-electrode gap, δ = 5 μm (Figure 79). After etching, the electrode was rinsed with demineralised water then dried with a stream of nitrogen gas, and copper tape was applied to give two electrode contacts.

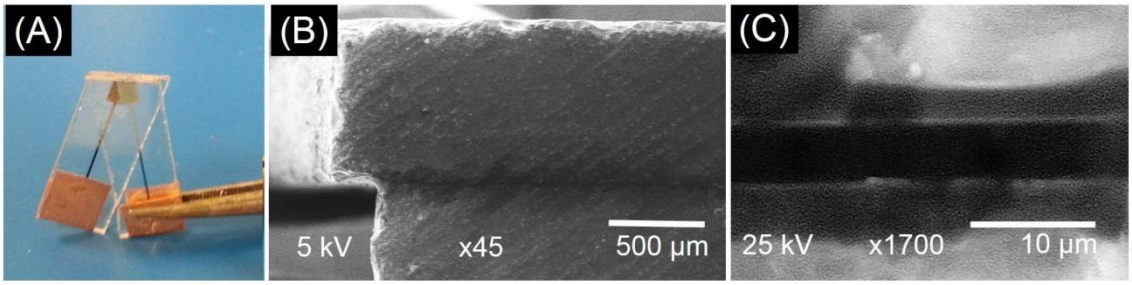

Figure 79 (A) Photograph of the Pt-Pt dual-plate micro-trench electrode. (B,C) Scanning electron microscopy images of the 2.5 mm long and 5 µm wide inter-electrode gap.

In order to estimate the depth of the Pt-Pt dual-plate electrode system, calibration voltammetric responses were recorded using the $Ru(NH_3)_6^{3+/2+}$ redox system (1 mM) in aqueous 0.1 M KCl (Figure 80B). From the mass transport controlled limiting current obtained, 0.7 µA, and assuming equal diffusion coefficients for $Ru(NH_3)_6^{3+}$ and $Ru(NH_3)_6^{2+}$ ($D = 0.9 \times 10^{-9}$ m^2s^{-1}),[172] the approximate depth can be obtained as 16 µm (see equation 1).[173]

$$depth = \frac{I_{\text{lim}} \times \delta}{nFDc \times length} = 16\mu m \qquad (1)$$

In this equation I_{lim} is the limiting current, δ is the inter-electrode gap, n is the number of electrons transferred for each molecule diffusing to the electrode surface, F is the Faraday constant, D is the diffusion coefficient, c is the bulk concentration, and *length*/*depth* refer to the micro-trench length and depth.

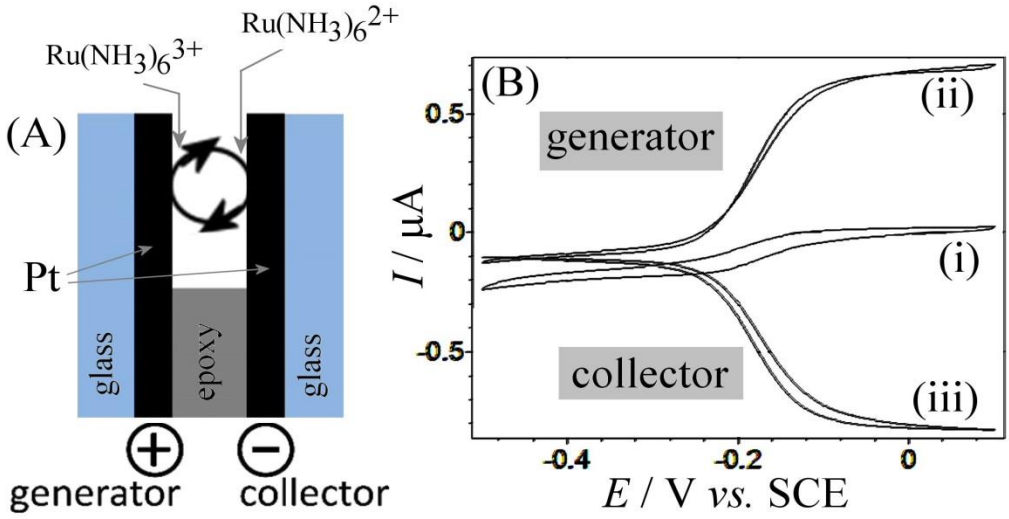

Figure 80 (A) Schematic drawing of the Ru(II/III) redox couple in the Pt-Pt dual-plate generator-collector experiment. (B) Cyclic voltammograms (scan rate 20 mVs^{-1}) for the reduction of 1 mM $Ru(NH_3)_6^{3+}$ in aqueous 0.1 M KCl (i) with only one electrode connected and (ii/iii) with both generator and collector working electrodes connected (collector potential = -0.5 V vs. SCE).

Rotating disk voltammetry experiments were performed with an RDE710 rotating electrode system (Gamry instruments) using a 4.57 mm diameter platinum disk at 22 ± 2 ℃. Voltammograms were recorded in 1 mM ferrocene-boronic acid in 0.1 M phosphate buffer pH 7 at a scan rate of 10 mV s^{-1}. The experimentally determined diffusion coefficient $D = 0.5 \times 10^{-9}$ cm^2 s^{-1} based on the Levich plot below (Figure 81).

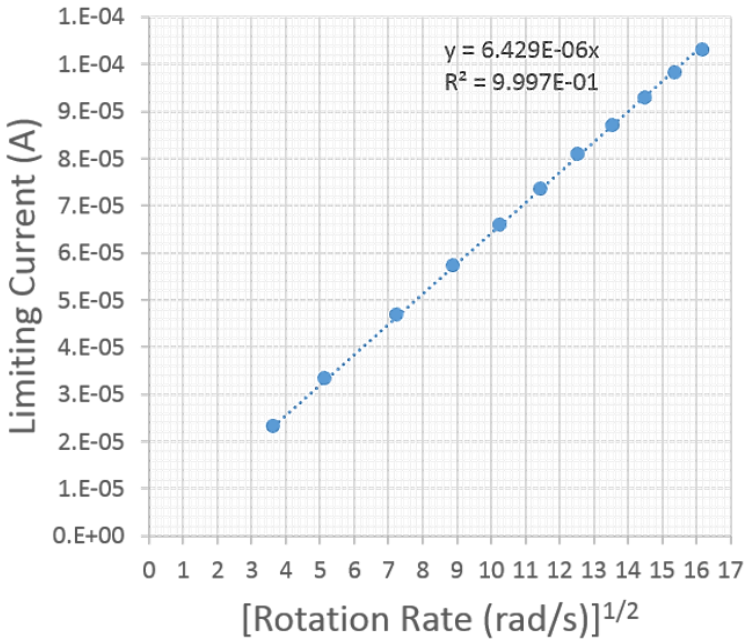

Figure 81 Levich plot for 1 mM ferrocene-boronic acid in 0.1 M phosphate buffer pH 7 at 22 ± 2°C.

4.3.2 Steady State Dual-Plate Generator-Collector Micro-Trench Voltammetry

The oxidation of ferrocene-boronic acid in 0.1 M phosphate buffer pH 7 occurs with a midpoint potential (E_{mid} = ½ E_{ox} + ½ E_{red}) of 0.14 V vs. SCE (Table 1) and is seen as an oxidation at the generator electrode and a corresponding reduction at the collector electrode (Figure 82A). Due to the collector potential being fixed at -0.3 V vs. SCE, the collector current signal is better defined and employed here for further analysis. Upon addition of fructose a new more negative voltammetric signal emerges at E_{mid} = -0.04 V vs. SCE and this can be attributed to a boronic acid - fructose complex ($E_{mid,2}$ < $E_{mid,1}$).[174, 175] When formulating the equilibrium equations,[176] this is consistent with the oxidised ferricenium-boronic acid forming a stronger complex (K_{ox} > K_{red}, see equation 2).

$$RT\ln\left(\frac{K_{ox}}{K_{red}}\right) = -nF(E_{mid,2} - E_{mid,1}) \qquad (2)$$

On the molecular scale this may be attributed to a more electro-positive boron, but also changes in ion association energies (e.g. involving phosphate anion - ferricenium cation interactions) could contribute to this effect. The mass transport controlled limiting current in the absence of fructose is close to 0.5 A, which translates to an approximate diffusion coefficient of 0.5 × 10^{-9} m^2s^{-1} (equation 3).[177, 178] This value is not unreasonable for the free ferrocene-boronic acid and it has been verified by independent rotating disc voltammetry measurements (D = 0.5 × 10^{-9} m^2s^{-1} in 0.1 M phosphate buffer pH 7).

$$D = \frac{I_{lim} \times \delta}{nFc \times depth \times length} = 0.5 \times 10^{-9}\, m^2 s^{-1} \qquad (3)$$

With increasing fructose levels the mass transport controlled limiting current decreases naturally due to underlying changes in solution viscosity. The plot in Figure 82A shows a gradual decrease in collector current followed by a stronger decline from [fructose] = 160 mM onwards. The more pronounced decline in mass transport limited current coincides with the appearance of the signal at $E_{mid,2}$ and is therefore assigned to binding

of boronic acid to fructose. Similar data sets are presented for pH 8 and pH 9 in Figure 82B and 82C, respectively.

In order to better describe the boronic acid to fructose binding process, "kinetic domains" are introduced (Figure 82D). In domain I, both ferrocene-boronic acid and ferricenium-boronic acid are "free" and the limiting current is relatively high. It is only in domain II that the ferricenium-boronic acid will bind to fructose and thereby lower the rate of diffusion (the lower diffusion coefficient dominates the inter-electrode transport).[179] In domain III, the fructose concentration is so high that both ferrocene- and ferricenium-boronic acid bind (with little further change in the transport). The transition point from domain I to II (Figure 82) is consistent with the reaction layer, which is approximately given by $\delta_{reaction} = \sqrt{\frac{D}{k_f[fructose]}}$,[180] being equal to the inter-electrode gap of 5 μm. Approximate rate constant data for $k_{f,ox}$ can be obtained (Table 1) and a clear trend of an increasing $k_{f,ox}$ with increasing pH is observed. At a molecular level this can be interpreted for example in terms of a fast pre-equilibrium involving hydroxide or HPO_4^{2-}.

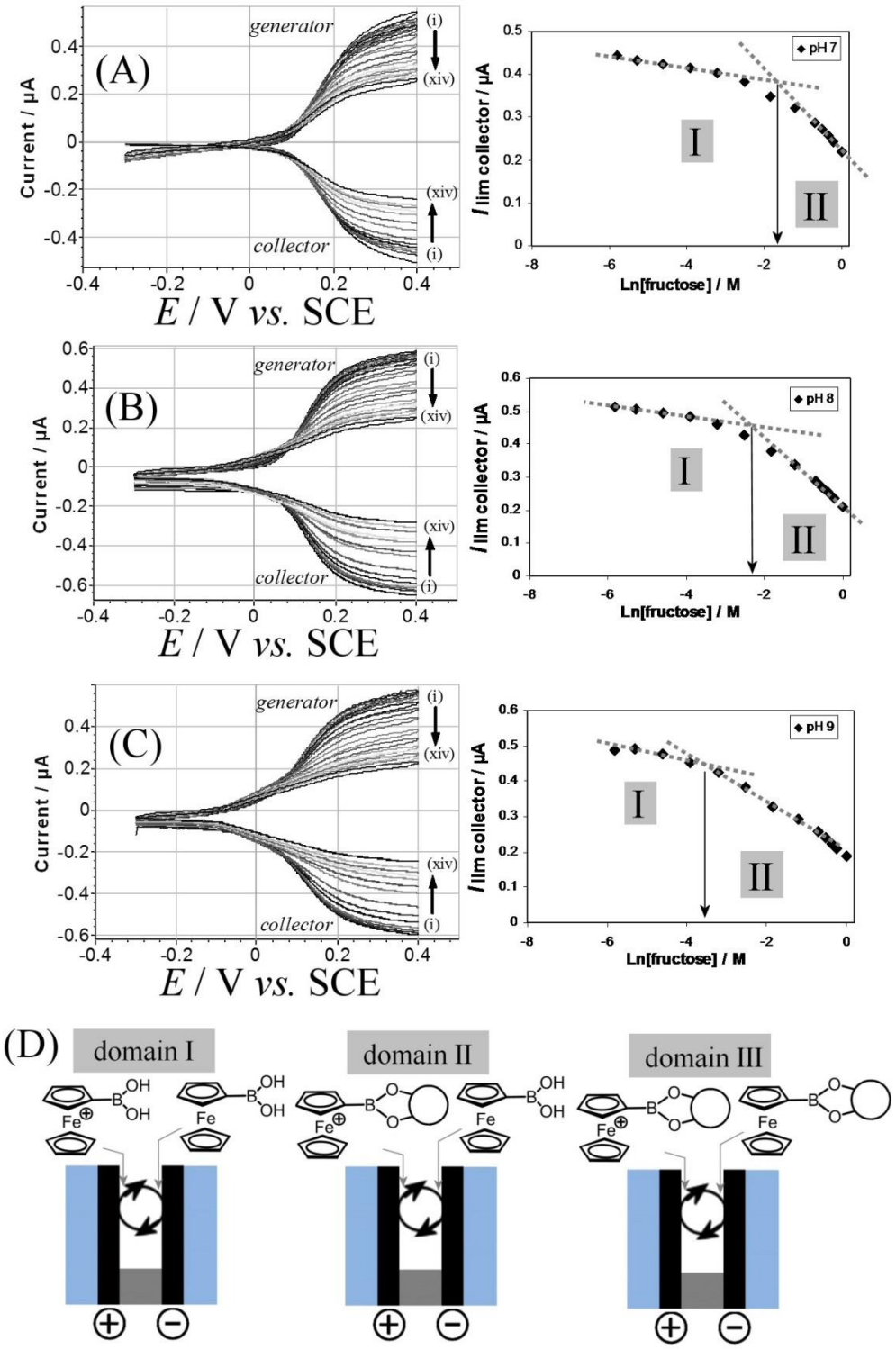

Figure 82 (A) Dual-plate generator-collector voltammograms (scan rate 20 mVs^{-1}, collector potential -0.3 V vs. SCE) for the oxidation of 1 mM ferrocene-boronic acid in 0.1 M phosphate buffer pH 7 with a fructose concentration of (i) 1, (ii) 3, (iii) 5, (iv) 10, (v) 20, (vi) 40, (vii) 80, (viii) 160, (ix) 300, (x) 500, (xi) 600, (xii) 700, (xiii) 800, and (xiv) 1000 mM. Plot of the collector limiting current versus logarithm of fructose concentration. (B) As above at pH 8. (C) As above at pH 9. (D) Schematic drawing of the redox cycle kinetic domains with (I) no fructose bound, (II) fructose binding to the ferricenium-boronic acid, and (III) fructose binding to both ferrocene- and ferricenium-boronic acid.

	$E_{mid,1}$ / V vs. SCE	$E_{mid,2}$ / V vs. SCE	$k_{f,ox}$ / $M^{-1}s^{-1}$	K_{ox} / M^{-1}	$k_{f,red}$ / $M^{-1}s^{-1}$	K_{red} / M^{-1}
pH 7	+0.14	-0.04	120	300	12	0.27
pH 8	+0.09	-0.04	240	400	24	2.5
pH 9	+0.04	-0.03	670	300	67	20

Table 1. Summary of voltammetric equilibrium potential and kinetic data for the binding of fructose to ferrocene-boronic acid and ferricenium-boronic acid in 0.1 M phosphate buffer.

Due to dual-plate generator-collector voltammetry offering a very fast steady state measurement tool, only kinetic information is obtained and additional information from a transient measurement method, for example from square wave voltammetry, is needed for the evaluation of the associated binding constants.

4.3.3 Transient Macro-Disc Square Wave Voltammetry

Square wave voltammetry is commonly employed as an analytical tool for binding and analytical assays.[181] Here the oxidation of ferrocene-boronic acid is studied at a 2 mm diameter platinum electrode immersed in 0.1 M phosphate buffer solution at pH 7, 8, and 9. Figure 83A shows a typical data set whereby addition of fructose causes an initial peak at 0.14 V vs. SCE to shift and then split to give a new peak at -0.04 V vs. SCE. These two peaks are associated with $E_{mid,1}$ and $E_{mid,2}$ for the oxidation of ferrocene-boronic acid without and with fructose attached.

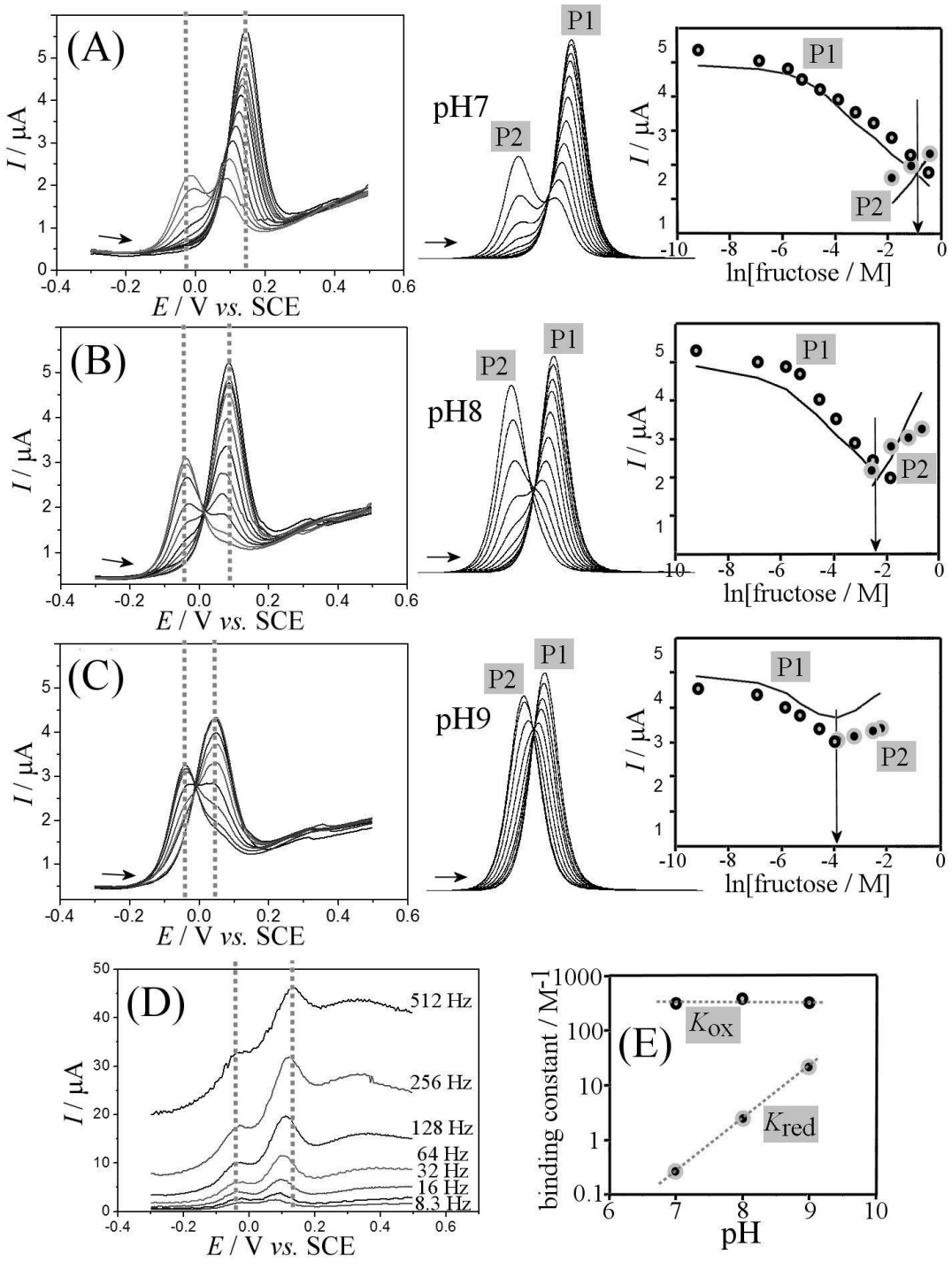

Figure 83 (A) Square wave voltammograms (f = 8.3 Hz, from -0.3 to +0.5 V vs. SCE, potential step 5 mV, amplitude 10 mV, 2 mm diameter platinum disk) for the oxidation of 1 mM ferrocene-boronic acid in 0.1 M phosphate buffer pH 7 with 0, 1, 3, 5, 10, 20, 40, 80, 160, 320, and 640 mM fructose. Also shown are the DigiElch simulation and the plot of peak currents for experimental (symbols) and simulation (line) data based on $D = 0.5 \times 10^{-9}$ m^2s^{-1} for all species. (B) As above at pH 8 and with 0, 1, 3, 5, 10, 20, 40, 80, 160, 300, and 500 mM fructose. (C) as above at pH 9 and with 0, 1, 3, 5, 10, 20, 40, 80, and 100 mM fructose. (D) Square wave voltammograms at pH 8 for 80 mM fructose as a function of frequency. (E) Plot of the binding constants K_{ox} and K_{red} versus pH.

Similar to the case of data from dual-plate generator-collector voltammetry, it is likely that the rate constant $k_{f,ox}$ is dominating in the shape of this voltammetric signal with the frequency of f = 8.3 Hz being linked to a typical diffusion layer of $\delta_{diffusion} = \sqrt{D/f} = 8\mu m$. Peak current data when plotted *versus* logarithm of fructose concentration shows a "crossing point" at 370 mM (Figure 83A), which is not too dissimilar to the transition point in the steady state voltammetric response (Figure 82A). Therefore the values for $k_{f,ox}$ evaluated above are employed as a starting point for the analysis.

When digital simulation is employed, $E_{mid,1}$, $E_{mid,2}$, and $k_{f,ox}$ can be used here as known input parameters. When first looking at the "crossing point" with 370 mM fructose, the peak ratio is consistent with K_{ox} = 300 M^{-1} (*via* rial and error simulation) and for then the peak-to-peak separation to be correct, $k_{f,red}$ requires to be approximately 10-times slower when compared to $k_{f,ox}$. This completes the set of 5 required parameters to solve the square scheme in Figure 78, at least in first approximation. A full optimisation of this solution with sensitivity analysis for each parameter with error evaluation would be desirable but is currently not possible. A full set of simulated square wave voltammetric curves for pH 7 is shown in Figure 83A. There are some remaining approximations in the input parameters (the diffusion coefficients are fixed at $D = 0.5 \times 10^{-9}$ m^2s^{-1} for all species and electron transfer is assumed reversible) and therefore the resulting equilibrium and rate constants need to be considered estimates. However, the relatively good agreement in shape of simulated signals with experimental data is re-assuring (simulated peak currents at high fructose levels appear slightly higher due to the missing effect of lower diffusion rates). A plot of the peak currents from simulation data versus logarithm of fructose concentration (see Figure 83A plot lines) confirms the agreement. Similarly data analysis was performed for pH 8 and pH 9 and parameters are summarised in Table 1.

The effect of the square wave frequency on the voltammetric signal (for pH 8 with 80 mM fructose) is demonstrated in Figure 83D where only a slight increase in peak-to-peak separation with frequency is observed, thus confirming the analysis method chosen above. At higher frequency a broad background response also emerges possibly associated with adsorbed species. The trend in binding constants with pH is shown in Figure 83E. Perhaps surprisingly, the binding constant K_{ox} for the ferricenium-boronic

acid is not significantly affected by pH and only the weaker K_{red} for the ferrocene-boronic acid strengthens with increasing pH. The observed trends could be linked to the formation of ternary complexes involving hydroxide or phosphate. The proposed mechanism could be that the ferricenium boronic acid has already bounded with hydroxide before binding with fructose; therefore the K_{ox} is pH independent. While ferrocene boronic works in the opposite way it binds with fructose together with hydroxide, which involves the hydroxide in the equilibrium. Thus, K_{red} is pH dependent.

4.4 Summary of Chapter 4

Voltammetric data for the interaction of ferrocene-boronic acid with fructose (or other saccharides) is time domain sensitive and here demonstrated for (i) a fast steady state method based on dual-plate generator-collector voltammetry and (ii) a fast transient method based on square wave voltammetry. Information from voltammetric peaks for bound and unbound forms of the ferrocene-boronic acid are predominantly due to the kinetic parameter $k_{f,ox}$ for the rate of binding to the oxidised ferricenium-boronic acid. In order to extract additional information (in particular binding constants) numerical simulation tools are required and data sets for a range of fructose concentrations need to be compared. In future similar experiments could be performed with a wider range of boronic acids to explore molecular structural effects.

CHAPTER FIVE

Results and Discussion

Published - Li, M., Guo, Z., Zhu, W., James, T. D., Marken, F., A redox-activated fluorescence switch based on a ferrocene-fluorophore-boronic ester conjugate" in *Chem. Comm.* 2015, **51 (7)**, 1293-1296.

5 Results and Discussion: A Redox-Activated Fluorescence Switch Based on A Ferrocene - Fluorophore - Boronic Ester Conjugate

5.1 Background

5.1.1 Molecular Switches and Logic Gates

The development of chemical sensing processes, including electrochemical and photochemical mechanisms, to integrate individual basic logic gates into combinational circuits, continues to receive a great deal of attention.[111, 182-194] In recent years efforts have been devoted to the exploitation of relatively simple logic operations, such as AND, OR, INHIBIT for the design of smart materials.[119, 195-204] Particularly, the fluorescence signals in logic gates[205-210] have become a focus of considerable research due to many advantages such as high sensitivity, low background, and wide dynamic range. Although fluorescent switches have been extensively explored,[4, 121] fluorescence switches based on the redox reaction centre ferrocene (Fc) are still rare and much less well studied.[5, 6, 117, 211-213] Therefore, it is very interesting to explore this multifunctional area.

5.1.2 The Properties and Application of Ferrocene and Its Derivatives

As a new type of organic iron compound - ferrocene was reported by Pauson and Kealy in 1951 in Nature.[214] After this, ferrocene compounds become popular molecules because of their special chemical properties and the chemical structure. The discovery of ferrocene and its many analogues has contributed a lot to the rapid growth of organometallic chemistry, which has become one of the important subjects of modern chemistry.

Ferrocene and its numerous derivatives have many significant applications such as ligand scaffolds, pharmaceutical candidates, anti-knock formulations, precursors to materials and redox standards.

Pharmaceutical application

In terms of anticancer activity an experimental drug has been prepared containing a ferrocenyl version of tamoxifen.[215] The mechanism is that the tamoxifen will bind to the estrogen binding sites, resulting in cytotoxic effects.

Materials chemistry

Due to its being readily decomposed to iron nanoparticles, ferrocene has been employed as a catalyst for the production of carbon nanotubes.[216] Through a Wittig reaction the vinyl ferrocene (from ferrocene aldehyde), can be prepared. This vinyl ferrocene can be transformed into a polymer which can be thought of as a ferrocenyl version of polystyrene.

5.2 Aim and Objective

The fluorescence signals in logic gates [205-210] have become a focus of considerable research due to many advantages such as high sensitivity, low background, and wide dynamic range. Although fluorescence switches have been extensively explored,[4, 121] switches based on the redox reaction centre ferrocene (Fc) are still rare and much less well studied.[5, 117, 211] Herein, we present a multifunctional molecule **59**, which behaves as a combinational serial INHIBIT gate as well as an electrochemical probe molecule.

59 consists of ferrocence as an electroactive unit and naphthalimide unit as the fluorophore, **59** becomes fluorescent when the ferrocene unit is oxidised for example with Fe^{3+}. The response of the oxidised **59** to sodium L-ascorbate (LAS, a reducing agent) can be utilised to directly control fluorescence. In contrast, the coordination of F^- to the boron atom of **59** only has an indirect effect on the intensity of the fluorescence *via* coordination with $Fe^{3+/2+}$. Considering these three "inputs", Fe^{3+}, LAS, and F^-, the system can be considered to function as an INHIBIT logic gate.

5.3 Investigations on Fluoride Sensing and Logic Gates

*5.3.1 Design and Synthesis of Compound **59***

Among all the fluorophores developed, naphthalimide unit is highly favourable because of its excellent photophysical properties, such as high extinction coefficient, excellent quantum yield, excellent photostability, and relatively long emission wavelengths. In addition, naphthalimide has a relatively simple structure for which facile and straight forward syntheses have been established.

Similarly, ferrocene (Fc) has various attractive features owing to its excellent reversible redox characteristics. Therefore, combination of the naphthalimide and ferrocene results in a system where fluorescence can be modulated by the ferrocene redox *via* control of the photoinduced electron transfer (PET) process. The Fc/Fc^{+} transformation, which can be operated reversibly by using chemical- and/or electrochemical methods, is a promising molecular building block for molecular devices with a significant change in its photophysical properties.

Finally, a boronic receptor group was added as a selective conjugating (linkage) group and/or fluoride receptor unit. Since the boronic acid group can be used to conjugate **59** to monomeric or polymeric carbohydrates.[217] For the purpose of developing a carbohydrate delivery vector or material based system by polymer attachment. While the Lewis acid - base interactions of a boron atom toward fluoride anion can be used for the detection of F^{-}. Thus, **59** also contains a boronic acid unit, introduced *via* a piperazine ring to explore both the conjugation and F^{-} sensing properties of the **59** system.

*Synthesis of Ferrocenylmethylamine **56***

Ferrocenylmethylamine **56** was synthesised through a two-step procedure (Scheme 9). The intermediate **55** was synthesised through the oxime formation. **54** and hydroxylamine hydrochloride were dissolved in ethanol and NaOH was added. The reaction mixture was heated at reflux under an N_2 atmosphere for 3 h. The mixture was allowed to cool to room temperature and then concentrated under reduced pressure. The residue was poured into water and extracted with CH_2Cl_2 three times. The organic layer was separated and combined and was evaporated under reduced pressure to give the crude product as dark brown solid. The precipitate **55** could be used directly without further purification.

Then, ferrocenylmethylamine was synthesised through a $LiAlH_4$ reduction. To a stirred solution of $LiAlH_4$ in anhydrous THF, a solution of **55** in anhydrous THF was added dropwise. After being stirred at room temperature for 30 mins, the mixture was refluxed for 6 h under an N_2 atmosphere. After cooling to RT, the reaction mixture was poured into water and a grey precipitate formed. After filtration, the filtrate was transferred to separatory funnel and extracted with ethyl acetate. The organic phase was evaporated under reduced pressure to give a yellow liquid in 80% yield. From the ^1H NMR spectrum, the emergence of the peaks at 4.19 - 4.08 and 3.40 ppm implied the completion of this reaction.

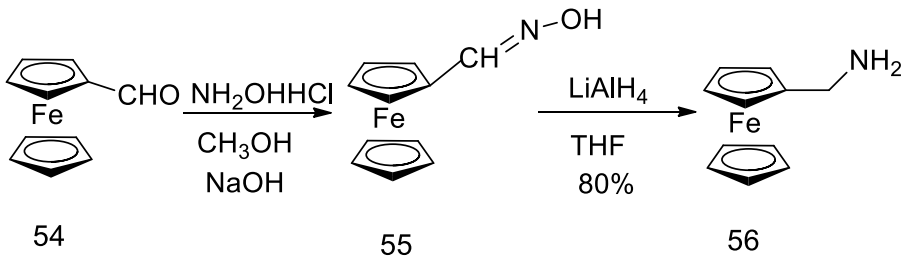

Scheme 9 Synthesis of **56**.

*Synthesis of compound **59***

59 was synthesised through a three-step procedure (Scheme 10). First, intermediate **57** was obtained by mixing 1.0 equiv. of **44** and 2.0 equiv. piperazine by refluxing in 2-methoxyethanol under nitrogen. This reaction is a typical nucleophilic aromatic substitution reaction. After the completion of the reaction, the mixture was allowed to cool to room temperature and then concentrated under reduced pressure. The precipitate **57** could be used directly without further purification. The reason why not to use the ferrocenylmethylamine to react with **44** first is that the ferrocene will affect the nucleophilic aromatic substitution between the piperazine and the naphthalimide derivative. Therefore, we choose to synthesise **57** first.

Next, ferrocenylmethylamine **56** was reacted with **57** through the imide formation, which was mentioned earlier. **56** and **57** were added into ethanol. The mixture was refluxed for 5 h under a nitrogen atmosphere. After completion of the reaction, the solvent was removed under vacuum and the residue was purified using column chromatography producing an orange solid in 16 % yield. From the ^{1}H NMR spectrum, the emergence of the peak at 2.9 - 3.2, 4.0 - 4.4 ppm implied the completion of this reaction.

Finally, the target compound **59** was obtained by S_N2 reaction. Compounds containing boronic acid groups are hard to purify, since the boronic acid moiety can interact with the hydroxyl surface groups in silica chromatography. Therefore, in order to improve yields, the boronic acid moiety needs to be protected first with pinacol or 2,2-dimethyl-1,3-propanediol. **58** and 2-(2-(bromomethyl)phenyl)-4,4,5,5-tetramethyl-1,3,2-dioxaborolane were dissolved in anhydrous acetonitrile. And K_2CO_3 (62.2 mg, 0.45 mmol) was added and the mixture was refluxed overnight. After completion of the reaction, most of the acetonitrile was evaporated and the residue was poured into water to give the precipitate with 67% yield. From the ^{1}H NMR spectrum, the emergence of the peak at 1.3 - 1.4, 7.2 - 7.5 ppm implied the completion of this reaction.

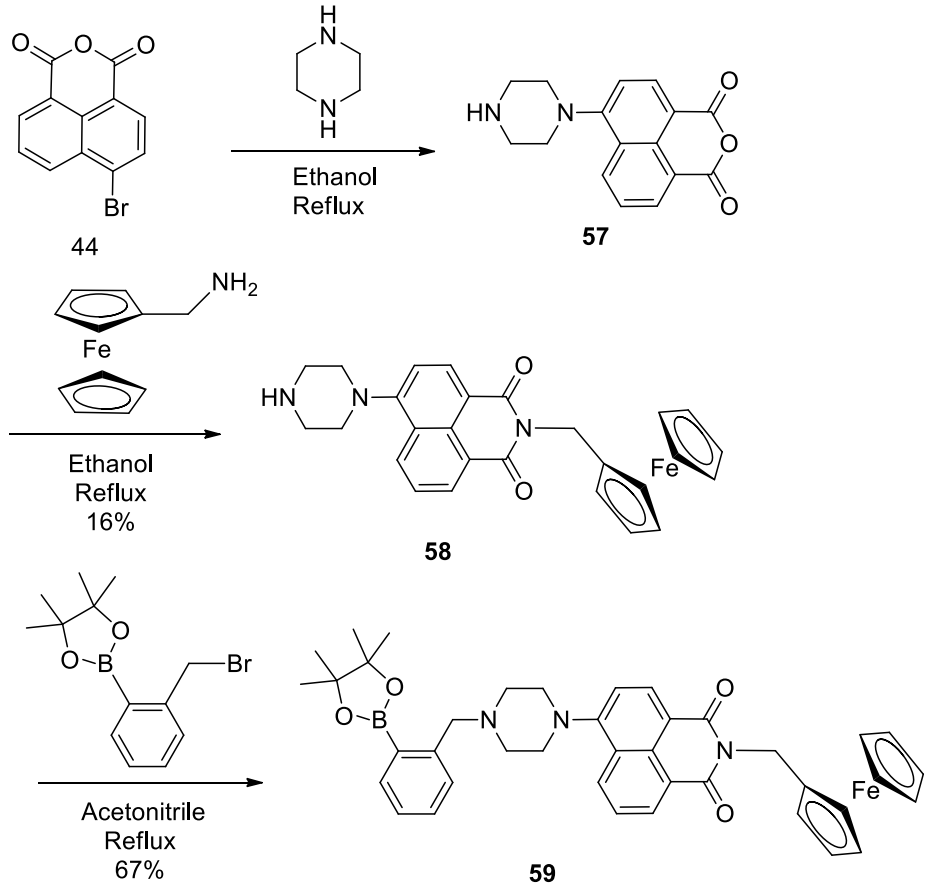

Scheme 10 Synthesis of **59**.

5.3.2 Chemical Redox Process of **59**

Initially, the chemical redox process and the photophysical properties of **59** were investigated using fluorescence spectroscopic measurements. Given that ferrocene is an active redox group, the function of Fe^{3+} as an oxidant was examined in THF solution. As shown in Figure 84a, **59** exhibits almost no fluorescence when excited at 403 nm. However, in the presence of Fe^{3+}, the fluorescence at 512 nm was dramatically enhanced. The 1:1 mechanism of Fe^{3+} "switching on" the fluorescence is indicative of a ferrocene-based redox process. The oxidation of the Fe^{2+} to Fe^{3+} in ferrocene interrupts the intramolecular photoinduced electron transfer (PET), which results in an enhanced fluorescence.[218] (ie The fluorescence maximum peak at 512 nm does not change, which is characteristic of a PET mechanism controlling the fluorescence intensity) After addition of 1 equivalent of Fe^{3+}, the fluorescence of **59** doesn't change any further, indicating that the ferrocene Fe^{2+} has been completely sto Fe^{3+}. Subsequently, the back-reduction can be achieved by adding sodium L-ascorbate (LAS), which is a reducing agent. Figure 84b shows that upon the addition of LAS from 0.5 to 2 equivalents to the oxidised solution, the fluorescence gradually decreases.

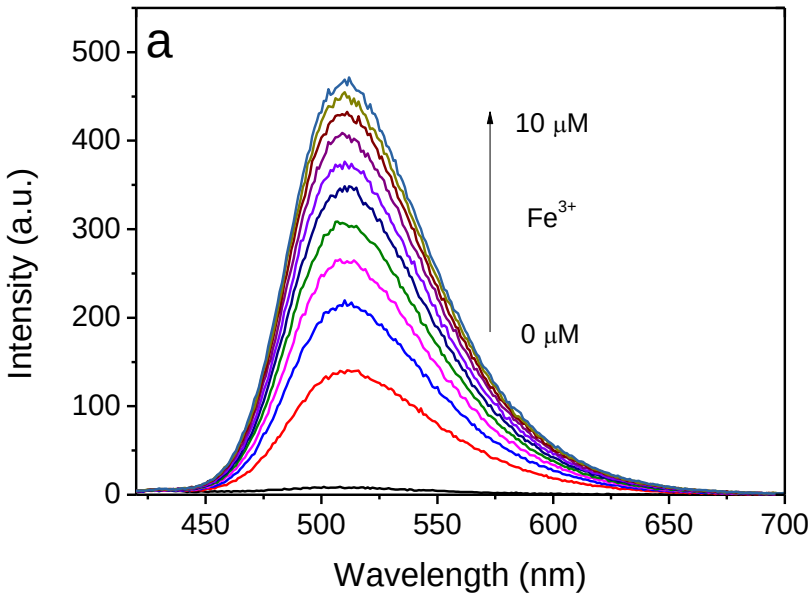

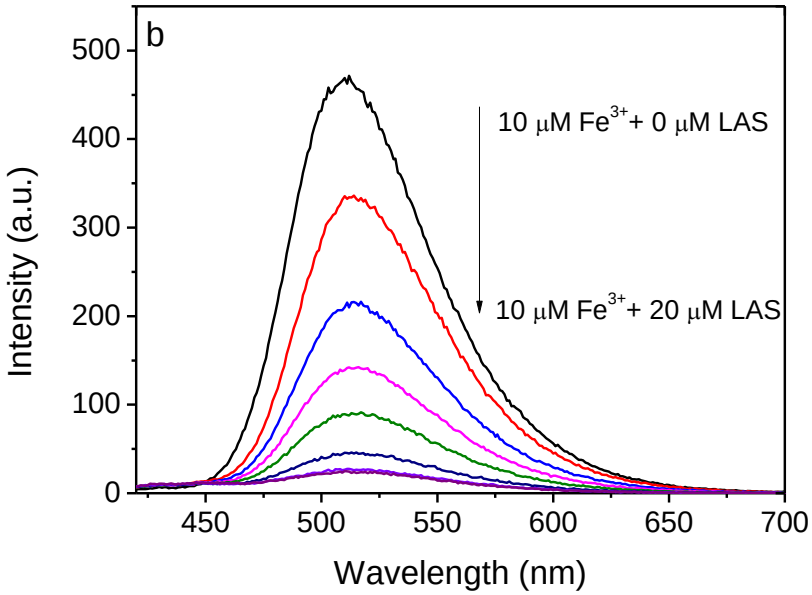

Figure 84 Emission change of of **59** (10 μM) in THF upon excitation at 403 nm: (a) Fluorescence enhancement upon titration of Fe^{3+} ($Fe(ClO_4)_3$) (0 - 1.0 equiv.); (b) Fluorescence quench when further chemically reduced by sodium *L*-ascorbate (LAS), in presence of 10 μM Fe^{3+} ($Fe(ClO_4)_3$).

However, by adding just LAS to a **59** solution produces no fluorescence changes (Figure 85), clearly indicating that, Fe^{3+} and LAS can be used to control the OFF-ON-OFF switching for the fluorescent **59** molecule.

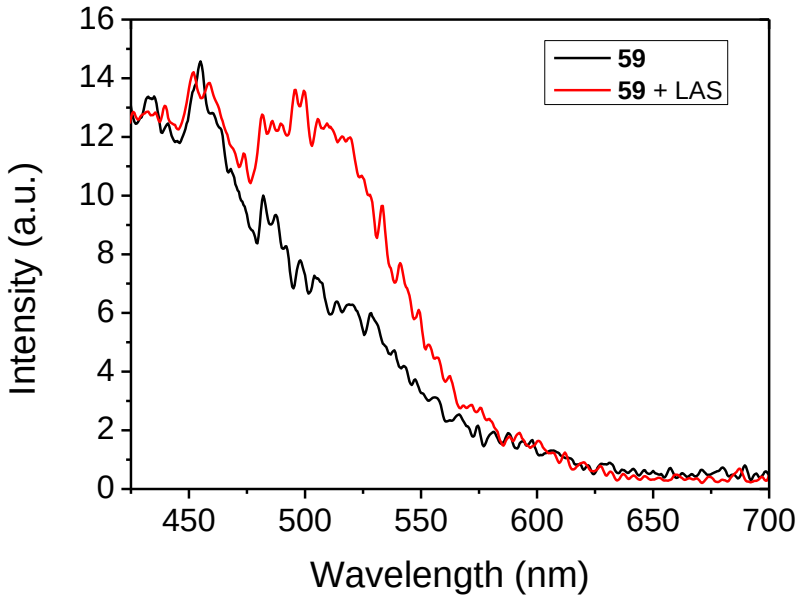

Figure 85 Emission spectra of **59** (10 μM) in THF upon titration of L-Ascorbic acid Sodium salt (LAS) by λ_{ex} = 403 nm (0, 10.0 equiv.).

As mentioned earlier the boronic acid group was incorporated into **59** for potential conjugation (to carbohydrate molecules or polymeric supports) and also for its fluoride sensing properties. The boronic acid group has been extensively employed as a ligand for fluoride (F^-) owing to its high affinity and excellent selectivity.[94] **59** should be a candidate as a fluoride ion chemosensor in that **59** contains a boronic acid moiety. However, perhaps surprisingly, the fluorescence was almost not changed by adding F^- (Figure 86). It is likely that the location of the boronic acid functionality is too far from the fluorescent part of the molecule. However, due to an interaction with $Fe^{2+/3+}$, fluoride can be indirectly detected (Figure 87), which indicates that the presence of F^- has an effect on the chemical redox process. Upon initial addition of 10 μM F^-, the weak fluorescence of **59** doesn't change. With subsequent addition of Fe^{3+}, the fluorescence enhancement is delayed until close to 10 μM Fe^{3+}. We then repeated the measurements using 20 μM **59** with an initial addition of 20 μM F^- in this case the fluorescence enhancement is delayed until close to 20 μM Fe^{3+} (Figure 88，89). We ascribe the indirect effect of fluoride to formation of a tetrahedral boronate anion $[-(OH)_2F]^-$ which forms an ion pair with the Fe^{3+}, which in turn reduces the availability of the Fe^{3+} and prevents the oxidation of the ferrocene. (Scheme 11)

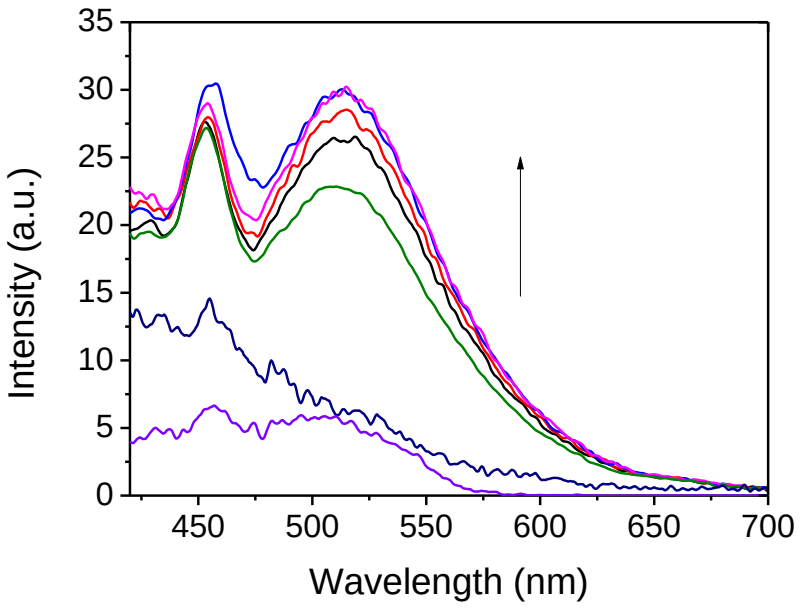

Figure 86 Emission spectra of **59** (10 μM) in THF upon titration of F^- by λ_{ex} = 403 nm (0, 1, 3, 5, 7, 8, 10.0 equiv.).

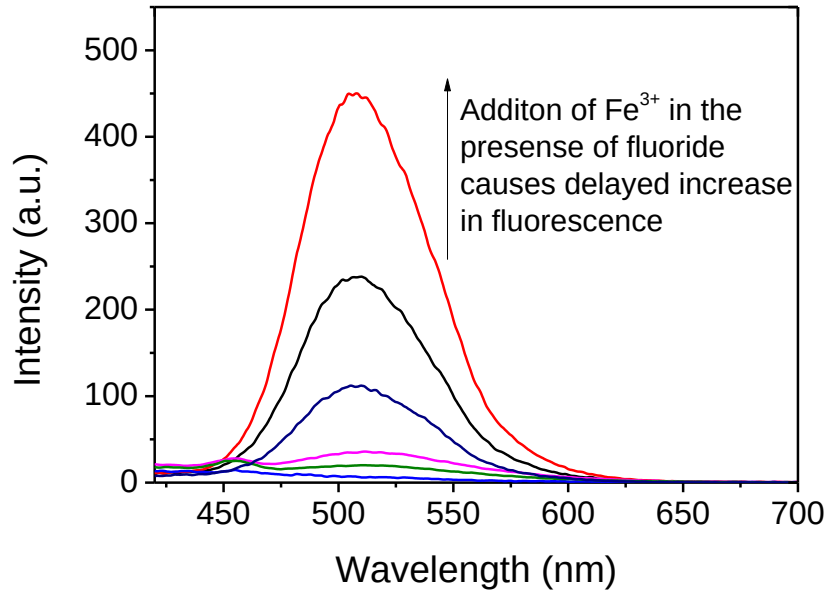

Figure 87 Fluorescent spectra of **59** (THF, 10 μM, λ_{ex} = 403 nm) with 10 μM F^- upon the addition of various Fe^{3+} (0, 2, 5, 10, 30, 50 μM) .

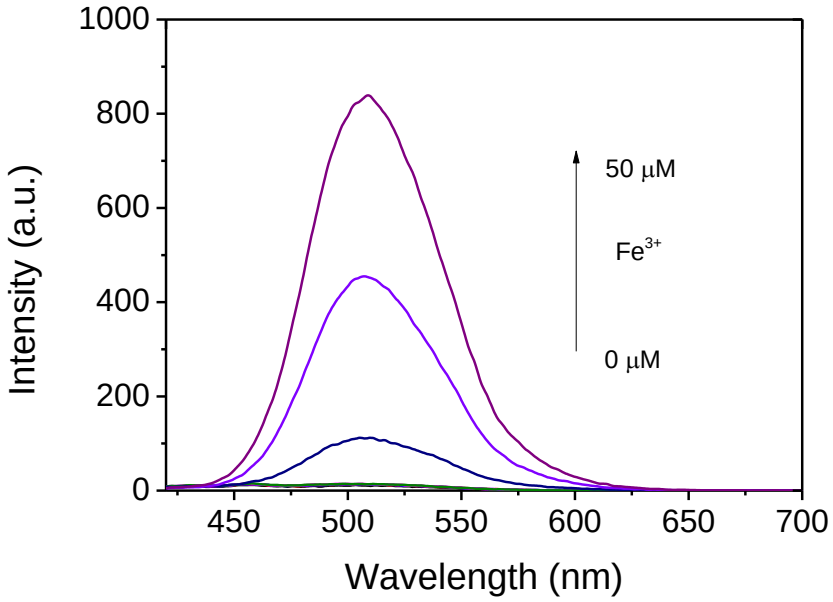

Figure 88 Fluorescent spectra of **59** (THF, 20 μM, λ_{ex} = 403 nm) in the presence of 20 μM F^- upon the addition of various Fe^{3+} (0, 2, 5, 10, 20, 30, 50 μM).

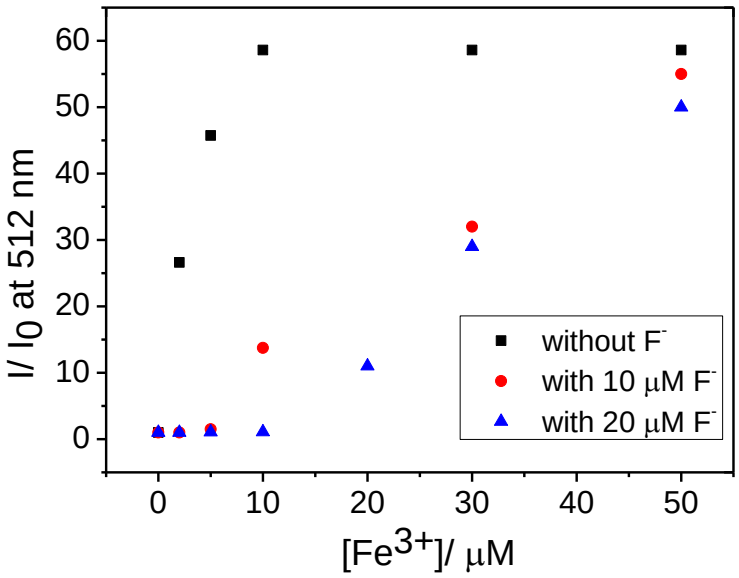

Figure 89 The values of I/I_0 at 512 nm of 10 μM and 20 μM **59** upon the addition of various Fe^{3+} (0, 2, 5, 10, 20, 30, 50 μM) with and without 10μM F^- and 20 μM F^-. Successive spectra were taken after 10 mins intervals.

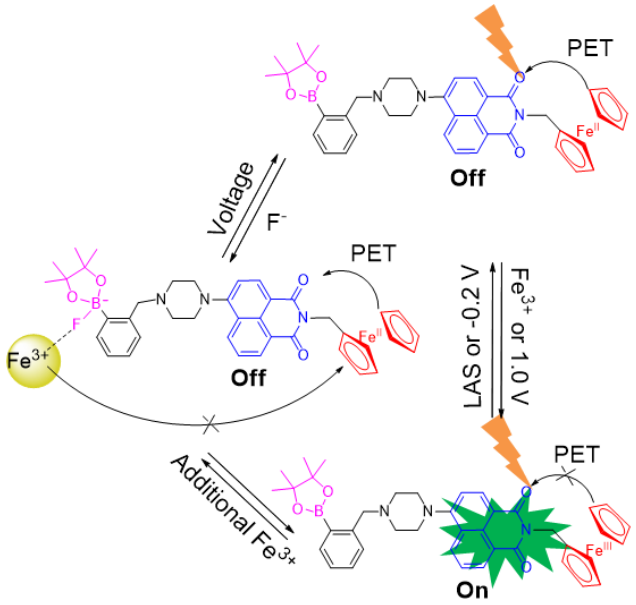

Scheme 11 Proposed schematic mechanism on PET and fluoride binding process.

In order to confirm the complexion of boron and fluoride, the same experiments were carried on with compound **58**. The results showed that there is no obvious difference with and without F^-, which means that the fluorescence was not delayed. The results also confirmed that the boron was linked with fluoride and the fluoride holds the Fe^{3+} back from oxidising the ferrocene, which cause the fluorescence enhancement delay (Figure 90-92).

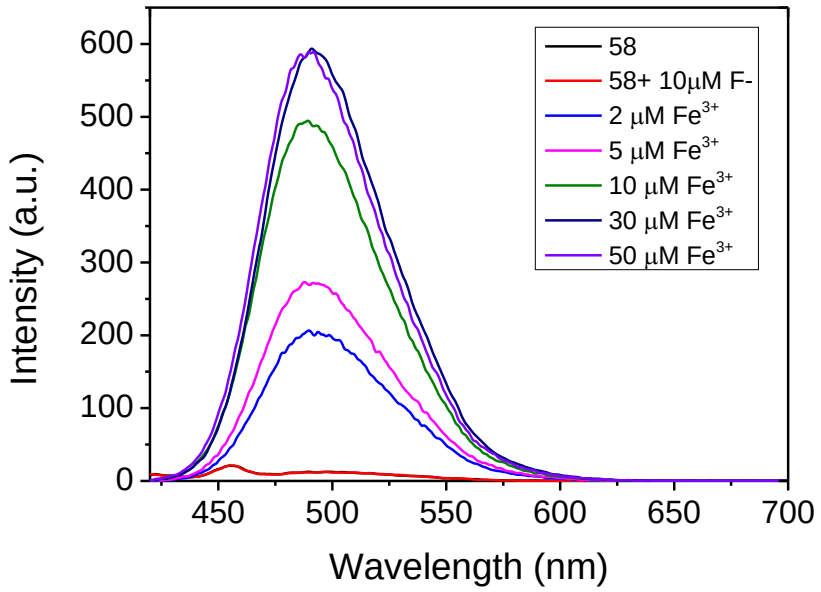

Figure 90 Fluorescent spectra of **58** (THF, 10 μM, λ_{ex} = 403 nm) and **58** with 10 μM F^- upon the addition of various Fe^{3+} (0,2, 5, 10, 30, 50 μM).

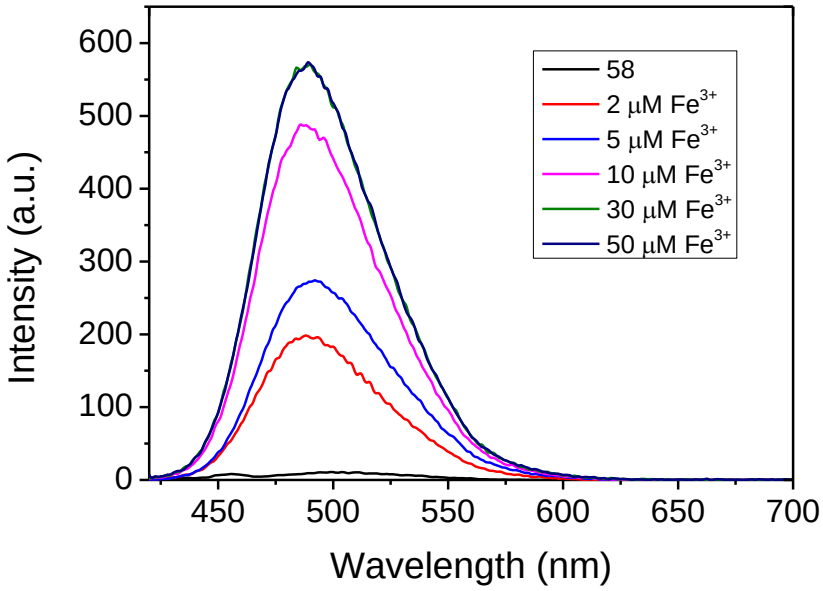

Figure 91 Fluorescent spectra of **58** (THF, 10 μM, λ_{ex} = 403 nm) upon the addition of various Fe^{3+} (0, 2, 5, 10, 30, 50 μM).

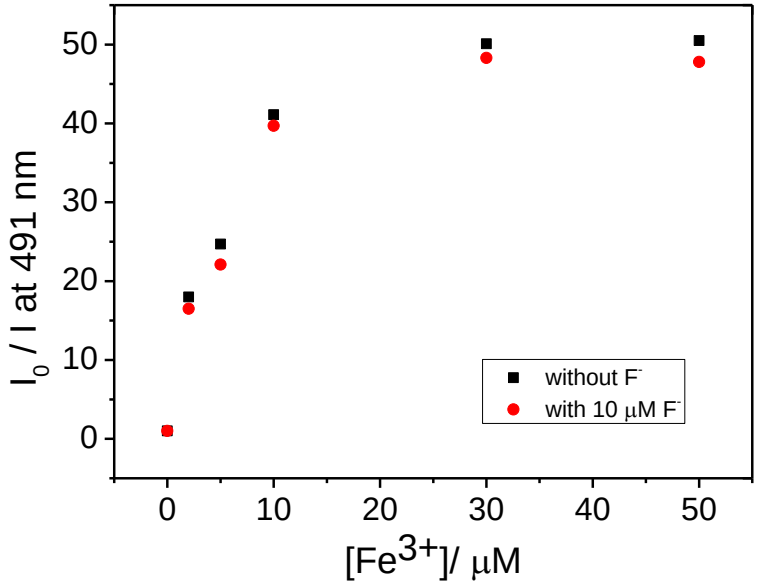

Figure 92 The values of I/I_0 at 491 nm upon the addition of various Fe^{3+} (0, 2, 5, 10, 30, 50 μM) with and without 10 μM F^-.

5.3.3 Combinational Logic Function

To take advantage of the OFF-ON fluorescence response of **59** driven by the redox process and the capture of F^-, a combinational serial INHIBIT logic operation as well as two INHIBIT logic gates were constructed with Fe^{3+} as an input and either LAS or F^- as another input (Figure 93).

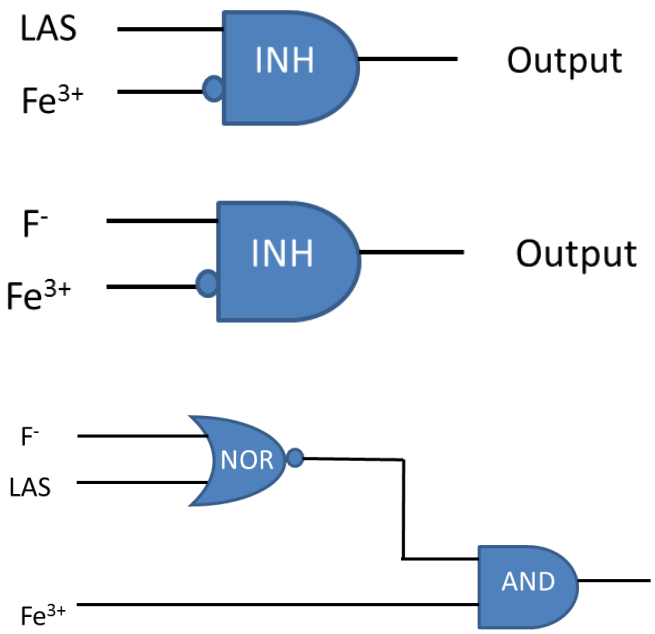

Figure 93 Schemes with logic symbols and the assignment of the chemicals to each of these inputs corresponding to Figure 93a, b, c in the text.

An INHIBIT logic gate is based on two-input AND gates with one input carrying a NOT gate. The values of I/ I_0 at 512 nm for **59** with different combinations of varying equivalents of Fe^{3+} and LAS correspond to an INHIBIT logic gate. Four situations are examined (Figure 94a), in which Fe^{3+} as input 1 is 10 μM (high, 1) or 0 μM (low, 0) and LAS as input 2 is 20 μM (high,1) or 0 μM (low, 0). As shown in Figure 93a, the value of I/I_0 at 512 nm (output) becomes high (I/I_0 = 58.6) only when 1 equivalent of Fe^{3+} is added. In contrast, the values of I/I_0 is at a low level (I/I_0 < 15) for any other combination. Similarly, the different input combinations of adding Fe^{3+} and F^- for **59** also behave like an INHIBIT logic gate, with the values of I/ I_0 (512 nm) as the output. These INHIBIT gate observations are presented in a truth table (Figure 94b). In this INHIBIT logic gate, Fe^{3+} as input 1 is 10 μM and the addition of F^- as input 2 is 10 μM.

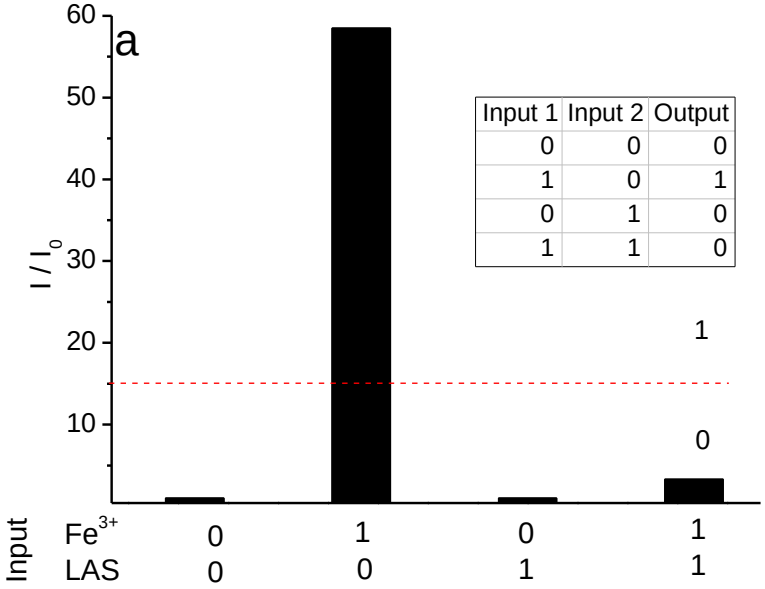
a
60
50
40
30
20
10
I / I0
Input 1 Input 2 Output
0 0 0
1 0 1
0 1 0
1 1 0
1
0
Input
Fe3+
LAS
0 1 0 1
0 0 1 1

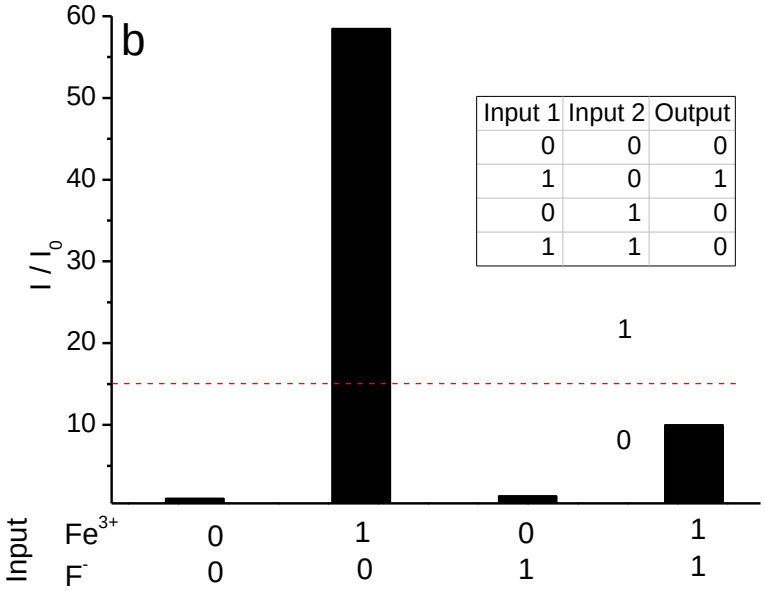
b
60
50
40
30
20
10
I / I0
Input 1 Input 2 Output
0 0 0
1 0 1
0 1 0
1 1 0
1
0
Input
Fe3+
F-
0 1 0 1
0 0 1 1

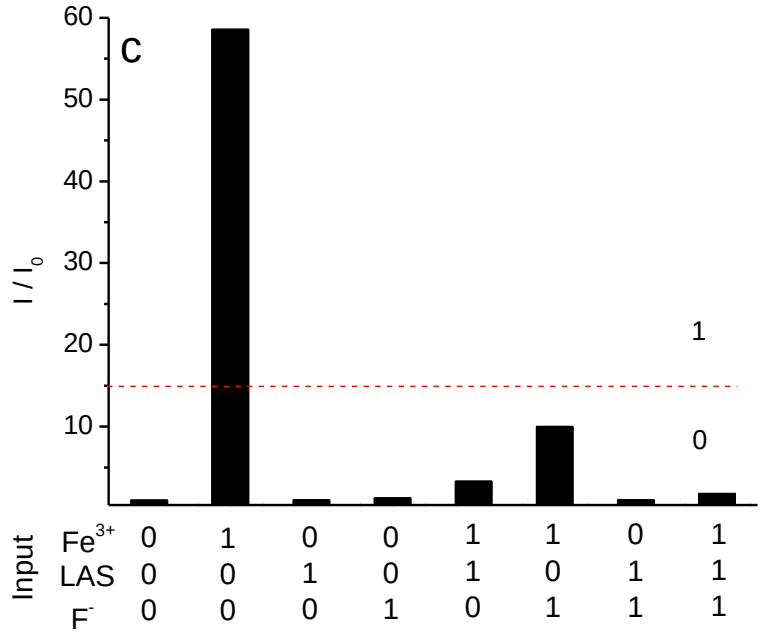

Figure 94 Two INHIBIT logic gates constructed with Fe^{3+} as an input and either LAS or F^- as another input. The values of I/I_0 at 512 nm as the output of the INHIBIT gate from the different inputs: (a) Fe^{3+} (10 μM) and LAS (20 μM); (b) Fe^{3+} (10 μM) and F^- (10 μM). (c) Combinational logic operation. The values of I/I_0 at 512 nm as the output of the combinational logic operation from the eight possible inputs.

Universally, combinational logic circuits play a key role in mimicking comprehensive arithmetic operations at the nanoscale level.[219] A combinational NOR and AND logic circuit can be constructed with three inputs: Fe^{3+}, LAS and F^- (Figure 94c). The NOR logic operation is the integration of a NOT and OR logic gate, in which the output is low when one or more of the inputs are high. The eight possible input combinations of varying Fe^{3+}, LAS and F^- are shown in Figure 94c. Obviously, the values of I/I_0 at 512 nm are only high (I/I_0 = 58.6) when Fe^{3+} is added. The output signals for the other four combinational input situations are low. The threshold for all of the logic operations given above has been set at 15.

5.3.4 Electrochemical Redox Investigation

Finally, the electrochemical characteristics of **59** (attached as microcrystals to a graphite electrode) immersed in aqueous media were studied. The ferrocene unit in the molecular structure produced well-defined chemically reversible oxidation - reduction signals (Figure 95) with a close to linear dependence of the peak current with the scan rate. This suggests an immobilised redox system with fast charge transport. This was confirmed when doubling the amount of deposit caused an approximate doubling of the current response. Given the size and complexity of the **59** molecule, anion penetration into the solid in conjunction with oxidation appears likely.

When fluoride is added to the aqueous solution (0.1 M ClO_4^-) an additional small signal is observed at 0.5 V vs. SCE (see Figure 95c). This is due to fluoride directly interacting with **59**.

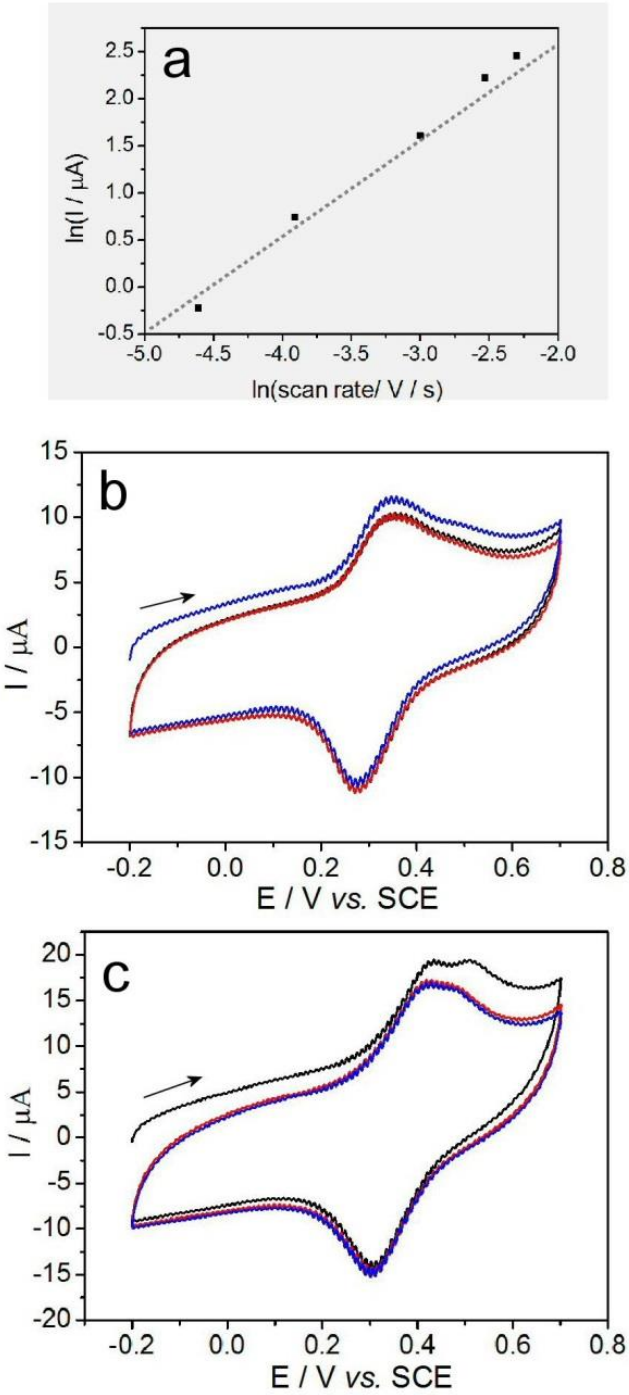

Figure 95 a) Plot of current peaks versus scan rates (10, 20, 50, 80, 100 mV s^{-1}) for 0.36 µg **59** immobilised at a graphite electrode surface and immersed in 0.1 M $NaClO_4$; b) First three scans of cyclic voltammograms (scan rate 50 mV s^{-1}) for 0.36 µg **59** immobilised at graphite electrode and immersed in 0.1 M $NaClO_4$; c) First three scans of cyclic voltammograms (scan rate 50 mV s^{-1}) for 0.36 µg **59** immobilised at graphite electrode and immersed in 0.1 M $NaClO_4$ with the addition of 0.1 M NaF.

Moreover, when the aqueous supporting electrolyte is systematically varied from ClO_4^- to NO_3^- to Cl^- and to F^- very similar voltammetric responses are observed (Figure 96). Only the position of the midpoint potential (here $E_{mid} = 0.5\ E_{p,ox} + 0.5\ E_{p,ed}$) shows the

effect of the electrolyte anion during the redox insertion process. The expected behaviour is the most positive shift in E_{mid} for the most hydrophilic anion, here fluoride.[220] However, the fluoride response is shifted negative of the chloride response presumably due to specific interaction with the boronic acid host crystal in the solid state.

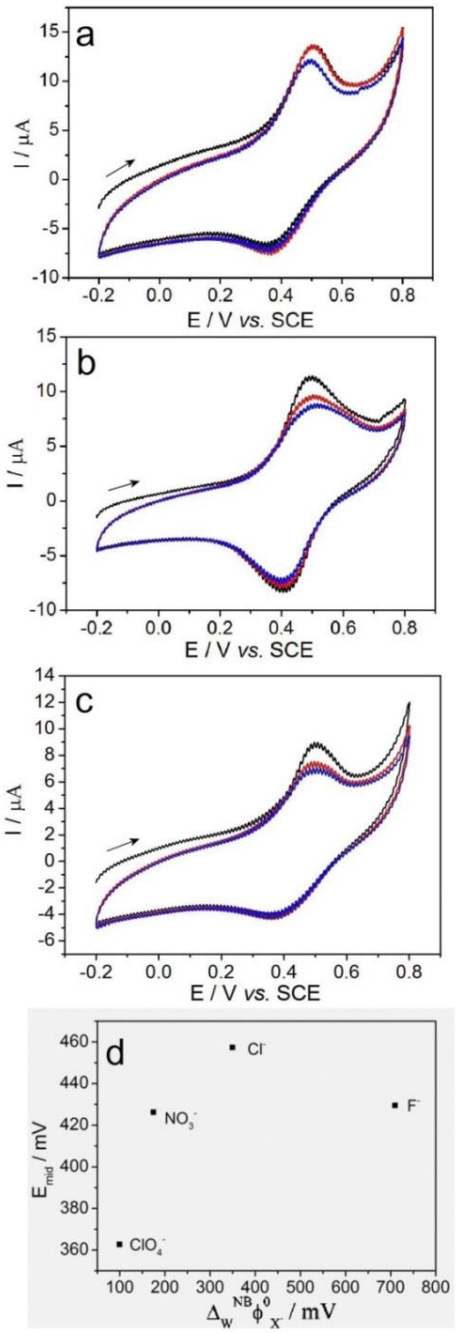

Figure 96 a)-c)First three scans of cyclic voltammograms (scan rate 50 mV s^{-1}) for 0.36 µg **59** immobilised at graphite electrode and immersed in 0.1 M $NaNO_3$, NaCl, NaF solutons; d) Plot of formal potentials of the first oxidation step for **59** in the presence of different electrolyte anions versus the standard membrane potentials

*5.3.5 Conjugating the **59** with Polymeric Carbohydrates*

We then explored the applicability of the boronic acid as a unit for conjugating **59** with polymeric carbohydrates (ie the cellulose found in filter paper). Two small volumes of **59** in THF were dropped onto a piece of filter paper that was allowed to air dry. To one of the spots a Fe^{3+}solution was added. The spot in contact with Fe^{3+} produced a green fluorescence while the untreated spot remained non fluorescent. This experiment clearly demonstrates that the boronic acid group can be used as a linkage group and for the development of material based sensors (Figure 97).

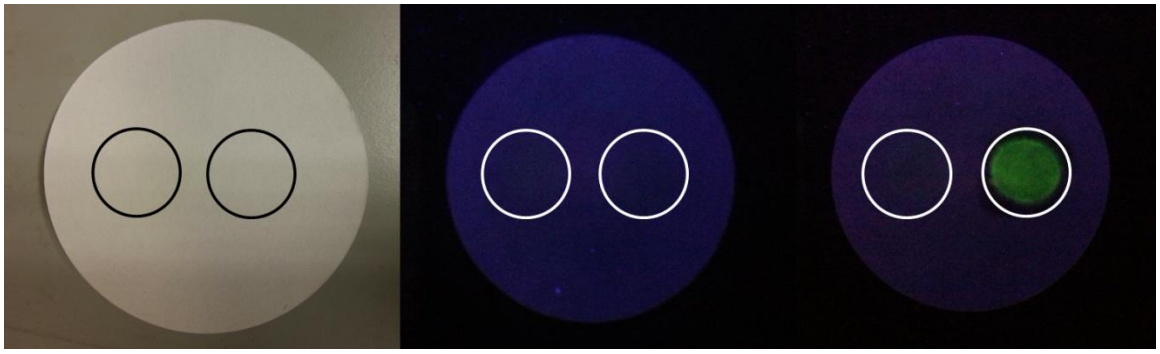

Figure 97 The photos were taken under day light and UV_{365}.a) Two drops of 10 μL **59** solution were dropped on filter paper in the black circle; b) No fluorescence can be seen under UV in the white circles; c) After dropping 10 μL Fe^{3+} solution on the right spot, green fluorescence can be seen under UV in the right circle.

5.4 Summary of Chapter 5

A smart molecule, **59**, derived from a naphthalimide chromophore, has been designed for logic fluorescence and electrochemical studies based on the ferrocence redox relationship for potential applications in ion sensing. Two INHIBIT logic gates constructed with Fe^{3+} as an input and either LAS or F^- as another input. Similarly, the combinational serial INHIBIT logic operation was also implemented using different combinations of three inputs: Fe^{3+}, LAS and F^-. The logic gate operates in organic solution but also *via* conjugation with cellulose as a material support (filter paper). The proposed combinational logic circuits play a key role in mimicking comprehensive arithmetic operations at the nanoscale level. Moreover, the application of **59** in electrochemistry has improved the sensing ability. The multiple logic fluorescent electrochemical system might contribute to the development of smarter fluorescent materials, which could be used in the development of controlled drug-release systems, and optical and rheological applications.

CHAPTER SIX

Conclusion and Future Work

6 Conclusion and Future Work

6.1 Conclusion

In terms of developing fluorescence and electrochemical sensor systems for biologically import species recognition, there are four projects involved in this thesis. Traditional fluorescent sensors are mainly developed on the protocol of the synthetic molecule containing a reporter site and a receptor side, which can exhibit responses in the presence of different analytes. While, electrochemical sensors are based on the redox process on the working electrode, which can be observed by a potentiostat. The dedicate design strategies play essential roles in attaining high selective and sensitive probes.

The supramolecular concept of nanotechnology and bioscience has promoted the formation of smart materials for high sensitive detection of biologically important species. With the rapid development, some biological molecular recognition events have already been realised both *in vitro* and *in vivo*. There are several sensing protocols, such as coordination-based sensors, reaction-based probes and electrochemical sensors, which are devoted to designing these sensors.

In the first chapter of this thesis, the mechanisms for fluorescence change and common design strategies for chemosensors were illustrated along with a basic introduction to electrochemistry. Firstly, details of molecular recognition in the area of coordination-based sensors for the detection of copper(II) ions were introduced. Secondly, a summary of the recent developments in reaction-based probes for the detection of biothiols was reported. And thirdly, a review about electrochemical sensors with boronic acid for saccharides recgonition was presented. Finally, information about molecular switches and molecular logic gates was presented.

In the second chapter, a naphthalimide based fluorescence sensor **47** containing a monoboronic acid group and reference compounds **48**, **50** were introduced. The ability of **47** for recognising metal ions were first investigated. The sensor displays high selectivity for copper(II) ions, which is one of the few examples of boronic acid based fluorescent chemosensors for copper(II) sensing. Subsequently, the chelate, **47**-Cu^{2+},

displayed fluorescence enhancement with fructose, and the system was designed as a fluorescence INHIBIT logic gate. Together with the fluorescent tests of **48**, **50** for copper(II) ions and the Job's plot results, we believe that the boronic acid and Schiff base worked together and the binding mode of **47** to Cu^{2+} is 2: 1 stoichiometry. Finally, **47** was demonstrated for detecting copper(II) ions in HeLa cells.

In the third chapter, a NIR fluorescent chemodosimeter **53** for GSH based on the DCM framework was introduced. Initially, UV spectrum was investigated. Probe **53** showed a colour change from yellow to pink upon addition of GSH, which could work as a ''naked-eye'' probe for GSH. Furthermore, the fluorescence enhancement at 690 nm demonstrated that the probe can be used for the detection of GSH. The fluorescence enhancement mechanism is based on the cleavage of DNBS from the fluorophore by GSH, which has been proved by the mass spectra. Finally, the confocal imaging experiments for detection of cellular thiols clearly demonstrated that **53** could be the good choice for biological applications.

In the fourth chapter, fructose binding with ferrocene-boronic acid was investigated with the employment of a fast steady state method based on dual-plate generator-collector voltammetry and a fast transient method based on square wave voltammetry. The voltammetric data for the interaction of ferrocene-boronic acid with fructose is time domain sensitive and the information from voltammetric peaks for bound and unbound forms of the ferrocene-boronic acid are predominantly due to the kinetic parameter $k_{f,ox}$ for the rate of binding to the oxidised ferricenium-boronic acid.

In the fifth chapter, a naphthalamide based sensor **59** has been designed and synthesised for logic fluorescence and electrochemical studies due to the ferrocence and Fe^{3+} redox relationship for potential applications in ion sensing. Firstly, the redox process of **59** upon the addition of Fe^{3+} and LAS was examined. Secondly, the indirect sensing of **59** for F^- was carried out. The same experiments were also employed for **58** in order to demonstrate the binding ability of boron to fluoride. According to the fluorescent tests above, two INHIBIT logic gates constructed with Fe^{3+} as an input and either LAS or F^- as another input. Furthermore, the combinational serial INHIBIT logic operation was also implemented using different combinations of three inputs: Fe^{3+}, LAS and F^-. Moreover, the application of **59** in electrochemistry has improved the sensing ability,

which shows better selectivity for F^- in aqueous media. Interestingly, **59** could conjugate with cellulose in filter paper and display fluorescence off-on, which might contribute to the development of smarter fluorescent materials.

The thesis is composed of four sub-projects, all of which focussed on the recognition of biologically importance species with different detection technique. The metal ion project was based on the coordination chemistry, an attempt to extend the application field of fluorescent sensor. The DCM project focused on the impact of the reaction between specific groups and biothiols. The electrochemcial project was aimed at exploring new strategy for saccharides sensing. And the molecular switch and logic gates project was focused on the multifunctional application and INHIBIT logic gate development.

6.2 Future Work

Although the research results presented in this thesis did answer some questions, some other new questions have arisen from these results at the same time, which needs to be addressed in future.

In the copper(II) ion detection project, poor solubility is the big issue for extending the applications. Therefore, further optimisation by preparing better water soluble fluorophores is required before use in biological experiments becomes generally applicable. The exact nature of the binding mode between receptor and metal ions could be understood if crystals could be obtained

Though the reaction based DCM probe had proved its potential ability for biothiol recognition, the ability of the system could be improved by better selectivity. Although the reaction based sensor is quite specific for some kind of groups, but it is not able to discriminate analytes containing the same functional group (SH). Therefore, more specific sensors should be designed and synthesised.

For the electrochemical sensor, a more detailed analysis of the data should take into account additional parameters for changes in diffusion coefficients with viscosity and changes in the rate of electron transfer. It is interesting to note that these results suggest "kinetic resolution" as an analytical approach where the boronic acid receptor is employed to detect "fast binding" analytes at higher sensitivity compared to "slow binding" analytes. A further conclusion emerging from this study is the possibility to develop a "switchable" boronic acid,[221] for example to be used in separation processes at suitably adjusted pH.

Although the developments of multifunctional systems that can integrate individual basic logic gates into combinational circuits are extremely interesting as smart materials, the poor solubility of the molecule has limited its application in biological systems. Therefore, further optimisations by preparing water soluble fluorophores are required.

CHAPTER SEVEN

Experimental

7 Experimental Section

7.1 General Procedures

Solvent and reagents:

All solvent and reagents used in this project were reagent-grade unless stated otherwise. These were purchased from Fisher UK, and Sigma Aldrich Company Ltd, and were used without further purification, unless stated otherwise.

Chromatography:

Thin layer chromatography was performed using commercially available Merck aluminium backed plates coated with 0.2 mm layer of silica gel 60 with fluorescent indicator UV 254. These plates were visualised using either ultraviolet light of 254 nm or 365 nm wavelength, or staining the plate with visualising solution. Silica gel column chromatography was carried out using Davisil LC 60A silica gel.

Nuclear magnetic resonance spectroscopy (NMR):

^{1}H NMR spectroscopy was carried out measured using a Bruker AVANCE 300 spectrometer in the Chemistry Department and spectra were recorded at 500, 400, 300 or 250 MHz respectively in deuterated DMSO, $CDCl_3$ depending on the sample solubility. Chemical shifts are expressed in parts per million (ppm) and reported relative to the residual solvent peak or to tetramethylsilane (TMS) as an internal standard. The multiplicity and general assignments of the spectroscopic data are denoted as: singlet (s), doublet (d), triplet(t), quartet (q), quintet (quint), doublet of doublet (dd),doublet of triplet (dt) triplet of triplet (tt), unresolved multiplet (m), apparent (app), broad (br) and aryl (Ar).

Mass spectrometry (MS):

Electrospray mass spectra (positive ions ESI^{+}) were recorded using a Bruker micro TOF spectrometer using reserpine as calibrant.

UV-vis Measurement

Absorption measurements were recorded by employing Perkin-Elmer UV-*vis* spectrometer Lambda20 with 10 mm path length and two sides' polished cuvettes. Blank solvent was exploited for baseline correction, which was carried out every time before the experiments. This instrument was operated by UV Winlab software. All solvent used in fluorescence measurements were HPLC grade and the water was deionised.

Fluorescence spectroscopy measurements:

Fluorescence measurements were performed on a Perkin Elmer Luminescence spectrophotometer LS 50B, utilising sterna silica (quartz) cuvettes with 10 mm path length and four sides polished. Data was collected *via* the FlWinLab software package. All solvent used in fluorescence measurements were HPLC grade and the water was deionised.

Electrochemical voltammetry measurements:

Square wave voltammetric experiments were performed on a microAutolab III system (Metrohm-Autolab, Netherlands) in staircase voltammetry mode. The step potential was maintained at approximately 1 mV. The counter and reference electrode were platinum gauze and saturated calomel (SCE, Radiometer), respectively. The working electrode was a 2.0 mm diameter platinum disk electrode. Rotating disc voltammetry was performed with a Gamry 710 system. Solutions were de-aerated with argon (BOC). All experiments were conducted at a temperature of $22 \pm 2\ ^{o}C$.

Dual-plate generator-collector electrochemical experiments were performed on a SP-300 bipotentiostat (Biologic, France). A four-electrode cell was employed with a Pt wire counted electrode, saturated calomel electrode (SCE, Radiometer), and the working electrodes of the micro-trench electrode. A PWM32 spin coater was used to spin photoresist. Platinum films on glass substrates were prepared by electron-beam evaporation.

pH measurement:

Hanna Instruments HI 9321 Microprocessor pH meter was employed for making buffers and normally calibrated by Fisher Chemicals standard buffer solution (pH 4.0 - phthalate, 7.0 - phosphate, and 10.0 - borate) before the experiment.

Melting point:

Melting points of compound were determined from Stuart Melting point SMP10. After set a plateau temperature, the unit quickly heats up and remains at the selected plateau temperature. Then the sample tubes were inserted and the instrument started heating again, which remained at a fixed rate of 2 °C per minute. Carefully watch the sample and note the temperature on the screen when the sample is seen to melt. After the experiments, the SMP10 was shut down and cooled to the room temperature.

Solid state infrared (IR) spectroscopy

Perkin Elmer 1000 FT-IR Express spectrometer was employed for the IR measurements. Samples were positioned directly onto the spectrometer diamond plat and compressed. Then “start” was pressed, the spectrum was automatically displayed and processed by the software. Characteristic absorption peaks are presented in wavelength (cm^{-1}).

7.2 Synthesis

2-amino-6-bromo-1H-benzo[de]isoquinoline-1,3(2H)-dione, 45

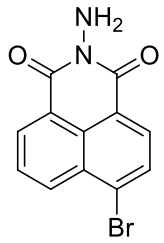

4-bromonaphthalic anhydride (2.77 g, 10 mmol) was dissolved in absolute ethanol (30 mL). An excess of hydrazine hydrate (85% w/w, 1.18 g, 20 mL) was added, after having refluxed for 4 h, the mixture was cooled and the precipitated solids were filtered and recrystallised from ethanol to give yellow solid (2.75 g, 95% yield). mp 220-225 ^{o}C (dec).

^{1}H NMR (300 MHz, DMSO-$d_{6,}$ ppm): δ_H 8.59 - 8.53 (m, 2H), 8.34 (d, J = 7.9 Hz, 1H), 8.21 (d, J = 7.9 Hz, 1H), 7.99 (apt, J = 7.4 Hz, 1H), 5.78 (s, 2H). ^{13}C NMR (75 MHz, DMSO-d_6, ppm): δ_C 160.3, 160.2, 133.1, 131.9, 131.7, 131.3, 129.6, 129.2, 127.3, 122.8, 122.0.

HRMS (ESI μTOF) m/z calcd for $C_{12}H_7N_2O_2Br$ $[M + H]^+$ 290.9769, found 290.9742.

IR (cm^{-1}) 1409, 1555, 1587, 1653, 1698, 3244, 3341

2-amino-6-(propylamino)-1H-benzo[de]isoquinoline-1,3(2H)-dione, 46

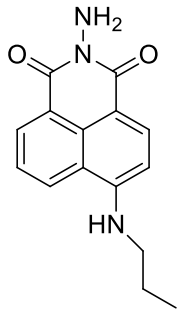

Compound **45** (1.16 g, 4 mmol) and 5 mL propylamine were added into 30 mL of 2-methoxyl ethanol and refluxed for 3 h. After the mixture cooled to room temperature, the mixture was poured into 100 mL water, the precipitated solids were filtered, was washed with ethanol and hexane, dried under vacuum to give a yellow solid (0.99 g, 92% yield). mp 215-218 ^{o}C (dec).

^{1}H NMR (300 MHz, DMSO-$d_{6,}$ ppm): δ_H 8.71 (dd, J_1 = 8.5 Hz, J_2 = 1.0 Hz, 1H), 8.59 (dd, J_1 = 7.3 Hz, J_2 = 1.0 Hz, 1H), 8.25 (d, J = 8.6 Hz, 1H), 7.84 (apt, J = 5.4 Hz, 1H), 7.69 - 7.64 (m，1H), 6.76 (d, J = 8.7 Hz, 1H), 5.70 (s, 2H), 3.40 - 3.44 (m, 2H), 1.76 - 1.64 (m, 2H), 0.97 (t, J = 7.4Hz, 3H,). ^{13}C NMR (75 MHz, DMSO-d_6, ppm): δ_C 160.5, 160.4, 151.4, 134.7, 130.9, 128.9, 124.6, 121.7, 120.5, 107.1, 104.2, 44.9, 21.5, 11.9.

HRMS (ESI μTOF) m/z calcd for $C_{15}H_{15}N_3O_2$ $[M + H]^+$ 270.1243, found 270.1241.

IR (cm^{-1}) 1398, 1567, 1611, 1673, 2878, 2961, 3222, 3317, 3379

(E)-6-(propylamino)-2-((2-(4,4,5,5-tetramethyl-1,3,2-dioxaborolan-2-yl)benzylidene)amino)-1H-benzo[de]isoquinoline-1,3(2H)-dione, 47

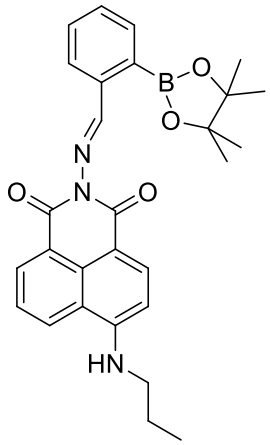

Compound **46** (0.27 g, 1.0 mmol) was dissolved in absolute ethanol (20 mL). An excess of 2-aldehyde boronic acid ester (0.50 g, 2.0 mmol) was added and the mixture was refluxed for 3 h. After the mixture was cooled to room temperature, the precipitate produced was filtered and washed with hexane (3×10 mL) to give a yellow solid (434.60 mg, 90% yield). mp 190-191 ^{o}C (dec).

^{1}H NMR (300 MHz, DMSO-$d_{6,}$ ppm): δ_H 9.14 (s, 1H), 8.72 (d, J = 10.0 Hz, 1H), 8.47 (d, J = 8.7 Hz, 1H), 8.29 (d, J = 10.1 Hz, 1H), 8.22 (d, J = 8.5 Hz, 1H), 7.86-7.81 (m, 2H), 7.72-7.60 (m, 3H), 6.78 (d, J = 10.3 Hz, 1H), 3.61-3.50 (m, 2H), 1.78-1.69 (m, 2H), 1.25 (s, 12H), 0.99 (t, J = 8.6 Hz, 3H,). ^{13}C NMR (75 MHz, DMSO-d_6, ppm): δ_C 170.8, 160.8, 160.3, 151.4, 137.7, 135.8, 135.1, 131.6, 131.5, 131.4, 129.2, 127.2, 124.6, 122.2, 120.5, 107.4, 104.4, 84.4, 44.9, 24.8, 21.5, 11.9.

HRMS (ESI μTOF) m/z calcd for $C_{28}H_{30}N_3O_4B$ $[M + H]^+$ 484.2408, found 484.2406.

IR (cm^{-1}) 1343, 1416, 1478, 1550, 1572, 1645, 1681, 2979, 3358

(E)-2-(benzylideneamino)-6-(propylamino)-1H-benzo[de]isoquinoline-1,3(2H)-dione, 48

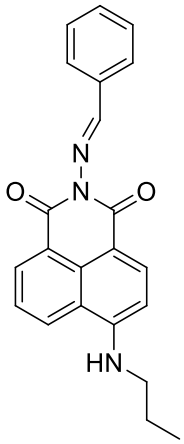

Compound **46** (0.06 g, 0.22 mmol) was dissolved in absolute ethanol (20 mL). An excess of benzaldehyde (0.04 g, 0.33 mmol) was added and the mixture was refluxed for 3 h. After the mixture was cooled to room temperature, the precipitate produced was filtered and washed with hexane (3×10 mL) to give a yellow solid (71.20 mg, 91% yield). mp 170-172 ^{o}C (dec).

^{1}HNMR (300 MHz, DMSO-d_6, ppm): δ_H 8.79 (d, J = 9.9 Hz, 1H), 8.71 (s, 1H), 8.49 (d, J = 8.7 Hz, 1H), 8.31 (d, J = 10.2 Hz, 1H), 8.00-7.89 (m, 3H), 7.34 (apt, J = 9.3 Hz, 1H), 7.67-7.55 (m, 3H), 6.84 (d, J = 10.5 Hz, 1H), 3.40 (t, J = 8.1 Hz, 2H), 1.82-1.68 (m, 2H), 1.02 (t, J = 8.7 Hz, 3H,). ^{13}C NMR (75 MHz, DMSO-d_6, ppm): δ_C 171.5, 160.8, 160.3, 151.4, 135.1, 133.0, 132.8, 131.3, 129.4, 129.3, 129.0, 124.7, 122.4, 120.6, 107.6, 104.4, 45.0, 21.5, 11.9.

HRMS (ESI μTOF) calcd m/z for $C_{22}H_{19}N_3O_2$ $[M+H]^+$ 358.1556, found 358.1564.

IR (cm^{-1}) 1372, 1447, 1571, 1632, 1681, 2874, 2960, 3290, 3427

(3-(6-bromo-1,3-dioxo-1H-benzo[de]isoquinolin-2(3H)-yl)phenyl)boronic acid, 49

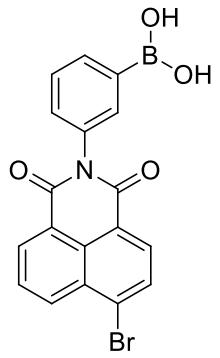

4-bromonaphthalic anhydride (2.00 g, 7.2 mmol) was dissolved in absolute ethanol (20 mL). An excess of 3-Aminobenzeneboronic acid (1.30 g, 8.6 mmol) was added and the mixture was refluxed for 2 h. After the mixture was cooled to room temperature, the precipitate produced was filtered and washed with hexane (3×10 mL) to give a yellow solid (2.57 g, 90% yield). mp 208-210 ^{o}C (dec).

^{1}H NMR (300 MHz, DMSO-$d_{6,}$ ppm): δ_H 8.65-8.58 (m, 2H), 8.39-8.33 (m, 1H), 8.29-8.24 (m, 1H), 8.20 (s, 1H), 8.08-8.00 (m, 1H), 7.90 (d, J = 8.6 Hz, 1H), 7.76 (d, J = 17.9 Hz, 1H), 7.55-7.43 (m, 1H). ^{13}C NMR (75 MHz, DMSO-d_6, ppm): δ_C 160.6, 160.5, 135.4, 133.9, 133.5, 132.3, 132.0，131.7, 130.6, 130.3, 129.5, 129.2, 123.6, 122.8, 120.2, 119.4.

HRMS (ESI μTOF) m/z calcd for $C_{18}H_{11}NO_4BBr$ $[M + H]^+$ 396.0043, found 396.0054.

IR (cm^{-1}) 1366, 1440, 1568, 1587, 1653, 1701, 1781, 3345

(3-(1,3-dioxo-6-(propylamino)-1H-benzo[de]isoquinolin-2(3H)-yl)phenyl)boronic acid, 50

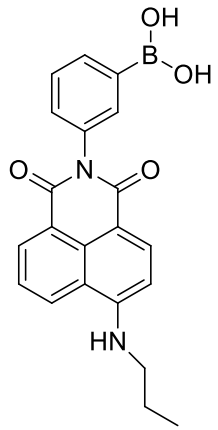

Compound **49** (0.80 g, 2 mmol) and 3 mL propylamine were added into 30 mL of 2-methoxyl ethanol and refluxed for 3 h. After the mixture cooled to room temperature, the solvent was removed under vacuum and the residue was purified using column chromatography (silica gel, DCM-MeOH, 20:1, v/v) to give a yellow solid (0.69 g, 92% yield). mp 221-223 ^{o}C (dec).

^{1}H NMR (300 MHz, DMSO-$d_{6,}$ ppm): δ_H 8.77-8.72 (m, 1H), 8.43-8.39 (m, 1H), 8.26-8.22 (m, 1H), 8.13 (s, 1H), 7.82 (d, J = 7.2 Hz, 1H), 7.72 - 7.62 (m, 1H), 7.62 - 7.43 (m, 1H), 7.33 - 7.2 2(m, 1H), 6.79 (dd, J_1 = 8.6 Hz, J_2 = 3.3 Hz, 1H), 6.69 - 6.65 (m, 1H), 3.40 - 3.35 (m, 2H), 1.78 - 1.66 (m, 2H), 0.98 (t, 3H, J = 7.3Hz). ^{13}C NMR (75 MHz, DMSO-$d_{6,}$ ppm): δc 164.4, 163.6 158.1, 151.2, 137.8, 136.2, 131.1, 129.7, 128.3, 124.6, 122.6, 120.6, 120.1, 116.6, 115.2, 107.9, 104.2, 44.9, 44.9, 21.5, 11.9.

HRMS (ESI μTOF) m/z calcd for $C_{21}H_{19}N_2O_4B$ $[M + H]^+$ 375.1516, found 375.1543.

IR (cm^{-1}) 1355, 1427, 1488, 1542, 1573, 1633, 1680, 2874, 2963, 3369

(E)-2-(2-(4-hydroxystyryl)-4H-chromen-4-ylidene)malononitrile, 52

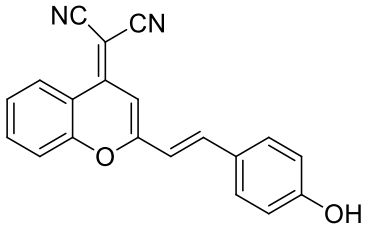

Compound **51** (0.21 mg, 1.00 mmol) and 4-hydroxybenzaldehyde (0.39 mg, 1.10 mmol) dissolved in 30 mL toluene. And then add 1.21 mL piperidine and 0.5 mL acetic acid. A Deam-Stark head was fitted and reaction mixture was heated under reflux for 8h. After the completion of the reaction, the mixture was allowed to cool to room temperature and then concentrated under reduced pressure. A red solid was obtained (0.20 g, 40.0%). mp 245-251 ^{o}C (dec).

^{1}H NMR(400MHz, DMSO-d_6, ppm):δ_H 10.16 (s, 1H), 8.73 (dd, J_1 = 8.4 Hz, J_2 = 1.2 Hz,1H), 7.91 (m, 1H), 7.79 (d, J = 7.6 Hz,1H), 7.70 (d, J = 16.0 Hz,1H), 7.60(m, 3H),7.28 (d, J = 16.0 Hz,1H), 6.96 (s, 1H), 6.85 (d, J = 8.8 Hz, 2H). ^{13}C NMR (100 MHz, DMSO-d_6, ppm): δ_C 165.3, 164.1, 158.1, 157.3, 144.5, 140.5, 135.6, 131.3, 129.8, 124.2, 122.6, 122.4, 121.3, 121.2, 121.1, 110.9, 64.3.

HRMS (ESI μTOF) calcd m/z for $C_{20}H_{12}N_2O_2$ $[M - H]^-$ 311.0843, found 311.0821.

IR (cm^{-1}) 811, 840, 970, 1168, 1201, 1618, 1456, 1550, 2210, 3375

(E)-4-(2-(4-(dicyanomethylene)-4H-chromen-2-yl)vinyl)phenyl2,4-dinitrobenzenesulfonate, 53

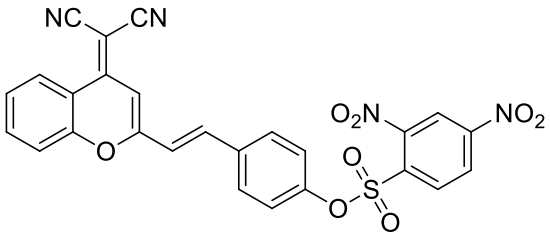

To a stirred solution of **52** (0.10 g, 0.32 mmol) in dry CH_2Cl_2 (15 mL) was added pyridine 0.5 mL. The mixture was then cooled to 0℃ and a solution of 2,4-dinitrobenzensulfonyl chloride (0.26 g, 0.96 mmol) in dry CH_2Cl_2 (5 mL) was added dropwise. After being stirred at 0℃for 30 minutes, the mixture continues to stir at room temperature for 3h. After the completion of the reaction, the mixture was concentrated under reduced pressure. The residue was purified with column chromatography (silica gel, DCM-MeOH, 20:1, v/v), and a red solid was obtained (0.05 g, 29.0%). mp 218 ^{o}C (dec).

^{1}H NMR(300MHz, $CDCl_3$, ppm):δ_H 8.86 (dd, J_1 = 8.4 Hz, J_2 = 1.3 Hz, 1H), 8.63 (d, J = 2.2 Hz,1H), 8.47 (dd, J_1 = 8.6 Hz, J_2 = 2.2 Hz, 1H), 8.20 (d, J = 8.6 Hz,1H), 7.70(m, 1H), 7.53 (m, 4H),7.41 (m, 1H), 7.25 (d, J = 8.8 Hz, 2H), 6.83 (s, 1H), 6.73 (d, J = 16.0 Hz, 1H). ^{13}C NMR(75 MHz, DMSO-d_6, ppm): δ_C 157.9, 153.9, 152.3, 151.9, 149.6, 148.5, 136.8, 135.9, 135.4, 133.9, 131.1, 130.4, 127.9, 126.6, 125.0, 123.1, 121.7, 121.5, 119.4, 117.4, 117.3, 116.0, 107.7, 61.4.

HRMS (ESI μTOF) calcd m/z for $C_{26}H_{14}N_4O_8S$ $[M - H]^-$ 541.0454, found 541.0472.

IR (cm^{-1}) 712, 855, 978, 1140, 1346, 1457, 1497, 1536, 1553, 1603, 2210, 3032

Ferrocenylmethylamine, 56

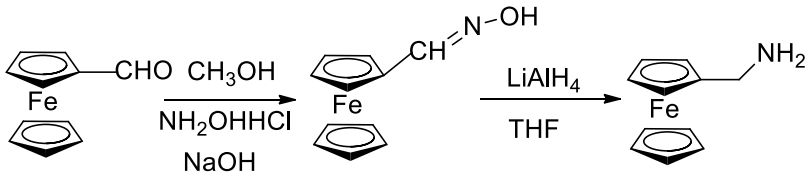

Ferrocenecarboxaldehyde (2.0 g, 9.34 mmol) and hydroxylamine hydrochloride (1.3 g, 18.68 mmol) were dissolved in 40 mL ethanol and NaOH (2.5 g, 62.27 mmol) was added. The reaction mixture was heated at reflux under an N_2 atmosphere for 3 h. The mixture was allowed to cool to room temperature and then concentrated under reduced pressure. The residue was poured into water (30 mL) and extracted with CH_2Cl_2 (3 × 50 mL). The organic layer was separated and combined and was evaporated under reduced pressure to give the crude product as dark brown solid 1.5g. The product was used for the next step without further purification.

To a stirred solution of $LiAlH_4$ (0.7 g, 18.4 mmol) in 10 ml anhydrous THF, a solution of ferrocenecarbaldehyde oxime (0.4 g, 1.75 mmol) in anhydrous THF (10 mL) was added dropwise. After being stirred at room temperature for 30 mins, the mixture was refluxed for 6 h under an N_2 atmosphere. After cooling to room temperature, the reaction mixture was poured into water (30 mL) and a grey precipitate formed. After filtration, the filtrate was transferred to separatory funnel and extracted with ethyl acetate (3 × 50 mL). The organic phase was evaporated under reduced pressure to give a yellow liquid (0.30 g, 80%). mp 113-115 ^{o}C (dec)

^{1}HNMR (300MHz, $CDCl_3$, ppm) δ_H 4.19 (s, 2H), 4.16 (s, 5H), 4.08 (s, 2H), 3.40 (s, 2H). ^{13}C NMR (125 MHz, $CDCl_3$, ppm): δ_C 68.3, 67.6, 67.1, 41.3.

IR (cm^{-1}) 999, 1103, 1304, 1470, 2200, 2622, 3080, 3431

2-ferrocenylmethyl-6-(piperazin-1-yl)benzo[de]isochromene-1,3-dione, 58

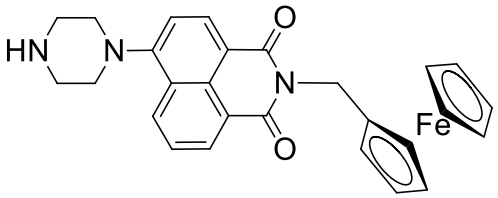

6-(Piperazin-1-yl)benzo[de]isochromene-1,3-dione (0.37 g, 1.30 mmol) and ferrocenylmethylamine (0.37 g, 1.72 mmol) were added into 30 mL ethanol. The mixture was refluxed for 5 h under a nitrogen atmosphere. After completion of the reaction, the solvent was removed *in vacuo* and the residue was purified with column chromatography (silica gel, DCM-MeOH, 1:1, v/v), and an orange solid was obtained (100 mg, 16%). mp 171-173 ^{o}C (dec).

^{1}H NMR (300 MHz, DMSO-$d_{6,}$ ppm): δ_H ^{1}HNMR (300 MHz, DMSO-d_6, ppm) δ_H 8.45 (d, J = 9.0 Hz, 1H), 8.39 (d, J = 8.5 Hz, 2H), 7.76 (apt, J = 7.5 Hz, 1H), 7.27 (d, J = 8.2 Hz, 1H), 4.95 (s, 2H), 4.32 (t, J = 1.8 Hz, 2H), 4.20 (s, 5H), 4.05 (t, J = 1.8 Hz, 2H), 3.13 (d, J = 2.8 Hz, 4H), 2.99 (d, J = 4.5 Hz, 4H). ^{13}C NMR (75 MHz, DMSO-d_6, ppm): δ_C 163.6, 163.0, 156.6, 132.8, 131.1, 129.4, 126.3, 125.6, 122.7, 115.4, 115.3, 83.8, 70.0, 68.8, 67.9, 54.1, 45.8.

HRMS (ESI µTOF) m/z calcd for $C_{27}H_{25}N_3O_2Fe$ $[M + Na]^+$ 502.1194, found 502.1203.

IR (cm^{-1}) 971, 1020, 1107, 1380, 1454, 1586, 1642, 1690, 2824, 2953, 3384

2-ferrocenylmethyl-6-(2-(bromomethy)phenyl-boronic ester-piperazin-1-yl)benzo[de]isochromene-1,3-dione, 59

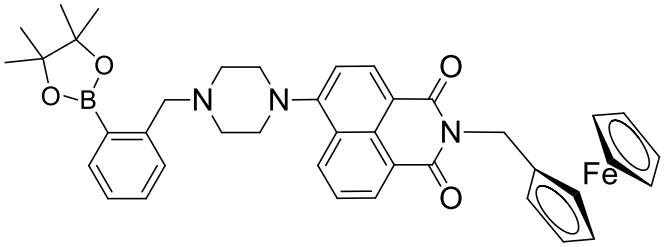

58 (70mg, 0.15 mmol) and 2-(2-(bromomethyl)phenyl)-4,4,5,5- tetramethyl-1,3,2-dioxaborolane (43.4 mg, 0.16 mmol) were dissolved in anhydrous acetonitrile. And K_2CO_3 (62.2 mg, 0.45 mmol) was added and the mixture was refluxed overnight. After completion of the reaction, most of the acetonitrile was evaporated and the residue was poured into water to give the precipitate (70 mg, 67%). mp 135 ^oC (dec).

^1H NMR (300 MHz, CD_3CN, ppm): δ_H 8.45 (dd, J_1 = 7.3 Hz, J_2 = 1.1 Hz, 1H), 8.37 (apt, J = 8.2 Hz, 2H), 7.69 - 7.66 (m, 1H), 7.65 - 7.63(m, 1H), 7.38 (dd, J_1 = 7.3 Hz, J_2 = 1.5 Hz, 1H), 7.33 - 7.25(m, 2H), 7.16 (d, J = 8.2 Hz, 1H), 5.00 (s, 2H), 4.38 (t, J = 1.8 Hz, 2H), 4.20 (s, 5H), 4.06 (t, J = 1.8 Hz, 2H), 3.77(s, 2H), 3.18 (s, 4H), 2.69 (t, J = 4.6 Hz, 4H), 1.36 (s, 12H). ^{13}C NMR (75 MHz, DMSO-d_6, ppm): δ_C 163.6, 163.0, 156.0, 143.9, 135.0, 132.7, 131.1, 131.0, 130.3, 129.5, 129.4, 126.8, 126.4, 125.5, 122.8, 115.6, 115.3, 83.8, 83.4, 70.0, 69.0, 67.9, 61.6, 52.9, 52.7, 25.2.

HRMS (ESI μTOF) m/z calcd for $C_{40}H_{42}N_3O_4BFe$ $[M + Na]^+$ 718.2515, found 718.2559.

IR (cm^{-1}) 1038, 1107, 1345, 1422, 1451, 1587, 1563, 1693, 2823, 2974

7.3 Cancer Cell Culturing

The cells were prepared by Dr. Rory Arrowsmith and Haobo Ge from Dr Sofia Pascu's group. The HeLa cells were cultured at 37 ^{o}C in 5% CO_2 in Earle's minimal essential medium supplemented with 10% heat inactivated FCS (Foetal Calf Serum), 1% L-glutamine and sodium bicarbonate, 0.5% penicillin/streptomycin. Medium needs to be refreshed every 2 - 3 days. Supernatant containing dead cells and metabolite was aspirated. The live adherent cells were then rinsed with 10 mL phosphate buffer saline (PBS) twice to remove any remaining FCS, which inactivates trypsin. Cells were resuspended by 10mL of PBS with 2.5 mL trypsin and incubate for 5 min at 37 ^{o}C. After cells detached, 5mL of serum medium was added to inactivate the trypsin and the solution was centrifuged for 5 min (1000 rpm at room temperature) to precipitate cultured cells. The supernatant was aspirated and 5 mL of medium was added. Cells were counted using a haemocytometer and then used for confocal imaging.

7.4 Confocal Microscope Imaging

The confocal image was prepared by Dr. Rory Arrowsmith and Haobe Ge from Dr Sofia Pascu's group. For confocal fluorescence microscopy HeLa cells were plated in 35 mm uncoated 1.5 mm thick glass-bottomed dishes as 3 x 105 cells per dish and incubated for at least 24 h. Cells were washed five times with 990µl Hank's solution, before adding SFM (990 µL). Subsequently, 1% compound in DMSO was added to obtain a final volume of 1 mL at 50 µm concentration. After 15 min incubation cells were washed 3 times with Hank's solution and incubated in SFM prior to imaging.

CHAPTER EIGHT

BIBLIOGRAPHY

8 Bibliography

1. X. Qian, Y. Xiao, Y. Xu, X. Guo, J. Qian and W. Zhu, *Chem. Commun.*, 2010, **46**, 6418-6436.
2. B. L. Feringa and W. R. Browne, *Molecular switches*, Wiley Online Library, 2001.
3. J. Andréasson, G. Kodis, Y. Terazono, P. A. Liddell, S. Bandyopadhyay, R. H. Mitchell, T. A. Moore, A. L. Moore and D. Gust, *J. Am. Chem. Soc.*, 2004, **126**, 15926-15927.
4. B. Rout, P. Milko, M. A. Iron, L. Motiei and D. Margulies, *J. Am. Chem. Soc.*, 2013, **135**, 15330-15333.
5. R. Martínez, I. Ratera, A. Tárraga, P. Molina and J. Veciana, *Chem. Commun.*, 2006, 3809-3811.
6. J. C. Spiteri, J. S. Schembri and D. C. Magri, *New J. Chem.*, 2015, **39**, 3349-3352.
7. J. R. Lakowicz, *Principles of fluorescence spectroscopy*, Springer Science & Business Media, 2007.
8. W. R. A. R. Lapouyade, *Top. Fluoresc. Spectrosc.*, 2002, **4**, 109-149.
9. A. W. Czarnik, *Top. Fluoresc. Spectrosc.*, 2002, **4**, 21-48.
10. T. D. James, *Top Curr Chem*, 2007, **277**, 107-152.
11. C. Gutsche, J. Atwood, J. Davies and D. MacNicol, *CD in inclusion compounds*, Oxford University Press Oxford, 1991.
12. C. D. Gutsche, *Calixarenes revisited*, *Royal Society of Chemistry, Cambridge*, 1998, **6**.
13. J. S. Kim and D. T. Quang, *Chem. Rev.*, 2007, **107**, 3780-3799.
14. Z. Xu, Y. Xiao, X. Qian, J. Cui and D. Cui, *Org. Lett.*, 2005, **7**, 889-892.
15. H.-F. Ji, R. Dabestani, G. M. Brown and R. A. Sachleben, *Chem. Commun.*, 2000, 833-834.
16. H.-F. Ji, R. Dabestani, G. M. Brown and R. L. Hettich, *J. Chem. Soc. Perkin. Trans. 2*, 2001, 585-591.
17. R. A. Bissell, A. P. de Silva, H. Q. N. Gunaratne, P. L. M. Lynch, G. E. M. Maguire and K. R. A. S. Sandanayake, *Chem. Soc. Rev.*, 1992, **21**, 187-195.
18. M. Fox and M. Chanon, *Photoduced electron transfer*, Amsterdam [etc.]: Elsevier, 1988.
19. G. He, X. Zhao, X. Zhang, H. Fan, S. Wu, H. Li, C. He and C. Duan, *New J. Chem.*, 2010, **34**, 1055-1058.
20. J. R. Lakowicz, *Principles of fluorescence spectroscopy*, Springer, 2009.
21. T. Förster, *Intermolecular energy transfer and fluorescence*, National Research Council of Canada, 1955.

22. Z. Hu, J. Hu, Y. Cui, G. Wang, X. Zhang, K. Uvdal and H.-W. Gao, *J. Mater. Chem. B*, 2014, **2**, 4467-4472.
23. J. Wu, W. Liu, J. Ge, H. Zhang and P. Wang, *Chem. Soc. Rev.*, 2011, **40**, 3483-3495.
24. B. Liu and B. Z. Tang, *Macromol. Rapid Commun.*, 2013, **34**, 704.
25. X. Chen, T. Pradhan, F. Wang, J. S. Kim and J. Yoon, *Chem. Rev.*, 2012, **112**, 1910-1956.
26. Y. Li, C. Chen, B. Li, J. Sun, J. Wang, Y. Gao, Y. Zhao and Z. Chai, *J. Anal. At. Spectrom.*, 2006, **21**, 94-96.
27. O. T. Butler, J. M. Cook, C. F. Harrington, S. J. Hill, J. Rieuwerts and D. L. Miles, *J. Anal. At. Spectrom.*, 2007, **22**, 187-221.
28. X. Chen, X. Tian, I. Shin and J. Yoon, *Chem. Soc. Rev.*, 2011, **40**, 4783-4804.
29. T. Yanagida and Y. Ishii, *Single molecule dynamics in life science*, John Wiley & Sons, 2008.
30. R. M. Duke, E. B. Veale, F. M. Pfeffer, P. E. Kruger and T. Gunnlaugsson, *Chem. Soc. Rev.*, 2010, **39**, 3936-3953.
31. M. Beija, C. A. Afonso and J. M. Martinho, *Chem. Soc. Rev.*, 2009, **38**, 2410-2433.
32. J.-T. Yeh, W.-C. Chen, S.-R. Liu and S.-P. Wu, *New J. Chem.*, 2014, **38**, 4434-4439.
33. Y. Zhou, F. Wang, Y. Kim, S.-J. Kim and J. Yoon, *Org. Lett.*, 2009, **11**, 4442-4445.
34. J. F. Zhang, Y. Zhou, J. Yoon, Y. Kim, S. J. Kim and J. S. Kim, *Org. Lett.*, 2010, **12**, 3852-3855.
35. S. Yin, V. Leen, S. V. Snick, N. Boens and W. Dehaen, *Chem. Commun.*, 2010, **46**, 6329-6331.
36. H. Y. Lee, H. Son, J. M. Lim, J. Oh, D. Kang, W. S. Han and J. H. Jung, *Analyst*, 2010, **135**, 2022-2027.
37. A. P. de Silva, H. Q. N. Gunaratne, T. Gunnlaugsson, A. J. M. Huxley, J. T. Rademacher, T. E. Rice, J. P. Desvergne and A. W. Czarnik, *Chemosensors of ion and molecule recognition*, Springer, 1997, 143.
38. J. Zhang, Q. Wu, B. Yu and C. Yu, *Sensors*, 2014, **14**, 24146-24155.
39. C. Zou, L. Gao, T. Liu, Z. Xu and J. Cui, *J. Inclusion Phenom. Macrocyclic Chem.*, 1-8.
40. Z. Chen, L. Wang, G. Zou, J. Tang, X. Cai, M. Teng and L. Chen, *Spectrochim Acta A Mol Biomol Spectrosc*, 2013, **105**, 57-61.
41. Z. Liu, C. Zhang, X. Wang, W. He and Z. Guo, *Org. Lett.*, 2012, **14**, 4378-4381.
42. J. Huang, Y. Xu and X. Qian, *Org. Biomol. Chem.*, 2009, **7**, 1299-1303.
43. J. P. Lorand and J. O. Edwards, *J. Org. Chem.*, 1959, **24**, 769-774.
44. J. Zhao, M. G. Davidson, M. F. Mahon, G. Kociok-Köhn and T. D. James, *J. Am. Chem. Soc.*, 2004, **126**, 16179-16186.
45. K. M. Swamy, S. K. Ko, S. K. Kwon, H. N. Lee, C. Mao, J. M. Kim, K. H. Lee, J. Kim, I. Shin and J. Yoon, *Chem Commun (Camb)*, 2008, 5915-5917.

46. S. K. Kim, K. M. K. Swamy, S.-Y. Chung, H. N. Kim, M. J. Kim, Y. Jeong and J. Yoon, *Tetrahedron Lett.*, 2010, **51**, 3286-3289.
47. S.-H. Li, F.-R. Chen, Y.-F. Zhou, J.-N. Wang, H. Zhang and J.-G. Xu, *Chem. Commun.*, 2009, 4179-4181.
48. D. W. Jacobsen, *Clin. Chem.*, 1998, **44**, 1833-1843.
49. D. M. Townsend, K. D. Tew and H. Tapiero, *Biomed. Pharmacother.*, 2004, **58**, 47-55.
50. C. Hwang, A. J. Sinskey and H. F. Lodish, *Science*, 1992, **257**, 1496-1502.
51. P. K. Pullela, T. Chiku, M. J. Carvan III and D. S. Sem, *Anal. Biochem.*, 2006, **352**, 265-273.
52. M. Rafii, R. Elango, G. Courtney-Martin, J. D. House, L. Fisher and P. B. Pencharz, *Anal. Biochem.*, 2007, **371**, 71-81.
53. W. Chen, Y. Zhao, T. Seefeldt and X. Guan, *J. Pharm. Biomed. Anal.*, 2008, **48**, 1375-1380.
54. A. Zinellu, S. Sotgia, B. Scanu, M. F. Usai, A. G. Fois, V. Spada, A. Deledda, L. Deiana, P. Pirina and C. Carru, *Amino Acids*, 2009, **37**, 395-400.
55. M. Wen, H. Liu, F. Zhang, Y. Zhu, D. Liu, Y. Tian and Q. Wu, *Chem. Commun.*, 2009, 4530-4532.
56. Y. Kanaoka, M. Machida, K. Ando and T. Sekine, *BBA Protein Struct.*, 1970, **207**, 269-277.
57. H. Kwon, K. Lee and H.-J. Kim, *Chem. Commun.*, 2011, **47**, 1773-1775.
58. H. S. Jung, J. H. Han, T. Pradhan, S. Kim, S. W. Lee, J. L. Sessler, T. W. Kim, C. Kang and J. S. Kim, *Biomaterials*, 2012, **33**, 945-953.
59. S. Ji, H. Guo, X. Yuan, X. Li, H. Ding, P. Gao, C. Zhao, W. Wu, W. Wu and J. Zhao, *Org. Lett.*, 2010, **12**, 2876-2879.
60. L. Yuan, W. Lin, S. Zhao, W. Gao, B. Chen, L. He and S. Zhu, *J. Am. Chem. Soc.*, 2012, **134**, 13510-13523.
61. L.-Y. Niu, Y.-S. Guan, Y.-Z. Chen, L.-Z. Wu, C.-H. Tung and Q.-Z. Yang, *J. Am. Chem. Soc.*, 2012, **134**, 18928-18931.
62. M. H. Lee, J. H. Han, P.-S. Kwon, S. Bhuniya, J. Y. Kim, J. L. Sessler, C. Kang and J. S. Kim, *J. Am. Chem. Soc.*, 2011, **134**, 1316-1322.
63. B. Zhu, X. Zhang, Y. Li, P. Wang, H. Zhang and X. Zhuang, *Chem. Commun.*, 2010, **46**, 5710-5712.
64. B. Zhu, X. Zhang, H. Jia, Y. Li, S. Chen and S. Zhang, *Dyes Pigm.*, 2010, **86**, 87-92.
65. R. Wang, L. Chen, P. Liu, Q. Zhang and Y. Wang, *Chem. -Eur. J.*, 2012, **18**, 11343-11349.
66. L. Long, W. Lin, B. Chen, W. Gao and L. Yuan, *Chem. Commun.*, 2011, **47**, 893-895.
67. H. S. Jung, J. H. Han, Y. Habata, C. Kang and J. S. Kim, *Chem. Commun.*, 2011, **47**, 5142-5144.

68. L. Zhou, Y. Lin, Z. Huang, J. Ren and X. Qu, *Chem. Commun.*, 2012, **48**, 1147-1149.
69. J. Bourson and B. Valeur, *J. Phys. Chem.*, 1989, **93**, 3871-3876.
70. B. Valeur and M. N. Berberan-Santos, *Molecular fluorescence: principles and applications*, John Wiley & Sons, 2012.
71. C. Tang, S. VanSlyke and C. Chen, *J. Appl. Phys.*, 1989, **65**, 3610-3616.
72. Z. Guo, W. Zhu and H. Tian, *Chem. Commun.*, 2012, **48**, 6073-6084.
73. J. F. Callan, A. P. de Silva and D. C. Magri, *Tetrahedron*, 2005, **61**, 8551-8588.
74. R. Martínez-Máñez and F. Sancenón, *Chem. Rev.*, 2003, **103**, 4419-4476.
75. X. Huang, Z. Guo, W. Zhu, Y. Xie and H. Tian, *Chem. Commun.*, 2008, 5143-5145.
76. W. Zhu, X. Huang, Z. Guo, X. Wu, H. Yu and H. Tian, *Chem. Commun.*, 2012, **48**, 1784-1786.
77. Z. Guo, W. Zhu and H. Tian, *Macromolecules*, 2009, **43**, 739-744.
78. J. Cao, C. Zhao and W. Zhu, *Tetrahedron Lett.*, 2012, **53**, 2107-2110.
79. A. Fisher, *Electrode dynamics*, Oxford University Press, 1996.
80. K. Lawrence, *Core-Shell functionalised carbon nanoparticles: synthesis, electrochemistry*, and fluorescence, University of Bath, 2013.
81. Carbon Monoixide Alarm, http://www.remastersys.com/sale/pz5285839-z58f683e-carbon-monoxide-alarm-with-electrochemical-sensor-and-90-to-270v-ac-operating-voltage.html.
82. S. D. Bull, M. G. Davidson, J. M. Van den Elsen, J. S. Fossey, A. T. A. Jenkins, Y.-B. Jiang, Y. Kubo, F. Marken, K. Sakurai and J. Zhao, *Acc. Chem. Res.*, 2012, **46**, 312-326.
83. T. D. James, M. D. Phillips and S. Shinkai, *Boronic acids in saccharide recognition*, Royal Society of Chemistry, 2006.
84. X. Wu, Z. Li, X.-X. Chen, J. S. Fossey, T. D. James and Y.-B. Jiang, *Chem. Soc. Rev.*, 2013, **42**, 8032-8048.
85. R. Nishiyabu, Y. Kubo, T. D. James and J. S. Fossey, *Chem. Commun.*, 2012, **47**, 1106-1123.
86. R. Nishiyabu, Y. Kubo, T. D. James and J. S. Fossey, *Chem. Commun.*, 2011, **47**, 1124-1150.
87. J. S. Fossey, F. D'Hooge, J. M. van den Elsen, M. P. Pereira Morais, S. I. Pascu, S. D. Bull, F. Marken, A. T. A. Jenkins, Y. B. Jiang and T. D. James, *Chem. Rec.*, 2012, **12**, 464-478.
88. G. F. Whyte, R. Vilar and R. Woscholski, *J. Chem. Biol.*, 2013, **6**, 161-174.
89. X. Wang, N. Xia and L. Liu, *Int. J. Mol. Sci.*, 2013, **14**, 20890-20912.
90. K. Lacina, P. Skládal and T. D. James, *Chem. Cent. J.*, 2014, **8**, 60.
91. E. Galbraith and T. D. James, *Chem. Soc. Rev.*, 2010, **39**, 3831-3842.
92. Z. Guo, I. Shin and J. Yoon, *Chem. Commun.*, 2012, **48**, 5956-5967.

93. X. Wu, X.-X. Chen, B.-N. Song, Y.-J. Huang, W.-J. Ouyang, Z. Li, T. D. James and Y.-B. Jiang, *Chem. Commun.*, 2014, **50**, 13987-13989.
94. T. Nishimura, S.-Y. Xu, Y.-B. Jiang, J. S. Fossey, K. Sakurai, S. D. Bull and T. D. James, *Chem. Commun.*, 2013, **49**, 478-480.
95. X.-P. He, X.-W. Wang, X.-P. Jin, H. Zhou, X.-X. Shi, G.-R. Chen and Y.-T. Long, *J. Am. Chem. Soc.*, 2011, **133**, 3649-3657.
96. J. L. Hammond, A. J. Gross, P. Estrela, J. Iniesta, S. J. Green, C. P. Winlove, P. G. Winyard, N. Benjamin and F. Marken, *Anal. Chem.*, 2014, **86**, 6748-6752.
97. X. R. Cheng, B. Y. Hau, T. Endo and K. Kerman, *Biosens. Bioelectron.*, 2014, **53**, 513-518.
98. J. H. Morris, H. J. Gysling and D. Reed, *Chem. Rev.*, 1985, **85**, 51-76.
99. L. Liu, N. Xia, Y. Xing and D. Deng, *Int. J. Electrochem. Sci*, 2013, **8**, 11161-11174.
100. M. Picot, L. Lapinsonnière, M. Rothballer and F. Barrière, *Biosens. Bioelectron.*, 2011, **28**, 181-188.
101. Z. Wang, F. Li, J. Xia, L. Xia, F. Zhang, S. Bi, G. Shi, Y. Xia, J. Liu and Y. Li, *Biosens. Bioelectron.*, 2014.
102. B. Wang, S. Takahashi, X. Du and J.-i. Anzai, *Biosensors*, 2014, **4**, 243-256.
103. K. V. Kong, C. J. H. Ho, T. Gong, W. K. O. Lau and M. Olivo, *Biosens. Bioelectron.*, 2014, **56**, 186-191.
104. C. Bresner, S. Aldridge, I. A. Fallis and L.-L. Ooi, *Acta Crystallogr. Sect. E Struct. Rep. Online*, 2004, **60**, m441-m443.
105. K. Lacina and P. Skládal, *Electrochim. Acta*, 2011, **56**, 10246-10252.
106. M. Şenel, C. Nergiz, M. Dervisevic and E. Çevik, *Electroanalysis*, 2013, **25**, 1194-1200.
107. K. Morita, N. Hirayama, H. Imura, A. Yamaguchi and N. Teramae, *J. Electroanal. Chem.*, 2011, **656**, 192-197.
108. Q. Wang, I. Kaminska, J. Niedziolka-Jonsson, M. Opallo, M. Li, R. Boukherroub and S. Szunerits, *Biosens. Bioelectron.*, 2013, **50**, 331-337.
109. H.-C. Wang, H. Zhou, B. Chen, P. M. Mendes, J. S. Fossey, T. D. James and Y.-T. Long, *Analyst*, 2013, **138**, 7146-7151.
110. V. Amendola and J.-P. Sauvage, *Molecular machines and motors*, Springer, 2001.
111. Y. Wu, Y. Xie, Q. Zhang, H. Tian, W. Zhu and A. D. Li, *Angew. Chem.-Int. Edit.*, 2014, **53**, 2090-2094.
112. S. Shinkai, T. Nakaji, Y. Nishida, T. Ogawa and O. Manabe, *J. Am. Chem. Soc.*, 1980, **102**, 5860-5865.
113. S. Shinkai, T. Nakaji, T. Ogawa, K. Shigematsu and O. Manabe, *J. Am. Chem. Soc.*, 1981, **103**, 111-115.
114. S. Shinkai, *Pure Appl. Chem.*, 1987, **59**, 425-430.

115. R. Martinez, I. Ratera, A. Tarraga, P. Molina and J. Veciana, *Chem. Commun.*, 2006, 3809-3811.
116. R. Zhang, Z. Wang, Y. Wu, H. Fu and J. Yao, *Org. Lett.*, 2008, **10**, 3065-3068.
117. W. Zhu, L. Song, Y. Yang and H. Tian, *Chem. -Eur. J.*, 2012, **18**, 13388-13394.
118. P. A. de Silva, N. H. Gunaratne and C. P. McCoy, *Nature*, 1993, **364**, 42-44.
119. D. C. Magri, G. J. Brown, G. D. McClean and A. P. de Silva, *J. Am. Chem. Soc.*, 2006, **128**, 4950-4951.
120. S. Ozlem and E. U. Akkaya, *J. Am. Chem. Soc.*, 2008, **131**, 48-49.
121. D. H. Qu, F. Y. Ji, Q. C. Wang and H. Tian, *Adv. Mater.*, 2006, **18**, 2035-2038.
122. A. Prasanna de Silva and N. D. McClenaghan, *J. Am. Chem. Soc.*, 2000, **122**, 3965-3966.
123. B. Wang, *Tetrahedron*, 2002, **58**, 5291-5300.
124. N. Y. Edwards, T. W. Sager, J. T. McDevitt and E. V. Anslyn, *J. Am. Chem. Soc.*, 2007, **129**, 13575-13583.
125. S. Gamsey, A. Miller, M. M. Olmstead, C. M. Beavers, L. C. Hirayama, S. Pradhan, R. A. Wessling and B. Singaram, *J. Am. Chem. Soc.*, 2007, **129**, 1278-1286.
126. P. Li, X. Duan, Z. Chen, Y. Liu, T. Xie, L. Fang, X. Li, M. Yin and B. Tang, *Chem. Commun.*, 2011, **47**, 7755-7757.
127. N. J. Robinson and D. R. Winge, *Biochemistry*, 2010, **79**, 537-562.
128. E. L. Que, D. W. Domaille and C. J. Chang, *Chem. Rev.*, 2008, **108**, 1517-1549.
129. S. G. Kaler, *Nat. Rev. Neurol.*, 2011, **7**, 15-29.
130. I. Bertini and A. Rosato, *Cell. Mol. Life Sci.*, 2008, **65**, 89-91.
131. T. Finkel, M. Serrano and M. A. Blasco, *Nature*, 2007, **448**, 767-774.
132. Q. Zou, X. Li, J. Zhang, J. Zhou, B. Sun and H. Tian, *Chem. Commun.*, 2012, **48**, 2095-2097.
133. Z.-Q. Guo, W.-Q. Chen and X.-M. Duan, *Org. Lett.*, 2010, **12**, 2202-2205.
134. S. Dalapati, S. Jana, M. A. Alam and N. Guchhait, *Sens. Actuators B Chem.*, 2011, **160**, 1106-1111.
135. N. Shao, G.-X. Pang, X.-R. Wang, R.-J. Wu and Y. Cheng, *Tetrahedron*, 2010, **66**, 7302-7308.
136. R. Hernández-Molina and A. Mederos, in *Comprehensive Coordination Chemistry II*, ed. J. A. M. J. Meyer, Pergamon, Oxford, 2003, pp. 411-446.
137. N. Aksuner, E. Henden, I. Yilmaz and A. Cukurovali, *Dyes Pigm.*, 2009, **83**, 211-217.
138. N. R. Chereddy and S. Thennarasu, *Dyes Pigm.*, 2011, **91**, 378-382.
139. S. Kyung áKwon and H. Na áLee, *Chem. Commun.*, 2008, 5915-5917.
140. H. S. Jung, P. S. Kwon, J. W. Lee, J. I. Kim, C. S. Hong, J. W. Kim, S. Yan, J. Y. Lee, J. H. Lee, T. Joo and J. S. Kim, *J. Am. Chem. Soc.*, 2009, **131**, 2008-2012.

141. P. A. A. J. Waghorn, Michael W. and Theobald, Mark B. M. and Arrowsmith, Rory L. and Pascu, Sofia I. and Botchway, Stanley W. and Faulkner, Stephen and Dilworth, Jonathan R., *Chem Sci.*, 2013, **4**, 1430-1441.

142. R. L. Arrowsmith, P. A. Waghorn, M. W. Jones, A. Bauman, S. K. Brayshaw, Z. Hu, G. Kociok-Köhn, T. L. Mindt, R. M. Tyrrell and S. W. Botchway, *Dalton Trans.*, 2011, **40**, 6238-6252.

143. B. McCranor, H. Szmacinski, H. H. Zeng, T. Hurst, A. Stoddard, C. A. Fierke, J. Lakowicz and R. B. Thompson, *Metallomics*, 2014, **6**, 1034–1042.

144. A. Renfrew, N. S. Bryce and T. Hambley, *Chem. Sci.*, 2013, **4**, 3731-3439.

145. J. R. Lakowicz, *Principles of fluorescence spectroscopy*, 4th Printing edn., Springer, 2006.

146. K. M. K. Swamy, S.-K. Ko, S. K. Kwon, H. N. Lee, C. Mao, J.-M. Kim, K.-H. Lee, J. Kim, I. Shin and J. Yoon, *Chem. Commun.*, 2008, 5915-5917.

147. H. Refsum, A. D. Smith, P. M. Ueland, E. Nexo, R. Clarke, J. McPartlin, C. Johnston, F. Engbaek, J. Schneede and C. McPartlin, *Clin. Chem.*, 2004, **50**, 3-32.

148. Z. A. Wood, E. Schröder, J. Robin Harris and L. B. Poole, *Trends Biochem. Sci.*, 2003, **28**, 32-40.

149. A. Pastore, F. Piemonte, M. Locatelli, A. L. Russo, L. M. Gaeta, G. Tozzi and G. Federici, *Clin. Chem.*, 2001, **47**, 1467-1469.

150. H. Tapiero, D. Townsend and K. Tew, *Biomed. Pharmacother.*, 2003, **57**, 134-144.

151. D. Zhai, S.-C. Lee, S.-W. Yun and Y.-T. Chang, *Chem. Commun.*, 2013, **49**, 7207-7209.

152. X. Chen, Y. Zhou, X. Peng and J. Yoon, *Chem. Soc. Rev.*, 2010, **39**, 2120-2135.

153. Y. Zhou, H. Zhou, T. Ma, J. Zhang and J. Niu, *Spectrochim. Acta, Part. A*, 2012, **88**, 56-59.

154. N. Zhao, Y.-H. Wu, L.-X. Shi, Q.-P. Lin and Z.-N. Chen, *Dalton Trans.*, 2010, **39**, 8288-8295.

155. R. Zhang, X. Yu, Z. Ye, G. Wang, W. Zhang and J. Yuan, *Inorg. Chem.*, 2010, **49**, 7898-7903.

156. J. Bouffard, Y. Kim, T. M. Swager, R. Weissleder and S. A. Hilderbrand, *Org. Lett.*, 2008, **10**, 37-40.

157. S.-P. Wang, W.-J. Deng, D. Sun, M. Yan, H. Zheng and J.-G. Xu, *Org. Biomol. Chem.*, 2009, **7**, 4017-4020.

158. T. D. James, M. D. Phillips and S. Shinkai, *Boronic acids in saccharide recognition*, Royal Society of Chemistry, 2006.

159. K. Lawrence, T. Nishimura, P. Haffenden, J. M. Mitchels, K. Sakurai, J. S. Fossey, S. D. Bull, T. D. James and F. Marken, *New J. Chem.*, 2013, **37**, 1883-1888.

160. N. Katif, R. A. Harries, A. M. Kelly, J. S. Fossey, T. D. James and F. Marken, *J. Solid State Electrochem.*, 2009, **13**, 1475-1482.
161. M. Li, G. E. M. Lewis, T. D. James, Y.-T. Long, B. Kasprzyk-Hordern, J. M. Mitchels and F. Marken, *ChemElectroChem*, 2014, **1**, 1640-1646.
162. Y.-J. Huang, W.-J. Ouyang, X. Wu, Z. Li, J. S. Fossey, T. D. James and Y.-B. Jiang, *J. Am. Chem. Soc.*, 2013, **135**, 1700-1703.
163. J. S. Hansen, J. B. Christensen, J. F. Petersen, T. Hoeg-Jensen and J. C. Norrild, *Sens. Actuators B Chem.*, 2012, **161**, 45-79.
164. C. Dusemund, K. S. Sandanayake and S. Shinkai, *J. Chem. Soc., Chem. Commun.*, 1995, 333-334.
165. S. Liu, U. Wollenberger, M. Katterle and F. W. Scheller, *Sens. Actuators B Chem.*, 2006, **113**, 623-629.
166. L. Bosch, T. Fyles and T. D. James, *Tetrahedron*, 2004, **60**, 11175-11190.
167. A. M. Bond, S. W. Feldberg, H. B. Greenhill, P. J. Mahon, R. Colton and T. Whyte, *Anal. Chem.*, 1992, **64**, 1014-1021.
168. S. E. Dale, Y. Chan, P. C. Bulman Page, E. O. Barnes, R. G. Compton and F. Marken, *Electrophoresis*, 2013, **34**, 1979-1984.
169. S. E. Dale, C. E. Hotchen and F. Marken, *Electrochim. Acta*, 2013, **101**, 196-200.
170. V. Mirceski and R. Gulaboski, *Maced. J. Chem. Chem. En.*, 2014, **33**, 1-12.
171. A. J. Gross and F. Marken, *Electrochem. Commun.*, 2014, **46**, 120-123.
172. F. Marken, J. C. Eklund and R. G. Compton, *J. Electroanal. Chem.*, 1995, **395**, 335-339.
173. A. J. Gross, S. Holmes, S. E. Dale, M. J. Smallwood, S. J. Green, C. P. Winlove, N. Benjamin, P. G. Winyard and F. Marken, *Talanta*, 2015, **131**, 228-235.
174. K. Lacina, J. Novotný, Z. Moravec and P. Skládal, *Electrochim. Acta*, 2015, **153**, 280-286.
175. J. W. Tomsho and S. J. Benkovic, *J. Org. Chem.*, 2012, **77**, 2098-2106.
176. S.-X. Guo, S. W. Feldberg, A. M. Bond, D. L. Callahan, P. J. Richardt and A. G. Wedd, *J. Phys. Chem. B*, 2005, **109**, 20641-20651.
177. A. T. Hubbard and D. Peters, *Electrochemistry in thin layers of solution*, 1973, **3**, 201-242.
178. M. A. Hasnat, A. J. Gross, S. E. Dale, E. O. Barnes, R. G. Compton and F. Marken, *Analyst*, 2014, **139**, 569-575.
179. S. E. Dale, A. Vuorema, M. Sillanpää, J. Weber, A. J. Wain, E. O. Barnes, R. G. Compton and F. Marken, *Electrochim. Acta*, 2014, **125**, 94-100.
180. A. N. F. Marken, A.M. Bond, Electroanalytical Methods, *Springer*, 2010, 89-106.
181. E. Laborda, J. González and Á. Molina, *Electrochem. Commun.*, 2014, **43**, 25-30.
182. A. P. de Silva and S. Uchiyama, *Nat. Nanotech.*, 2007, **2**, 399-410.

183. J. Andréasson and U. Pischel, *Chem. Soc. Rev.*, 2010, **39**, 174-188.
184. E. Katz and V. Privman, *Chem. Soc. Rev.*, 2010, **39**, 1835-1857.
185. H. Tian, *Angew. Chem.-Int. Edit.*, 2010, **49**, 4710-4712.
186. G. de Ruiter and M. E. van der Boom, *Acc. Chem. Res.*, 2011, **44**, 563-573.
187. A. P. de Silva, *Chem. Asian J.*, 2011, **6**, 750-766.
188. D. Gust, J. Andréasson, U. Pischel, T. A. Moore and A. L. Moore, *Chem. Commun.*, 2012, **48**, 1947-1957.
189. U. Pischel, J. Andréasson, D. Gust and V. F. Pais, *ChemPhysChem*, 2013, **14**, 28-46.
190. U. Pischel, *Angew. Chem.-Int. Edit.*, 2007, **46**, 4026-4040.
191. A. Credi, *Angew. Chem.-Int. Edit.*, 2007, **46**, 5472-5475.
192. F. M. Raymo, *Adv. Mater.*, 2002, **14**, 401.
193. A. P. de Silva and N. D. McClenaghan, *Chem. -Eur. J.*, 2004, **10**, 574-586.
194. J. Yoon, *Angew. Chem.-Int. Edit.*, 2014.
195. G. von Maltzahn, T. J. Harris, J.-H. Park, D.-H. Min, A. J. Schmidt, M. J. Sailor and S. N. Bhatia, *J. Am. Chem. Soc.*, 2007, **129**, 6064-6065.
196. S. Angelos, N. M. Khashab, Y.-W. Yang, A. Trabolsi, H. A. Khatib, J. F. Stoddart and J. I. Zink, *J. Am. Chem. Soc.*, 2009, **131**, 12912-12914.
197. S. Uchiyama, G. D. McClean, K. Iwai and A. P. de Silva, *J. Am. Chem. Soc.*, 2005, **127**, 8920-8921.
198. A. P. de Silva, M. R. James, B. O. McKinney, D. A. Pears and S. M. Weir, *Nat. Mater.*, 2006, **5**, 787-789.
199. M. Motornov, J. Zhou, M. Pita, V. Gopishetty, I. Tokarev, E. Katz and S. Minko, *Nano Lett.*, 2008, **8**, 2993-2997.
200. I. Tokarev, V. Gopishetty, J. Zhou, M. Pita, M. Motornov, E. Katz and S. Minko, *ACS Appl. Mater. Inter.*, 2009, **1**, 532-536.
201. G. de Ruiter, L. Motiei, J. Choudhury, N. Oded and M. E. van der Boom, *Angew. Chem.-Int. Edit.*, 2010, **122**, 4890-4893.
202. R. J. Amir, M. Popkov, R. A. Lerner, C. F. Barbas and D. Shabat, *Angew. Chem.-Int. Edit.*, 2005, **117**, 4452-4455.
203. D. Margulies and A. D. Hamilton, *J. Am. Chem. Soc.*, 2009, **131**, 9142-9143.
204. S. Chen, Z. Guo, S. Zhu, W.-E. Shi and W. Zhu, *ACS Appl. Mater. Inter.*, 2013, **5**, 5623-5629.
205. J. Andréasson, S. D. Straight, T. A. Moore, A. L. Moore and D. Gust, *J. Am. Chem. Soc.*, 2008, **130**, 11122-11128.
206. M. Suresh, D. A. Jose and A. Das, *Org. Lett.*, 2007, **9**, 441-444.
207. T. Konry and D. R. Walt, *J. Am. Chem. Soc.*, 2009, **131**, 13232-13233.
208. W. Sun, C. Zhou, C. H. Xu, C. J. Fang, C. Zhang, Z. X. Li and C. H. Yan, *Chem. -Eur. J.*, 2008, **14**, 6342-6351.

209. S. Kou, H. N. Lee, D. van Noort, K. e. M. e. K. Swamy, S. H. Kim, J. H. Soh, K. M. Lee, S. W. Nam, J. Yoon and S. Park, *Angew. Chem.-Int. Edit.*, 2008, **120**, 886-890.
210. J. Andréasson, U. Pischel, S. D. Straight, T. A. Moore, A. L. Moore and D. Gust, *J. Am. Chem. Soc.*, 2011, **133**, 11641-11648.
211. L. Sun and H. Tian, *Tetrahedron Lett.*, 2006, **47**, 9227-9231.
212. D. C. Magri, M. Camilleri Fava and C. J. Mallia, *Chem. Commun.*, 2014, **50**, 1009-1011.
213. T. J. Farrugia and D. C. Magri, *New J. Chem.*, 2013, **37**, 148-151.
214. T. Kealy and P. Pauson, *Nature*, 1951, **168**, 1039-1040.
215. S. Top, A. Vessières, G. Leclercq, J. Quivy, J. Tang, J. Vaissermann, M. Huché and G. Jaouen, *Chem. -Eur. J.*, 2003, **9**, 5223-5236.
216. D. Conroy, A. Moisala, S. Cardoso, A. Windle and J. Davidson, *Chem. Eng. Sci.*, 2010, **65**, 2965-2977.
217. A. J. Cross, M. G. Davidson, D. Garcia-Vivo and T. D. James, *RSC Adv.*, 2012, **2**, 5954-5956.
218. J. Zhang, W. Tan, X. Meng and H. Tian, *J. Mater. Chem.*, 2009, **19**, 5726-5729.
219. V. Balzani, A. Credi and M. Venturi, *Molecular devices and machines*, Wiley-VCH Weinheim, Germany, 2004.
220. U. Schröder, J. Wadhawan, R. G. Evans, R. G. Compton, B. Wood, D. J. Walton, R. R. France, F. Marken, P. C. Bulman Page and C. M. Hayman, *J. Phys. Chem. B*, 2002, **106**, 8697-8704.
221. A. N. Moore and D. Wayner, *Can. J. Chem.*, 1999, **77**, 681-686.

CHAPTER NINE

Appendix

9 Appendix

9.1 List of NMR Spectra

9.1.1 NMR for Naphthalimide Derivetives

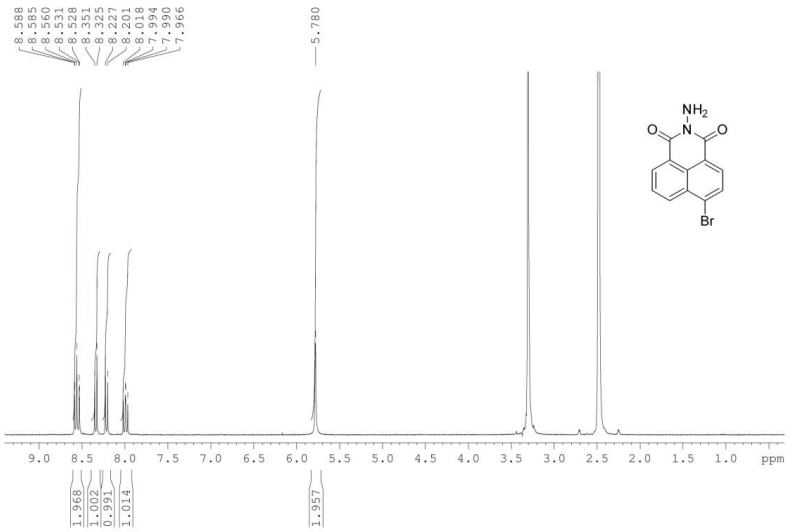

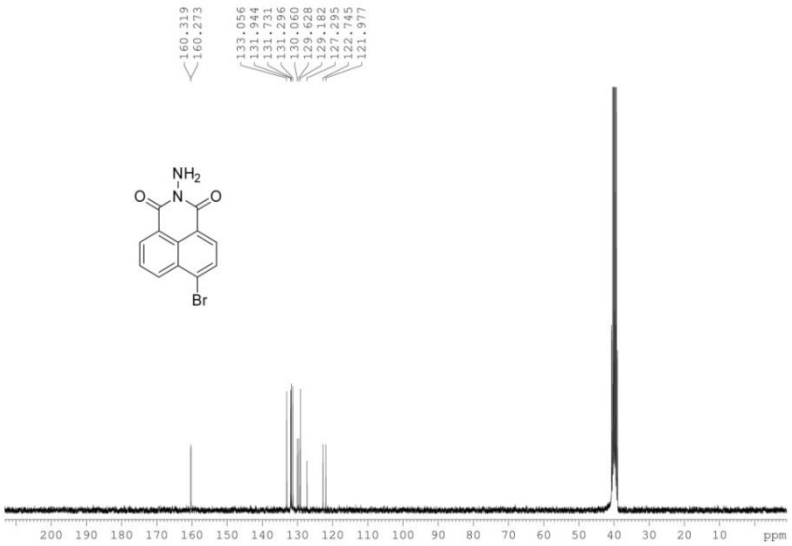

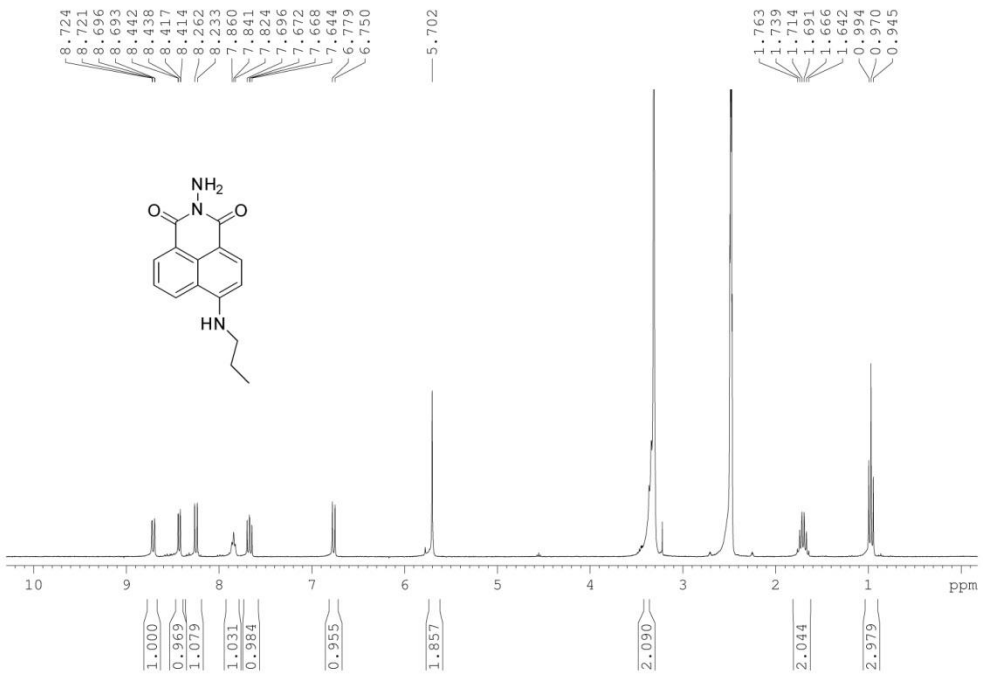
8.724
8.721
8.696
8.693
8.442
8.438
8.417
8.414
8.262
8.233
7.860
7.841
7.824
7.696
7.672
7.668
7.644
6.779
6.750
5.702
1.763
1.739
1.714
1.691
1.666
1.642
0.994
0.970
0.945
NH2
N
O
O
HN
10
9
8
7
6
5
4
3
2
1
ppm
1.000
0.969
1.079
1.031
0.984
0.955
1.857
2.090
2.044
2.979

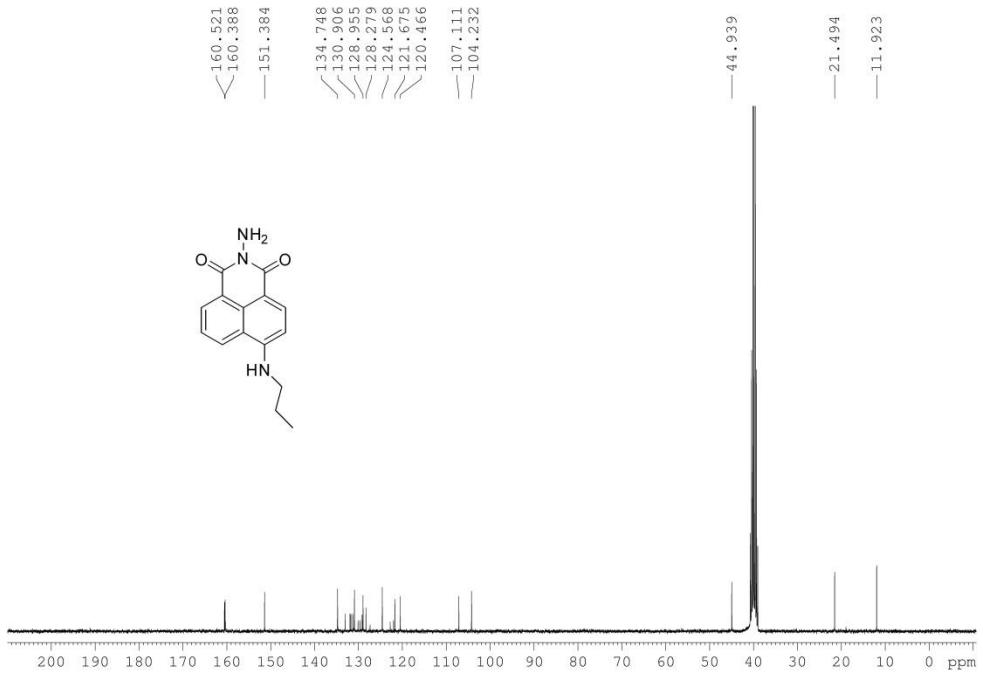
160.521
160.388
151.384
134.748
130.906
128.955
128.279
124.568
121.675
120.466
107.111
104.232
44.939
21.494
11.923
NH2
N
O
O
HN
200
190
180
170
160
150
140
130
120
110
100
90
80
70
60
50
40
30
20
10
0
ppm

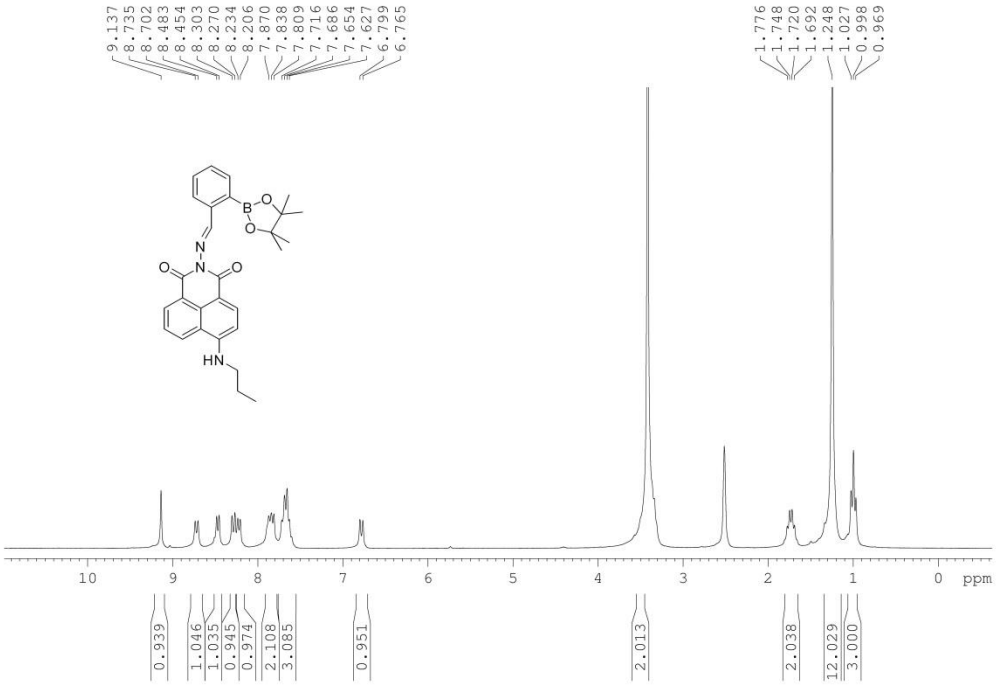
9.137
8.735
8.702
8.483
8.454
8.303
8.270
8.234
8.206
7.870
7.838
7.809
7.716
7.686
7.654
7.627
6.799
6.765
1.776
1.748
1.720
1.692
1.248
1.027
0.998
0.969
B
O
O
N
N
O
O
HN
10
9
8
7
6
5
4
3
2
1
0
ppm
0.939
1.046
1.035
0.945
0.974
2.108
3.085
0.951
2.013
2.038
12.029
3.000

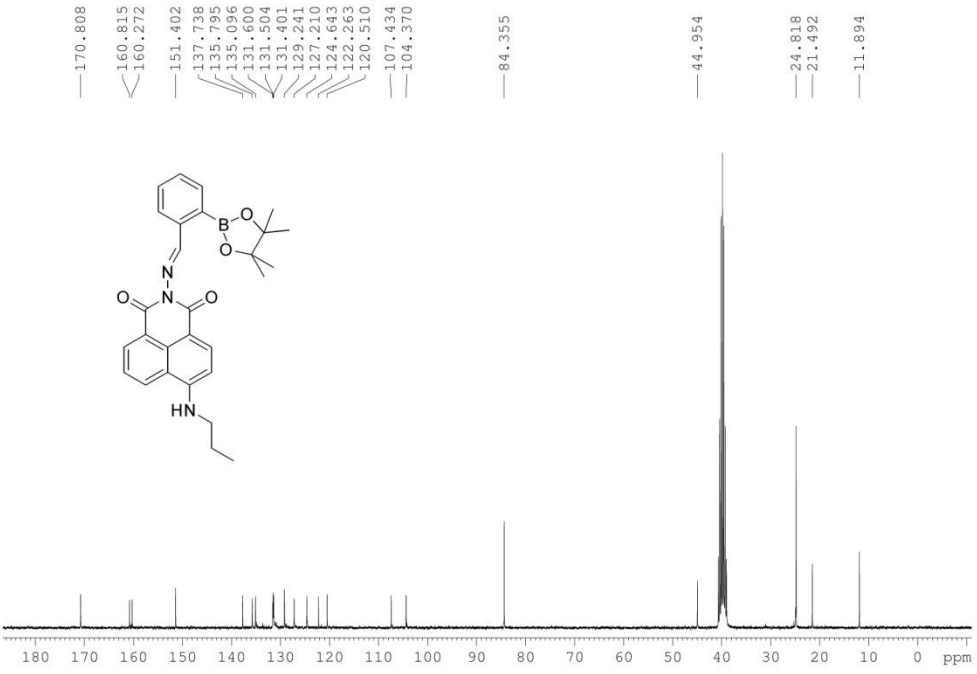
170.808
160.815
160.272
151.402
137.738
135.795
135.096
131.600
131.504
131.401
129.241
127.210
124.643
122.263
120.510
107.434
104.370
84.355
44.954
24.818
21.492
11.894
B
O
O
N
N
O
O
HN
180
170
160
150
140
130
120
110
100
90
80
70
60
50
40
30
20
10
0
ppm

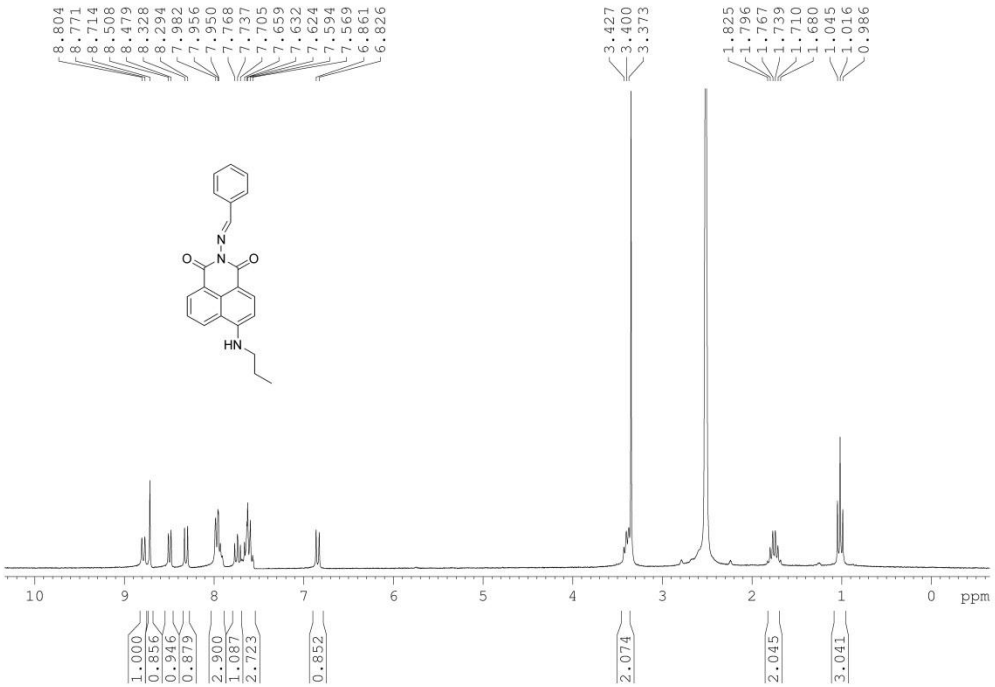
8.804
8.771
8.714
8.508
8.479
8.328
8.294
7.982
7.956
7.950
7.768
7.737
7.705
7.659
7.632
7.624
7.594
7.569
6.861
6.826
3.427
3.400
3.373
1.825
1.796
1.767
1.739
1.710
1.680
1.045
1.016
0.986
HN
10 9 8 7 6 5 4 3 2 1 0 ppm
1.000
0.856
0.946
0.879
2.900
1.087
2.723
0.852
2.074
2.045
3.041

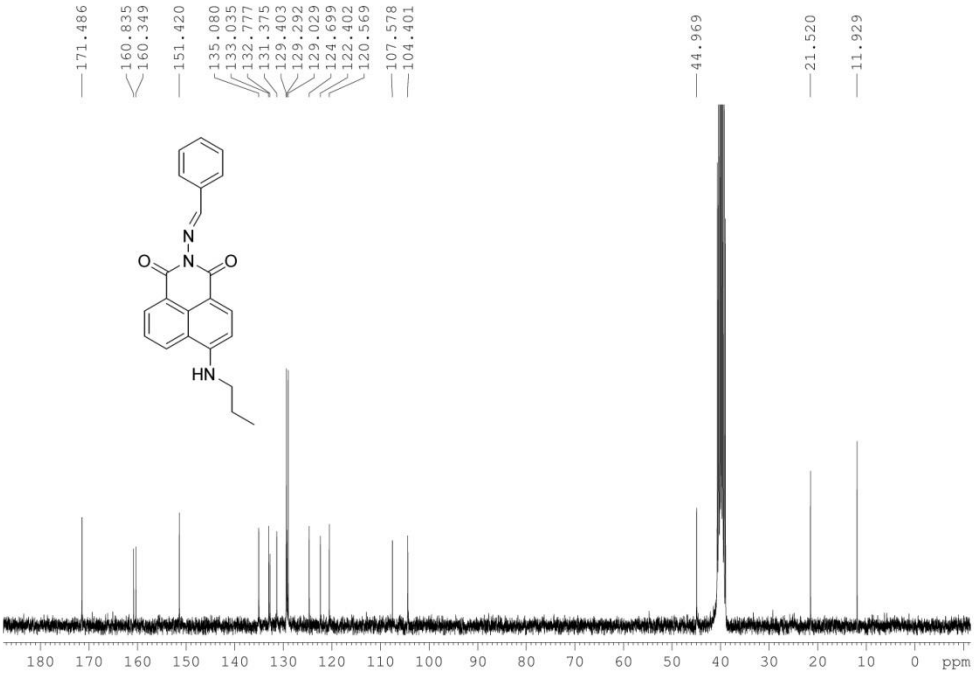
171.486
160.835
160.349
151.420
135.080
133.035
132.777
131.375
129.403
129.292
129.029
124.699
122.402
120.569
107.578
104.401
44.969
21.520
11.929
HN
180 170 160 150 140 130 120 110 100 90 80 70 60 50 40 30 20 10 0 ppm

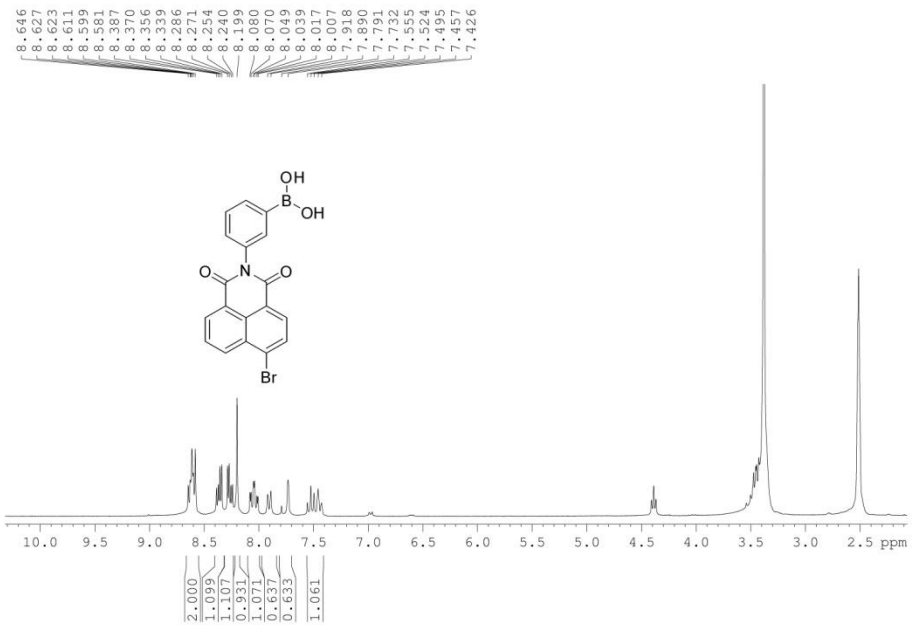
8.646
8.627
8.623
8.611
8.599
8.581
8.387
8.370
8.356
8.339
8.286
8.271
8.254
8.240
8.199
8.080
8.070
8.049
8.039
8.017
8.007
7.918
7.890
7.791
7.732
7.555
7.524
7.495
7.457
7.426
OH
B
OH
O
N
O
Br
10.0 9.5 9.0 8.5 8.0 7.5 7.0 6.5 6.0 5.5 5.0 4.5 4.0 3.5 3.0 2.5 ppm
2.000
1.099
1.107
0.931
1.071
0.637
0.633
1.061

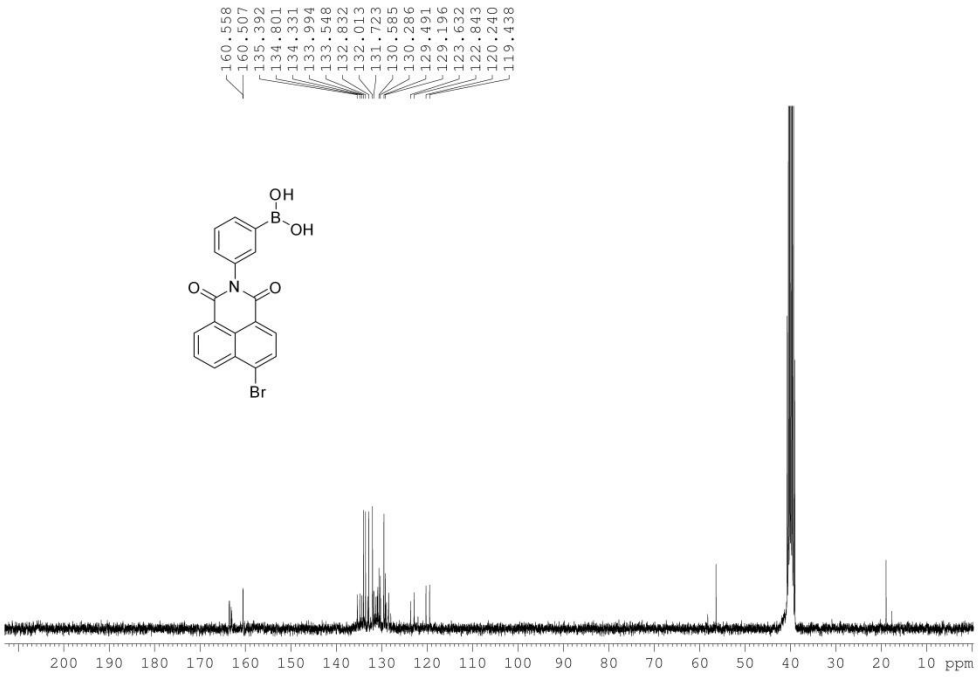
160.558
160.507
135.392
134.801
134.331
133.994
133.548
132.832
132.013
131.723
130.585
130.286
129.491
129.196
123.632
122.843
120.240
119.438
OH
B
OH
O
N
O
Br
200 190 180 170 160 150 140 130 120 110 100 90 80 70 60 50 40 30 20 10 ppm

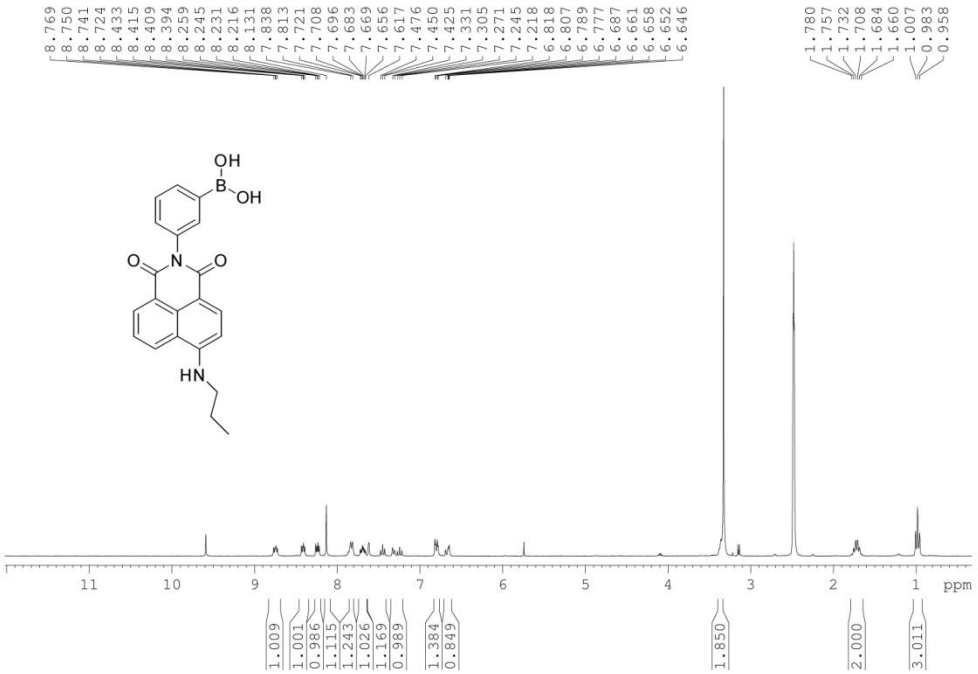
8.769
8.750
8.741
8.724
8.433
8.415
8.409
8.394
8.259
8.245
8.231
8.216
8.131
7.838
7.813
7.721
7.708
7.696
7.683
7.669
7.656
7.617
7.476
7.450
7.425
7.331
7.305
7.271
7.245
7.218
6.818
6.807
6.789
6.777
6.687
6.661
6.658
6.652
6.646
1.780
1.757
1.732
1.708
1.684
1.660
1.007
0.983
0.958
OH
B
OH
O
N
O
HN
11
10
9
8
7
6
5
4
3
2
1
ppm
1.009
1.001
0.986
1.115
1.243
1.026
1.169
0.989
1.384
0.849
1.850
2.000
3.011

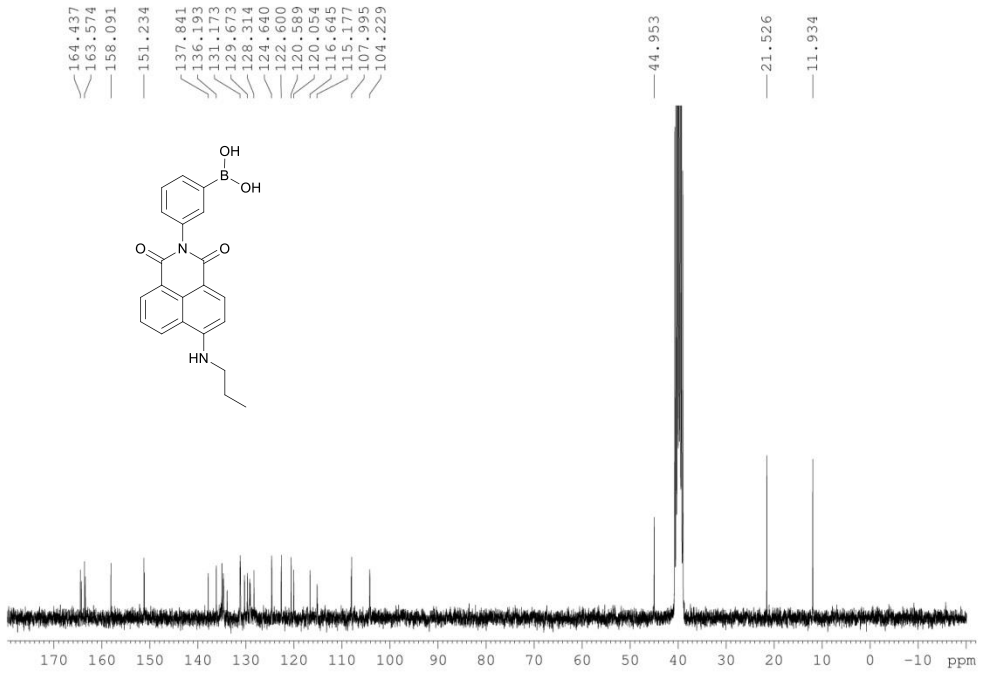
164.437
163.574
158.091
151.234
137.841
136.193
131.173
129.673
128.314
124.640
122.600
120.589
120.054
116.645
115.177
107.995
104.229
44.953
21.526
11.934
OH
B
OH
O
N
O
HN
170
160
150
140
130
120
110
100
90
80
70
60
50
40
30
20
10
0
-10
ppm

9.1.2 NMR for DCM Derivatives

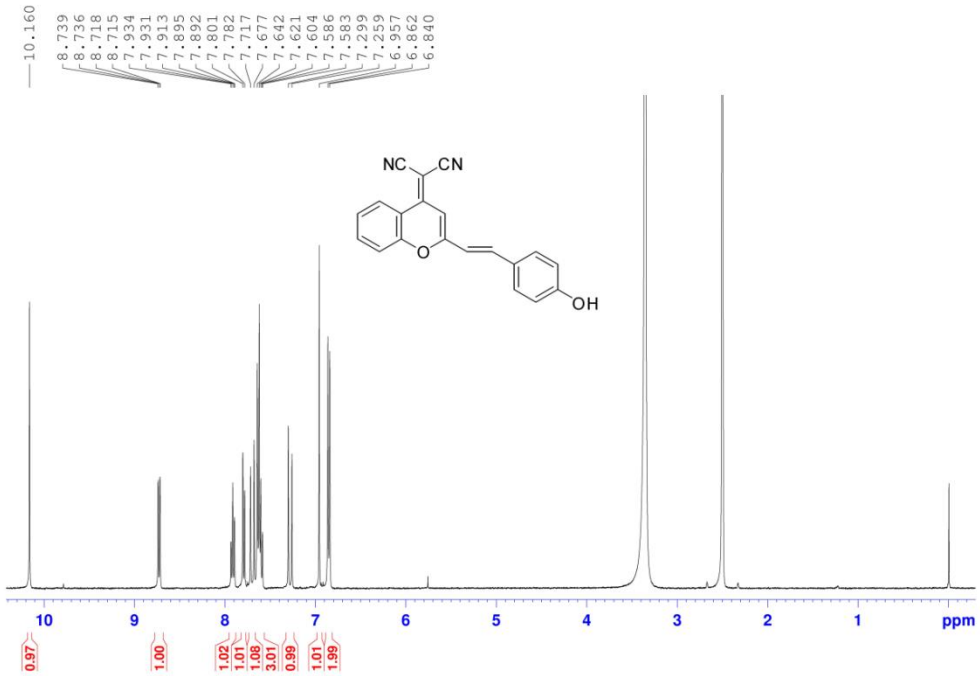

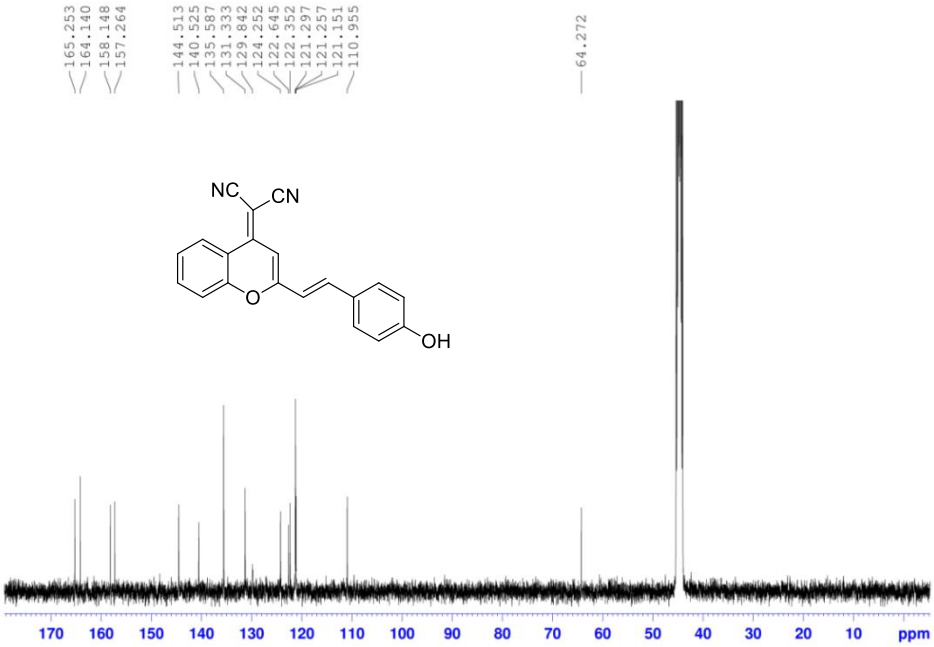

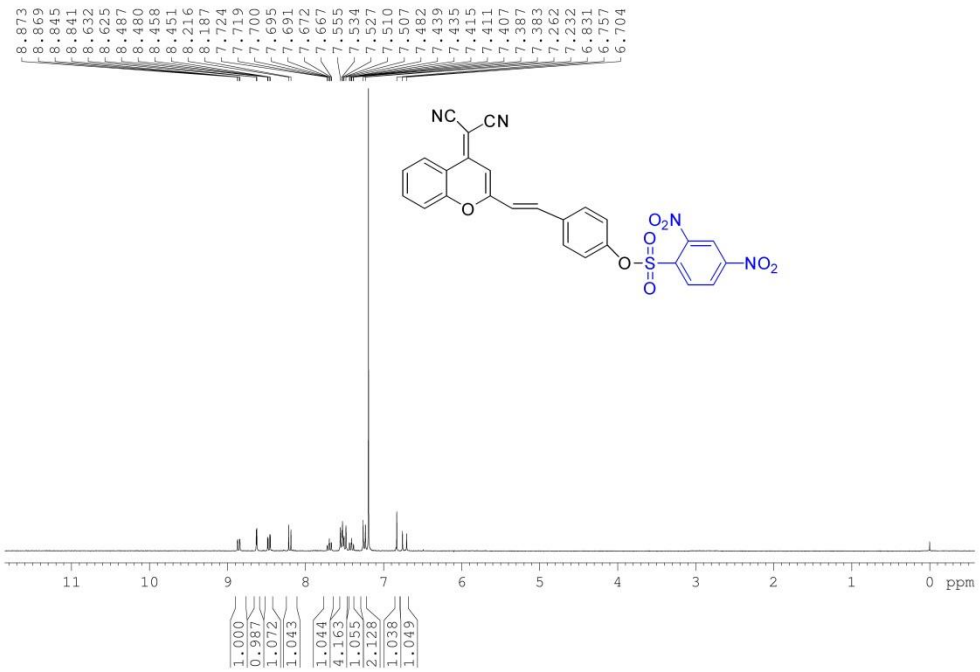
8.873
8.869
8.845
8.841
8.632
8.625
8.487
8.480
8.458
8.451
8.216
8.187
7.724
7.719
7.700
7.695
7.691
7.672
7.667
7.555
7.534
7.527
7.510
7.507
7.482
7.439
7.435
7.415
7.411
7.407
7.387
7.383
7.262
7.232
6.831
6.757
6.704
NC
CN
O
O2N
O
O
S
O
NO2
11
10
9
8
7
6
5
4
3
2
1
0 ppm
1.000
0.987
1.072
1.043
1.044
4.163
1.055
2.128
1.038
1.049

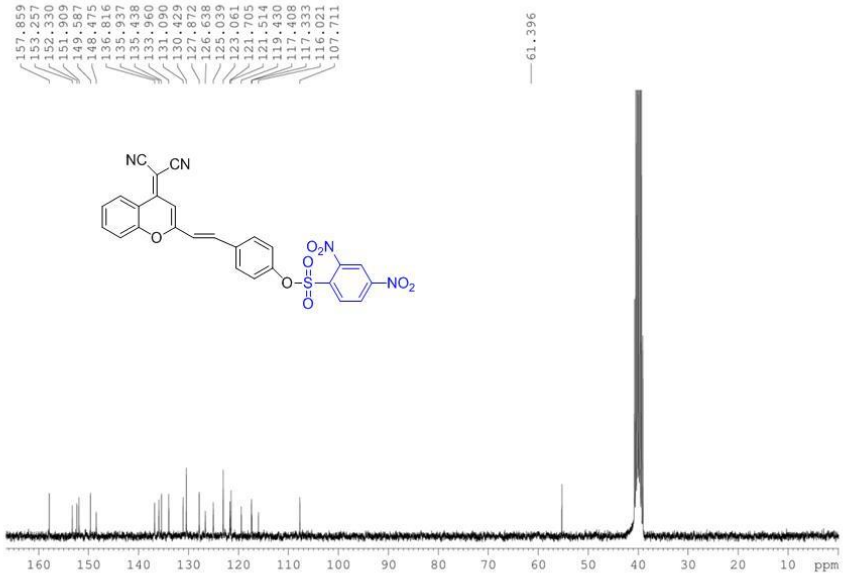
157.859
153.257
152.330
151.909
149.587
148.475
136.816
135.937
135.438
133.960
131.090
130.429
127.872
126.638
125.039
123.061
121.705
121.514
119.430
117.408
117.333
116.021
107.711
61.396
NC
CN
O
O2N
O
O
S
O
NO2
160
150
140
130
120
110
100
90
80
70
60
50
40
30
20
10
ppm

9.1.3 NMR for Ferrocene Derivatives

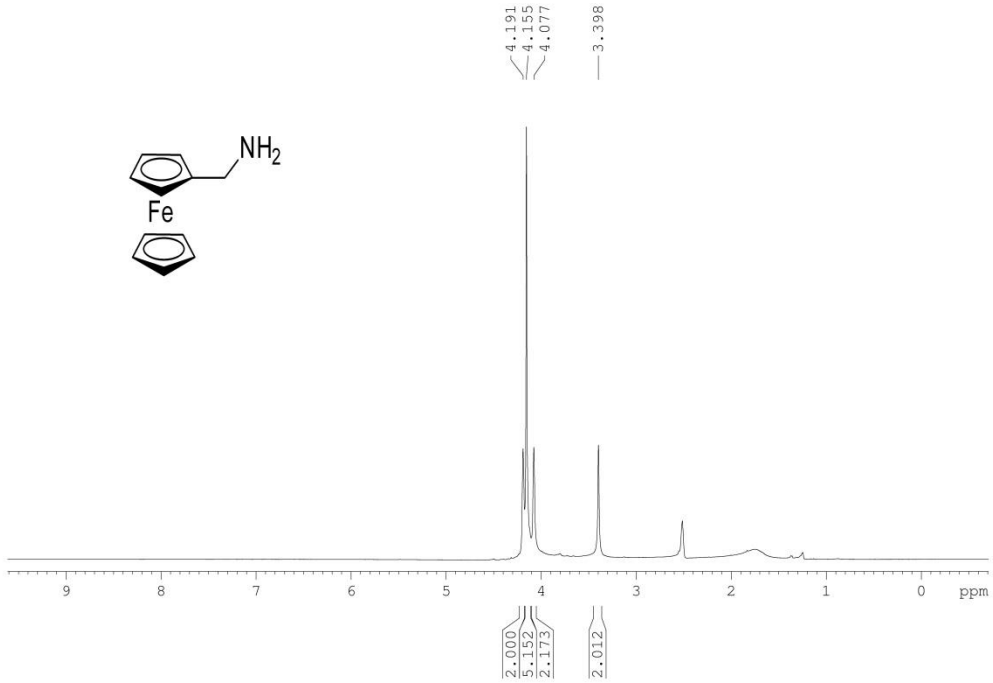

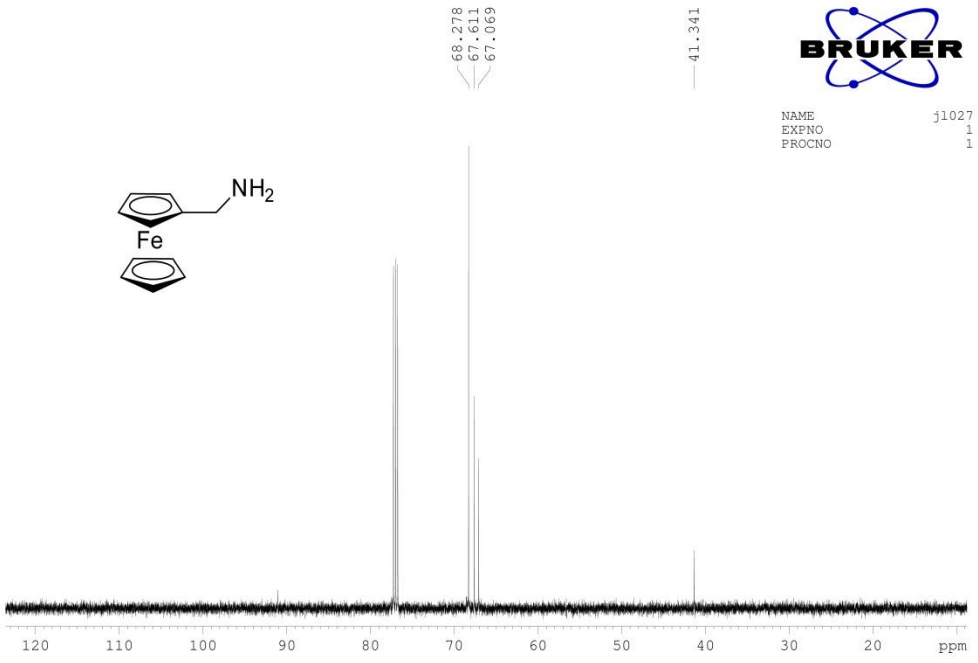

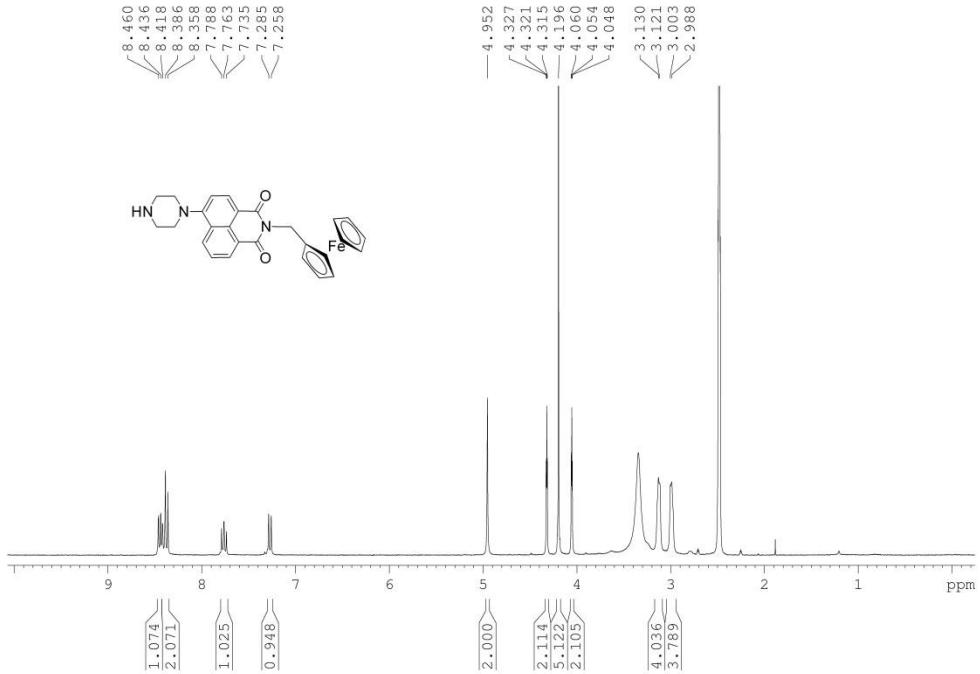
8.460
8.436
8.418
8.386
8.358
7.788
7.763
7.735
7.285
7.258
4.952
4.327
4.321
4.315
4.196
4.060
4.054
4.048
3.130
3.121
3.003
2.988
HN
N
O
N
O
Fe
9
8
7
6
5
4
3
2
1
ppm
1.074
2.071
1.025
0.948
2.000
2.114
5.122
2.105
4.036
3.789

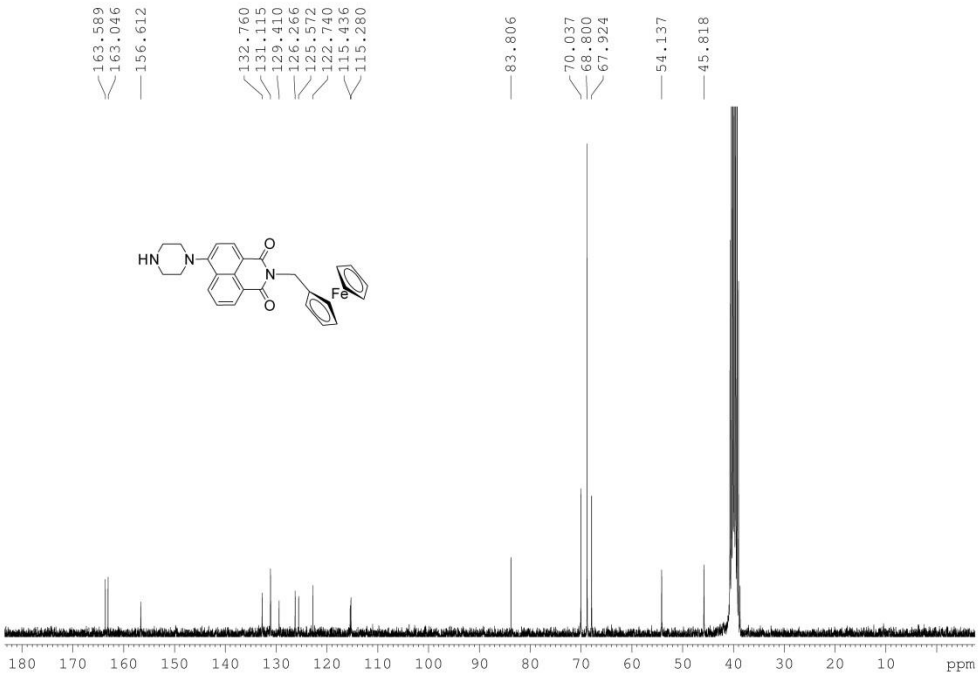
163.589
163.046
156.612
132.760
131.115
129.410
126.266
125.572
122.740
115.436
115.280
83.806
70.037
68.800
67.924
54.137
45.818
HN
N
O
N
O
Fe
180
170
160
150
140
130
120
110
100
90
80
70
60
50
40
30
20
10
ppm

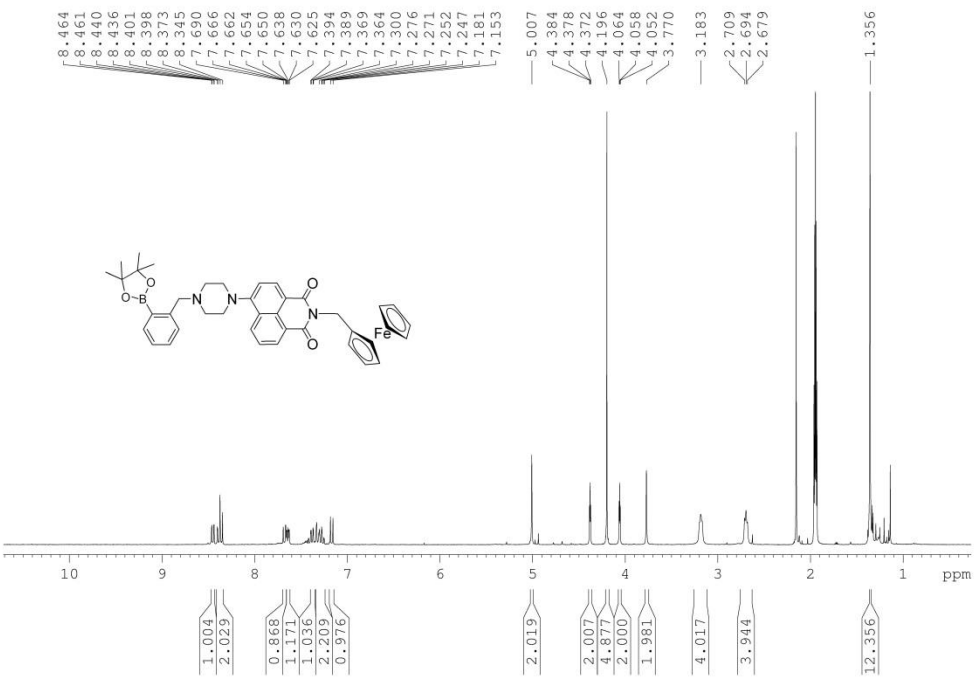
8.464
8.461
8.440
8.436
8.401
8.398
8.373
8.345
7.690
7.666
7.662
7.654
7.650
7.638
7.630
7.625
7.394
7.389
7.369
7.364
7.300
7.276
7.271
7.252
7.247
7.181
7.153
5.007
4.384
4.378
4.372
4.196
4.064
4.058
4.052
3.770
3.183
2.709
2.694
2.679
1.356
Fe
10
9
8
7
6
5
4
3
2
1
ppm
1.004
2.029
0.868
1.171
1.036
2.209
0.976
2.019
2.007
4.877
2.000
1.981
4.017
3.944
12.356

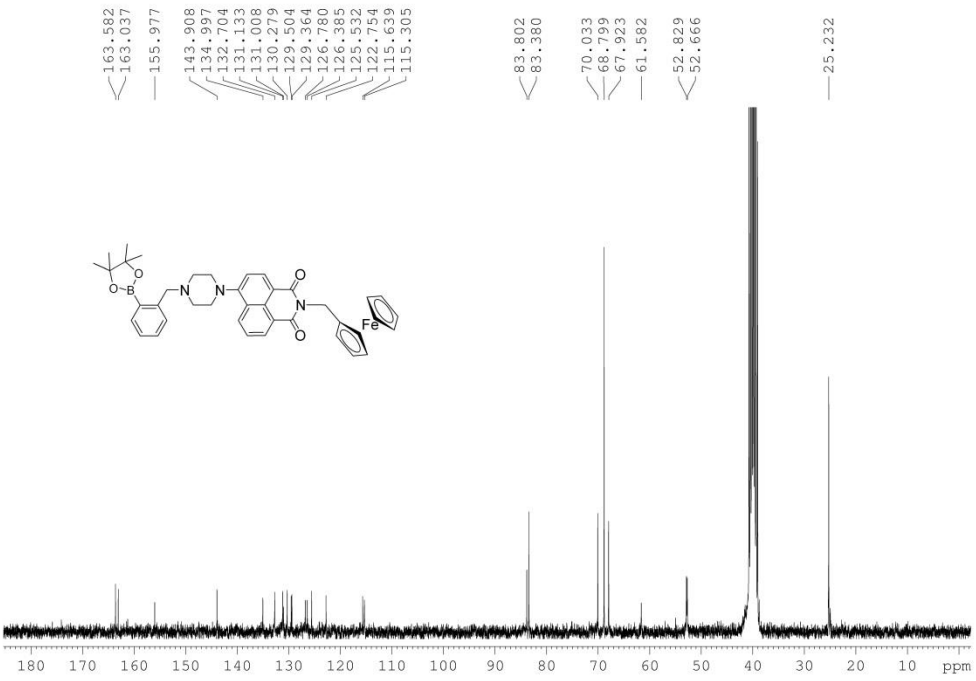
163.582
163.037
155.977
143.908
134.997
132.704
131.133
131.008
130.279
129.504
129.364
126.780
126.385
125.532
122.754
115.639
115.305
83.802
83.380
70.033
68.799
67.923
61.582
52.829
52.666
25.232
Fe
180
170
160
150
140
130
120
110
100
90
80
70
60
50
40
30
20
10
ppm